VANADIUM RECOVERY IN THE ELECTRO-ALUMINOTHERMIC PRODUCTION OF FERROVANADIUM.

deur

Matthys Karel Gerhardus Vermaak

Voorgelê ter vervulling van 'n deel van die vereistes vir die graad

Magister in Ingenieurswese

in die Departement van Materiaalkunde en Metallurgiese Ingenieurswese, Universiteit van Pretoria, Pretoria, Republiek van Suid-Afrika.

Projekleier : Professor P.C. Pistorius

Januarie, 2000

Aan Ilse met liefde.

ACKNOWLEDGEMENTS

I would like to thank and herewith express my sincere appreciation to the following people and institutes:

- Prof. Chris Pistorius, my supervisor, for guidance and continuous support.
- S. Havenga for all her support.
- Eben Bernardo and A. Brugman, for appreciating the need for this research and the opportunity.
- Highveld Steel and Vanadium Corporation Limited for financial support.
- Department of Material Science and Metallurgical Engineering, Pretoria University, for facilities.
- S. Verryn and M. Loubscher of the Geology Department for help in various analyses.
- A. Botha of the Electron-microscopy section for assistance and thrust bestowed upon me to use the electron-microscope after-hours.
- R. Muir, for manufacture and repair of countless special glassware equipment.
- My father, mother, Leslie, Pieter, Batsie, Ilse and her parents, Muller and other friends for their, prayers, continuous support and patience throughout.
- My fellow graduate students, Rian, Giel, Josè, Michelle, Niel, Riaan, Ferdus, Colette, Nana, Daudet and Alain for their support and advice.
- The Lord, for the abilities He gave me and the opportunities to develop them.

SOLI DEO GLORIA

VANADIUM RECOVERY IN THE ELECTRO-ALUMINOTHERMIC PRODUCTION OF FERROVANADIUM.

by

Matthys Karel Gerhardus Vermaak

Prof. P.C. Pistorius

Department of Material Science and Metallurgical Engineering

Master Degree in Engineering

Abstract.

Ferrovanadium is sometimes produced from V_2O_3 in electric arc furnaces, using aluminium as reductant. CaO fluxes the alumina which forms during reduction of the vanadium oxide. Vanadium recovery in the electro-aluminothermic process is mainly controlled by losses to the slag. These include metal droplet entrainment (these droplets remain in the slag after solidification) and unreduced vanadium oxides in the slag. Both these factors might be a significant cause of vanadium losses.

To quantify factors which can affect the equilibrium vanadium loss, the vanadium oxide activity coefficient was measured experimentally for different slag compositions. Hydrogen-water mixtures were used to control the partial oxygen pressure (ca. 10^{-13} atm) over CaO-Al_2O_3 slags contained in vanadium crucibles at 1700°C; gas phase mass transfer was controlled by jetting the gas mixture onto the slag surface. Manipulation of the redox conditions at a single slag composition and temperature showed that – as expected – the vanadium is present in the trivalent state in the slag. The slag basicity (CaO/Al_2O_3 ratio) was found to have a very strong effect on the activity coefficient of $VO_{1.5}$, with clear implications for the effect of plant practice on vanadium loss. The laboratory equilibrium results were compared to EDX analyses obtained from actual industrial slag samples. Analysis of the industrial slags indicate that slags with higher Al_2O_3 contents clearly have lower vanadium oxide contents.

An alteration of the slag composition by adding less CaO will lower the soluble vanadium loss, inevitably changing the separation of the solid ferrovanadium phase from the slag phase. The effect of slag basicity on metal droplet entrainment was assessed by

investigating solidified slag samples. The effect of droplet entrainment on vanadium loss could not be fully quantified due to the strong segregation behavior and crowding close to the slag-metal surface. Samples which were taken close to this interface showed unusually high vanadium losses, compared to samples taken at the top of the bulk slag sample.

Equilibrium calculations were also performed to predict the relative influence of temperature, MgO content of the slag, and aluminium content of the ferrovanadium on oxidic vanadium loss. The activity-composition relations for the species in the slag and ferrovanadium were estimated using the Chemsage software package. The lower predicted vanadium content of the slag compared to industry is probably the result of uncertainties regarding the aluminium activity. Nevertheless, lower MgO contents of the slag, higher aluminium contents of the ferrovanadium and lower tap temperatures will yield lower vanadium oxide losses to the slag.

Keywords: Key Words: electro-aluminothermic process, ferrovanadium, vanadium, activity coefficient, slag-metal equilibrium, basicity, slag losses, metal droplet entrainment.

VANADIUMHERWINNING IN DIE ELEKTRO-ALUMINOTERMIESE PRODUKSIE VAN FERROVANADIUM

deur

Matthys Karel Gerhardus Vermaak

Prof. P.C. Pistorius

Departement Materiaalkunde en Metallurgiese Ingenieurswese

Meestersgraad in Ingenieurswese

Opsomming

Ferrovanadium word soms van V_2O_3 in 'n elektriese boogoond vervaardig, met aluminium as reduktant. CaO dien as vloeimiddel vir die alumina wat gevorm word tydens die reduksie van die vanadiumoksied. Vanadiumherwinning in die elektro-aluminotermiese proses word hoofsaaklik deur metaaldruppelvasvanging (die druppels bly vasgevang in die slak nadat stolling plaasgevind het) en ongereduseerde vanadiumoksied in die slak beheer. Beide die meganismes is moontlik verantwoordelik vir beduidende vanadiumverliese.

Faktore wat die ewewigvanadiumverliese kan beïnvloed, kan gekwantifiseer word deur die vanadiumoksiedaktiwiteitskoëffisiënt eksperimenteel, vir verskillende slaksamestellings, te bepaal. Water-waterstofgasmengsels is gebruik om die parsiële suurstofdruk (ca. 10^{-13} atm) by 1700°C oor $CaO\text{-}Al_2O_3$ slakke wat in suiwer vanadiumkroese geplaas is, te beheer. Gasmassa-oordrag is beheer deur die gasmengsel direk op die slakoppervlakte te spuit. Verandering van die redokstoestande vir 'n enkele slaksamestelling en temperatuur toon, soos verwag, dat V^{3+} die stabiele oksidasietoestand is. Dit is bevind dat die slakbasisiteit (CaO/Al_2O_3-verhouding) 'n baie sterk invloed op die vanadiumoksiedaktiwiteitskoëffisiënt ($VO_{1.5}$) het, met duidelike implikasies vir die aanlegpraktyk ten opsigte van vanadiumverliese. Die laboratoriumewewigsresultate is toe met EDS analises van industriële slakke vergelyk. Die analises toon aan dat slakke met 'n laer alumina-inhoud laer vanadiumoksiedvlakke het.

'n Wysiging van die slaksamestelling deur minder CaO by te voeg, sal vanadiumoksiedverliese verlaag, maar die skeidingsgedrag van die vaste ferrovanadiumfase sal noodwendig ook verander. Die effek van slakbasisiteit op

metaaldruppelvasvanging is aangespreek deur industriële slakke te ondersoek. Die effek van slakbasisiteit kon nie ten volle gekwantifiseer word nie weens die sterk segregasiegedrag en die versameling van die metaaldruppels naby die slak-metaalintervlak. Monsters wat in die omgewing van die intervlak geneem is, het ongewoon hoë vanadiumverliese getoon vergeleke met monsters wat aan die bokant van die blokslakmonster geneem is.

Die relatiewe invloed van die MgO-inhoud van die slak, die aluminiuminhoud van ferrovanadium en die taptemperatuur is voorspel deur ewewigsberekeninge uit te voer. Die beraamde samestelling-aktiwiteitsverwantskappe van die spesies in ferrovanadium en in die slak is verkry deur van die Chemsage sagtewarepakket gebruik te maak. Die laer voorspelde vanadiumoksiedinhoud van die slak vergeleke met aanlegdata is toe te skryf aan onsekerhede wat betref die aluminiumaktiwiteit. Ten spyte hiervan, sal laer MgO-vlakke in die slak, hoër aluminiumvlakke en laer taptemperature die vanadiumopbrengs verhoog.

Sleutelwoorde: elektro-aluminotermiese proses, ferrovanadium, vanadium, aktiwiteitskoëffisiënt, slak-metaalewewig, basisiteit, slakverliese, metaaldruppelvasvanging.

Table of contents

1. Literature study

1.1. Introduction

Vanadium recovery in the electro-aluminothermic process is influenced by a number of factors relating to the production process, for instance raw materials handling, flux additions, temperature control and tapping procedure. Because of the high selling price of the final product, is it essential to identify and investigate the relative effect of each factor on the vanadium recovery, aiming to optimize the process. The most important recovery-linked factors that still await clarification can, if possible, be addressed by performing experiments. The objective of the following discussion is to provide background on some areas that were studied experimentally by the author.

1.2. Production of ferrovanadium

1.2.1. Introduction

Ferrovanadium represents today a group of vanadium compounds and alloys some of which do not even contain iron, but all of which serve the function of introducing vanadium into iron and steel. It is difficult to produce pure vanadium metal because vanadium readily reacts and absorbs oxygen, nitrogen and carbon. Furthermore the presence of impurities renders the vanadium metal brittle (Gupta,1992).

Ferrovanadium is produced by the reduction of vanadium bearing starter materials including slags, boiler residues, fly ash and vanadium oxides, using carbon, silicon or aluminium as reductant. The vanadium oxides can be in the form of V_2O_5, V_2O_4, V_2O_3 or mixtures of these oxides. The exothermicity of the reaction is a function of the level of vanadium oxidation and the concentration of each species in the raw material. This would therefore determine to what extent external energy is required. Depending on the production process and raw materials used, the concentration of vanadium in ferrovanadium generally ranges from 40 to 85 % by weight, and the industry classifies ferrovanadium into grades accordingly. Table 1 shows typical chemical specifications for commercial forms of ferrovanadium.

Alloy	Composition (Mass %)							
	V	C	N	Al	Si	P	S	Mn
50 –60 % ferrovanadium	50-60	0.2 max		2 max	1 max	0.05 max	0.05 max	
70 –80 % ferrovanadium	70-80			1 max	2.5 max	0.05 max	0.10 max	
80 % ferrovanadium	77-83	0.5 max		0.5 max	1.25 max	0.05 max	0.05 max	0.05 max
Carvan	82-86	10.5-14.5		0.1 max	0.1 max	0.05 max	0.10 max	
Ferrovanadium carbide	70-73	10-12			0.5 max	0.05 max	0.05 max	0.05 max
Ferrovan	42 min	0.85 max			7 max			4.5 max
Nitrovan	78-82	10-12	6 min	0.10 max	0.1 max	0.05 max	0.05 max	0.05 max

Table 1: Typical chemical compositions, with Fe as balance, for commercial forms of ferrovanadium (Gupta,1992).

The methods of producing ferrovanadium are discussed below

1.2.2. Carbothermic reduction

Reduction with carbon is conducted in a submerged-arc furnace. Carbon in the form of coke, coal, "char" or charcoal can be used. Carbothermic reduction is endothermic and so the process is energy intensive. Thus, successful production of ferrovanadium by carbon reduction of vanadium pentoxide requires the introduction of the furnace charge into the high temperature zone under strongly reducing conditions. The furnace usually has a rectangular cross section, using either two or three electrodes arranged in line. The electrodes create a high temperature reduction zone (Gupta,1992). The charge mainly consists of vanadium oxide, carbon source, steel scrap and fluxing agents.

The charge is fed into the high-energy reduction zone and ferrovanadium and slag accumulate below the arc and are tapped at 4-12h intervals (Hayward,1952).

A typical ferrovanadium composition for this process is as follows: 33-42 % V, 3-5 % Si, 3-3.5%C and balance Fe (Gupta,1992). The high residual carbon content in the alloy and the difficulty in regulating the carbon content have made carbothermic reduction in the arc furnace less attractive than alternative routes. The carbon reduction process is mainly used for the production of high C-grade ferrovanadium for example "Carvan" (85 %

Vanadium, 12 % Carbon, 2 % iron), used in applications where carbon and carbides are not detrimental.

The development of a falling film plasma reactor has changed the limited use of carbothermic reduction considerably. Plasma reactors enable endothermic reactions in carbothermic reduction to be carried out at very high temperatures, thus establishing higher yields. MacRae et al (1976) developed a falling film plasma reactor to produce ferrovanadium, shown in figure 1.

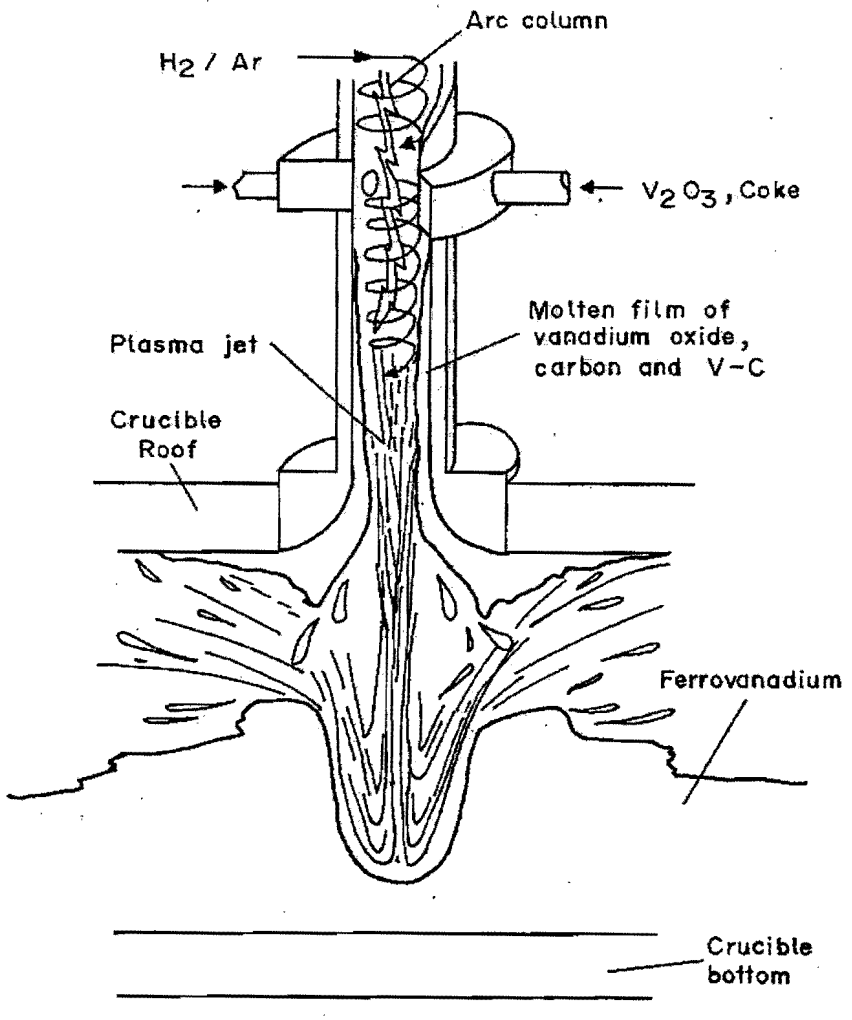

Figure 1: Falling film plasma reactor (Gupta,1992).

Vanadium oxide and coke fines are injected into the arc which is struck between a tungsten cathode and a tubular copper anode. The molten liquid flows down the anode wall into a receiving crucible. In essence the film enables intimate contact between the

reactants and the long residence time provides sufficient time for heat transfer, thus driving the reaction almost to completion. The product contains typically 42 % V, 53% Fe and 3 % C. Despite the good heat transfer to the reactants, the power consumption is still 3200 kWh/ton ferrovanadium produced.

1.2.3. Silicon reduction

In this route the reductant is a high-grade ferrosilicon containing 75% silicon. Silicon is not a powerful reducer of vanadium oxides; thus a two-stage process is required. Technical grade vanadium pentoxide is smelted to produce ferrovanadium containing about 30% vanadium with a considerable amount of residual silicon. According to Khodorovsky et al (1967), the slag composition is 50-55% CaO, 5-10% MgO, 28-30% SiO_2 and 0.5% V. The overall reaction can be represented by

$$2V_2O_5 + 5(Fe_{y/5}Si)_{alloy} + 10CaO = 4(Fe_{y/4}V)_{alloy} + 5Ca_2SiO_4 \qquad (1)$$

The primary metal is refined with vanadium pentoxide and lime in a second step and the secondary slag is returned as part of the charge to produce primary metal. Lower vanadium oxides such as V_2O_3 and VO interact with silica to form vanadium silicates, thus making the reduction process difficult and more complicated. As a result the slag traps some vanadium and the recovery rarely exceeds 75-80% (Gupta,1992).

1.2.4. Aluminium reduction

The reduction of vanadium oxide with aluminium can be further subdivided into the aluminothermic (thermit) and the electro-aluminothermic processes. The nature of the vanadium oxide used as input material governs the production route as is indicated in the next sections.

1.2.4.1. Reduction of vanadium oxides

The reduction of vanadium oxides by aluminium can be represented by the following set of reactions. (The heats of the reactions were calculated using correlations of

Kubaschewski et al. (1993) for enthalpy values at 298 K and 2073 K for the reactants and products respectively):

$$3V_2O_5 + 10Al \rightarrow 6V + 5Al_2O_3 \; ; \Delta H^\circ = -4.28 * 10^5 \text{ J/mol V} \quad (2)$$

$$3V_2O_4 + 8Al \rightarrow 6V + 4Al_2O_3 \; ; \Delta H^\circ = -2.37 * 10^5 \text{ J/mol V} \quad (3)$$

$$V_2O_3 + 2Al \rightarrow 2V + Al_2O_3 \; ; \Delta H^\circ = -9.25 * 10^4 \text{ J/mol V} \quad (4)$$

$$3VO + 2Al \rightarrow 3V + Al_2O_3 \; ; \Delta H^\circ = -1.52 * 10^4 \text{ J/mol V} \quad (5)$$

The enthalpy of the exothermic reaction can be used to predict whether the reaction releases enough energy to melt the metal and slag. The ratio of the heat of the reaction and the molecular weight of the products is generally used to determine the exothermicity of the reaction. If the ratio >4 500 J/gram, then the reaction is violent, under 2250 J/gram external supply of heat is necessary and between 2250 J/gram and 4500 J/gram the reaction develops in a controlled manner and external energy is not necessary (Yücel,1996). Only slag reaction 2 is sufficiently exothermic to obtain liquid metal given the very high melting temperature of ferrovanadium (typically 1750 °C).

1.2.4.2. Aluminothermic reduction

The process can be characterized by reaction 2. This reaction is strongly exothermic and once it has been initiated it can both melt the iron added to make the alloy and allow for effective separation of the alloy and the high aluminium slag. The aluminothermic reactor is presented in figure 2.

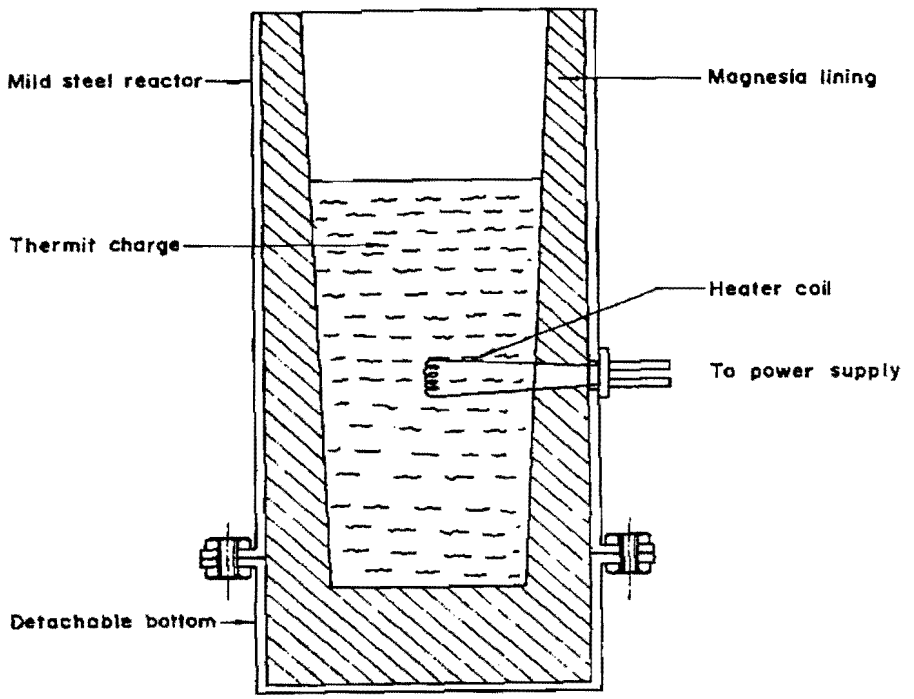

Figure 2: Aluminothermic reactor (Gupta,1992).

The charge mix consists mainly of V_2O_5, scrap iron, aluminium (particle size: 0.7 - 1.1 mm, Nyirfa[1985]) and lime. The materials are thoroughly mixed before being fed to the reactor. Two distinct smelting methods can be distinguished namely "the reverse reaction" and "feeded reaction" methods. In the feeded reaction method only part of the charge mix is fed to the reactor and then this is ignited. The remainder of the charge mix is fed progressively according to the speed of the reactions. The method requires well-trained operators. In the reverse reaction method the entire charge mix is loaded into the reactor and ignited in such a way that the reaction can proceed downwards. The heater coil is embedded in the mixture so that the reaction can be initiated remotely by passing a current through the coil. Once initiated the reaction proceeds to completion.

Adjusting the feed rate and the particle size of especially aluminium can control the rate of the feeded reaction. If the aluminium granules are too big the reaction interfaces are small resulting in slow and incomplete reactions. The rate of fusion of the initial charge increases with an increase of the specific surface area and with greater addition of aluminium shot. Figure 3 shows the effect of granule size and the amount of Al added on the rate of fusion of the charge. The rate of charge fusion determines the rate of the reduction process.

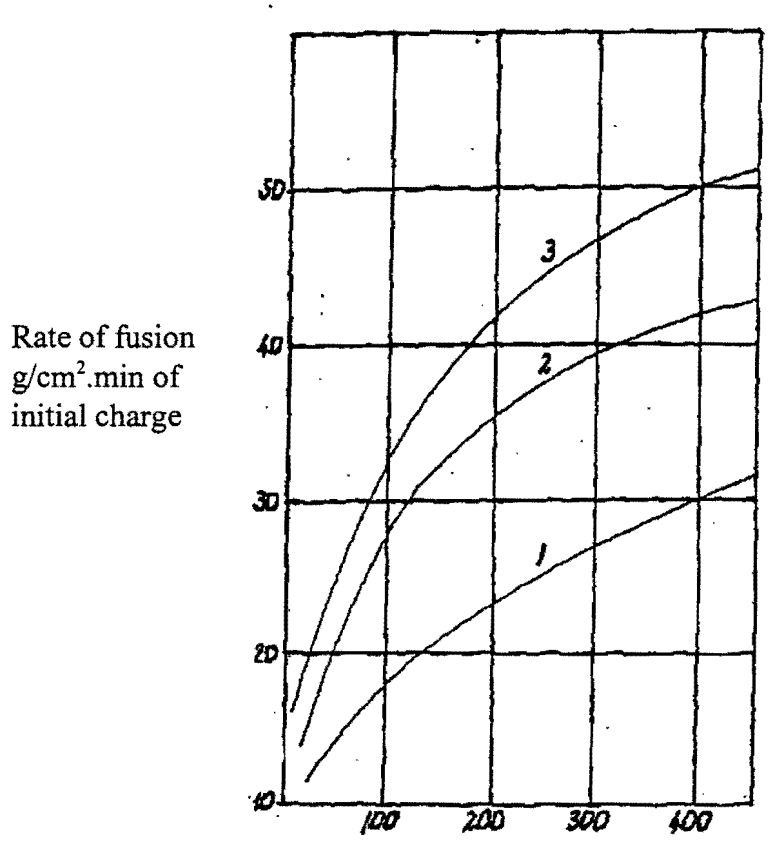

Figure 3: Effect of the amount of aluminium and of its specific surface area on the fusion rate of the charge (Nyirfa,1985). Curve 2 represents the stoichiometric amount of aluminium added. The other curves are where this amount is reduced by 20 % (Curve 1) and increased by 20 % (Curve3).

Large size granules cause increased amounts of large-size drops of alloy being trapped in the slag. Although the increase of aluminium above the stoichiometrically needed amount results in faster reactions and improves the vanadium recovery, it does increase the final Al content of the alloy. There are strict specifications set by the consumer regarding the aluminium content of the alloy, indicated by Table 1, thus necessitating the optimization of the recovery process by adjusting parameters influencing the vanadium distribution between slag and metal. One such parameter is the slag basicity. The slag basicity has a dual influence on the vanadium recovery in the sense that it influences the vanadium activity coefficient and the slag viscosity, which in turn has an effect on the separation of metal droplets from the liquid slag. In addition to this, the slag volume also increases with an increase in basicity. Figure 4 shows the effect of the slag basicity on the V_2O_5 content

of the slag. No indication is given whether the metal particles in the slag were avoided during analysis.

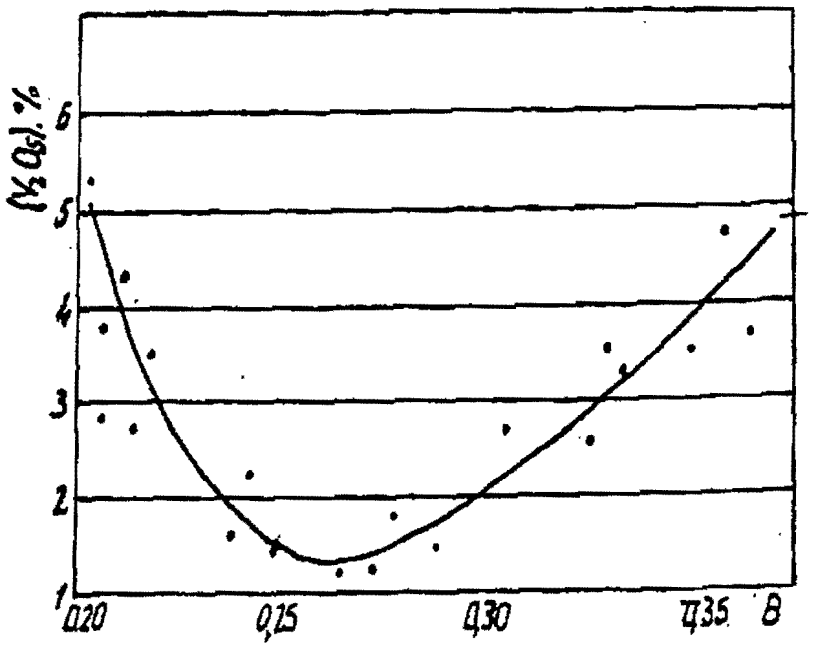

Figure 4: Effect of the slag basicity (mass %CaO / mass %Al_2O_3) on the V_2O_5 content of the slag (Nyirfa,1985).

From this figure it is evident that an optimum exists at a ratio mass % CaO: mass % Al_2O_3 of around 0.25 –0.3, which must be achieved if the recovery is to be maximized, if the effect of viscosity on the recovery can be neglected. In other words the effect of slag basicity on droplet entrainment and its subsequent contribution to the total vanadium loss to the slag are not taken into account. Nothing is mentioned about the type of refractory lining this industrial smelting process (Nyirfa,1985). As indicated later in this work a substantial amount of magnesite refractory lining dissolves in the presence of a high-alumina slag. If it is assumed that effect of MgO is similar to CaO then the effect of the former on the vanadium distribution cannot be neglected and should be incorporated in the basicity relationship. No indication is given in this work regarding the effect of slag basicity on the phenomenon of droplet entrainment.

In the next paragraph the second of the Al-based reduction processes will be discussed (i.e. electro-aluminothermic reduction).

1.2.4.3. Electro-aluminothermic production of ferrovanadium

As indicated by the title of this work, factors influencing vanadium recovery in the electro-aluminothermic process will be under detailed investigation. For a lower vanadium oxidation level in the feed material less Al is required and consequently the reaction is less exothermic. The use of V_2O_3 and V_2O_4 as raw materials necessitates the addition of external energy to sustain the reduction process. This process is much less violent and thus more controllable than the aluminothermic process. This allows the operator better control over the process because temperature is an important factor concerning the quality of the product, vanadium yield, viscosity of the slag, the separability of the slag and the metal, and the dissolution of the refractory lining. The equilibrium constant of this reduction reaction is strongly temperature dependent, thus co-determining the distribution of vanadium between the metal and the slag. Electric power consumption in ferro-alloy production is compared in Table 2. Although the production of ferrovanadium by an electric arc furnace process does not require as much power as other ferro-alloy processes, it can still amount to a substantial percentage of the total cost and should therefore be carefully controlled.

Alloy	Specification	Energy consumption (kWh/ton) of alloy
Ferrochrome	0.06 % C	18000
	1 % C	10000
	4 - 6 % C	7000
Ferrosilicon	45 % Si	6000
	75 % Si	9000
Ferromanganese	0.5 % C	7000
	1-2 % C	3000
Silico-manganese	65 % Mn	9000
Ferrotitanium	26 % Ti	7500
Ferrovanadium	80 % V	1100

Table 2: Electric power consumption in ferro-alloy production. All the electric power consumption estimates, were taken from Sieveking(1945) except that of ferrovanadium which is typical of a South African producer, with V_2O_3 as feed.

Ferrovanadium can be produced from the trivalent oxide (V_2O_3) by reduction with aluminium in an electric arc furnace, adding iron in the form of scrap, and lime (CaO) to flux the alumina (Al_2O_3) - the byproduct from the reduction reaction.

Typical compositions of the metallic product and the slag are given in Table 3, based on figures for a South African producer. A corresponding mass balance is depicted schematically in Figure 5; the mass balance shows a mismatch of some 140 kg per tonne of ferrovanadium. This is largely the result of the substantial wear of the magnesia refractory lining of the furnace for which data could be obtained; the entire MgO content of the slag (see Table 3) is the result of refractory wear in this furnace.

Table 3: Typical metal and slag compositions (mass persentages).

Metal:

V	Al	Fe	Si
80	2	17	1

Slag:

Al_2O_3	MgO	CaO	V_2O_3
65	11	21	3

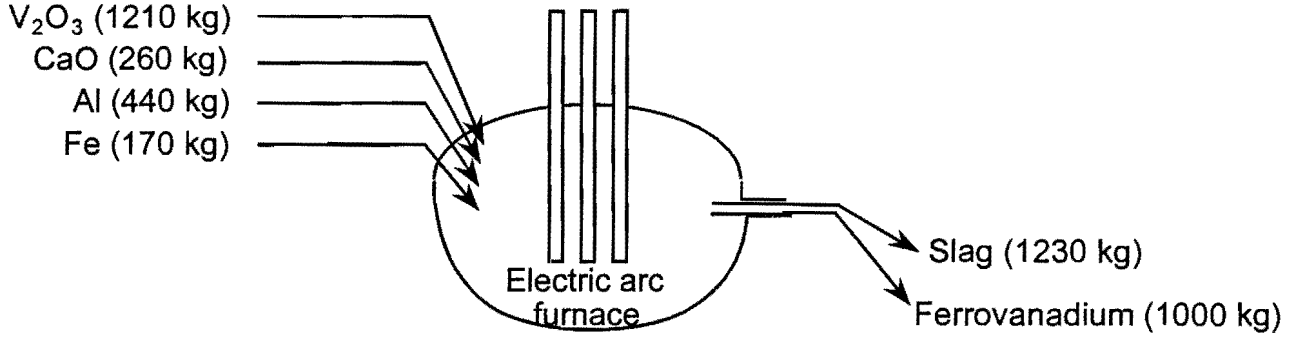

Figure 5. Schematic depiction of a ferrovanadium furnace which uses V_2O_3 as feed, with an approximate mass balance.

Excessive tap temperature can reduce the life of the magnesite refractory lining quite substantially. Recorded tap temperatures as high as 1900 °C are reported from industry. The high temperature necessitates a magnesite refractory lining, although the incompatibility between the Al_2O_3-rich slag and the lining results in excessive wear.

Point E on the line D-G in figure 6 depicts the average industrial slag composition of the South African ferrovanadium producer. If a slag, with average composition E, is brought is contact with the refractory lining, mainly MgO, the average composition of the reacting slag will change along line D-G. At a temperature of 1800°C, the slag would only be saturated with spinel ($MgO.Al_2O_3$) when the average composition reached point F, indicating that the industrial slag is not saturated with MgO.

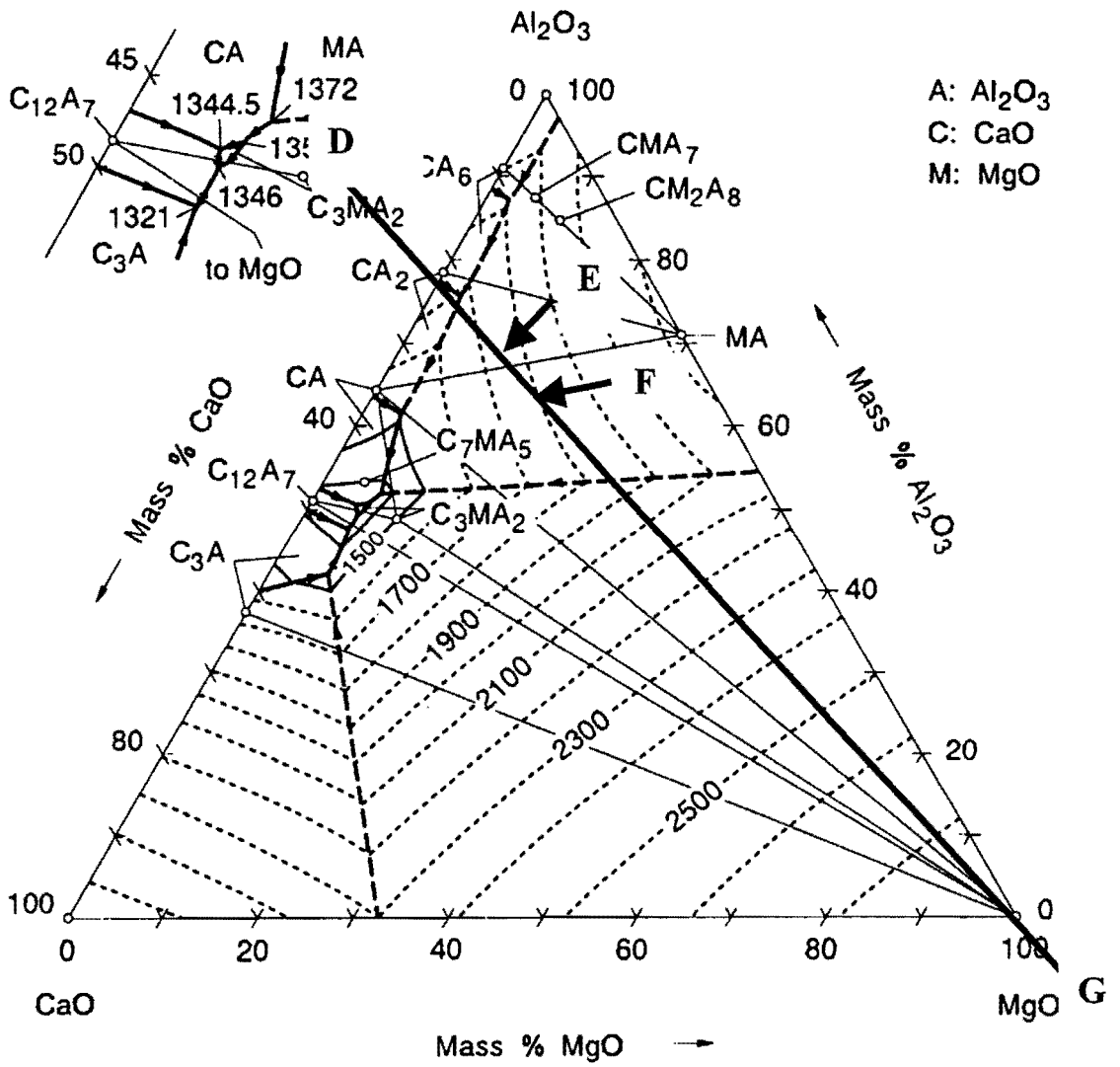

Figure 6: Al_2O_3-CaO-MgO ternary phase diagram, (Verein Deutscher Eisenhüttenleute,1995).

Industry observations indicate that deep furrows, especially around the tap hole, are observed after the completion of each heat. These deep furrows are from time to time patched up with fettling material containing around 90 % MgO. The consumption of the fettling material is on average about 70 – 100 kg per heat and this value gradually increases as more excessive wear occurs at the later stages of the lining life. This fettling practice allows the ferrovanadium producers to attain between 200 and 300 heats on a lining.

Mass balances performed and depicted in figure 5 on the smelting process showed that the high MgO content of the slag has its source from the refractory lining and the fettling

material being used to extend the life of the refractory lining. The MgO content of the slag can, thus, serve as marker of lining wear and should therefore be carefully monitored.

In addition to refractory wear due to the dissolution of the magnesite refractory lining in the Al_2O_3-rich slag, the evaporation of Mg (produced by the reduction of MgO) is possible under the prevailing conditions. The typical tap temperature is around 1800°C and an estimation of the reigning partial oxygen pressure (see section 1.5.1. on activity-composition relations) reveals values $Po_2 \approx 10^{-15}$ atmospheres. Magnesia vaporizes at low oxygen pressures and high temperatures according to the following reaction

$$MgO = Mg(g) + O_2 \qquad (6)$$

The calculated equilibrium partial magnesium vapour pressure (P_{Mg}) is 0.135 atm for a $Po_2 = 1.88 * 10^{-14}$ atm (see Table 10) at 2073K. (This was calculated using correlations of Kubaschewski et al. [1993] for free energy values.) All the fume and dust liberated during the smelting process are withdrawn from the furnace using an external suction fan. The dust is subsequently separated from the smelter exhaust gas using bag filters. The magnesium fumes emitted from the furnace re-oxidize at the colder regions higher up in the furnace during its ascent. The high MgO content of the recycled dust, shown in Table 4, is indicative of magnesium vaporisation.

Component	%
V_2O_5	54.8
CaO	2.7
Al_2O_3	32.6
MgO	8.2
Fe_2O_3	0.9
SiO_2	0.5

Table 4: Chemical composition of recycled bag filter dust of a South African ferrovanadium producer.

The flow sheet of a South African ferrovanadium producer is shown in figure 7.

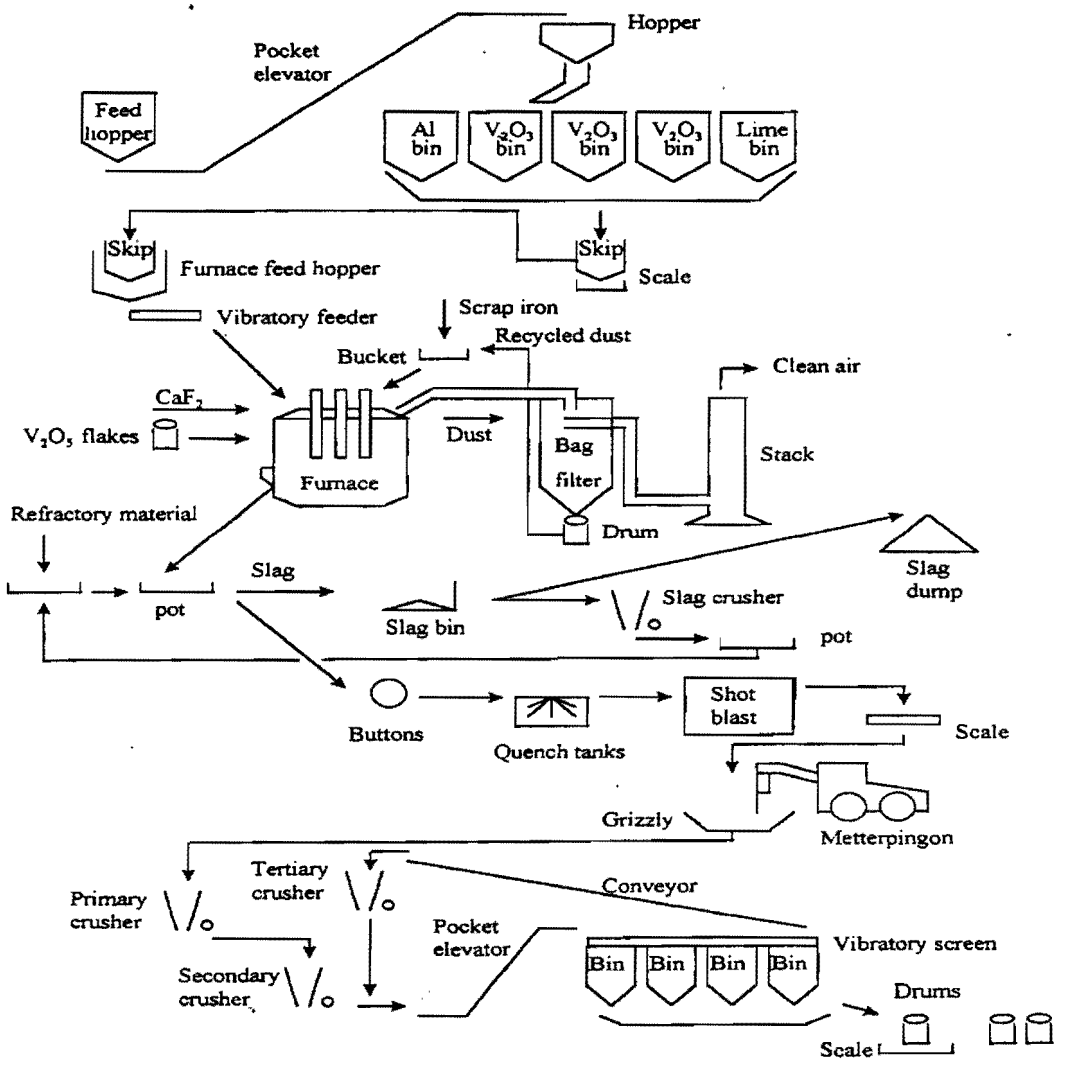

Figure 7: FeV process flow sheet of a South African producer

Fluorite is added just prior to tapping to lower the solidification temperature of the slag. The lower solidification temperature increases time available for separation of the droplets, thus increasing vanadium recovery. During the reduction process vanadium oxide is reduced to vanadium metal which subsequently reacts with molten iron and aluminium to form the metal particles. Not all metal particles, especially not the smaller ones, settle out of the slag while in the liquid state. This results in the entrainment of metal droplets. CaF_2 further enhances refractory wear leading to more vanadium oxide in the slag because MgO increases the alumina activity coefficient (See section 6.2). The time between the addition of the CaF_2 and tapping is kept as short as possible to limit the effect of the CaF_2 on the refractory lining. V_2O_5 flakes (around 230 kg for a heat size of 1100 kg FeV) are added with the raw materials to enrich the metal with vanadium.

1.2.4.4. Factors influencing vanadium recovery in the electro-aluminothermic production of ferrovanadium

The aim of this next section is to identify and evaluate all possible factors influencing vanadium recovery in the electro-aluminothermic production of ferrovanadium. The limited availability of applicable information in some instances hinders the evaluation of the process.

1.2.4.4.1. The loss of vanadium units due to theft

As in case of many valuable commodities, such as copper and nickel, a lucrative trade exists also in ferrovanadium on the black market. The price of ferrovanadium is linked mainly to the steel price and ranges from $7/kg up to $32/kg. Sporadic instances of theft are reported from time to time, but one gets the impression that this is only the tip of the iceberg. Especially the disappearance of small quantities of ferrovanadium on a daily basis will go undetected through the system. This integrated over a certain period will lead to substantial losses. A number of precautionary measures such as high fencing, security and a good and strict practice can be taken to minimize the effect of theft, although the total elimination of such trade is very unlikely. Due to the lack of information available no further discussion of theft as a possible cause of vanadium loss will be given here.

1.2.4.4.2. Loss of vanadium units as oxide spillages during handling and transportation

The fine vanadium oxide powder (consisting mainly of V_2O_3 and small quantities of VO_2) is transported by truck in metal containers (known as kibbles) from the oxide producing plant to the ferrovanadium plant. The kibbles are lifted with a fork lift onto the discharge unit located near the raw material silos. The kibble discharge hatch is subsequently opened releasing the contents into a bucket elevator unit from where the oxide is transported into the silos. An appreciable amount of oxide dust is generated during the discharge stage. The dust escapes from the bucket elevator unit through openings and is

released into the plant. In addition to the health risk posed by the dust, a substantial amount of vanadium is lost during the handling activities such as charging of the furnace. Ways have to be found to eliminate vanadium loss due to dust formation; these may include pelletizing, sintering, briquetting or the installation of a pneumatic conveying unit.

1.2.4.4.3. Loss of vanadium units as reverts

Recyclable ferrovanadium spillages which occur during the tapping process are commonly known as reverts. Some ferrovanadium smelting processes utilize a number of small tapping pots instead of one large pot. This sometimes leads to the phenomenon where metal is tapped onto solidified slag. The first few pots taking mainly the slag constituent from the furnace, are not completely filled. When on subsequent tapping the remainder of the furnace contents, now mostly ferrovanadium metal, is tapped into the remainder of the tapping pots, the capacity is sometimes exceeded. This forces the operator to re-use to the first few tapping pots, now containing solidified slag, to overcome the lack of capacity. As a result, some of the reverts are dumped together with the slag.

The reverts can be recovered by crushing and jigging of the old dump on an annual basis. Most of the misplaced ferrovanadium is now recycled as feed material to the furnace. The loss of ferrovanadium as reverts can be eliminated by utilizing a single slag pot with a capacity which exceeds that of the furnace slag content. In addition to the savings in spillage losses, a large slag pot also promotes the separation of the metal phase from the slag phase during solidification, as indicated in the next session on metal droplet separation.

1.2.4.4.4. Metal droplet entrainment

Preliminary investigations conducted on industrial slag samples show two primary mechanisms of droplet entrainment. Figure 8 and 9 show images of entrained droplets underlining the dual mechanisms leading to droplet entrainment.

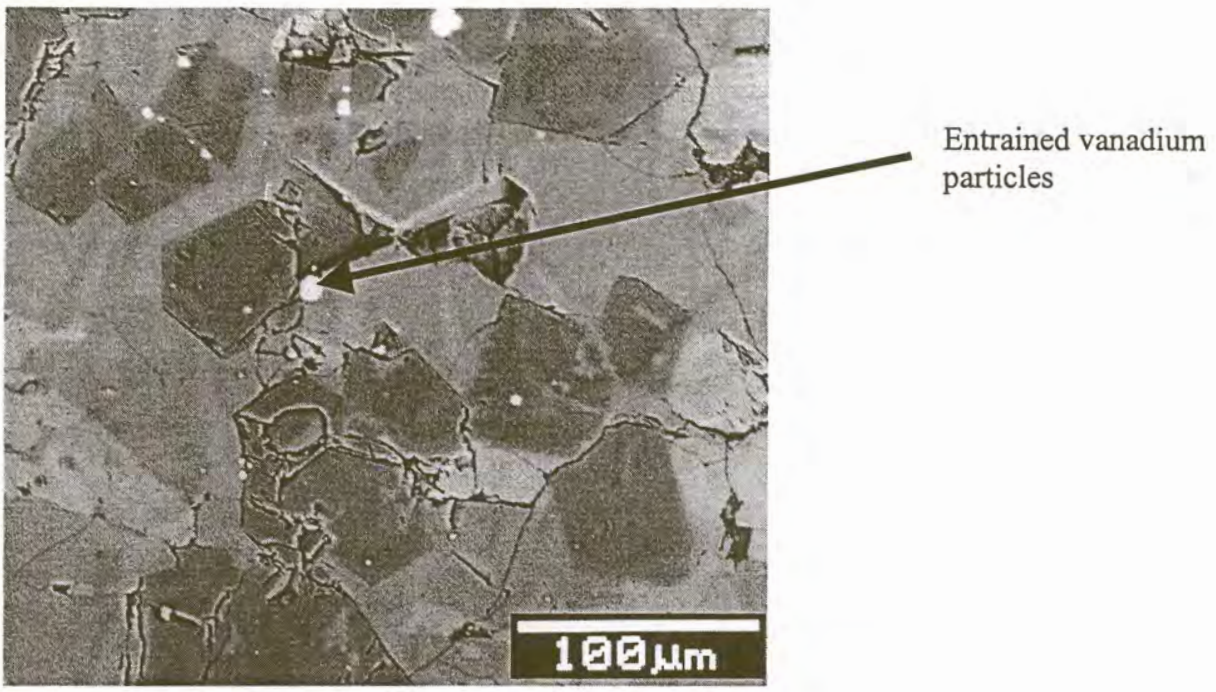

Figure 8: Back scattered electron image of vanadium droplets embedded in industrial slag sample.

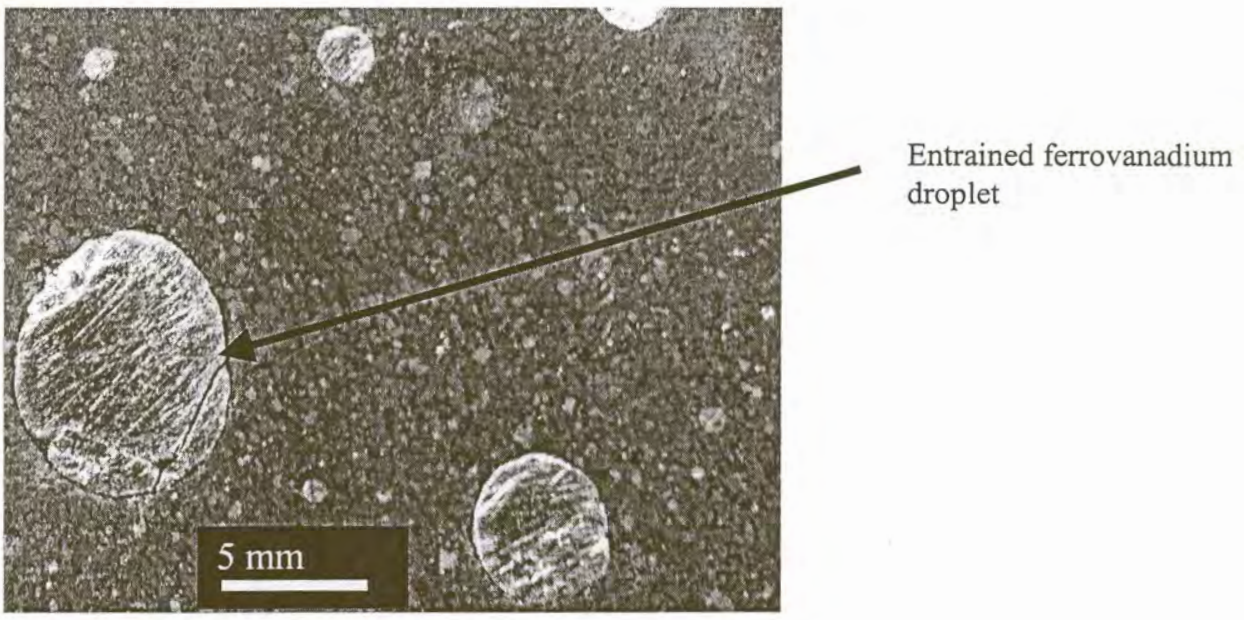

Figure 9: Entrained ferrovanadium droplets in industrial slag sample.

The results of EDS analysis conducted on the entrained droplets, depicted in figure 8 and 9, are showed in Table 5.

	V-droplets	FeV-droplets
% V	72-96	82
% Fe	0-20	15.4
% Al	0-11	1.2

Table 5: EDS-results on entrained droplets showed in figure 8 and 9

The vanadium content of the entrained droplets showed in figure 9 corresponds to the ferrovanadium bulk composition given in Table 5, indicating entrainment as a result of an incorrect tapping procedure. In other words, the entrainment can be a result of a too slow tapping stage by which ferrovanadium is tapped onto "cold" liquid slag. Not enough time is allowed before complete solidification resulting in large entrained metal droplets with a composition similar to that of the bulk metal. A re-evaluation of the tapping practice could eliminate the loss of vanadium as entrained ferrovanadium droplets.

The high vanadium content and small droplet size indicate that the droplets showed in figure 8 are most probably as formed during the reduction process before alloying with iron. Pure vanadium droplets are formed when the vanadium containing oxides are initially reduced by molten aluminium. The metallic droplets now agglomerate and separate from the slag phase under their combined weight. The pure vanadium droplets subsequently form an alloy with the molten scrap iron in the bottom of the furnace. The generally low iron content of the vanadium droplets indicates the lack of intimate contact between the droplets and the molten iron pool. The vanadium recovery will increase with the utilization of larger tapping pots due to the decrease in the cooling rate and the subsequent increase in the metal separation periods, thus, yielding higher metal recoveries. The influence of slag properties on the separation of the solid phase will be discussed in the section on the influence of physicochemical properties of the slag on the separation of the solid phase

1.2.4.4.4.1. Influence of physicochemical properties of the slag on the separation of the solid phase.

Any liquid-solid separation process can be divided into either free or hindered settling conditions. The crowding of particles is negligible in free settling conditions, whilst particle crowding becomes more apparent in hindered-settling conditions. Effectively all the resistance to motion in viscous slag systems is due to the shear forces or viscosity of the fluid. In addition to this, preliminary results show the average entrained droplet diameter to be 0.5 μm for V-particles and 5 mm for FeV-particles. The separation of metal particles or droplets from the slag therefore obeys Stokes' law, which assumes the drag force of spherical particles to be entirely due to viscous resistance, giving the expression.(Wills,1993)

$$D = 3\pi d\eta v \qquad (7)$$

With d = spherical particle diameter(m)
D = drag force (N)
η = slag viscosity (Pa.s)
v = terminal velocity (m/s)

and

$$v = gd^2(\rho_s - \rho_f)/18\eta \qquad (8)$$

with ρ_s = particle density (kg/m^3)
ρ_f = slag density(kg/m^3)

$\rho_s - \rho_f$ is know as the effective density of the particle and is fairly constant when slag and ferrovanadium with constant composition are produced.

Thus, the viscosity of the slag has a large effect on the settling rate of solid particles. The viscosity of the slag is mainly influenced by temperature, slag composition and the presence of solid particles. The relative viscous resistance on small spherical particles is

much larger than on large spherical particles with the same effective density. If the entrained particles are large enough to benefit from a lower slag viscosity, a rise in the tap temperature will reduce droplet entrainment. The beneficial effect of temperature on droplet entrainment may unfortunately be counterbalanced by the increase of soluble vanadium in the slag. The effect of slag composition on the viscosity of the slag will now be addressed.

Al_2O_3-rich Al_2O_3-CaO slags are formed during the manufacture of ferrovanadium. The dissolution of the magnesite refractory lining in the acidic slag has a fluxing effect on the slag. Figure 10 shows the Al_2O_3-CaO-MgO ternary phase diagram. (Verein Deutscher Eisenhüttenleute,1995)

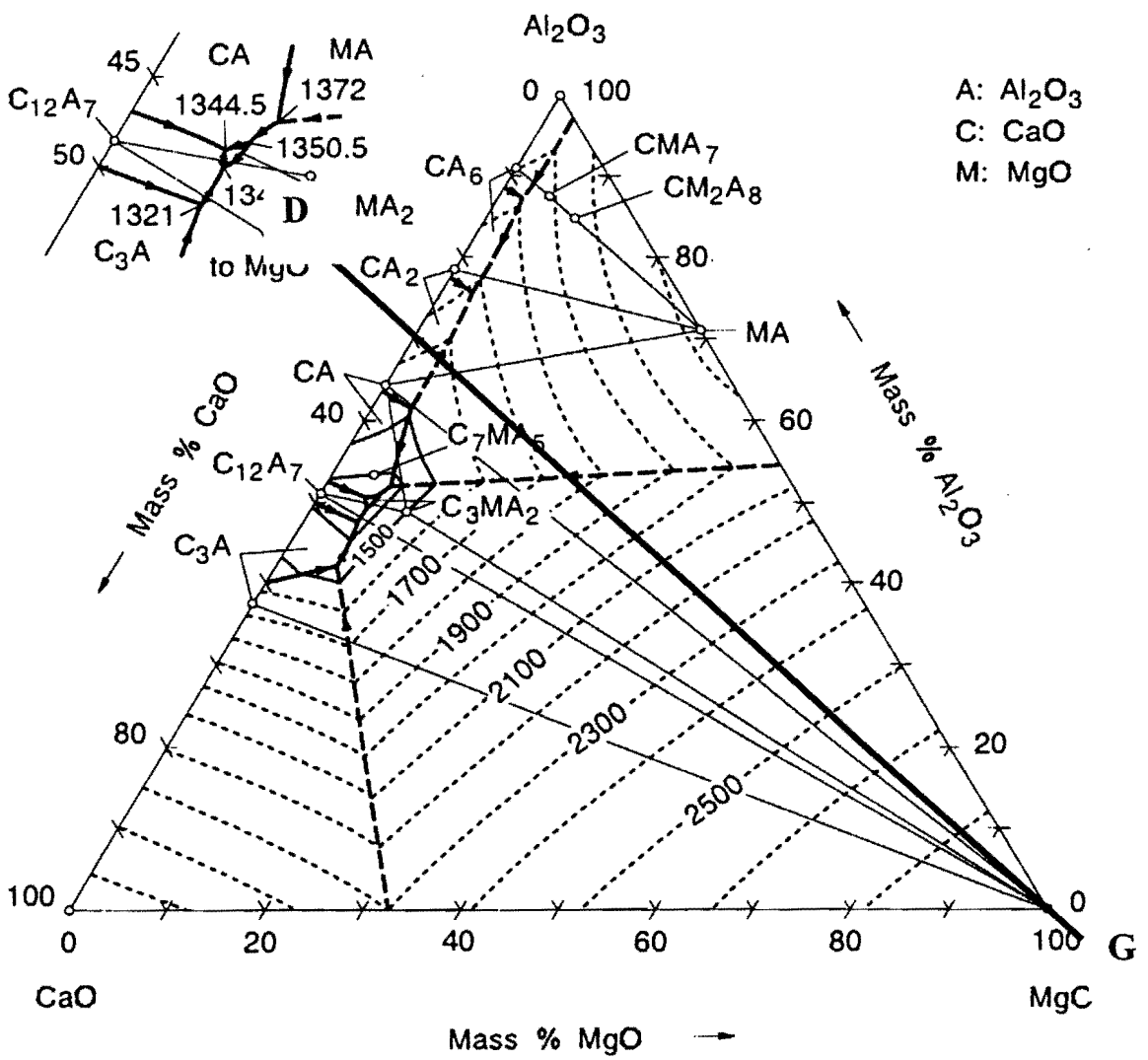

Figure 10: Al_2O_3-CaO-MgO ternary phase diagram (Verein Deutscher Eisenhüttenleute,1995).

If, for example, 70 % Al_2O_3- 30 % CaO slag is brought into contact with MgO from the lining the nominal composition will change alongside the line D-G. A small quantity of MgO (~4 %) will reduce the melting point of the slag from 1650 °C (the melting point of a 70 % Al_2O_3-CaO slag) to ~1580 °C. At the industry-reported maximum of around 10 % MgO, the liquidus temperature again reaches 1650°C. Upon further dissolution of MgO the melting point will increase and presumably so too the viscosity of the slag (at a given temperature).

The longer the slag is in the liquid state and the lower its viscosity when molten the more complete will be the separation of metal and slag. The effect of CaO and MgO fluxing additions on the viscosity of high-alumina slags can be seen in figure 11 (Arkhipov,1965). Their study focused on factors effecting the more complete separation of the metal and slag phases. Physicochemical properties such as slag viscosity, composition, surface tension, interfacial tension and liquidus range of around 100 laboratory heats were studied. Three distinct slags were used to illustrate the influence of fluxing additions on the metal droplet separability. The composition of the three slags used is shown in Table 6.

	SiO_2	Al_2O_3	CaO	TiO_2	MgO
Slag 1	0.07	86.9	2.2	0.35	1.41
Slag 2	0.11	84.5	6.6	0.37	0.98
Slag 3	0.22	80.2	6.4	0.32	4.73

Table 6: Composition (mass percentages) of the three slags used to illustrate the effect of fluxing additions on droplet entrainment(Arkhipov,1965). Despite the chemical compositions not adding up to 100%, it can still be assumed that three slags with distinct alumina contents were employed.

Nothing is mentioned about the nature of the laboratory experiments conducted to give rise to the results shown in figure 11. A nominal vanadium content of 85 % in the ferrovanadium was aimed for. Figure 11 depicts the results as obtained from the three slag samples.

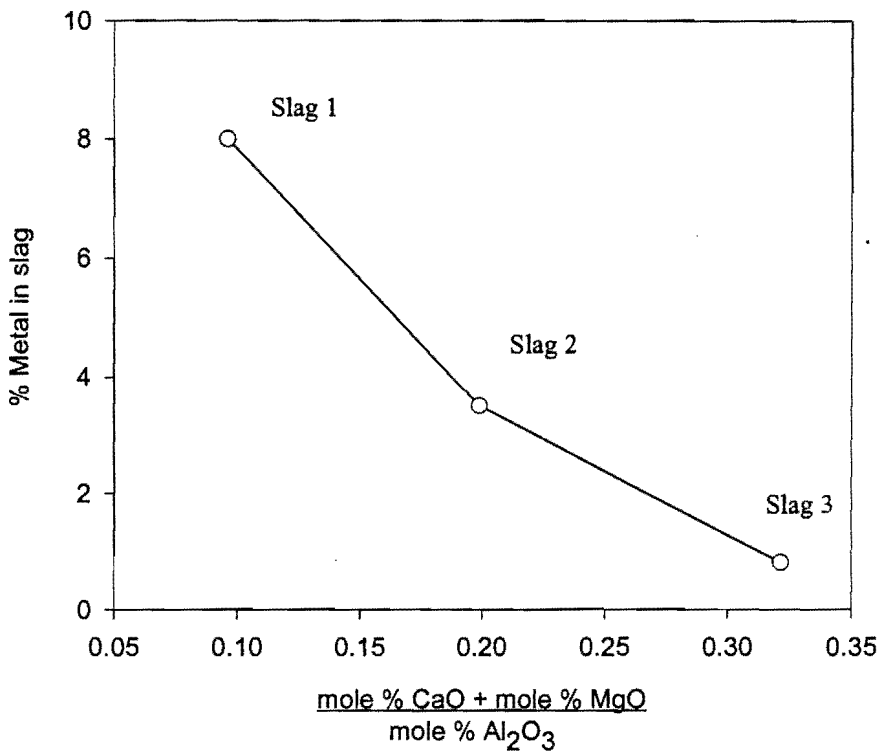

Figure 11: Metal droplet entrainment (expressed as percentage metal in the slag) as a function of slag basicity (after Arkhipov, 1965).

The Al_2O_3 content of the slag of the South African ferrovanadium producer is considerably lower, see Table 3, than the tabulated values reported by the authors. The results depicted in figure 11, show that a slight alteration in the chemical composition of the slag formed in the aluminothermic production of ferrovanadium has a considerable effect on the separation of the liquid phases, at low basicity.

In order to attain a better understanding in the causes behind the more complete separation of the liquid phases, viscosity measurements can be carried out on synthetic slags. Viscosity investigations were carried out by Arkhipov et al (1965) on slags produced in the production of ferrovanadium. Table 6 show the composition of the high-alumina slags used in these investigations. The viscosity measurements were carried out in a vertical resistance tube furnace using a carbon reduction tube in which temperatures around 2100°C were reported. The temperature within the furnace was measured by

means of a tungsten-molybdenum thermocouple, and the viscosity of the slag was determined by means of a vibration viscosimeter. The influence of the fluxing additions CaO and MgO on the viscosity on high-alumina slags is depicted in figure 12.

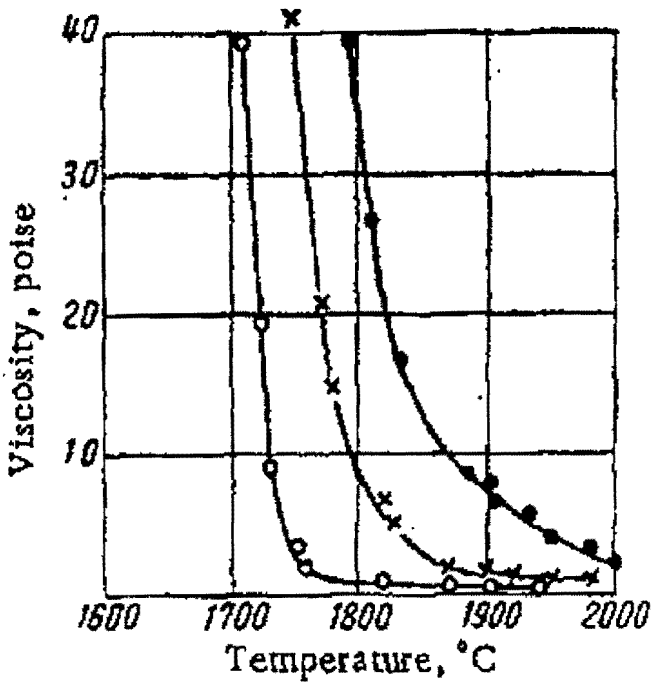

Figure 12: Viscosity curves of high-alumina slags (• Slag1, × Slag2, o Slag3) (Arkhipov,1965)

It is evident from the curve that slag 3 provides the best conditions of droplet separation in the temperature range of 1750 °C – 2000 °C. Slags which give optimum vanadium recovery must have a minimum viscosity prior to solidification as well as an optimum composition to ensure minimum soluble vanadium loss. The term soluble vanadium loss refers to oxidic vanadium in the slag. If, for example, the alteration of the slag composition by adding fluxing agents, is not beneficial to vanadium recovery with respect to soluble vanadium loss, then the separation of the liquid phases can be optimized by tapping at a slightly higher temperature and utilizing a larger melt volume. The smaller the volume of the melt the more rapid the heat transfer to the surrounding environments. Figure 13 shows cooling curves of a range of slag compositions as well as that of an alloy containing 85 % vanadium and 8.2% iron. The composition of each slag used is given in

Table 6 and the cooling curve of each slag is numbered accordingly. Cooling curve four refers to the cooling curve of the alloy.

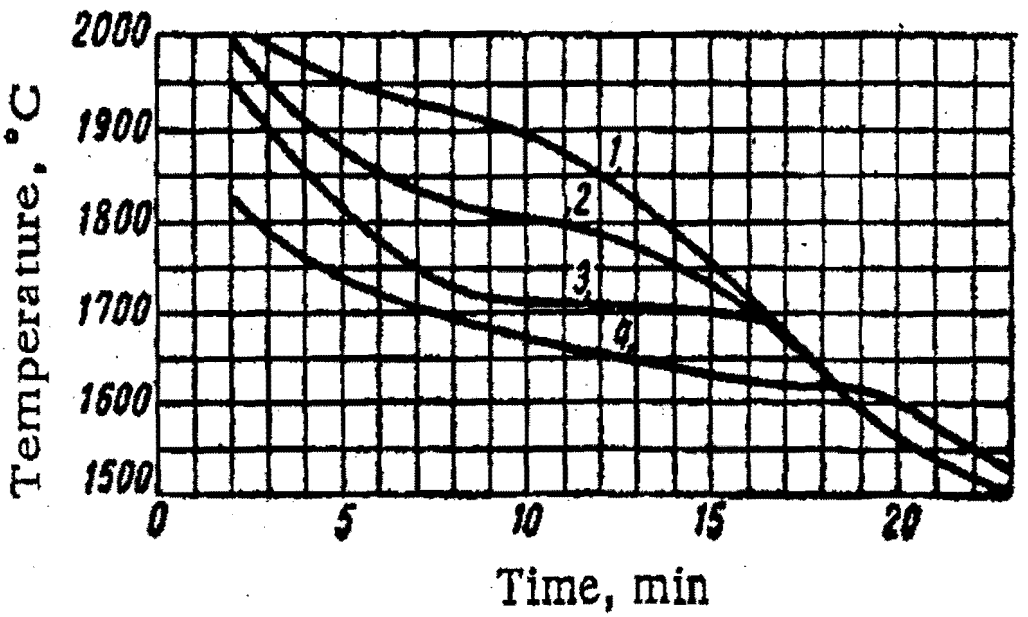

Figure 13: Cooling curves of slags after termination of smelting process (Arkhipov,1965). 1) Slag 1; 2) Slag 2; 3) Slag3; 4)Alloy, containing 85% vanadium and 8.2% iron.

Figure 11 shows that slag 3 has the lowest melting point and it remains in the liquid state longer thus representing the most favorable conditions for separation.

In addition to slag composition and temperature, solid particles in the slag also have an influence on the viscosity of liquid slag. The effect of solid particles on the viscosity behavior of slag was studied by Reddy et al (1993). The existence of solid particles result in significant increase in the slag viscosity as shown in figure 14.

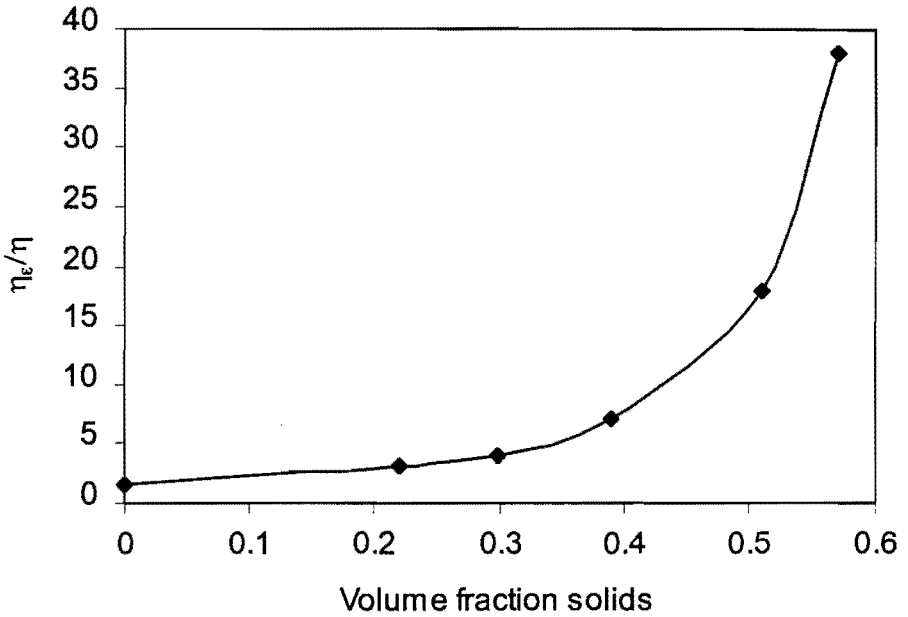

Figure 14: Influence of the solid content of the melt on the ratio of apparent viscosity to that of the pure liquid.(Reddy,1993)

When the volume fraction of solid particles increases to 0.57 the effective viscosity increases almost to 38 times the viscosity of the pure liquid. The melting point of the ferrovanadium droplets is higher than the liquidus temperature of the slag (See figure 17 for a 80 % V alloy. The binary Fe-Al and Al-V phase diagrams [Baker,1992] show the small effect of small amounts of aluminium on the melting points of these alloys. It may be assumed that small amounts of Al have a similar effect on the melting point of ferrovanadium), resulting in the formation of solid particles while the slag is still in the liquid state. It is debatable whether the entrained droplets in the ferrovanadium slag will have this appreciable effect on the viscosity due to the comparatively low concentration of droplets in the slag. Arkhipov and co-workers (1965) reported values between 0.8 and 8 % of metal produced end up in the slag. (This works out to be around 3 volume % particles in the slag, assuming 1000 kg metal and 1400 kg slag produced, with the slag containing 8 % of total mass of alloy produced. Metal and slag densities were taken to be 5800 kg/m^3 and 2600 kg/m^3 respectively.)

With regard to the viscosity, the slag with the lowest melting point and the fewest droplets should be used to maximize metal droplet separation. This does not, of course, mean that vanadium recovery in total will also benefit because the effects of viscosity, temperature

and slag basicity in vanadium recovery are interwoven. The aim of this study is to address this issue in order to optimize vanadium recovery.

1.2.4.4.5. Vanadium loss due to unreduced oxides in the high alumina slag

One way to decrease the amount of unreduced oxides in the slag is to add excess aluminium as reducing agent to the feed material. A certain amount of aluminium reductant ends up in the product as an impurity since aluminium readily alloys with many metals and alloys. In addition to aluminium loss to side reactions and atmospheric oxidation, some aluminium is vaporized at the tip of the electrodes.

International consumer specification on the residual aluminium content of ferrovanadium limits the use of too much excess aluminium. Optimum vanadium content of the slag should be aimed for while still meeting international consumer specifications. One way to accomplish high vanadium yields without adding too much excess aluminium is to manipulate factors influencing the vanadium activity coefficient in the slag. The overall oxidation reaction can be expressed as

$$2(V)_{FeV} + (Al_2O_3)_{slag} = 2(Al)_{FeV} + (V_2O_3)_{slag} \qquad (9)$$

The experimental work(reported later in this thesis) determined the oxidation state of oxidic vanadium, but for illustrative purposes the oxidation state vanadium is here taken as V^{3+}. The equilibrium activity of vanadium oxide in the slag is given by

$$a_{V_2O_3} = K\frac{a_V^{\,2}\, a_{Al_2O_3}}{a_{Al}^{\,2}} \qquad (10)$$

with

a_x = activity of species x

K = equilibrium constant

The activity coefficient of vanadium oxide is likely to be strongly influenced by the slag basicity, thus strongly influencing the vanadium distribution between the metal and the slag. By optimizing the activity coefficient through the careful adjustment of the slag basicity the tendency of oxide formation can be greatly reduced. The effect of slag basicity on the vanadium content of the slag is depicted in figure 4. The same strong effect is also expected to hold for the electro-aluminothermic reduction.

In practice the adjustment of the slag basicity by adding large quantities of fluxing agents is limited by the furnace dimensions, power rating and whether the large slag volumes will prevent the electrodes from arcing. Nevertheless, a strong vanadium-content composition relation as depicted in figure 4 indicates that only small adjustments in slag composition are necessary to increase recoveries.

1.3. Thermodynamic properties

1.3.1. Systems similar to vanadium system

There is not much literature available on the influence of slag basicity on the vanadium oxide activity in the Al_2O_3-CaO-MgO systems. It is known that species with the same ionic radii and oxidation state will behave similarly in liquid slags. Table 7 below shows corresponding ionic radii for the same oxidation state of a few different species.

Species	Ionic radius (nm)	Species	Ionic radius (nm)	Species	Ionic radius (nm)
V^{2+}	0,88	Ti^{2+}	0,94	Cr^{2+}	0,89
V^{3+}	0,74	Ti^{3+}	0,76	Cr^{3+}	0,63
V^{4+}	0,63	Ti^{4+}	0,68	Cr^{6+}	0,52
V^{5+}	0,59				

Table 7: Ionic radii of a few oxidized species.(Weast,1982)

It is evident that V^{2+} and Cr^{2+}, Ti^{3+} and V^{3+} are expected to behave similarly in liquid slag systems. Figure 15 below shows the effect of slag basicity on the partitioning of chromium between the Cr^{2+} and Cr^{3+} oxidation states.

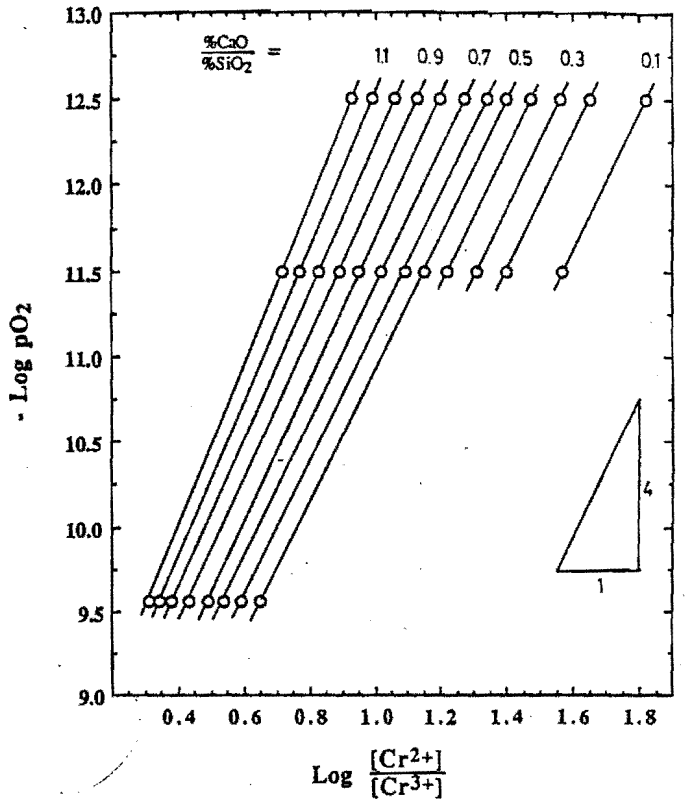

Figure 15: Effect of slag basicity on the partitioning of chromium between the oxidation states (Pretorius,1989).

The figure indicates Cr^{2+} to be more stable at low oxygen partial pressures and low basicities. According to this V^{2+} is expected to be the prominent oxidation state where conditions of low oxygen pressure and low basicities prevail in silica melts. The interactions between species in liquid melts are usually non-ideal and highly species dependent. Because of this it cannot be said that V^{2+} will be the more stable oxidation state in Al_2O_3-CaO melts where conditions of low partial oxygen pressure and low basicities prevail.

1.3.2. Estimation of the reigning partial oxygen pressures in the industrial FeV-production process.

The oxidation equilibrium of vanadium at fixed partial pressures in the industrial FeV-production process can be either reaction (13) or (14)

$$V + 0.5O_2 \rightarrow VO \quad (13)$$

$$2V + 1.5O_2 \rightarrow VO_{1.5} \quad (14)$$

The oxygen partial pressure in industrial smelting processes is governed by those reactions which remain closest to equilibrium. In the vanadium smelting process where Al is used as a reductant the Po_2 partial pressure is most probably governed by reaction (15)

$$2Al + 1.5O_2 \rightarrow Al_2O_3 \quad (15)$$

The overall reactions can thus be expressed as

$$V + Al_2O_3 \rightarrow Al + VO \quad (16)$$

$$V + Al_2O_3 \rightarrow Al + V_2O_3 \quad (17)$$

The reigning partial oxygen pressure in the vanadium smelting process can be calculated as follows

$$P_{O_2} = \left(\frac{a_{Al_2O_3}}{a^2_{Al}\, e^{-\frac{\Delta G^0}{RT}}} \right)^{\frac{2}{3}} \quad (18)$$

The assumption is that reaction 15 is at equilibrium. As indicated by equation 18, the Al_2O_3 and Al activities govern the oxygen partial pressure. Figure 16 shows the activity of Al_2O_3 in binary $CaO\text{-}Al_2O_3$ slags a function of slag composition and temperature.

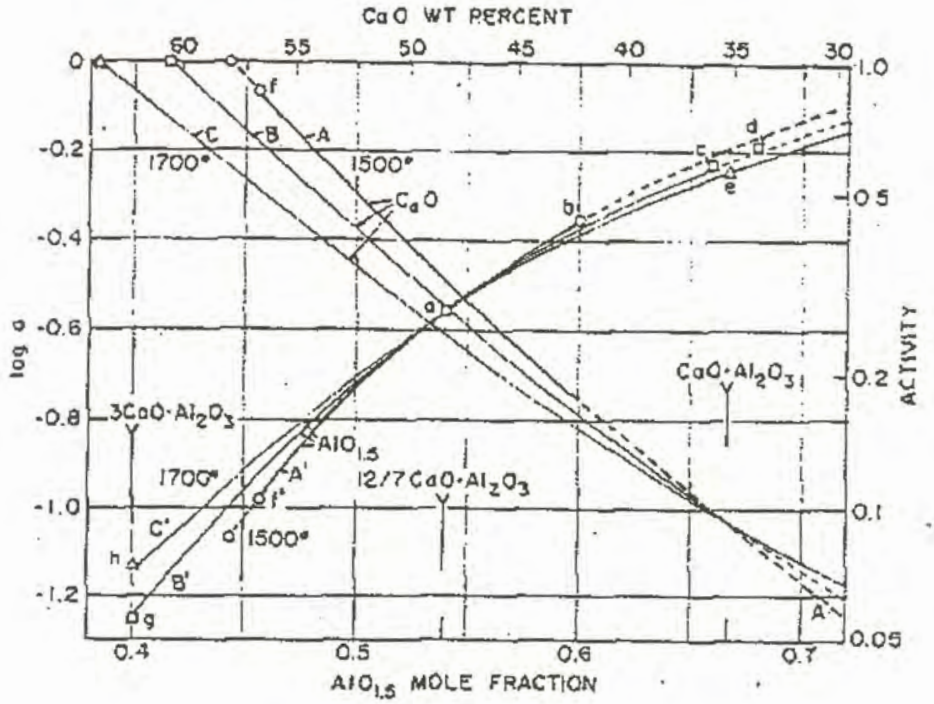

Figure 16: Al_2O_3-activity as a function of temperature and slag composition.(Rein & Chipman,1965).

Unfortunately Al_2O_3 – activity values are given in figure 16 only for melts containing a minimum of 30 % CaO (industrial slags contain 23 % CaO and 9 % MgO). The activity of Al_2O_3 in 30 % CaO-Al_2O_3 melts was hence be used for further calculations in this section.

All forms of vanadium dissolve completely and evenly in liquid steel and do not give rise to segregation nor do they form gross inclusions. The complete liquid and solid (at high temperature) solubility of vanadium and iron is depicted by the vanadium-iron phase diagram in figure 17.

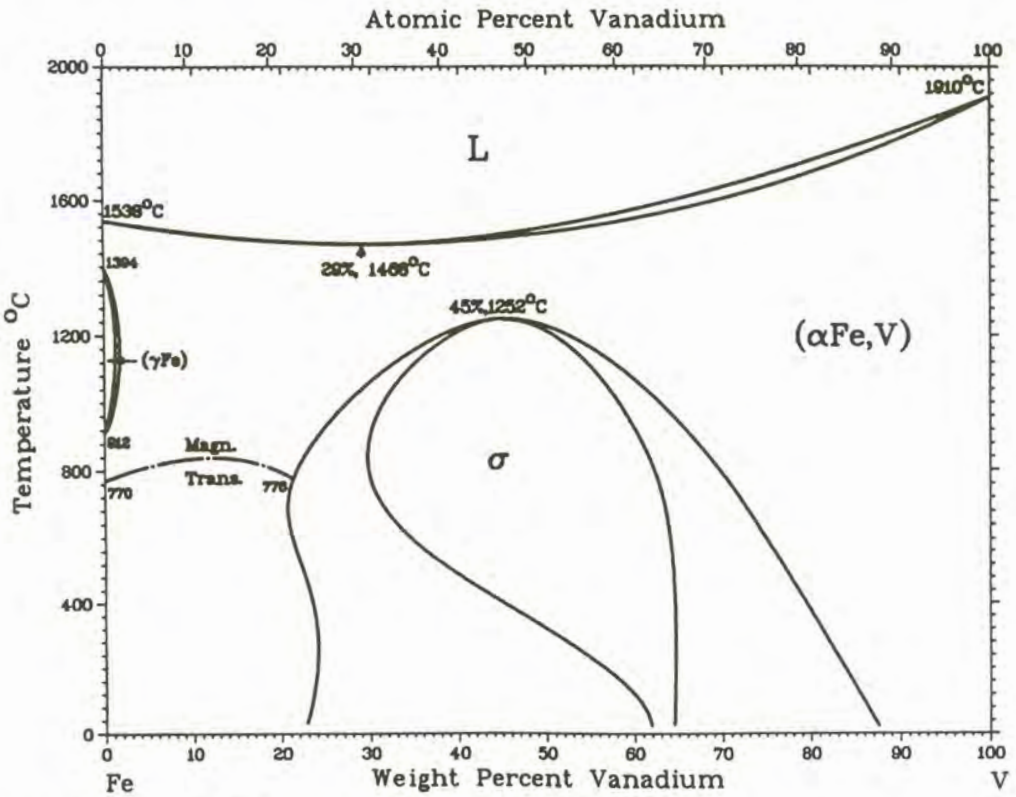

Figure 17: Binary V-Fe phase diagram. (Baker(ed))

The activity coefficient of dilute aluminium in ferrovanadium can be estimated by assuming it to be similar to that in binary Fe-Al alloys (because of the nearly ideal behavior between iron and vanadium).

Consider the following reaction for liquid iron

$$Al(l) \rightarrow Al\,(l)_{1\%} \tag{19}$$

According to Sigworth & Elliott (1974) the free energy change can be calculated

$$\Delta Gs = RT \ln\left(\gamma^{\infty}_{Al}\frac{0.5585}{M_i}\right) \tag{20}$$

With Fe as solvent and M_i = molar mass of aluminium, and γ^{∞}_{Al} the Raoultian activity coefficient for Al in a highly dilute solution. ΔGs for reaction (14) expressed as a function of temperature is as follows (Sigworth & Elliott,1974)

$$\Delta Gs = (-3609 - 1.594T) * (4.184)^2 \text{ (J/g-atom)} \tag{21}$$

The Henrian activity is simply proportional to the Raultian activity as follows

$$a_i = h_i C_i \tag{22}$$

Where the value of C_{Al} for Aluminium dissolved in liquid iron is given by:

$$C_{Al} = \frac{M_{Al}}{0.5585\gamma^{\infty}_{Al}} \tag{23}$$

and

$$h_{Al} = f_{Al}(\%\ Al) \tag{24}$$

$$\text{with } \log f_{Al} = \sum e^{j}_{Al}(\%j) + \sum r^{j}_{Al}(\%j)^2 \tag{25}$$

Where e^{j}_{Al} and r^{j}_{Al} are the first and second order interaction coefficients of species j with Al.

The following average metal composition is assumed for the sake of the calculation.

	Mass %	N_i(mole fraction)
C	0,6	0,02
Al	2	0,04
Si	0,8	0,14
Fe	14,2	0,126
V	82,4	0,8

Table 8: Average metal analysis.

The activity of Al in FeV as estimated using the metal composition given in Table 8 is shown in Table 9.

Temp(K)	Gamma Al	Ci	f_0	a_{Al}
1873	0.0291	0.0006	1.3908	0.0017
1898	0.0307	0.0006	1.3908	0.0018
1923	0.0324	0.0007	1.3908	0.0019
1948	0.0340	0.0007	1.3908	0.0020
1973	0.0358	0.0007	1.3908	0.0021
1998	0.0375	0.0008	1.3908	0.0022
2023	0.0393	0.0008	1.3908	0.0023
2048	0.0412	0.0009	1.3908	0.0024
2073	0.0431	0.0009	1.3908	0.0025
2098	0.0450	0.0009	1.3908	0.0026
2123	0.0470	0.0010	1.3908	0.0027
2148	0.0490	0.0010	1.3908	0.0028
2173	0.0510	0.0011	1.3908	0.0029
2198	0.0531	0.0011	1.3908	0.0031
2223	0.0552	0.0011	1.3908	0.0032
2248	0.0573	0.0012	1.3908	0.0033
2273	0.0595	0.0012	1.3908	0.0034

Table 9: Estimated Al-activity as function of temperature for FeV containing 2 mass % Al.

The calculated partial oxygen pressures, assumed to be fixed by Al/Al_2O_3 and $VO/VO_{1.5}$-equilibrium, are given in Figure 8.

These were calculated using correlations of Kubaschewski et al. (1993) for free energy values.

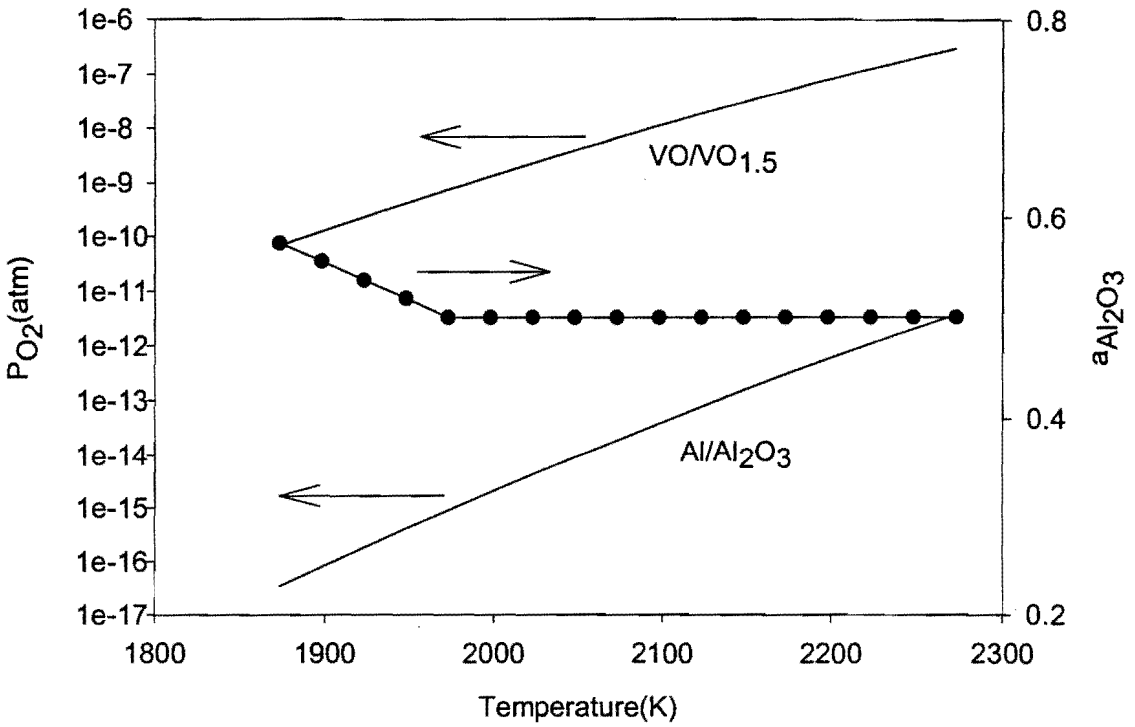

Figure 18: Comparative oxygen activities as function of temperature for the Al/Al_2O_3 and $VO/VO_{1.5}$- equilibrium. The dotted line gives the data on the activity of Al_2O_3 in 30 % $CaO\text{-}Al_2O_3$ slags. Unfortunately the literature data are given only for the 1600-1650 °C temperature range. The activity of Al_2O_3 above this range was assumed to be constant due to the lack of more accurate relations. Unit activities of VO and $VO_{1.5}$ were assumed.

Figure 18 depicts the calculated oxygen activity for the two different equilibria in the industrial ferrovanadium reduction process. This figure further indicates that V^{2+} will be the stable oxidation state if the oxygen activity is governed by the Al/Al_2O_3-equilibrium and $\gamma_{VO} \approx \gamma_{VO1.5}$. The oxidation state of vanadium in the slag clearly needs to be clarified by performing high-temperature equilibrium experiments.

These approximate oxygen activities serve to indicate the range of the oxygen activities to be used for experimental purposes in order to simulate conditions in the industrial smelting process.

1.4. Research problem and objectives

During the submerged-arc smelting process, vanadium oxide is reduced with aluminum to form ferrovanadium and Al_2O_3-CaO-MgO-slag. In addition to vanadium lost as unreduced oxides in the slag, vanadium yield is also decreased by entrained droplets, which remain in the slag after solidification. The high-alumina slag is fluxed with CaO and MgO. The entire MgO content of the slag is the result of refractory wear. A strong effect on vanadium activity of the Al_2O_3 content of the slag is expected. Adding fluxing agents in moderate quantities should minimize the detrimental effect of droplet entrainment. The South African ferrovanadium producers operate the smelting process at considerably lower Al_2O_3-values compared to aluminothermic processes, which is not necessary beneficial to vanadium recovery. The aim of this work is to quantify the effect of slag composition on the equilibrium vanadium oxide content, and on the entrainment of droplets in the slag. Knowing these relations, certain adjustments can be made to optimize vanadium recovery in the electro-aluminothermic process.

The experimental work aimed to determine the following:

- To determine the activity coefficient of VO_x as a function of the slag composition. The experiments involve fixing the oxygen activity, to a level which corresponds to the oxygen activity in the industrial smelting process, by using an appropriate gas mixture

- To determine the activity coefficient of VO_x as a function of temperature.

- To determine the oxidation state of vanadium in the slag.

- To quantify the losses of vanadium as entrained droplets as a function of slag composition.

- To quantify the total vanadium loss as a function of slag composition.

The aim of the next section is to survey different experimental techniques and procedures necessary to generate the appropriate results.

1.5. Investigation into experimental techniques and procedures

1.5.1. Evaluation of different gas mixing systems

The most versatile method used to obtain desired oxygen fugacities at high temperature is the use of two gases, which react with each other at high temperatures to release or consume oxygen. This buffering action serves to maintain the oxygen activity at a constant value.

In other words equilibrium is restored by the dissociation of the gas phase by the following reactions (as examples).

$$2H_2O = 2H_2 + O_2 \quad (26)$$

$$2CO_2 = 2CO + O_2 \quad (27)$$

In these two-gas systems the oxygen pressures are a function of temperature as well as the gas composition. The two most widely used two-gas systems are the CO_2-CO and the CO_2-H_2 systems. The complexity of the gas systems is reduced because the gas species are bought in separate cylinders ready for mixing to their specified volumetric proportions. However, at high experimental temperatures and low partial oxygen pressures, C tends to precipitate according to the following reactions.

$$2CO(g) = CO_2(g) + C(s) \quad (28)$$

or

$$CO_2 = C + O_2 \quad (29)$$

The applicability of the CO/CO_2 gas mixtures at low partial oxygen pressures is therefore limited. Working at very low oxygen partial pressures, and high temperature also limits the use of the H_2-CO_2 system because very low CO_2 flow rates are required. (for example: Volume % $CO_2 \approx 0{,}01$ at 2000 °C and $Po_2 = 1*10^{-14}$ atmosphere (Janaf table,1965).

Rotameters to control the exact volumetric flow rates of the gas species are not sensitive enough for such low flow rates, thus limiting the application range of the H_2/CO_2 gas mixtures as well.

Since oxygen partial pressures, in the range of 10^{-12}-10^{-17}, require CO/CO_2 and H_2/CO_2 ratios outside the limits of the gas mixing system, one should revert to H_2/H_2O gas mixtures as last alternative.

Table 10 gives the required water vapor partial pressure in hydrogen if the oxygen fugacity in the industrial smelting process is governed by the Al/Al_2O_3-reaction. According to Belton (1998) the lowest water/hydrogen ratio which have been used successfully was 0.002. The problem with lower ratios is that the equilibrium can only be approached practically from one direction because of the low oxygen capacity of the gas mixture. One should keep in mind that the approximations of the oxygen activity governed by the Al/Al_2O_3-equilibrium is based on the assumption that Al in ferrovanadium behaves like aluminium in dilute iron alloys. Performing an equilibrium run at the ultra-low water/hydrogen ratios at a corresponding industrial slag basicity, to see if the same vanadium content can be obtained can test the validity of this assumption. If not, the water/hydrogen ratio can be adjusted accordingly.

Although very low oxygen partial pressures can be attained certain complexities are introduced, specially referring to the gas mixing apparatus. With H_2-H_20 mixtures, hydrogen is saturated with water vapour by passing it through distilled H_20 or any other liquid substance with a well-known water partial pressure (as function of temperature). The vapour pressure of the water is only temperature dependent while the total gas flow is also pressure (total pressure above solution surface) dependent, resulting in a complex system. The gas mixing apparatus will be discussed in more detail in the next section.

Temp	ΔG°_{rxn}	Po_2	PH_2/PH_2O	PH_2O
1873	285811.8	3.36E-17	17827.2	5.609E-05
1898	282902.0	7.91E-17	14386.5	6.950E-05
1923	279990.7	1.82E-16	11684.6	8.558E-05
1948	277077.9	4.08E-16	9548.4	1.047E-04
1973	274163.9	8.94E-16	7850.1	1.274E-04
1998	271248.7	1.97E-15	6410.0	1.560E-04
2023	268332.4	4.26E-15	5261.1	1.900E-04
2048	265415.1	9.02E-15	4339.6	2.304E-04
2073	262496.9	1.88E-14	3596.6	2.780E-04
2098	259577.9	3.84E-14	2994.5	3.338E-04
2123	256658.1	7.72E-14	2504.3	3.992E-04
2148	253737.7	1.53E-13	2103.3	4.752E-04
2173	250816.8	2.97E-13	1773.9	5.634E-04
2198	247895.3	5.69E-13	1501.9	6.654E-04
2223	244973.5	1.08E-12	1276.6	7.827E-04
2248	242051.3	2E-12	1089.1	9.173E-04
2273	239128.9	3.67E-12	932.5	1.071E-03

Table 10: Required partial water pressure as a function of temperature, for Po_2 governed by the Al/Al_2O_3-reaction .

1.5.2. Experimental evaporation technique and procedure

Evaporation techniques involve a pure gas being passed over or through a liquid to produce a mixture between the gas and vapour from the liquid.

Gas entering the dispersion bottles shown in figure 19 is dispersed into bubbles, which rise in close contact with the liquid to the surface.

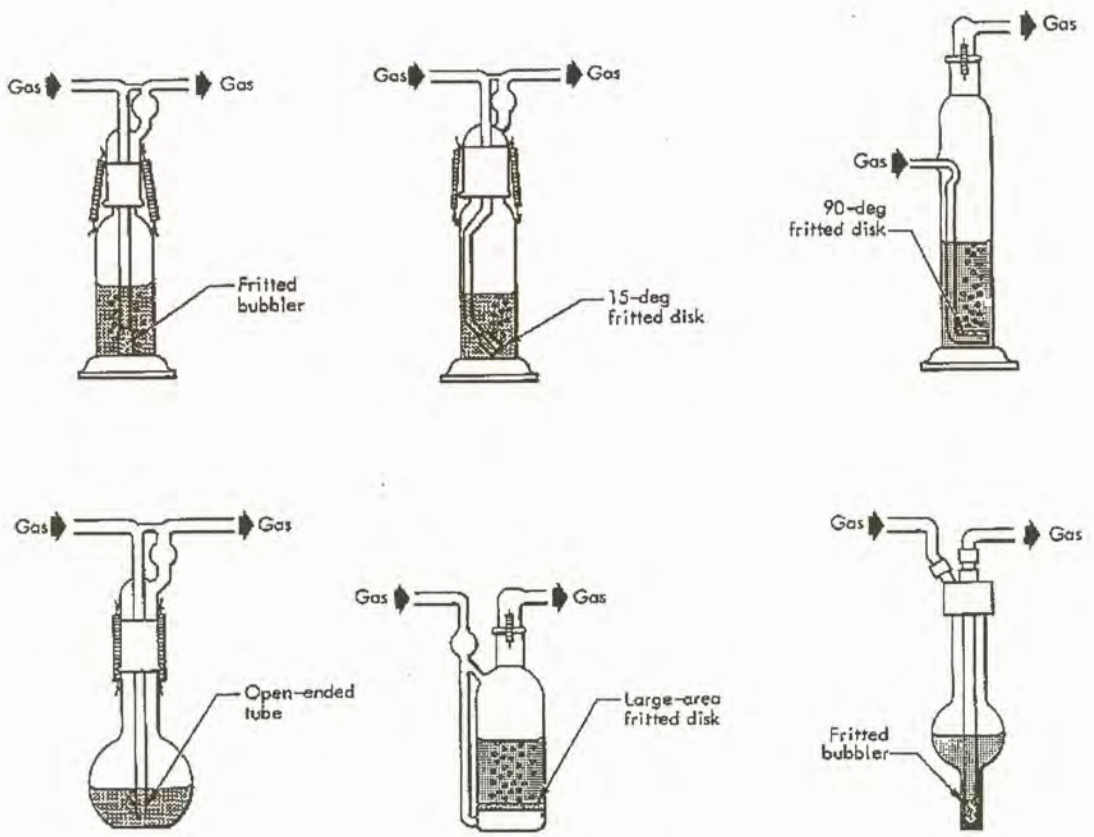

Figure 19: Sketches of six typical gas dispersion bottles.(Nelson,1992)

The smaller the bubbles the larger the cumulative surface area, and the better the efficiency of evaporation. The degree of evaporation is a function of the bubble size, rate of ascent, temperature of liquid, the retention time, total pressure on system, vapour pressure and viscosity.

Checks on the exit gas composition are absolutely essential due to the complexities being introduced by the H_2O-H_2 mixtures. Analysis may be accomplished by mass spectrometry, dew point determination, or by the weighing the water and measuring the volume hydrogen per unit time. The flow meters must be calibrated in-line to determine the exact volume of gas passing through in a measured time. Nagasaka et al.(1994) used a Drierite-filled column to check the weight gain in every experimental run for measured water vapor pressures reigning from 0.002 to 0.3 atmosphere. The calculated water vapour pressure, if the oxygen activity is fixed by the Al/Al_2O_3-reaction, is much lower than the values reported by Nagasaka et al(1994), thus needing long adsorption times to yield measurable quantities of water.

Very low oxygen pressures, as in this study, can be obtained with the following dynamic methods:

- Saturation of hydrogen with water vapour by passing it over or through an ice bed
- By passing hydrogen through a saturated salt solution e.g.. Lithium chloride solution. (Chipman,1953)
- The amount of water vapour can be fixed by contacting the hydrogen gas with a sulphuric acid solution at a controlled temperature.
- Using the oxalic acid dihydrate/ oxalic acid equilibrium (Belton,1998)

The application of ice is limited by very slow kinetics and very intimate contact between the ice and the hydrogen gas must be obtained. A further drawback is difficulty in controlling and measuring the ice temperature to maintain a constant gas composition throughout an experimental run.

According to Belton(1998) early workers very precisely established the water vapor pressure of oxalic acid dihydrate / oxalic acid mixtures, and obtained

$$\text{Log P (mm Hg)} = 18.053 - 9661/(T + 250) \qquad (30)$$

With

T = Temperature (K)

At a temperature of 273K water/hydrogen ratios as low as 0.0005 can be conveniently obtained, using the oxalic acid dihydrate / oxalic acid equilibrium.

The application of sulphuric acid as solvent enables better temperature control by immersion of the contactors in a well stirred bath, but the constant removal of water from the sulphuric acid leads to the alteration of gas composition with time. The time dependence can be estimated by means of dynamic mass balance calculations

The partial water vapour pressure as a function of temperature and solution composition can be obtained by fitting curves to experimental data given in Perry et al (1985). The temperature-composition dependance of the partial water pressure, temperature range: 30 – 60 °C and 70 –85 % sulphuric acid solutions, is represented by the following equation.

$$P_{H2O}(bar) = (-3.372 + 0.2584\,T - 0.00616\,T^2 + 5.017*10^{-5}\,T^3) + (0.1449 - 0.011\,T + 2.628*10^{-4}\,T^2 - 2.122*10^{-6}\,T^3) * \%\,H_2SO_4 + (0.002068 + 1.569*10^{-4}\,T - 3.736*10^{-6}\,T^2 + 2.972*10^{-8}\,T^3) * (\%\,H_2SO_4)^2 + (9.8*10^{-6} - 7.4*10^{-7} * T + 1.7*10^{-8} * T^2 + 1.389 * 10^{-10}\,T^3) * ((\%\,H_2SO_4)^3 \quad (31)$$

with

T = Temperature (K)

Using this information and a simple mass balance, the change in solution composition with time can be estimated. This was performed by calculating the amount of water stripped out of the saturator for a given period assuming equilibrium between the water in the sulphuric acid and in the gas stream. The composition of the sulphuric acid was recalculated after each period. The calculations were repeated utilizing the new composition of the sulphuric acid and equation 31 to calculate the amount of water stripped out of the saturators for the next incremental period. The values used in this calculation, depicted in figure 20, are as follows

Initial sulphuric acid composition	80 %
Temperature of water bath	36 °C
Mass of solution	2025 g
Total pressure above contactor	0.87 atmosphere
Gas flow rate	0.18Nm^3/min
Equilibration temperature.	1700 °C

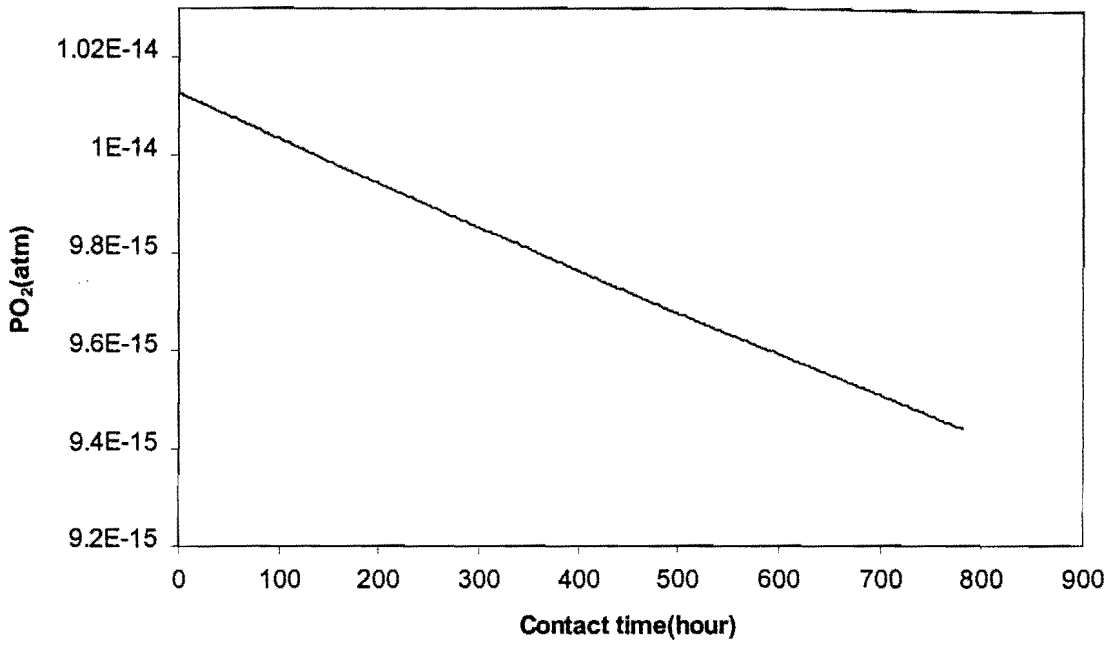

Figure 20: Calculated change of oxygen activity at 1700 °C for a H_2-H_2O mixture prepared with a 80 % sulphuric acid solution, for a hydrogen gas flow rate of 0.18Nm^3/min through an acid bath of 2025 g.

The figure depicts a 7.8 % change in the partial oxygen pressure for a 200 hour exposure period.

The effect of this change on the accuracy of the equilibrium measurements can be estimated as follows.

$$2V + 1.5\ O_2 = 2\ VO_{1.5} \qquad (32)$$

The vanadium oxide activity depends on the oxygen activity as follows

$$a_{VO1.5} \propto Po_2^{0.75} \qquad (33)$$

A variation of 7.8% in the oxygen activity thus yields an uncertainty of 4.7% in the vanadium oxide activity coefficient. This is expected to be well in the range of

experimental errors, indicating that the sulfuric acid needs only be replaced every 200 hours.

The temperature of the water bath in which the saturators are immersed should be carefully controlled because the water vapor pressure over the solvent depends exponentially on the temperature, as indicated by figure 21.

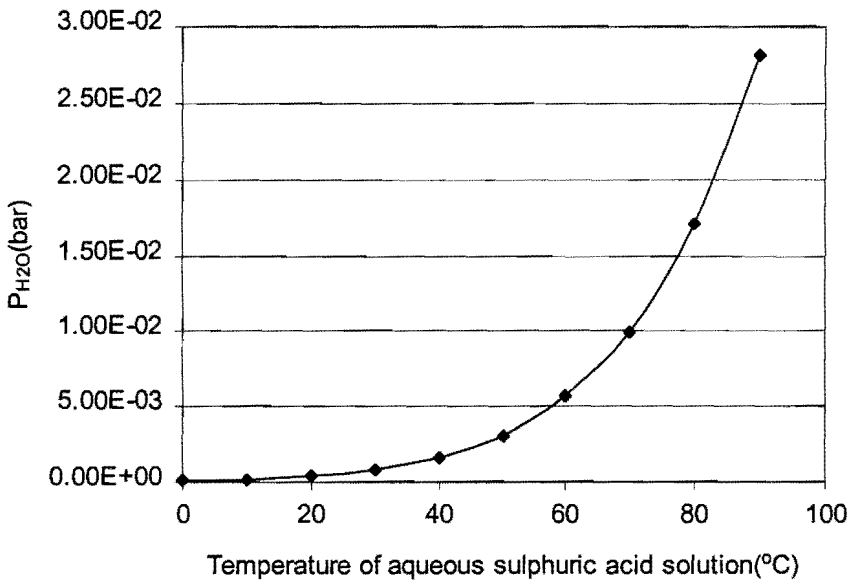

Figure 21: Effect of temperature on the partial water pressure above a 85 % sulphuric acid solution, (Perry,1985)

A circulating water bath with a controller will ensure uniform temperatures where a number of saturators are used in series. To prevent alteration of the gas mixture being used all the gas-carrying tubes must be heated to prevent condensation. Minu et al.(1948) reported tube temperatures around 80 °C, for a mole fraction water in the gas stream of 0.175, to prevent condensation.

All the adjustable parameters should be carefully controlled if accurate results are to be obtained.

1.5.3. Kinetics of the vanadium oxidation reaction

The overall reaction can be divided in a number of steps taking place in series. The first step is the mass transfer of H_20 as a gas across the boundary layer, to the gas-slag interface. The second step is the actual chemical reaction of H_20 at the the gas-slag interface by adsorption and reaction with the slag phase. The next step entails the mass transfer of the absorbed species to the slag-metal interface. Another chemical reaction takes place at this interface whereby vanadium is oxidized. The step following the oxidation reaction is the mass transfer of the vanadium oxide from the interface to the bulk of the slag, increasing the average vanadium content in the slag. The slowest of these steps will govern the overall rate of the overall reaction.

Chemical reactions are activation energy controlled remaining close to equilibrium at high temperatures. Thus mass transfer may be the rate-limiting step. The purpose of this discussion is to evaluate the mass transfer of water to the slag-gas interface as a possible rate-determining step. Unfortunately not much is known about the diffusion of vanadium species in slags.

If the rate of the overall reaction is determined by the rate of mass transfer of H_20 to the interface, then the rate of water vapor diffusion can be expressed according to the following reaction.

$$\frac{dN_{H_2O}}{dt} = m\,A\left(C_{H_2O}^{bulk} - C_{H_2O}^{inter}\right) \qquad (34)$$

The rate of vanadium oxidation(mol/hr) is 0.66 times the rate of mass transfer of H_20 to the interface In this equation $\frac{dN_{H_2O}}{dt}$ is the rate of mass transfer of H_20 to the interface and m is the mass transfer coefficient.

Assume $C_{H_2O}^{inter} = 0$ and P_{H_2O} is smaller than 0.1 atmosphere, (Nagasaka,1994), then

$$\frac{dN_{H_2O}}{dt} = \frac{m}{RT}\left(P_{H_2O}^{bulk}\right) \text{ (mol/cm}^2\text{s}^{-1}\text{)} \qquad (35)$$

With R the universal gas constant, T the temperature in K and $P_{H_2O}^{bulk}$ the partial water pressure of the bulk gas phase.

Assume the following oxidation isotherm for vanadium

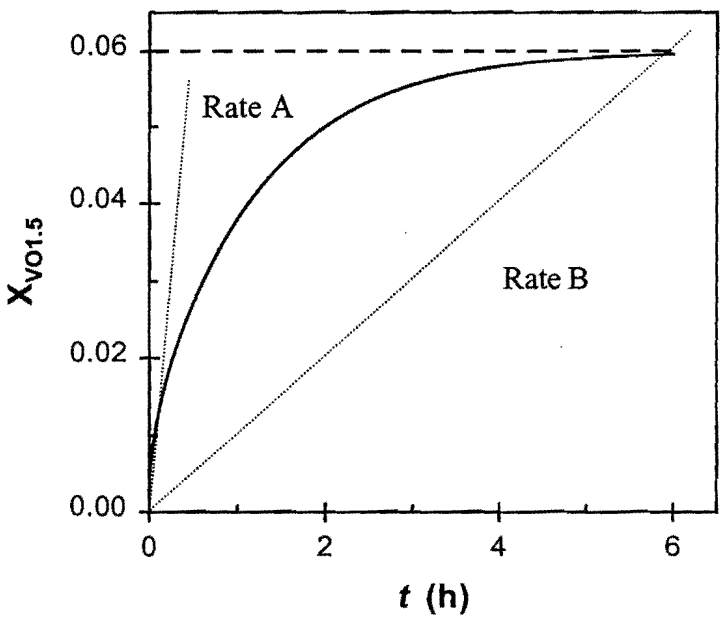

Figure 22: Assumed vanadium oxidation isotherm

Six hours is the assumed duration time for each experimental trial to reach equilibrium at a given temperature. It is further assumed (based on industrial slags) that the equilibrium mole fraction vanadium is 0.06. Two oxidation rates are now considered, Rate A (the initial rate) and Rate B (the average oxidation rate). See figure 22.

Fluid dynamics calculations for a specific experimental setup can evaluate the mass transfer coefficient(m) in equation 34. Mannion et al.(1991) and Nagasaka et al.(1993) used these equations to good effect to investigate gas mass transfer control in reactions where the chemical reactions were sufficiently fast. The experimental setup of this study, correlating with their studies, is as follows:

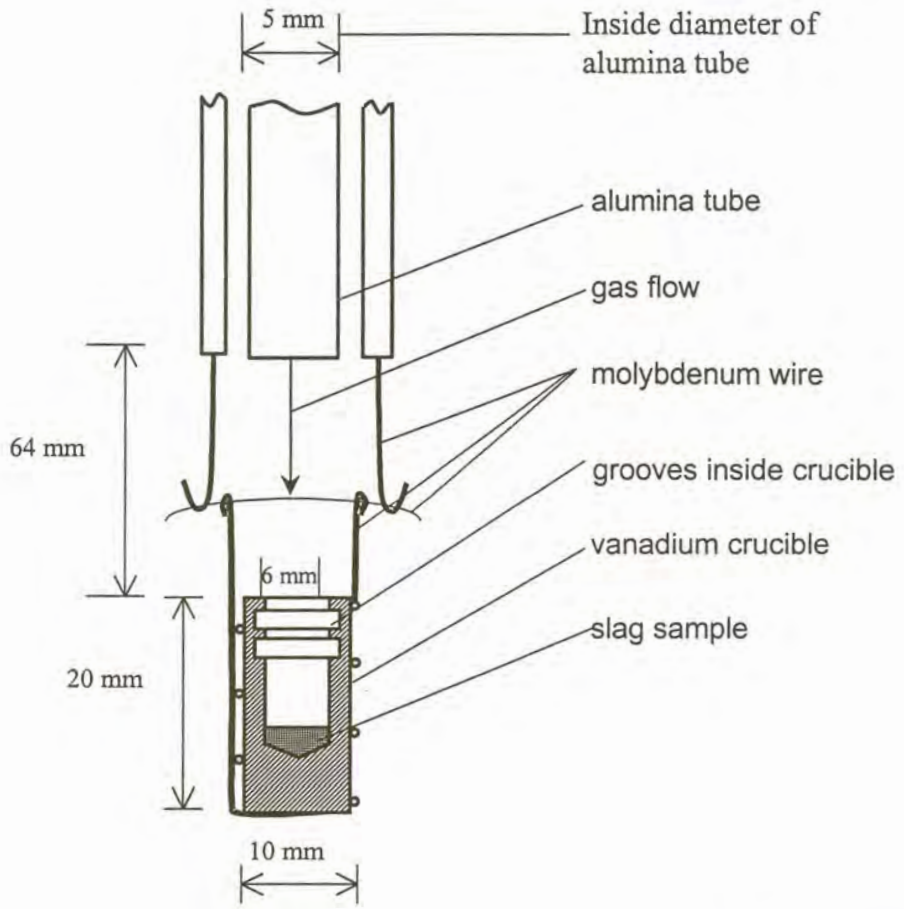

Figure 23: Planned configuration to suspend vanadium crucible inside the tube furnace.

The average mass transfer coefficient may be calculated using the following empirical equations. The Sherwood number (*Sh*) enables the calculation of the average mass transfer coefficient and was proposed to be as in equation 36, by Mannion(1992) and 37 by Nagasaka(1994).

$$Sh = 0.4(\pm 0.13)\left(\frac{d}{r}\right) Re^{0.66}\, Sc^{0.55} \qquad (36)$$

Or

$$Sh = 0.27(\pm 0.07)\left(\frac{d}{r}\right)^{1.5} Re^{0.76}\, Sc^{0.5} \qquad (37)$$

And

$$\mathrm{Sh} = m\frac{d}{D} \tag{38}$$

With

d = diameter of nozzle (m)

r = radius of crucible (m)

μ = viscosity (Pa.s)

ρ = density (kg/m^3)

D = interdiffusivity (m^2/s)

u = linear velocity (m/s)

m = mass transfer coefficient.(m/s)

Using the gas properties of interest the dimensionless Reynolds (*Re*) and Schmidt (*Sc*) numbers can now be calculated as in equation 39 and 40 respectively.

$$Re = \frac{du\rho}{\mu} \tag{39}$$

$$Sc = \frac{\mu}{\rho D} \tag{40}$$

Because of the low P_{H_2O} needed (see Table 10) the gas mixture can be considered to be pure H_2 and the gas properties of H_2 are shown in Table 11 for a gas temperature which is the average of the slightly preheated gas (330K) and the metal surface (1973-2123K).

Properties of H_2 (1200K)	
ρ	0.0176 kg/m^3 (calculated using ideal gas law)
μ	0.000024 Pa.s (Fruehan,1998)
D	9.97 *10^{-4} m^2/s (Szekely,1971)

Table 11: Properties of H_2 at 1200 K

The values used in the calculation are shown in Table 12

Values used in calculations	
Slag mass	0.0002 kg
Molar mass of slag (CaO: Al2O3 1:1)	0.079 kg/mol
Mole slag	0.00253 mol
Total pressure	0.876 atm
Bulk P_{H2O}	0.0004*101300 Pa

Table 12: Values of constants used to perform the calculations

In addition to the value of D reported by Perry et al.(1985) to be 9.97 cm^2/s, it may also be calculated using the empirical equation also proposed by Perry et al.(1985).

$$D_{AB} = \frac{10^{-3} T^{1.75} \left[\frac{(M_A + M_B)}{M_A M_B} \right]^{0.5}}{P\left[\left(\sum V_A \right)^{\frac{1}{3}} + \left(\sum V_B \right)^{\frac{1}{3}} \right]^2} \qquad (41)$$

where

T = temperature in K (1200K)

P = pressure in atmosphere

D = interdiffusivity

$M_A M_B$ = molar mass of specie A and B respectively.

$\sum V_A, \sum V_B$ = Atomic diffusion volumes

Table 13 shows atomic diffusion volumes of some of the gases found in metallurgical processing.

Specie	atomic diffusion volumes
H_2	7.07
N_2	17.9
O_2	16.6
Air	20.1
CO	18.9
CO_2	26.9
H_2O	12.7
SO_2	41.1

Table 13: Atomic diffusion volumes for use in estimating D_{AB} (Perry et al.,1985).

The gas diffusivity of H_20-H_2 was calculated to be 10.08 cm^2/s, at 1200 K, using equation 41.

The two correlations used to calculate the minimum gas flow rate needed to maintain the oxidation rates showed in figure 22, resulted in slightly different results as seen in Table 14.

		Mannion	Nagasaka
		Gas flow rates(ml/min)	Gas flow rates(ml/min)
Oxidation rate A	$1.41 * 10^{-7}$ mol/s	4015	5065
Oxidation rate B	$7.03 * 10^{-9}$ mol/s	43	54.2

Table 14: Results of fluid flow calculations for different oxidation rates. Flow rates are for 25 °C and 0.865 atm pressure.

Darken et al (1945) have established that approximately 0.9cm/s (10.6 ml/min through a tube, I.D. 5mm) is an optimum linear flow rate through a cylindrical tube to minimize thermal diffusion and temperature uncertainties.

It is evident from the results that very low flow rates are sufficient for an assumed oxidation rate if gas mass transfer is the rate-determining step (rate B). Thus, the gas mass

transfer does not have a profound effect on the kinetics of the oxidation rate and should therefore not be the rate determining step. One of the other reaction mechanisms proposed could therefore be rate limiting.

1.6. Conclusion

It can be concluded that the Al_2O_3 content of the slag (or slag basicity) has a strong effect on the amount of oxidic vanadium in the slag. In addition to this, the amount of vanadium in metallic form is also dependent on the slag basicity. Both of these mechanisms of vanadium loss to the slag should be quantified in order to maximize vanadium recovery. The oxidic vanadium loss to the slag can be quantified by performing high temperature equilibrium experiments utilizing hydrogen-water mixtures to fix the oxygen activity.

2. Experimental techniques

2.1. Introduction

Little information is available on activity-composition relations of vanadium in contact with high Al_2O_3-CaO-MgO slags, as indicated by the previous section. Although metal droplet entrainment has been identified as one of the possible mechanisms of vanadium loss to the slag, this section will concentrate solely on the quantification of the effect of the slag basicity on soluble vanadium loss to the slag. The experimental technique involved the equilibration of synthetic $CaO-Al_2O_3$ slags with a vanadium crucible by maintaining the required oxygen activity using H_2-H_2O gas mixtures. After equilibration the slags were quenched, polished and analysed using energy dispersive X-ray analysis (EDX) techniques. Knowing the mole fraction of $VO_{1.5}$ in the slag and the mole fraction of water in the reaction gas, the vanadium activity coefficient $\gamma_{VO1.5}$ was determined for a range of CaO/Al_2O_3 - ratios.

2.2. Experimental set-up

2.2.1. Gas system set-up

As indicated previously, ultra-low oxygen activities based on the assumption that the oxygen activity in the industrial smelting furnace is fixed by the Al_2O_3/Al- equilibrium can only be obtained using hydrogen gas equilibrated with water vapour. The amount of water vapour was fixed by contracting hydrogen gas with 75.7 % sulphuric acid at a controlled temperature of 42±0.1°C. A schematic representation of the gas system is depicted in figure 24, while figure 25 shows the complete experimental set-up used in the present study.

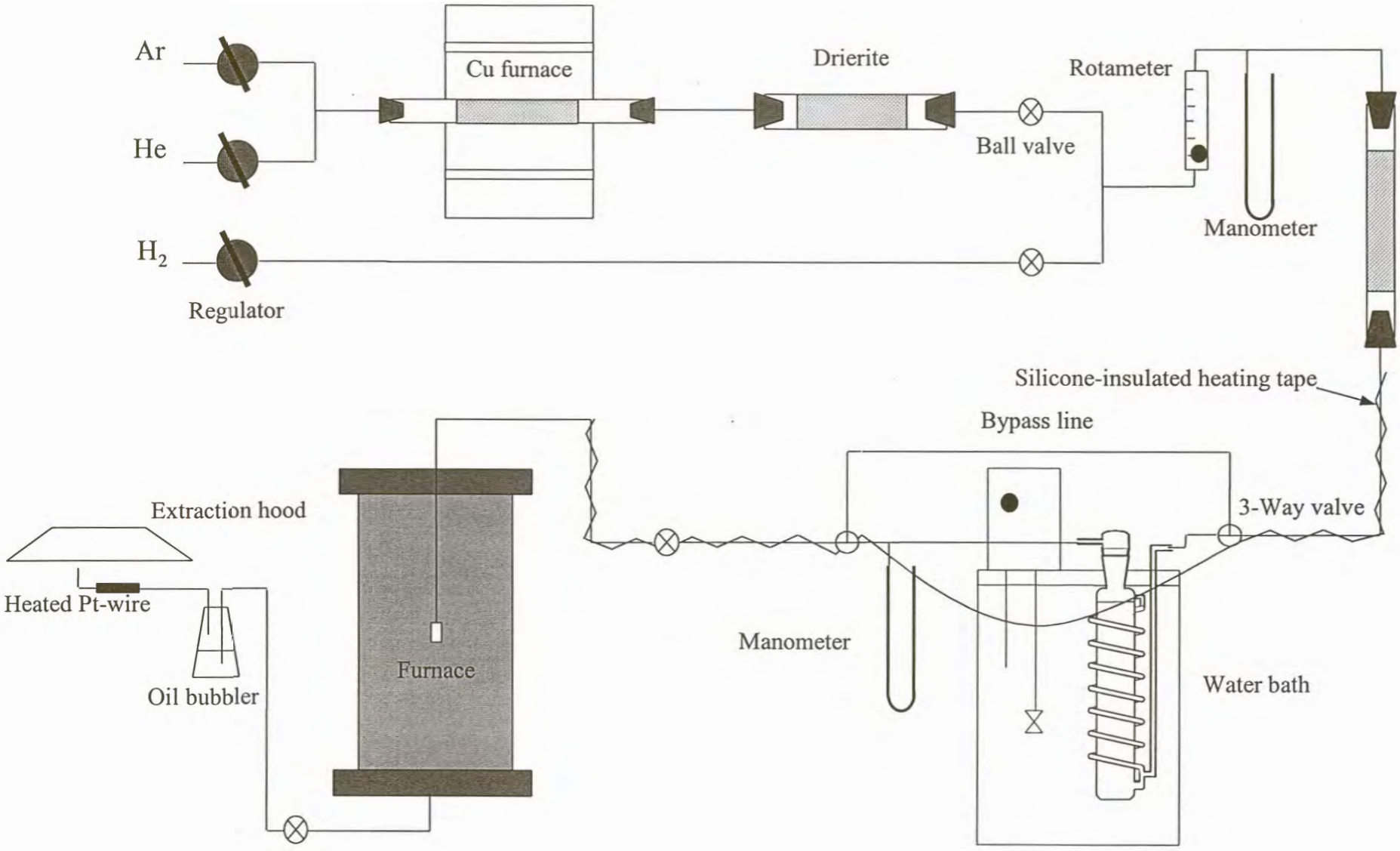

Figure 24: Schematic of gas system.

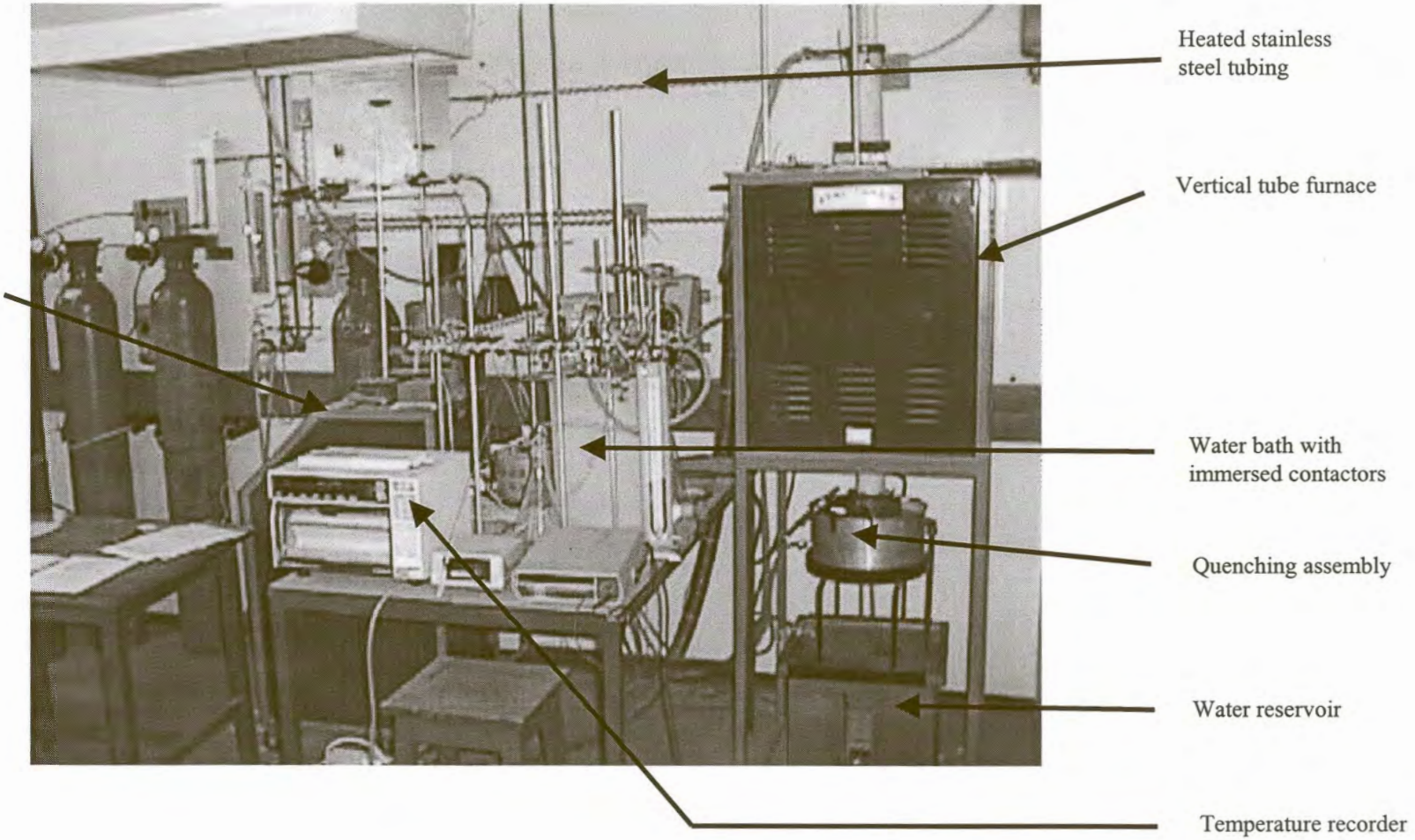

Figure 25: The complete experimental set-up used in the present study showing the gas system and furnace set-up

Tygon high-density tubing was originally used to convey the reaction gas, but difficulties in establishing a constant water vapour level led to the replacement of the tubing by stainless steel tubing. Pieces of stainless steel tubing were connected using stainless steel Swagelok couplings ensuring good tight seals. The stainless tubing (O.D. 10 mm, I.D., 8 mm) was heated to 80 °C using silicone-insulated heating tape connected to a 220 V power source. The power rating of the heating tape was 30 W/m, and 18m of heating tape was helically wound, with a 2.5 cm pitch, around the stainless steel tubing. Desorption of the absorbed water from the inner surface of the stainless steel tubing was enhanced by the continuous flushing of the tubing with Argon gas for a few days. The dryness of the tubing was monitored by passing the humid Argon stream through a Drierite-filled column, subsequently weighing the column to measure the mass increase due to water uptake as shown in figure 26.

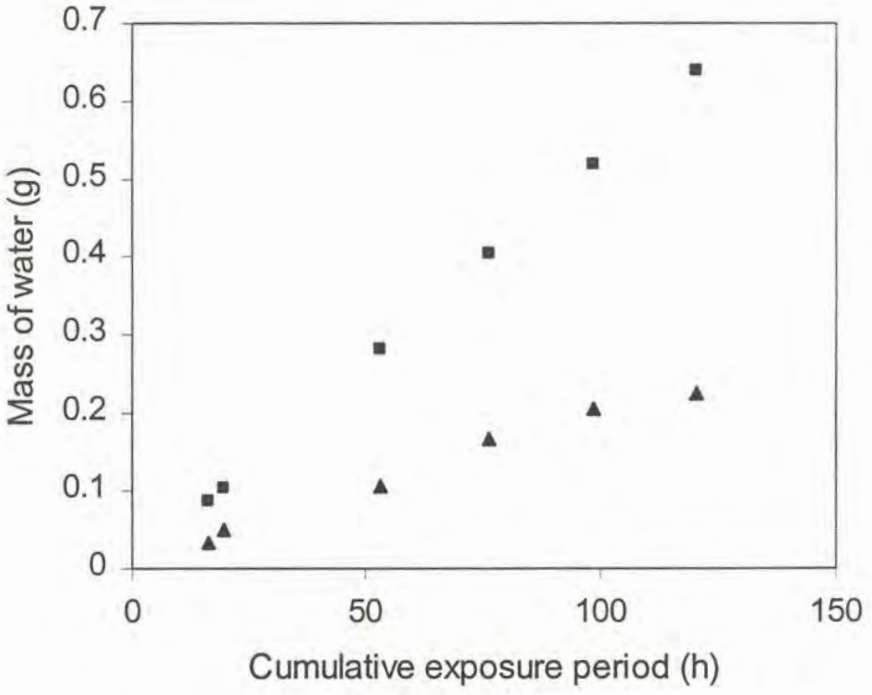

Figure 26: Humidity measurements performed on Argon gas used to convey desorbed water which originated from the walls of the stainless steel tubing. In this figure, the squares show the expected amount of water transferred for equilibrium with 85% sulphuric acid at 60 °C, and the triangles show the amount of water stripped from the tube surface if dry argon is used.

Figure 26 indicates that at least 120 hours of flushing is necessary to remove most of the absorbed water, before commencement of the equilibrium runs.

It was found that care had to be taken when weighing the Drierite-filled columns to measure the amount of water uptake, because the columns slowly changed weight over periods of tens of minutes after removal from the gas line. This effect is presumed to reflect a slightly higher pressure within the porous bed in the columns. As the gas flows out of the pores and exchange occurs between the gas inside the column with air (which has a different density), the column mass decreases, as illustrated by figure 27.

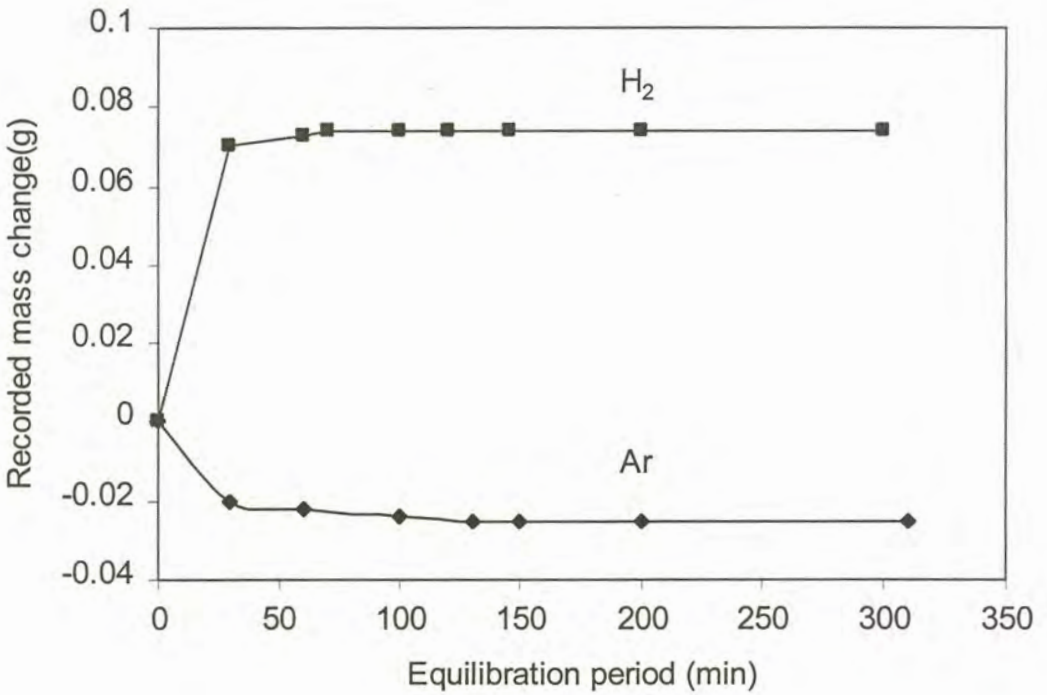

Figure 27: Change in the weight of two Drierite-filled columns containing argon and hydrogen carrier gases, after removal from the gas line.

Figure 27 serves to illustrate the required equilibration period for the two Drierite-filled columns, for the two different carrier gases. This figure reveals that at least 130 minutes should be allowed for the argon-filled column to equilibrate (after removal from the gas line), compared to the 70 minutes for the hydrogen-filled column. The Argon-filled column shows a net weighed decrease while the hydrogen filled-column increased. The equilibration period for argon-filled columns was throughout the moisture measurements

much shorter compared to instances when hydrogen was used. Argon was used only initially to assist in the desorption of water form the stainless steel tubing and was replaced by hydrogen as soon as the gas system was dry enough to start performing equilibrium experiments. The large difference in the equilibration period is presumably due to the large difference in gas viscosity values existing between the gases. The gas viscosity values relate to the molar mass of the gases and gases with large viscosity values exhibit lower diffusion rates. The equilibration period also depend on the size of Drierite particles (larger particles impose less restriction on gas diffusion) as well as the diffusion distance. Clearly, care has to be taken to determine the equilibration period for each individual case, if more than one type of Drierite column is used.

As indicated earlier, after a few days of monitoring the water content in the Argon gas stream, the water levels were sufficiently low to proceed with the experimental work. For this, glass reactors were used to contact the hydrogen with sulphuric acid solutions.

The already immersed reactors in the water bath are shown in figure 28.

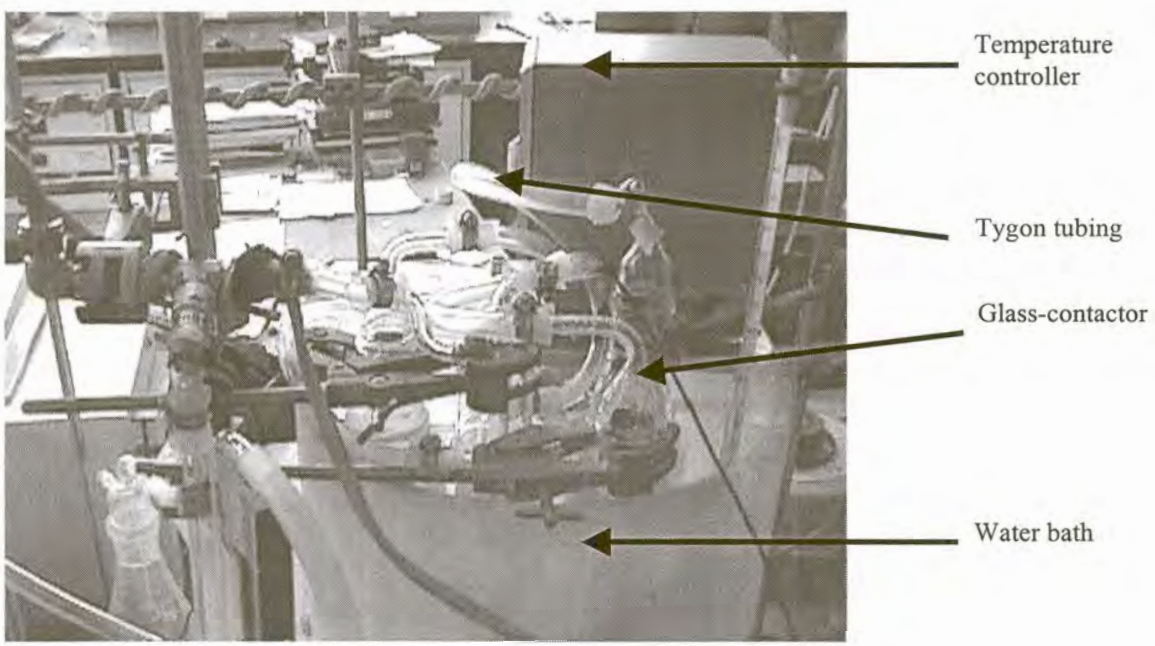

Figure 28: Photograph showing immersed glass reactors with temperature controller.

The inlets and outlets of two reactors were connected in series using flexible Tygon tubing. Hose clamps were used to ensure gas tightness of the connections. A pressure

drop of 11cm Hg over the reactors was observed. Although a dense polymer, the Tygon could not prevent gas from diffusing out resulting in a pressure drop within the gas line when not in use, causing the withdrawal of sulphuric acid from the reactors into the tubing. Attack of the tubing was prevented by keeping the reactors pressurised between experimental runs.

Each reactor contained about 0.5 dm^3 of sulphuric acid solution. The amount of water vapour in the gas stream was originally fixed by contacting the hydrogen gas with 85% sulphuric acid at a controlled temperature of 60 ± 0.1°C. The first equilibrium run served the purpose to test the assumption that the activity of Al in FeV is similar to that of Al in dilute steel. This assumption was originally made in order to perform calculations to estimate the oxygen potential in the industrial smelting process. Results obtained will be discussed in more detail later in this work. (See section). Before this experiment could be performed, checks had to be performed on the exist gas composition to determine the consistency as well as the deviation from equilibrium, as been depicted by figure 29.

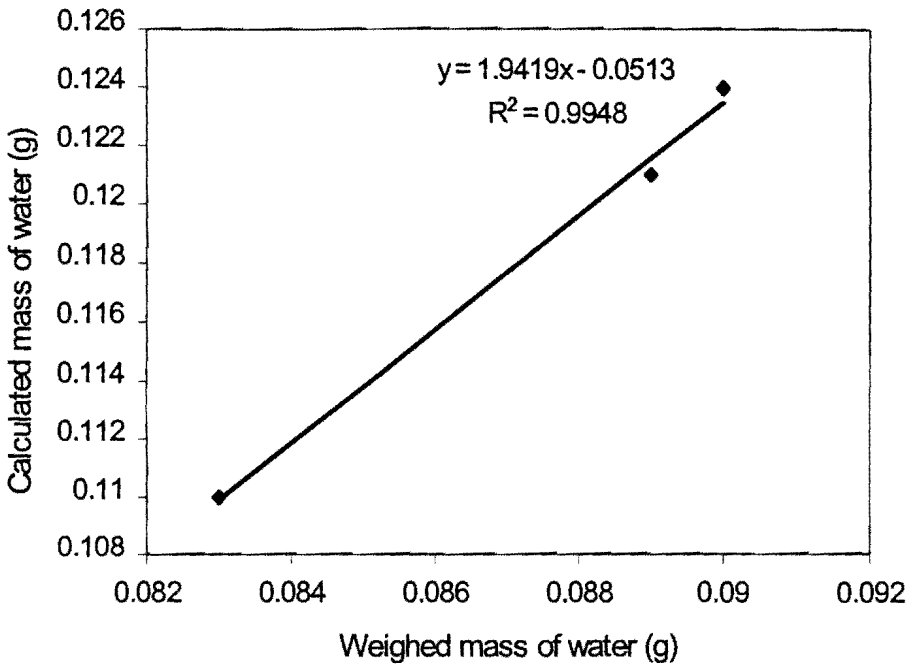

Figure 29: Comparison between the actual mass of water transported by the gas stream and the mass of water calculated assuming equilibrium between the water vapour in gas stream and acid. Calculations were performed for a 85 % sulphuric acid solution kept at 60°C. Gas flow rate of 0.18 Nl/min and total pressure 0.877 atm were used. Tabulated correlations in Perry et al (1984) of the partial water pressure as a function of temperature and acid composition were also implemented. Values are for different times of gas flow, ranging from 19 to 24 hours.

Figure 29 shows that the amount of water in the reaction gas deviates considerably from the equilibrium calculated amount, thus indicating that the equilibrium could not be obtained within the saturators. In any case, equilibration of the lime-alumina slag with a vanadium crucible under this atmosphere caused a low vanadium oxide contact (of only 1%) compared with the 3% in plant slag. Because of too reducing condition the 85% sulphuric acid solution was replaced by a 75 % sulphuric acid solution at a controlled temperature of 42 ± 0.1°C. The equilibrium partial water pressure above the surface of the sulfuric acid was thus increased by 2.7 times. The composition of the sulphuric acid solution was monitored prior to filling of the columns, by measuring of the density of sulphuric acid solutions. The density measurements were performed by immersing a piece of 316 stainless steel plate, the volume of which was accurately pre-determined ($33.72cm^3$), into the sulphuric acid solution at a known temperature. After immersion, the

flat plate was weighed accurately to three decimal places, to measure the decrease in weight due to the buoyancy force acting on the flat plate. On average, the mass readings showed around 10 mg decrease due to the corrosion of the stainless steel in the sulphuric acid solution from the moment the reading stabilised until the reading was recorded. The density of the sulphuric acid can be calculated using the equation 45

$$\rho_{H_2SO_4} = \frac{\text{Weight of flat plate before immersion - Weight of flat plate after immersion}}{\text{Volume of flat plate}}$$

With $\rho_{H_2SO_4}$: density of sulphuric acid (g/cm^3)

(42)

A variation of 0.010g/33.72 cm^3 yields an uncertainty of ± 0.03% in the density of the sulphuric acid.

Accurate tabulation of sulphuric acid densities as a function of temperature and composition is found in literature (Perry (1984)).

To ensure that conditions proceed as close as possible to equilibrium between the water vapour in the gas stream and acid, three glass reactors containing a helical gas-liquid contractor were employed in series. One such reactor is depicted in figure 30.

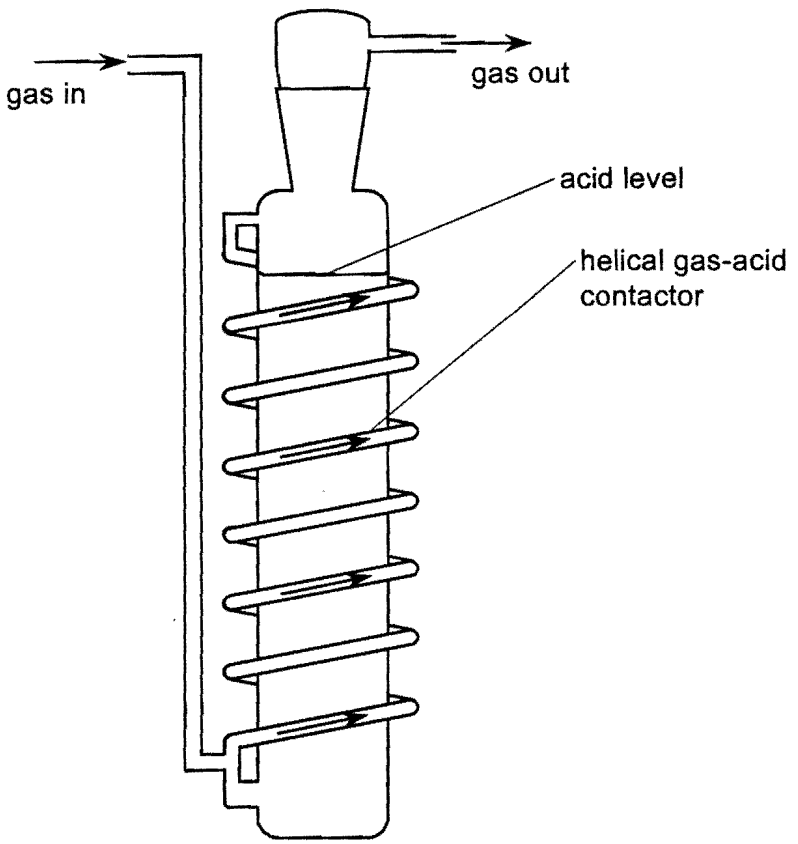

Figure 30: Glass contactor containing sulphuric acid, showing the path of the carrier gas.

The stainless steel tubing was protected from possible acid attack by using glass traps at the inlet and outlet of the sulphuric acid contractors as depicted in figure 31. The glass reactor preceding the water bath was dried at 200°C to ensure no gas stream contamination during its exposure to the atmosphere when the sulphuric acid was replaced. Concentrated sulphuric acid attacks 316 stainless steel tubing and precautionary measures had to taken against sharp pressure fluctuations which may cause acid reaching the tubing.

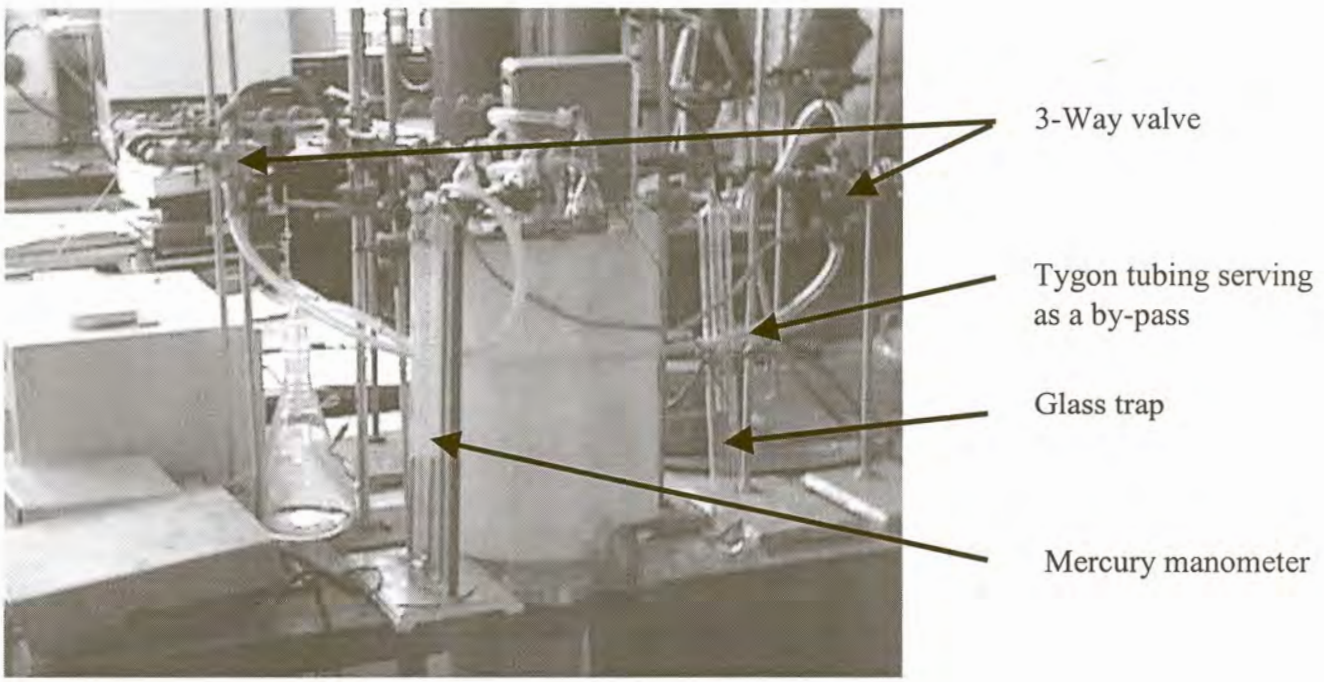

Figure 31: Glass traps used to protect 316 stainless steel tubing against acid spurts.

All three the reactors were immersed in a 25-liter plastic water bath ensuring good insulation against heat transfer to the environment. Atmospheric water pick-up, between experimental runs and during the replacement of the sulphuric acid reactors, was eliminated by using valves at the exposed open-ends of the stainless tubing, as depicted in figure 24. Three-way valves located on either side of the sulphuric acid reactors made it possible to by-pass the reactors when flushing with Argon gas was required. Unnecessary stripping of water out of sulphuric acid solutions was therefore avoided. The temperature of the water bath was accurately controlled to within 0.1°C using a Grant VFP thermostatic circulator. Calibrated thermometers were used additionally to monitor the water bath temperature in case the immersion thermostat failed to measure the temperature accurately. Recordings of the bath temperature were also continuously made for future reference.

The gas system contained two separate gas lines for Ar/He and H_2, which joined just before the rotameter. Oxygen was removed from the Argon or Helium by passing it over copper turnings held at 600°C. The copper-turning furnace was directly followed by an

anhydrous $CaSO_4$-filled column to remove any water. A second anhydrous $CaSO_4$-filled column was inserted just after the rotameter to remove any excess water entering the system through the hydrogen. At the outlet from the furnace, the hydrogen gas was burnt on a heated platinum wire after passing through an oil trap. Figure 32 shows the heated Pt-wire assembly.

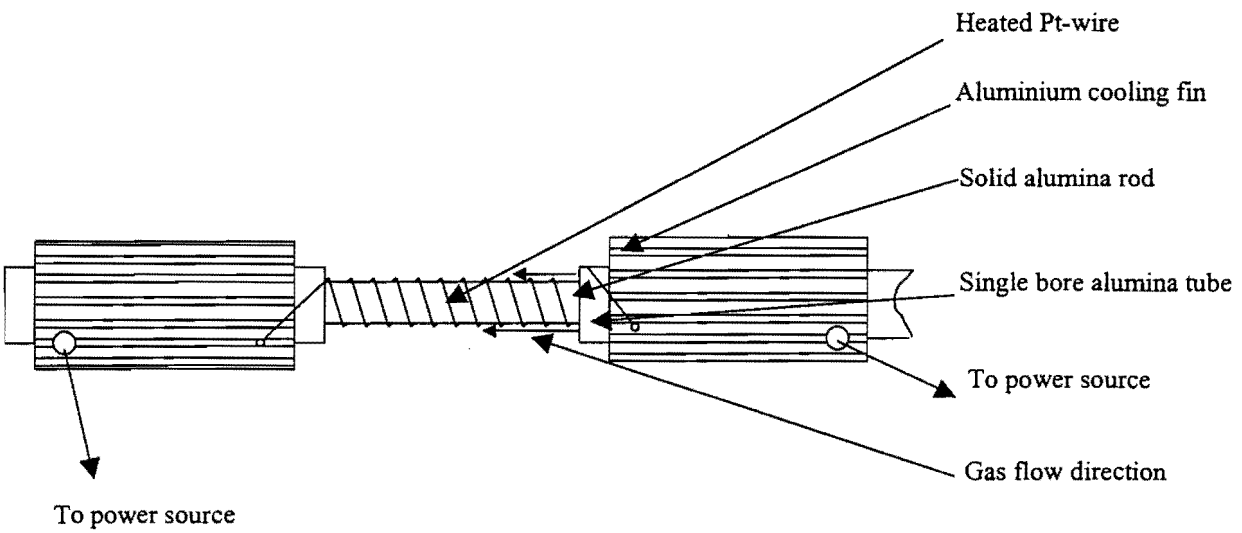

Figure 32: Heated platinum wire assembly.

The platinum wire assembly proved to be a safe alternative to the traditional bunsen-flame method of oxidation of hydrogen gas. The platinum wire was kept at around 1000 °C for weeks on end without failure. This enables experiments to be safely carried out throughout the night if no power failure occurs. The completeness of the oxidation reaction was determined by holding a hydrogen detector in the close vicinity of the heated platinum wire. No traces of excess hydrogen could be detected around the platinum wire. As can be indicated by the figure, the Pt-wire was wound around an alumina tube that fitted snugly into a larger alumina tube which directed the hydrogen gas through the small opening between the two tubes onto the hot Pt-wire. This ensured intimate contact between the hydrogen gas and the Pt-wire.

Gas flow rates were measured and controlled by a single rotameter which was calibrated in-line using a bubble meter. In-line calibration of the rotameter was required to establish the exact flow rate of the gas mixture because a back pressure in the gas line does affect

the flow rate. For this calibration purpose, the outlet from the oil trap at the end of the gas system was connected to the bottom of bubble meter cylinder. The gas was introduced into the bottom of the apparatus, displacing a soap bubble along the length to the top end of the cylinder. A stopwatch was used to establish the time required for one bubble to traverse the indicated volume. This measurement was repeated around 20 times to establish a good average value for each rotameter setting.

During actual equilibration runs, the hydrogen flow rate was kept at 0.18 Ndm^3/min throughout. Because equilibrium between the water vapour in the gas and acid can not be assumed, the actual amount of water in the gas was monitored (between equilibration runs) by passing the humid gas stream through a Drierite-filled column for a period of 5 hours. The mass increase was weighed accurately to the nearest milligram. The 5 hour exposure period yielded a typical mass increase of 85 mg. Figure 33 depicts the actual mass of water transferred per unit time, as a function of the total time that the sulphuric acid reactors were in use

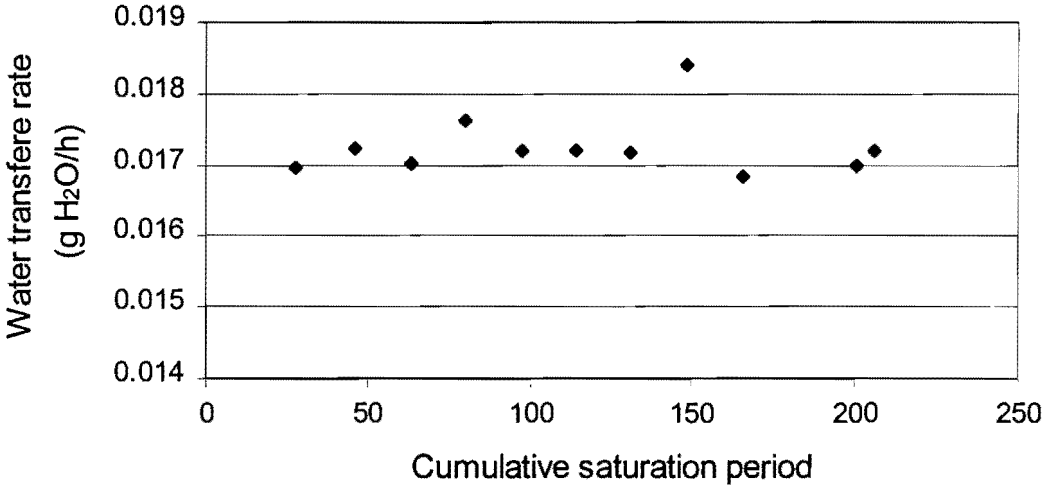

Figure 33: The actual mass of water measured per unit time as a function of the time the sulphuric acid reactors were in use.

As indicated by figure 33, no appreciable change in the water content of the reaction gas due to stripping of water out of the sulphuric acid occurred during the 200 hour saturation period.

The reliability of the measured mole fraction of water vapour depends on the accuracy of the weight measurements. A three-digit scale is in effect only accurate to two decimal places. The weighing practice was kept as consistent as possible to increase the reliability of the measurements. The resulting average calculated mole fraction of water vapour in the gas stream was $(2.00 \pm 0.05) \times 10^{-3}$ for the equilibrium runs. In one experiment the mole fraction water vapour in the hydrogen gas was increased to $(3.52 \pm 0.02) \times 10^{-3}$ to determine the oxidation state of vanadium in the slag.

Leak detection was performed before each equilibrium run by filling the gas line with pressurised Helium gas (pressures around 12 cm Hg were applied) and checking for leaks with a hand-held helium detector. Leak checks performed on the furnace itself will be discussed later this section.

The line pressure before and after the water bath was measured using mercury manometers. The pressure above the acid solution is important for calculating the actual as well as equilibrium amount of water (mole fraction) in the hydrogen stream. Figure 34 compares the actual amount of water transferred, with the equilibrium amount of water (calculated using the following values and equation 25 in the literature section).

Acid composition: 75.7% H_2SO_4 (determined from density measurements)
Water bath temperature: See appendix 1
Exposure period to acid reactors: See appendix 1
Gas flow rate: 0.18 Nl/min
Total pressure above acid solution: 0.877 atmosphere

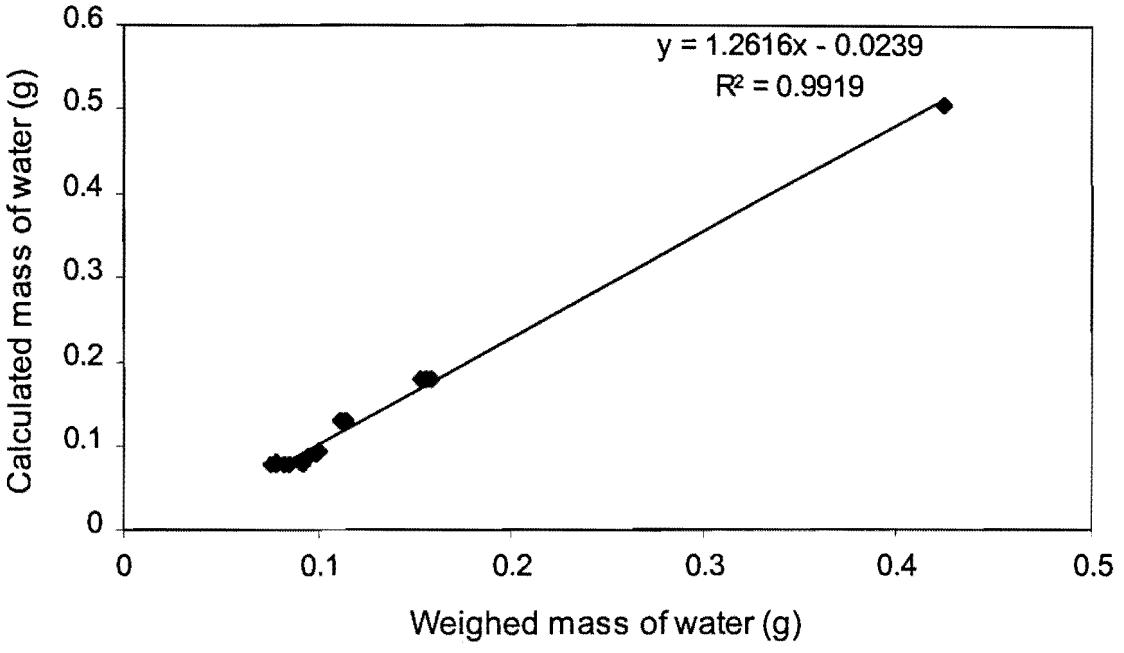

Figure 34: Comparison between the actual weighed mass of water and mass of water calculated assuming equilibrium between water vapour in the gas stream and the acid.

As figure 34 shows, checks performed on the exit gas composition using Drierite-filled columns show a definite deviation from the calculated water content of the reaction gas (calculated assuming equilibrium between the water vapour in the reaction gas and the sulphuric acid solution.) The amount of water in the reaction gas is consistently lower than the predicted content indicating that three reactors in series are not capable of obtaining the equilibrium water content in the reaction gas.

The slopes of the straight lines fitted through the data points in figure 29 and 34, indicate that the system utilising a 75 % sulphuric acid solution is closer to equilibrium than the system utilising a 85% sulphuric acid solution. It is thus easier to obtain equilibrium between the water vapour in the gas stream and the acid if the lower concentration sulphuric acid solution is utilised.

The reactors were designed at first with helical contactors, measuring a total length of around 6 meters, to ensure long intimate contact between the reaction gas and sulphuric acid solution. Despite obvious measures to ensure equilibrium, at the end equilibrium

could not be obtained. This underlines the fact that checks on the exit gas composition between equilibrium runs are absolutely essential. Any published data based on H_2/H_2O-equilibrium utilised to fix the oxygen activity should contain the method used to determine the gas composition. An assumption that equilibrium conditions prevail in the saturator may decrease the value of the work. It can further be concluded that the water content of the reaction gas can be successfully monitored using Drierite as absorbent.

The sulphuric acid solution (after more than 200 hours exposure period) was replaced after the completion of the first series of experiments investigating activity-composition relations. Table 15 shows the calculated composition of the sulphuric acid in the reactors before and after the completion of the experiments

	Initial Composition	Final composition
First reactor	75.7	75.5
Second reactor	75.7	75.2
Last reactor	75.7	75.2

Table 15: Change in sulphuric acid composition. (mass percentages)

It is evident that no appreciable change of the sulphuric acid composition occurred and that 200 hours' exposure with 3 reactors containing 0.5 dm^3 acid can comfortably maintain a constant water vapour level in the hydrogen gas.

2.2.2. The furnace set-up

A schematic representation of the furnace assembly set-up is shown in figure 35.

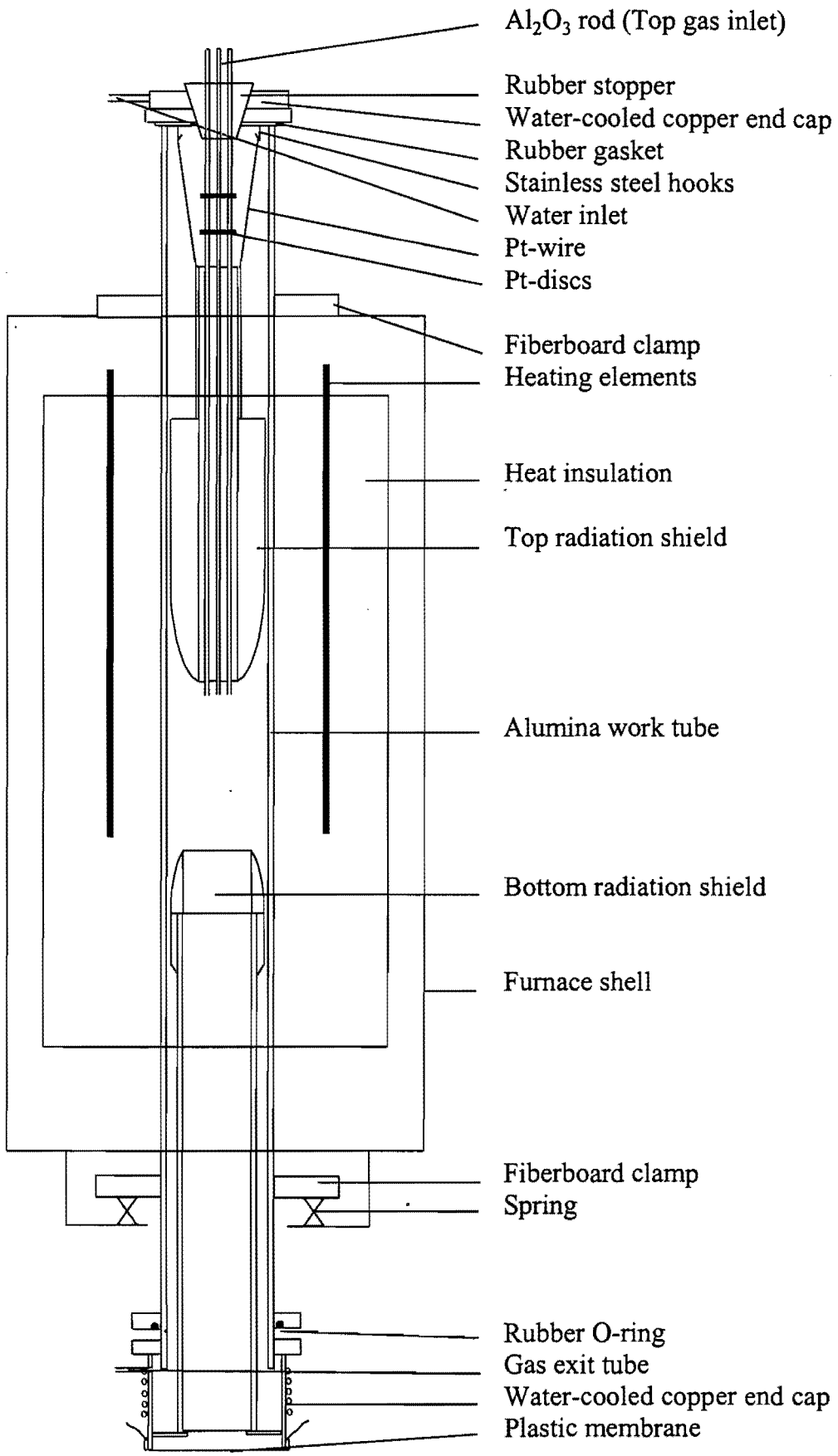

Figure 35: Schematic representation of the furnace assembly set-up

The vertical tube resistance furnace from Pirotherm which employed six equidistant molybdenum disilicide-tungsten carbide heating elements, situated around the furnace tube, was utilized. The specified temperature rating of the furnace is maximum 1800°C for normal heating and cooling cycle. If necessary the furnace could reach 1850°C whereafter the elements should never be switched off and kept at or above 900°C indefinitely.

The maximum temperature that could reliably be obtained in the available laboratory furnace without drastically reducing the life of the elements, was 1700°C. To test the temperature influence on the activity coefficient of vanadium, an experiment was conducted at 1750°C. Due to severe SiO_2 pick-up in the slag no more experiments were performed at this temperature. A single run at 1650 °C was performed to test the influence of temperature on the activity coefficient of vanadium.

The furnace temperature was controlled by an Eurotherm controller/programmer using a Pt-40%Rh/Pt-20%Rh thermocouple that was positioned next to the furnace tube, close to the hot zone. The exact position and temperature of the hot zone was measured with a hand-held Pt-40%Rh/Pt-20%Rh thermocouple (Bedford,1965) placed at various depths in the furnace tube. During this procedure the lower end of the alumina tube was covered with a plastic film to prevent an updraft of hot air through the furnace tube leading to inaccurate measurements. The temperature profile as a function of position at a programmed temperature of 1600°C is shown in figure 36.

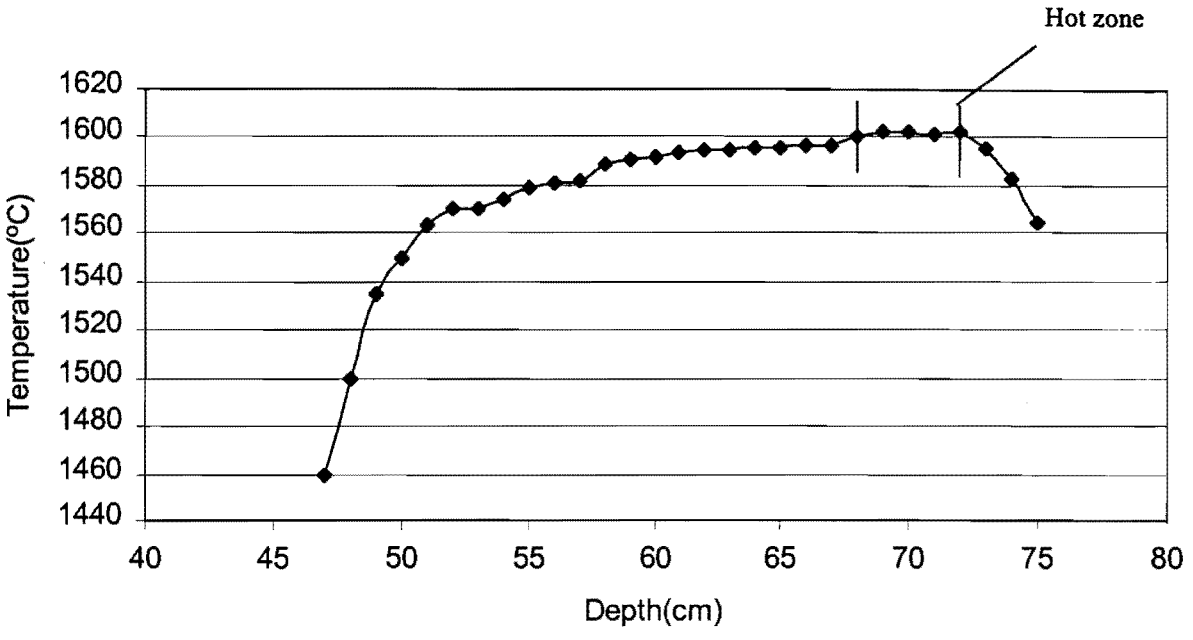

Figure 36: Temperature profile as a function of position. Depth measured from top of alumina tube. Programmed furnace temperature:1600°C; the furnace hot zone was determined to be 50 mm in length. The average measured temperature in this zone was (1601±0.5 °C).

The average temperature of the hot zone measured with the hand-held thermocouple was within 1°C of that indicated by the furnace controller.

The re-crystallized alumina (99.8% Al_2O_3) furnace tube (length 1.2m, O.D. 75 mm, and I.D. 65 mm) was fitted with water-cooled copper heads at both ends. The bottom fitting extended below the alumina tube and was sealed with O-rings lubricated with high temperature vacuum grease. The upper end cap was sealed, before each equilibrium run, to the open flat end of the tube, sealing with a rubber gasket between the tube and the fitting. A steel bracket attached to the furnace tube exerted pressure on the gasket. The upper end cap contained the rubber plug sealed to the fitting, to prevent gas leakage due to the high pressure within the work tube. The rubber plug was used as exit seal for the three alumina tubes used to suspend the vanadium crucible inside the tube and to introduce gas to the synthetic slag. The tubes were sealed to the rubber plug with silicone sealer.

Possible thermal damage (by radiation from the hot zone) to the rubber plug and silicone sealant was prevented by using two round Pt discs fixed to the alumina tubes using Pt-wire. The Pt-disc diameters corresponded to the inside diameter of the alumina tube, which formed part of the upper radiation shield. No thermal damage whatsoever was observed at the surface of the rubber plug.

Radiation shields were present within the furnace tube above and below the crucible. The purpose of top radiation shield was to protect the elements as well as copper end cap from excessive temperatures. The top radiation shield was suspended from the water cooled end cap using 0.5 mm O.D. Pt-wire.

Failure of the vanadium crucible during the first equilibrium run due to complete melting was found to be the result of severe phosphorus pick-up. The radiation shields consisted of fibreboard rings made from a high-temperature fibreboard, temperature rating of 1800°C, and glued together using high temperature cement. The cement originally used to manufacture the radiation shield was an alumina-phosphate cement. Under reducing high-temperature conditions, the cement can be reduced to Al_2O_3 and P_2 (gas). The phosphorus gas apparently alloyed with the vanadium crucible to form a low melting point eutectic component resulting in failure at a temperature 200°C below the melting point of pure vanadium. The radiation shields were reconstructed using the same high-temperature fibreboard rings and pure high-temperature alumina cement. Following severe silica pick-up in the slag within the crucible during early runs, these radiation shields were found to contain mullite, which can be reduced to Al_2O_3 and SiO(g) under reducing high-temperature conditions employed here. In support of this mechanism, silica crystals were observed on the cooler regions of the radiation shields. The continuous precipitation of silica onto the gas carrying alumina tube over extended periods led to failure of the tube due to glass formation. A glass phase could clearly be observed in the vicinity of the crack formed in the alumina tube.

The radiation shields were originally coated with a ±5 mm thick layer of alumina (98% Al_2O_3), applied as a slurry. The alumina layer was subsequently sintered at 1400°C for at least 8 hours in a muffle furnace. The alumina coating and sintering cycle were repeated a number of times, if considered necessary, after the radiation shield was examined for

large cracks. Some cracking of the alumina coating did still occur during subsequent use, causing sporadic contamination of the samples by silica. Those samples which showed more than 2 % silica (mass percentage) pick-up were discarded. Silica pick-up was more severe in slags with higher basicities, presumably due to low silica activity coefficients in these slags. Furthermore, there was a direct correlation between the creep behaviour and the silica content of the slags. Severe slag creep was observed in some early experiments due to severe silica pick-up from radiation shields. Slag creep was prevented, to an extent, by reducing silica pick-up by coating the radiation shields, machining two grooves into the inner wall near the top of crucible and also by dividing the opening of the crucible into two using a 0.1mm vanadium wire (See figure 38).

2.2.3. Quenching set-up.

The lower-end of the furnace tube was sealed with a PVC membrane, thickness of 30 μm, wrapped over the furnace tube opening, with a layer of vacuum grease as sealant between the copper end cap tube and the plastic film. The PVC film was held in position by using a hose clamp pressing onto a (0.1 mm-thick, 20mm wide) PVC band preventing the thin plastic film from being cut by the clamp.

The PVC-covered end cap was immersed in water, contained in an aluminium container through which water ran continuously. A large container/reservoir situated below the aluminium container was continuously filled by the overflow of the top container. When the water level within the reservoir reached a certain height, a pressure sensitive switch activated a pump located at the bottom of the reservoir.

The quenching set-up shown in figure 37, consisted of two single bore alumina tubes (I.D. 2.5 mm) containing molybdenum wires of 1 mm in diameter. The bottom protruding molybdenum wires were bent to form two hooks. The top hole from which the thick wires protruded (above the furnace tube) was sealed by silicone sealant. The crucible was suspended from the two molybdenum wire hooks by means of a thinner (0.3 mm diameter) connecting molybdenum wire. Solid-state diffusion is very much possible at 1700 °C and ultra-low partial oxygen pressures result in oxide-free contact surfaces. Solid-state welding occurred between the thick molybdenum hooks and the thin

anhydrous $CaSO_4$-filled column to remove any water. A second anhydrous $CaSO_4$-filled column was inserted just after the rotameter to remove any excess water entering the system through the hydrogen. At the outlet from the furnace, the hydrogen gas was burnt on a heated platinum wire after passing through an oil trap. Figure 32 shows the heated Pt-wire assembly.

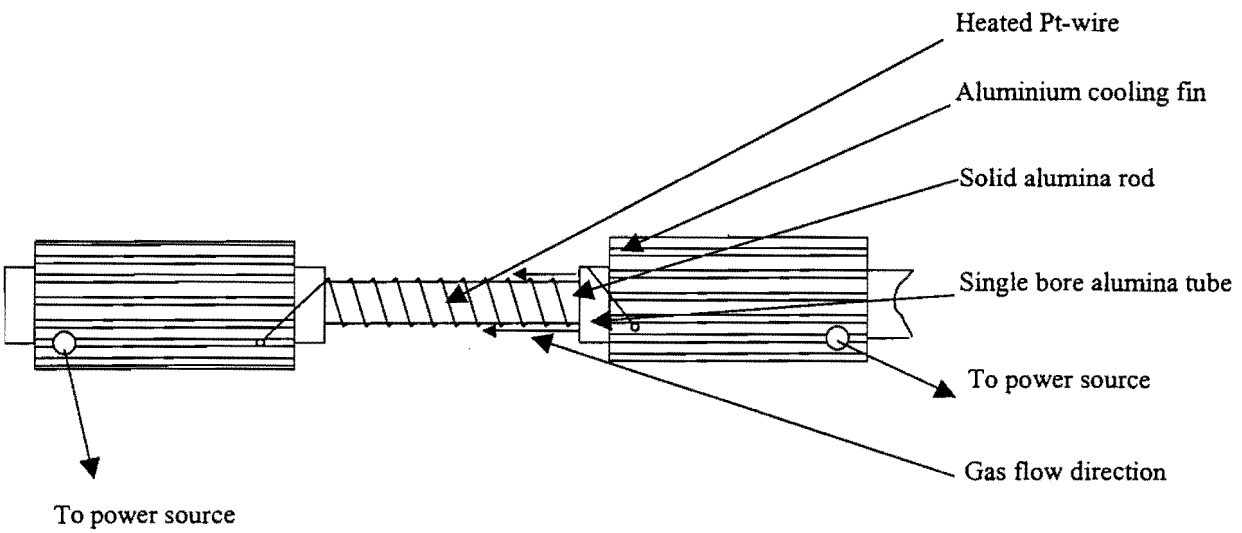

Figure 32: Heated platinum wire assembly.

The platinum wire assembly proved to be a safe alternative to the traditional bunsen-flame method of oxidation of hydrogen gas. The platinum wire was kept at around 1000 °C for weeks on end without failure. This enables experiments to be safely carried out throughout the night if no power failure occurs. The completeness of the oxidation reaction was determined by holding a hydrogen detector in the close vicinity of the heated platinum wire. No traces of excess hydrogen could be detected around the platinum wire. As can be indicated by the figure, the Pt-wire was wound around an alumina tube that fitted snugly into a larger alumina tube which directed the hydrogen gas through the small opening between the two tubes onto the hot Pt-wire. This ensured intimate contact between the hydrogen gas and the Pt-wire.

Gas flow rates were measured and controlled by a single rotameter which was calibrated in-line using a bubble meter. In-line calibration of the rotameter was required to establish the exact flow rate of the gas mixture because a back pressure in the gas line does affect

the flow rate. For this calibration purpose, the outlet from the oil trap at the end of the gas system was connected to the bottom of bubble meter cylinder. The gas was introduced into the bottom of the apparatus, displacing a soap bubble along the length to the top end of the cylinder. A stopwatch was used to establish the time required for one bubble to traverse the indicated volume. This measurement was repeated around 20 times to establish a good average value for each rotameter setting.

During actual equilibration runs, the hydrogen flow rate was kept at 0.18 Ndm^3/min throughout. Because equilibrium between the water vapour in the gas and acid can not be assumed, the actual amount of water in the gas was monitored (between equilibration runs) by passing the humid gas stream through a Drierite-filled column for a period of 5 hours. The mass increase was weighed accurately to the nearest milligram. The 5 hour exposure period yielded a typical mass increase of 85 mg. Figure 33 depicts the actual mass of water transferred per unit time, as a function of the total time that the sulphuric acid reactors were in use

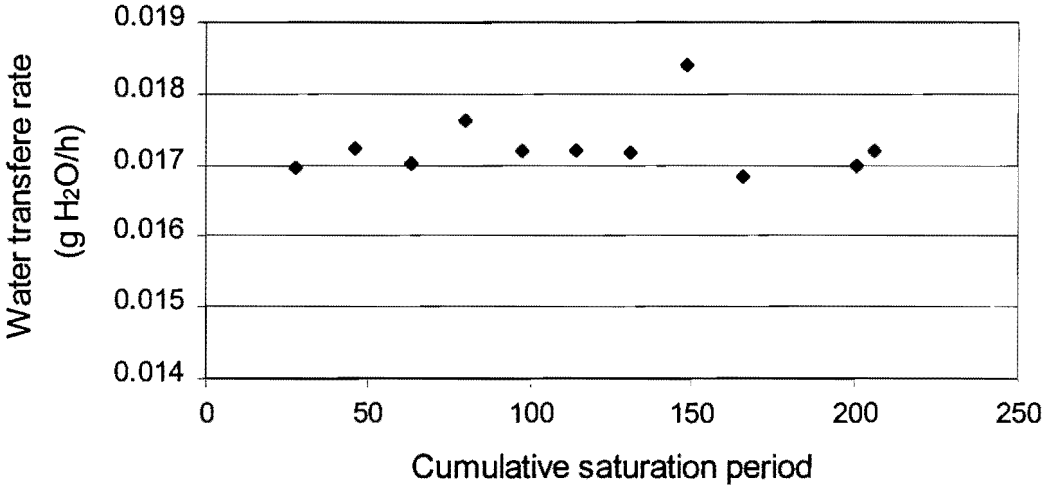

Figure 33: The actual mass of water measured per unit time as a function of the time the sulphuric acid reactors were in use.

As indicated by figure 33, no appreciable change in the water content of the reaction gas due to stripping of water out of the sulphuric acid occurred during the 200 hour saturation period.

The reliability of the measured mole fraction of water vapour depends on the accuracy of the weight measurements. A three-digit scale is in effect only accurate to two decimal places. The weighing practice was kept as consistent as possible to increase the reliability of the measurements. The resulting average calculated mole fraction of water vapour in the gas stream was $(2.00 \pm 0.05) \times 10^{-3}$ for the equilibrium runs. In one experiment the mole fraction water vapour in the hydrogen gas was increased to $(3.52 \pm 0.02) \times 10^{-3}$ to determine the oxidation state of vanadium in the slag.

Leak detection was performed before each equilibrium run by filling the gas line with pressurised Helium gas (pressures around 12 cm Hg were applied) and checking for leaks with a hand-held helium detector. Leak checks performed on the furnace itself will be discussed later this section.

The line pressure before and after the water bath was measured using mercury manometers. The pressure above the acid solution is important for calculating the actual as well as equilibrium amount of water (mole fraction) in the hydrogen stream. Figure 34 compares the actual amount of water transferred, with the equilibrium amount of water (calculated using the following values and equation 25 in the literature section).

Acid composition: 75.7% H_2SO_4 (determined from density measurements)
Water bath temperature: See appendix 1
Exposure period to acid reactors: See appendix 1
Gas flow rate: 0.18 Nl/min
Total pressure above acid solution: 0.877 atmosphere

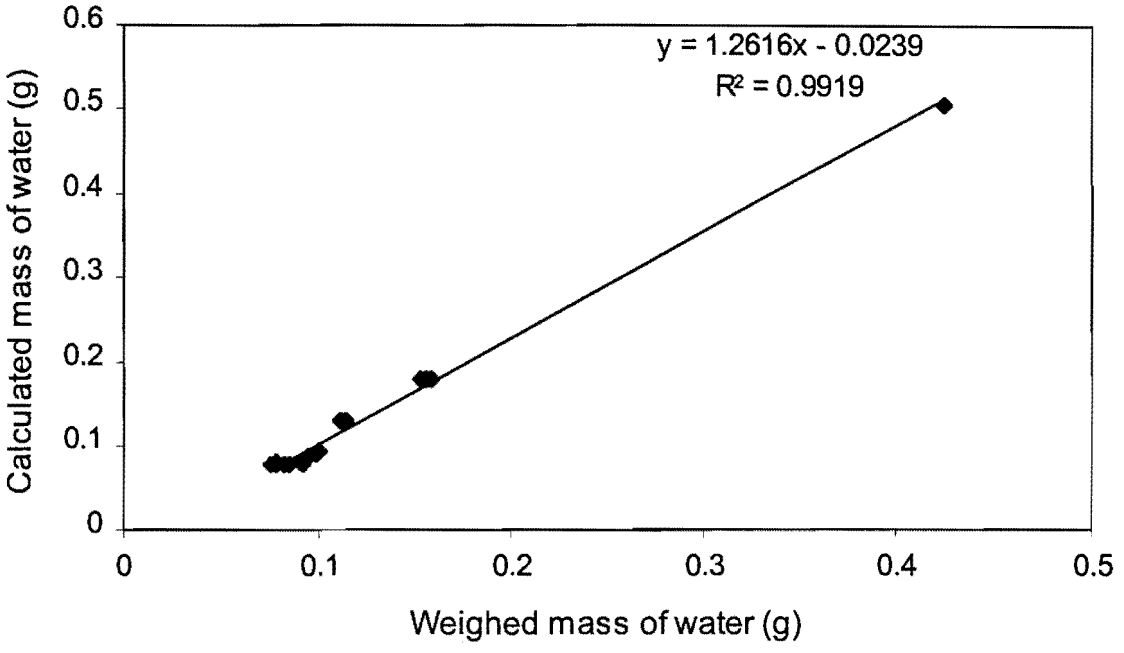

Figure 34: Comparison between the actual weighed mass of water and mass of water calculated assuming equilibrium between water vapour in the gas stream and the acid.

As figure 34 shows, checks performed on the exit gas composition using Drierite-filled columns show a definite deviation from the calculated water content of the reaction gas (calculated assuming equilibrium between the water vapour in the reaction gas and the sulphuric acid solution.) The amount of water in the reaction gas is consistently lower than the predicted content indicating that three reactors in series are not capable of obtaining the equilibrium water content in the reaction gas.

The slopes of the straight lines fitted through the data points in figure 29 and 34, indicate that the system utilising a 75 % sulphuric acid solution is closer to equilibrium than the system utilising a 85% sulphuric acid solution. It is thus easier to obtain equilibrium between the water vapour in the gas stream and the acid if the lower concentration sulphuric acid solution is utilised.

The reactors were designed at first with helical contactors, measuring a total length of around 6 meters, to ensure long intimate contact between the reaction gas and sulphuric acid solution. Despite obvious measures to ensure equilibrium, at the end equilibrium

could not be obtained. This underlines the fact that checks on the exit gas composition between equilibrium runs are absolutely essential. Any published data based on H_2/H_2O-equilibrium utilised to fix the oxygen activity should contain the method used to determine the gas composition. An assumption that equilibrium conditions prevail in the saturator may decrease the value of the work. It can further be concluded that the water content of the reaction gas can be successfully monitored using Drierite as absorbent.

The sulphuric acid solution (after more than 200 hours exposure period) was replaced after the completion of the first series of experiments investigating activity-composition relations. Table 15 shows the calculated composition of the sulphuric acid in the reactors before and after the completion of the experiments

	Initial Composition	Final composition
First reactor	75.7	75.5
Second reactor	75.7	75.2
Last reactor	75.7	75.2

Table 15: Change in sulphuric acid composition. (mass percentages)

It is evident that no appreciable change of the sulphuric acid composition occurred and that 200 hours' exposure with 3 reactors containing 0.5 dm^3 acid can comfortably maintain a constant water vapour level in the hydrogen gas.

2.2.2. The furnace set-up

A schematic representation of the furnace assembly set-up is shown in figure 35.

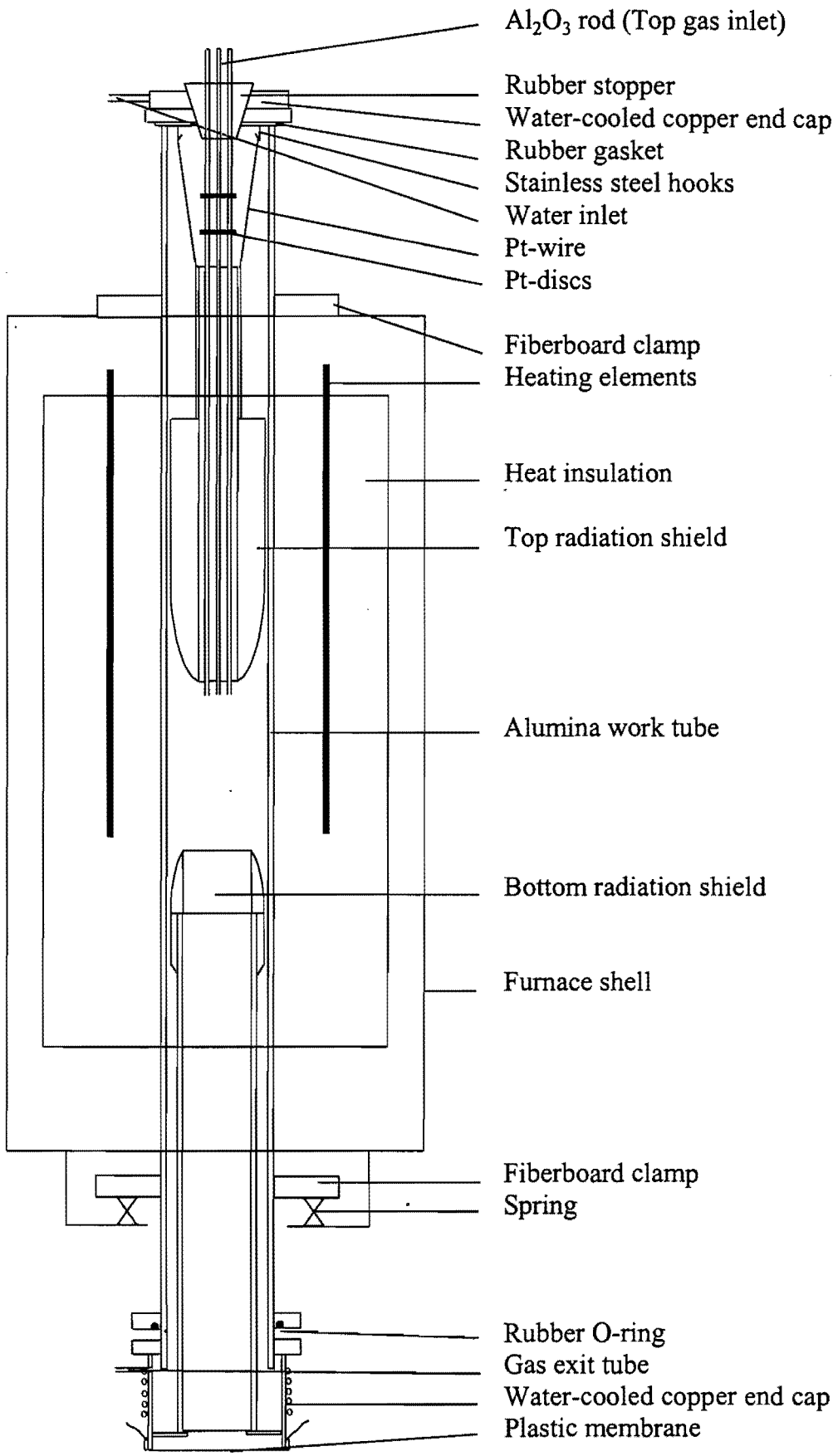

Figure 35: Schematic representation of the furnace assembly set-up

The vertical tube resistance furnace from Pirotherm which employed six equidistant molybdenum disilicide-tungsten carbide heating elements, situated around the furnace tube, was utilized. The specified temperature rating of the furnace is maximum 1800°C for normal heating and cooling cycle. If necessary the furnace could reach 1850°C whereafter the elements should never be switched off and kept at or above 900°C indefinitely.

The maximum temperature that could reliably be obtained in the available laboratory furnace without drastically reducing the life of the elements, was 1700°C. To test the temperature influence on the activity coefficient of vanadium, an experiment was conducted at 1750°C. Due to severe SiO_2 pick-up in the slag no more experiments were performed at this temperature. A single run at 1650 °C was performed to test the influence of temperature on the activity coefficient of vanadium.

The furnace temperature was controlled by an Eurotherm controller/programmer using a Pt-40%Rh/Pt-20%Rh thermocouple that was positioned next to the furnace tube, close to the hot zone. The exact position and temperature of the hot zone was measured with a hand-held Pt-40%Rh/Pt-20%Rh thermocouple (Bedford,1965) placed at various depths in the furnace tube. During this procedure the lower end of the alumina tube was covered with a plastic film to prevent an updraft of hot air through the furnace tube leading to inaccurate measurements. The temperature profile as a function of position at a programmed temperature of 1600°C is shown in figure 36.

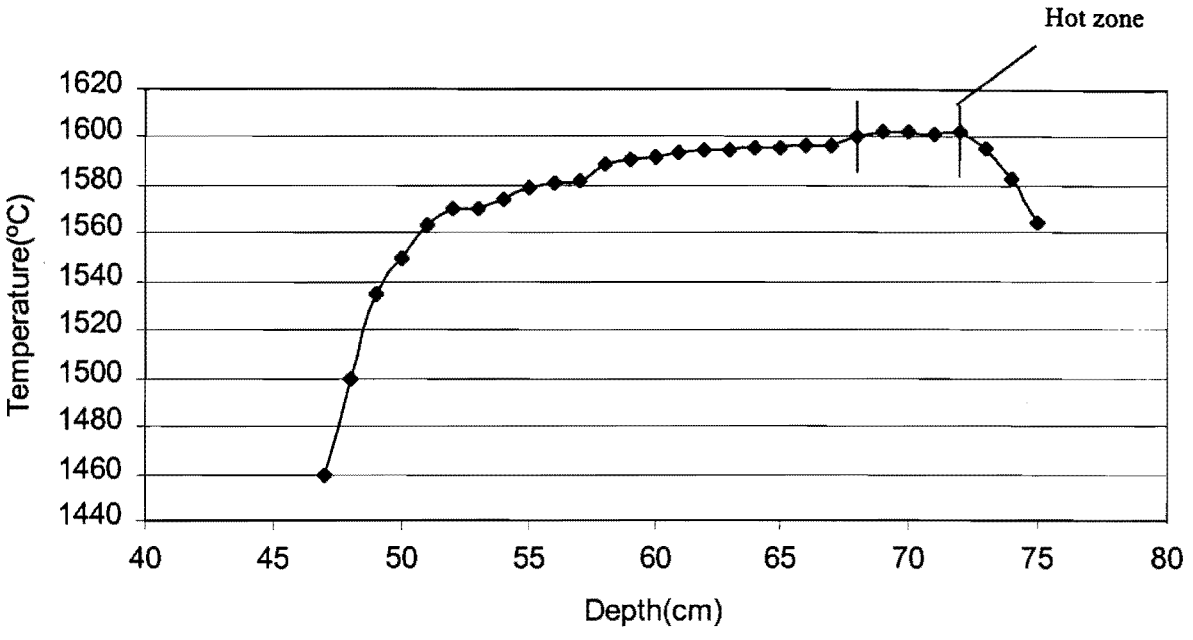

Figure 36: Temperature profile as a function of position. Depth measured from top of alumina tube. Programmed furnace temperature:1600°C; the furnace hot zone was determined to be 50 mm in length. The average measured temperature in this zone was (1601±0.5 °C).

The average temperature of the hot zone measured with the hand-held thermocouple was within 1°C of that indicated by the furnace controller.

The re-crystallized alumina (99.8% Al_2O_3) furnace tube (length 1.2m, O.D. 75 mm, and I.D. 65 mm) was fitted with water-cooled copper heads at both ends. The bottom fitting extended below the alumina tube and was sealed with O-rings lubricated with high temperature vacuum grease. The upper end cap was sealed, before each equilibrium run, to the open flat end of the tube, sealing with a rubber gasket between the tube and the fitting. A steel bracket attached to the furnace tube exerted pressure on the gasket. The upper end cap contained the rubber plug sealed to the fitting, to prevent gas leakage due to the high pressure within the work tube. The rubber plug was used as exit seal for the three alumina tubes used to suspend the vanadium crucible inside the tube and to introduce gas to the synthetic slag. The tubes were sealed to the rubber plug with silicone sealer.

Possible thermal damage (by radiation from the hot zone) to the rubber plug and silicone sealant was prevented by using two round Pt discs fixed to the alumina tubes using Pt-wire. The Pt-disc diameters corresponded to the inside diameter of the alumina tube, which formed part of the upper radiation shield. No thermal damage whatsoever was observed at the surface of the rubber plug.

Radiation shields were present within the furnace tube above and below the crucible. The purpose of top radiation shield was to protect the elements as well as copper end cap from excessive temperatures. The top radiation shield was suspended from the water cooled end cap using 0.5 mm O.D. Pt-wire.

Failure of the vanadium crucible during the first equilibrium run due to complete melting was found to be the result of severe phosphorus pick-up. The radiation shields consisted of fibreboard rings made from a high-temperature fibreboard, temperature rating of 1800°C, and glued together using high temperature cement. The cement originally used to manufacture the radiation shield was an alumina-phosphate cement. Under reducing high-temperature conditions, the cement can be reduced to Al_2O_3 and P_2 (gas). The phosphorus gas apparently alloyed with the vanadium crucible to form a low melting point eutectic component resulting in failure at a temperature 200°C below the melting point of pure vanadium. The radiation shields were reconstructed using the same high-temperature fibreboard rings and pure high-temperature alumina cement. Following severe silica pick-up in the slag within the crucible during early runs, these radiation shields were found to contain mullite, which can be reduced to Al_2O_3 and SiO(g) under reducing high-temperature conditions employed here. In support of this mechanism, silica crystals were observed on the cooler regions of the radiation shields. The continuous precipitation of silica onto the gas carrying alumina tube over extended periods led to failure of the tube due to glass formation. A glass phase could clearly be observed in the vicinity of the crack formed in the alumina tube.

The radiation shields were originally coated with a ±5 mm thick layer of alumina (98% Al_2O_3), applied as a slurry. The alumina layer was subsequently sintered at 1400°C for at least 8 hours in a muffle furnace. The alumina coating and sintering cycle were repeated a number of times, if considered necessary, after the radiation shield was examined for

large cracks. Some cracking of the alumina coating did still occur during subsequent use, causing sporadic contamination of the samples by silica. Those samples which showed more than 2 % silica (mass percentage) pick-up were discarded. Silica pick-up was more severe in slags with higher basicities, presumably due to low silica activity coefficients in these slags. Furthermore, there was a direct correlation between the creep behaviour and the silica content of the slags. Severe slag creep was observed in some early experiments due to severe silica pick-up from radiation shields. Slag creep was prevented, to an extent, by reducing silica pick-up by coating the radiation shields, machining two grooves into the inner wall near the top of crucible and also by dividing the opening of the crucible into two using a 0.1mm vanadium wire (See figure 38).

2.2.3. Quenching set-up.

The lower-end of the furnace tube was sealed with a PVC membrane, thickness of 30 μm, wrapped over the furnace tube opening, with a layer of vacuum grease as sealant between the copper end cap tube and the plastic film. The PVC film was held in position by using a hose clamp pressing onto a (0.1 mm-thick, 20mm wide) PVC band preventing the thin plastic film from being cut by the clamp.

The PVC-covered end cap was immersed in water, contained in an aluminium container through which water ran continuously. A large container/reservoir situated below the aluminium container was continuously filled by the overflow of the top container. When the water level within the reservoir reached a certain height, a pressure sensitive switch activated a pump located at the bottom of the reservoir.

The quenching set-up shown in figure 37, consisted of two single bore alumina tubes (I.D. 2.5 mm) containing molybdenum wires of 1 mm in diameter. The bottom protruding molybdenum wires were bent to form two hooks. The top hole from which the thick wires protruded (above the furnace tube) was sealed by silicone sealant. The crucible was suspended from the two molybdenum wire hooks by means of a thinner (0.3 mm diameter) connecting molybdenum wire. Solid-state diffusion is very much possible at 1700 °C and ultra-low partial oxygen pressures result in oxide-free contact surfaces. Solid-state welding occurred between the thick molybdenum hooks and the thin

connecting wire preventing quenching of the sample after equilibration when a current was passed through the molybdenum wires. This welding problem was prevented by applying graphite dag to the molybdenum wire hooks.

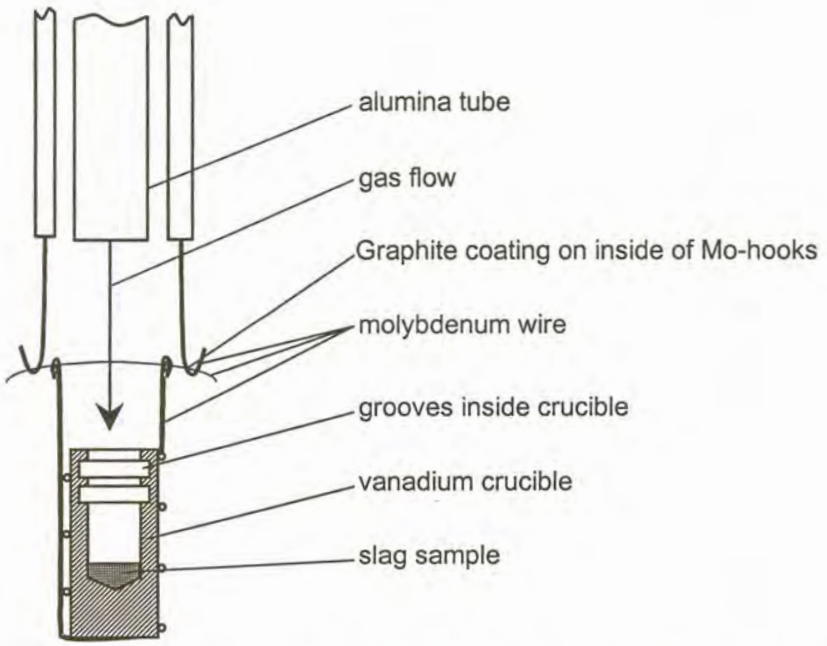

Figure 37: Detail of the configuration used to suspend the vanadium crucible inside the tube furnace, and to bring the reaction gas into contact with the slag.

Post-experimental investigations of the alumina tubes containing the thick Mo-wire showed a continuous layer of black dust, suggesting possible sublimation of the carbon at the experimental conditions. No visible carbon layer was observed on the Molybdenum hooks exposed to 1700°C, in contrast with the experiment performed at 1650°C where a small amount of carbon could be observed. A much larger applied potential was needed to melt the bridge wire in case of the 1650°C-experiment indicating the possible occurrence of a relative thick layer of carbon compared to the layer at 1700°C. Nevertheless, the carbon coating of the hooks has proven to be a successful measure against molybdenum welding under high-temperature reducing conditions.

The sample was hence removed from the furnace by applying an electrical current to the thick molybdenum wires protruding from the top of the alumina tube. This led to the melting of the thinner wire, subsequently releasing the crucible to fall through the PVC membrane into the container containing water. Rapid cooling of the quenched sample was hindered by a water vapour "blanket" surrounding the crucible. Despite expecting a

homogenous glass phase to be present in the vanadium crucible, some slags contained a number of non-equilibrium phases resulting in larger variations on the analysed mole fraction vanadium in the slag. (See the section 2.3.3. on sample analysis).

2.2.4. Crucibles

Equilibration of the slag with the selected gas composition was performed in vanadium crucibles. The crucibles were manufactured by turning and drilling the crucibles out of high purity vanadium rod. (99,9%). The dimensions of the crucible are given in figure 38.

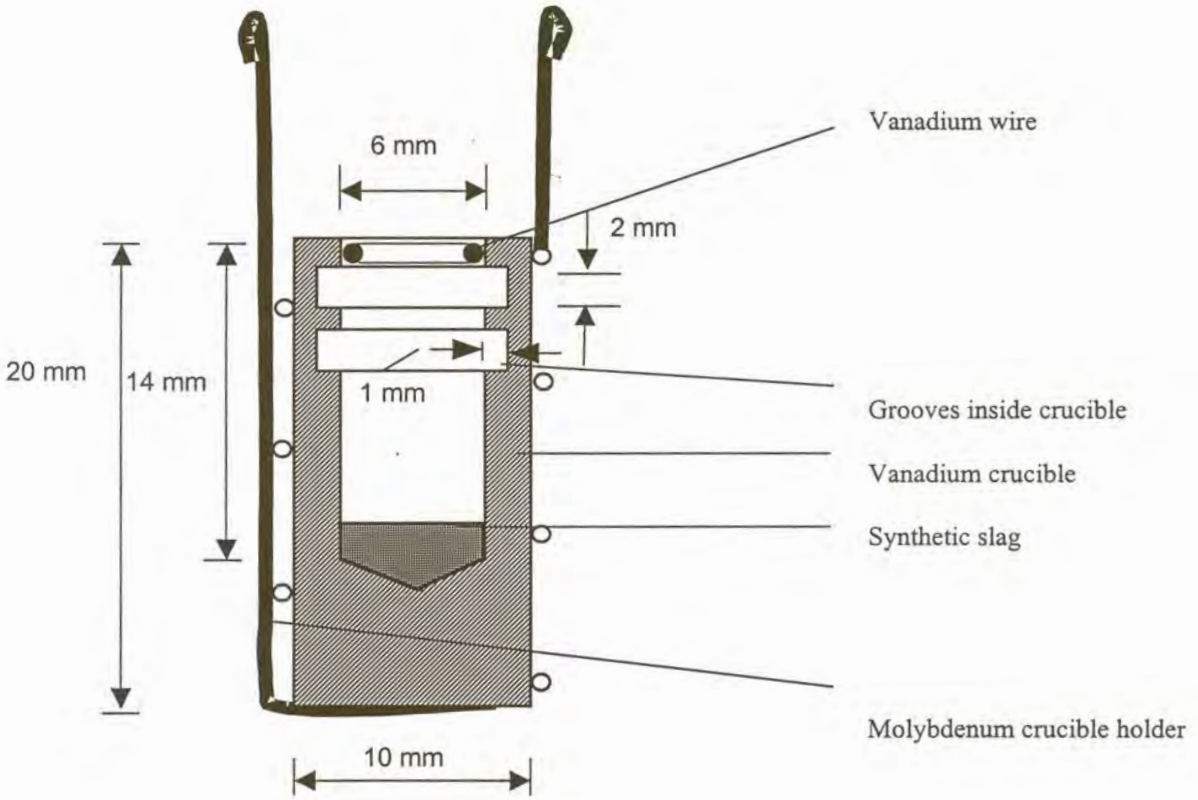

Figure 38: Schematic representation of pure vanadium crucible being used.

By using a pure vanadium crucible, the use of a separate metal phase was avoided. The vanadium crucible supplied all the vanadium needed to attain equilibrium between the container and vanadium oxide in the synthetic slag. Each crucible was contained in a wire crucible holder made from 1 mm diameter molybdenum wire. The crucible holder

2.3. Experimental procedure

2.3.1. Slag preparation

The maximum temperature that could be obtained reliably in the available laboratory furnace was 1700 °C. The $CaO-Al_2O_3$ slag investigated in this study covered the range of liquid compositions at 1700°C as shown in figure 39 and Table 16.

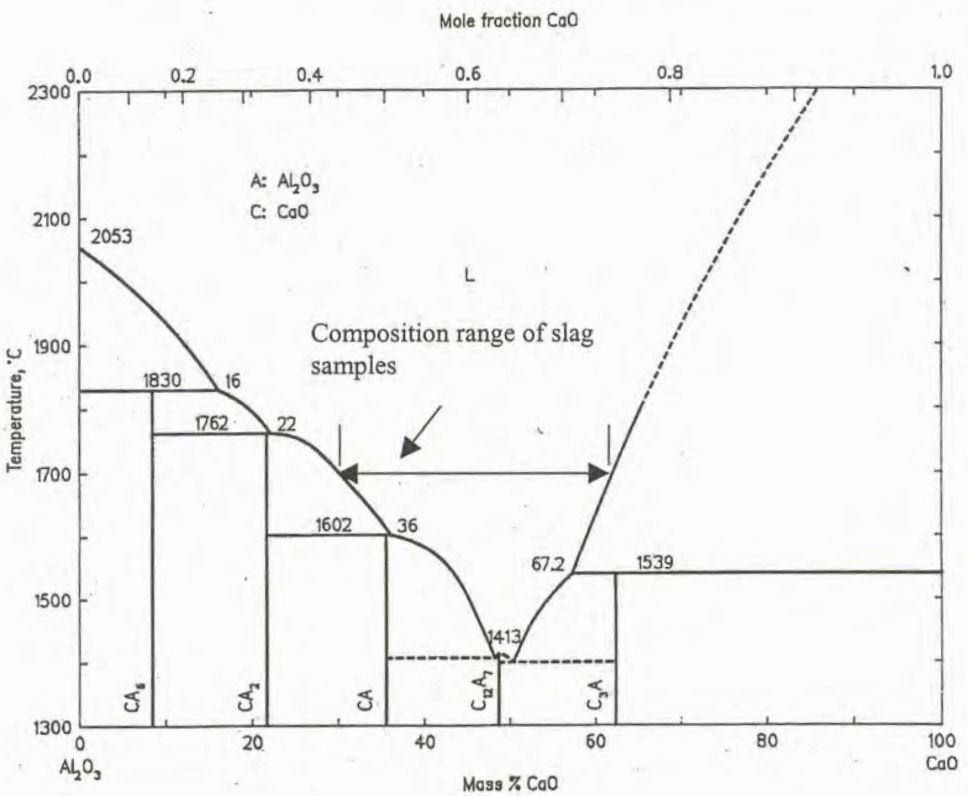

Figure 39: $CaO-Al_2O_3$ phase diagram showing the composition range of the slag samples (Verein Deutscher Eisenhüttenleute,1995).

	Slag 1	Slag 2	Slag 3	Slag 4	Slag 5	Slag 6	Slag 7
% CaO	25	33	29	41	49	37	45
% Al_2O_3	75	67	71	59	51	63	55

Table 16 : As-mixed compositions (mass percent) of the slag melts studied.

The following chemicals were used to make up the slag mixtures shown in Table 15 before equilibration: GP-grade V_2O_5 (assay: >99%), V (assay: 99.9%), $CaCO_3$ (assay: 99.5%), MgO (assay: 98%) and Al_2O_3 (assay: 99%). The first few experiments concentrated on the effect of MgO on the amount of oxidic vanadium in slag. Unfortunately, it was not possible to establish the effect of MgO under equilibrium conditions. No MgO originally added to the slag samples could be retained after equilibration because magnesium has a significant equilibrium vapour pressure.(See section in literature study). It was subsequently assumed that MgO behaves similarly to CaO in the industrial furnace on a molar basis (as far as the effect on VO_x activity is concerned) because both oxides show strong basic behavior in low basicity slags. For this reason, the experimental work concentrated on CaO-Al_2O_3 slags.

Due to the problem of hydration of the CaO in pure form, high grade $CaCO_3$ was used as source of CaO. Calcination of the $CaCO_3$ was performed at 1200°C for 5 hours in a muffle furnace, heated by silicon carbide heating elements, and using a Pt-crucible for containment of the powder. After calcination, the calcium oxide was cooled in a water free atmosphere by placing the Pt-crucible with the contents, still at 1200°C, directly into a desicator. Only a few minutes was allowed between the subsequent crushing of the CaO pellet and the weighing of the powders, to prevent any changes occurring in the composition of the CaO.

The Al_2O_3 powder was dried by heating at 800°C for 5 hours. Samples (typically 20g) were made up by weighing the required mass of powders on an electronic mass-balance, reporting the weight to the nearest milligram, and mixing these powders thoroughly in a swing mill for 5 minutes. After thorough mixing, the pellets (15mm diameter and 20mm in height) were pressed and sintered for 3 hours at 1200°C, crushed and re-mixed. This was followed by another pelletizing and sintering cycle. According to need, pieces of 0.2g were chipped from the pellet and enriched with vanadium by adding pre-determined amounts of V_2O_5 or metallic vanadium powder (particle size: 5μm) to the chunks. The chunks with the vanadium additions were thoroughly mixed in a swing mill before charging into the vanadium crucible. The mixed powder was compacted to ensure the maximum amount of reagents to be present within the crucible. The crucible was filled to

just below the first groove, which was machined into the inner wall. The slag depth in the crucible after melting was about 2.5 mm, yielding a slag mass of ca. 0.2g.

2.3.2. Experimental run.

The crucible containing the slag was introduced cold to the furnace, then heated at 2°C/min to 1400°C under purified argon. The gas stream was switched to the hydrogen-water mixture at 1400°C. Subsequent heating to the equilibration temperature was at 1°C/min holding the sample at this final temperature for 6 hours before quenching. Some minutes before quenching the hydrogen-water mixture was replaced by purified Argon for safety reasons. After quenching the sample was retrieved from the water, and the perforated PVC membrane was replaced with a new layer of PVC with the furnace still at the equilibration temperature. Oxidation of molybdenum occurs even in deoxygenated Argon at 1700°C. Hence, after the replacement of the PVC membrane the Argon was again replaced by hydrogen, for the duration of the cooling cycle. Prior to opening, the furnace was once more flushed with Argon. The thick Molybdenum wires lasted for 5 equilibration cycles before needing replacement.

2.3.3. Sample analysis

After being retrieved from the water the crucible with slag was dried for 10 minutes at 100°C. The crucible was mounted in an epoxy resin (impregnated under vacuum). Polymerization of the resin was performed at 90°C for 4 hours. Following polymerization, the crucible was sectioned along its axis using a diamond cut-off wheel. Despite using a diamond cut-off wheel, it still took half an hour to cut through the supposedly pure vanadium crucible.

From the XRD-pattern, shown in Figure 40, the presence of vanadium nitride phases are identified in the vanadium crucible after equilibration.

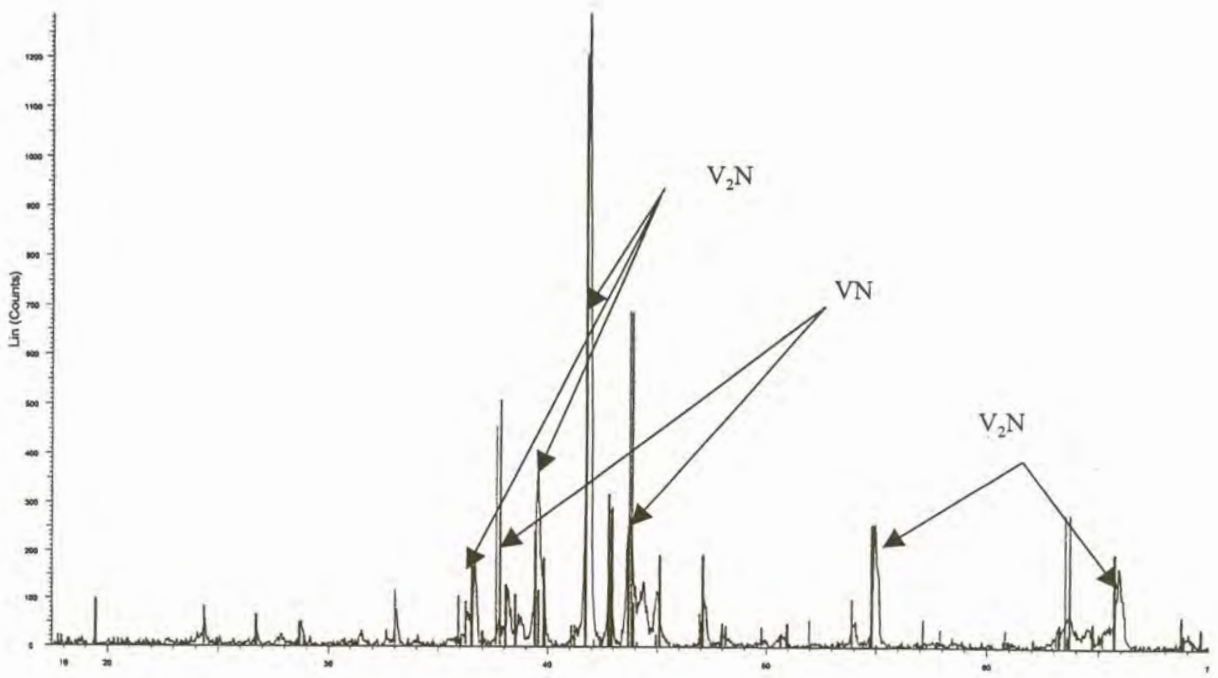

Figure 40: XRD-pattern of vanadium crucible after equilibration.

Vanadium readily reacts with nitrogen, most probably an impurity in the Argon, at 1700°C to give rise to the vanadium nitride phases. These vanadium nitride phases are extremely hard and show great cutting resistence. The sectioned vanadium crucible was subsequently polished down to 3 microns using diamond paste. Following polishing, the crucible was coated with a thin layer of carbon before chemically analysed by energy dispersive x-ray analysis (EDX) using a Joel 5800 Electron microscope with a microanalyser. Other bulk chemical analysis techniques could not by used, since the slag, specially low basicity slags, contained vanadium metal particles (whether as a result of partial reduction of the vanadium oxide which had been added as V_2O_5 to the slag mixture, or of unreacted vanadium metal powder). Entrained vanadium metal particles are shown in figure 41.

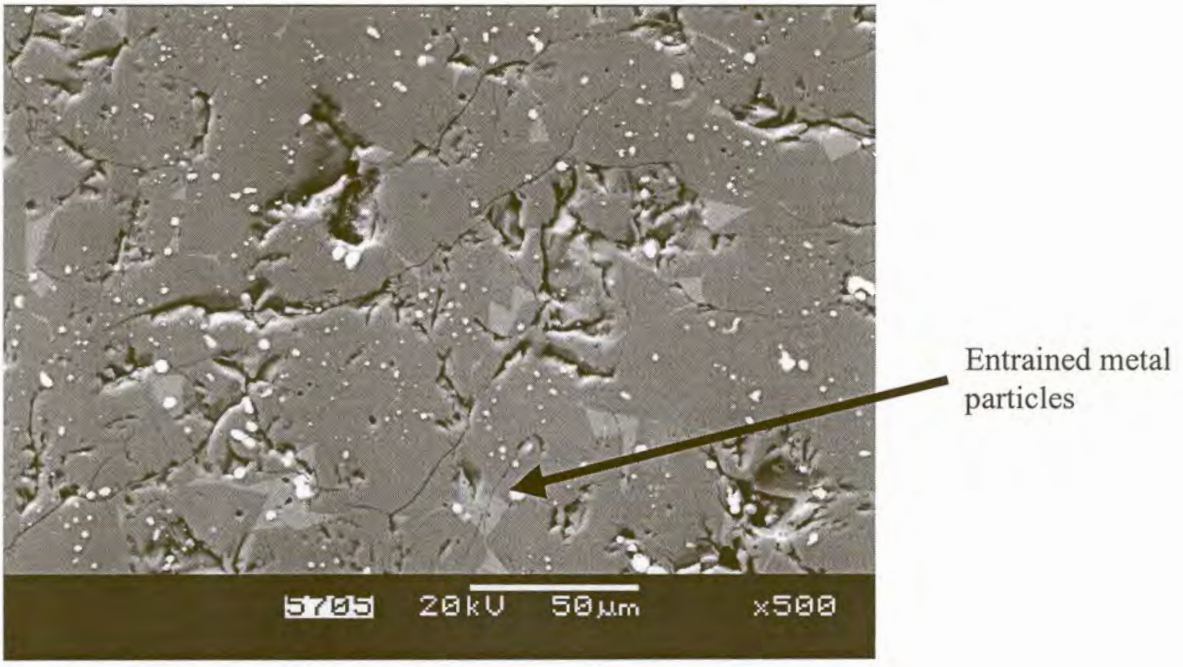

Figure 41: Back-scattered electron image of equilibrated slag sample showing entrained metal particles.

By examining the sample with back-scattered electron imaging, such metal particles were readily discerned, and avoided during EDX analysis. The analyses were performed using 20 kV acceleration voltage at a working distance of 10mm, using 100 seconds of analysis time. A total of 30 fields was typically analysed per sample, using this set of analyses to calculate the 95% confidence intervals on the average $CaO:Al_2O_3$ ratio, and average mole fraction of vanadium.

The solidified slag typically contained two or more crystalline phase, and care was taken to ensure representative sampling of all the phases. Figure 42 and 43 depict cases where more than two crystalline phases were identified.

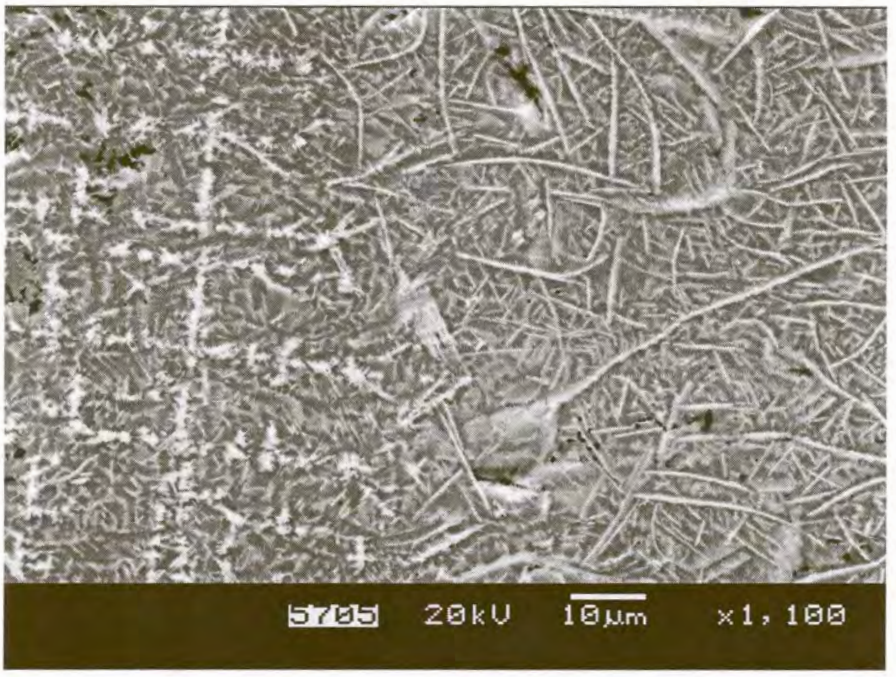

Figure 42: Back-scattered electron image of slag 7 after equilibration, showing more than two crystalline phases.

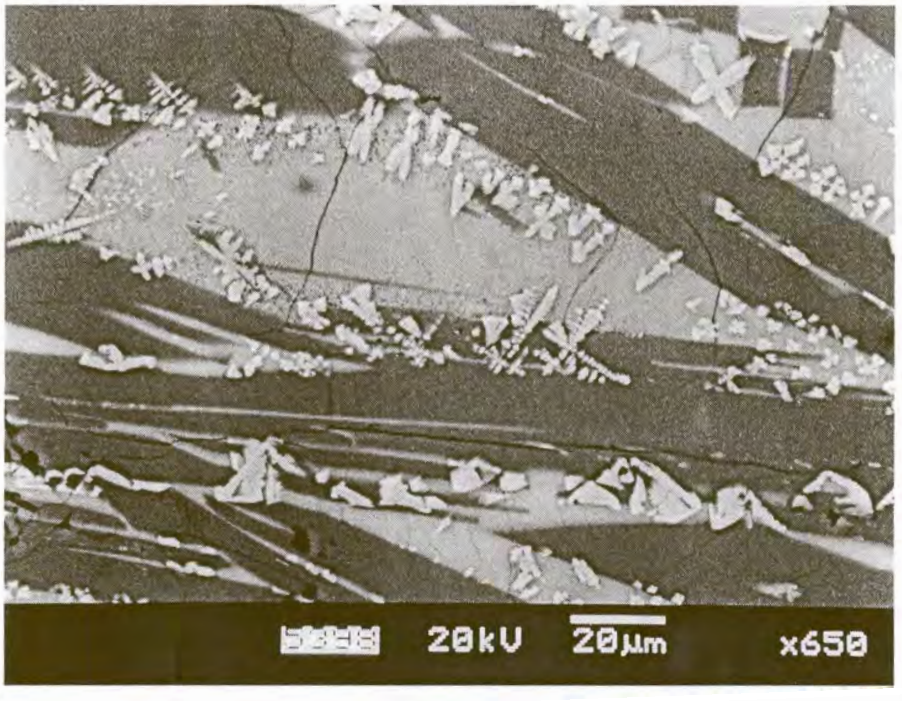

Figure 43: Back-scattered electron image of slag 5 after equilibration, showing more than two crystalline phases.

A combination of relatively slow cooling, due to the water vapour cloud surrounding the crucible during quenching, and the phase stabilizing effect of vanadium on the high basicity slags ($CaO:Al_2O_3$ >0.7) gave rise to formation of multiple crystalline phases. The high basicity slags ($CaO:Al_2O_3$ >0.7) usually did not contain any entrained vanadium metal particles.

3. Equilibrium time determination

Two possible rate-determining steps were considered – gas-phase mass transfer (of H_2O to or from the gas-slag interface) and mass transfer of $VO_{1.5}$ within the slag. To quantify the former, the correlation as used by Belton & Belton (1980) was employed to find the mass transfer constant of H_2O in the gas. No data on the diffusivity of vanadium cations in $CaO\text{-}Al_2O_3$ could be found, but data for transition metal cations (Fe^{2+}, Fe^{3+} and Mn^{2+}) were used to estimate the likely range of diffusivities (Verein Deutscher Eisenhüttenleute,1995). These data are given in Figure 44, with extrapolations to the equilibration temperature of 1700°C. From these data, the diffusivity is estimated to be at least 6×10^{-10} m^2/s.

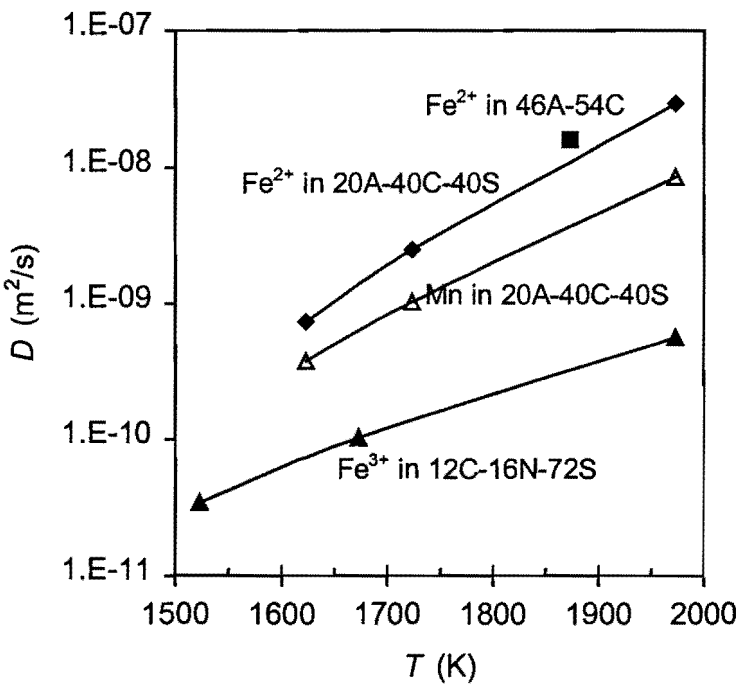

Figure 44. Literature data on diffusion coefficients of transition metal ions in slags similar to those used in this work. Slag compositions are given as mass percentages, where "A" refers to Al_2O_3, "C" is CaO, "S" is SiO_2, and "N" is Na_2O. The two data points at the lower temperatures give the temperature range for which the data are reported, and the line to 1973 K gives the extrapolation to the temperature used in this work.

Because of the low oxidizing capacity of the H_2O/H_2 ratios implemented in this work, care had to be taken that equilibrium could be obtained from both sides i.e. both from higher than equilibrium and lower than equilibrium vanadium oxide concentrations in the slags.

$VO_{1.5}$ mass transfer in the slag is possibly rate determining. Vanadium metal powder was charged in the initial mixtures to assist with the diffusion process by reducing the actual diffusion distance, which would have been 3mm if no powder was used (i.e. the radius of the pure vanadium crucible). Thorough mixing was ensured by grinding of the chunks of pellets with the vanadium or vanadium powder addition to a powder in a tungsten carbide grinding vessel. Another sample was loaded with vanadium oxide in the initial slag mixture to determine if the same final vanadium content, as in case of the sample containing pure vanadium metal, could be obtained. All these equilibration runs were conducted at a CaO: Al_2O_3 ratio of 1 and at 1700 °C (See experiment 1 and 3 in Table 16). The activity of oxygen was kept constant by using constant H_2O/H_2 ratios. The initial assumption that 6 hours should be sufficient if slag-mass transfer is the rate-determining step (for the lower band of the estimated diffusion) was confirmed by the two experiments.

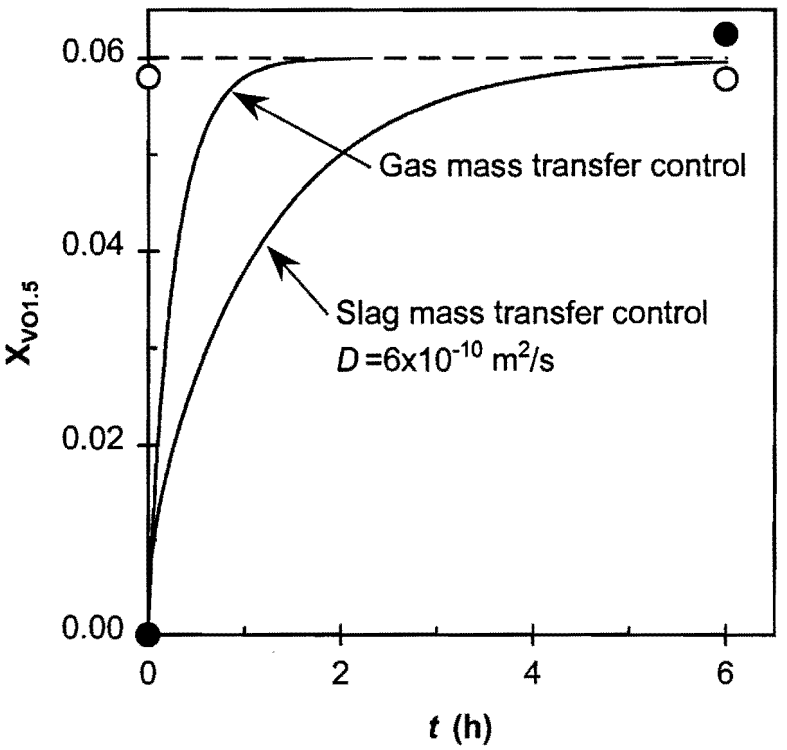

Figure 45. Calculated change in the average $VO_{1.5}$ content of the slag, for respectively gas phase mass transfer control and slag mass transfer control (lower-bound estimate of diffusivity). The data points give the actual change in vanadium content for a slag which contained no vanadium oxide to start with (filled circles), and one which contained a mole fraction of 0.058 of vanadium oxide at the start of the 6-hour equilibration period at 1700°C.

The same final vanadium oxide content in the synthetic slag was essentially reached, indicating that six hours should be sufficient to reach equilibrium. In this case, the standard amount of vanadium pentoxide, initially added to the synthetic slags, corresponding to a $VO_{1.5}$ mole fraction of about 0.06, happened to be very close to the equilibrium level.

4. Results and discussion.

4.1. Activity coefficient relations.

Table 16 gives a summary of all the experiments conducted, containing the H_2O/H_2 ratio, sample composition, equilibration temperature and vanadium cation mole fraction as well as the respective 95% confidence intervals. (for analyzed vanadium mole fraction and calculated basicity).

The activity of vanadium oxide in the slag, shown in Table 16, was calculated from the equation 41 shown below.

$$K_2 = \frac{a_{VO_{1.5}} p_{H_2}^{1.5}}{a_V \; p_{H_2O}^{1.5}} \qquad (41)$$

After completion of the experimental runs the crucibles were analyzed by EDX, and was found to be pure, with no measurable aluminium pick-up. Hence, the activity of vanadium in equation 41 was taken to be 1. The activity of water and hydrogen was fixed by the gas mixture. After analysing the the mole fraction of vanadium oxide in the slag, the activity coefficient of $VO_{1.5}$ was calculated from equation 42

$$\gamma_{VO_{1.5}} = \frac{a_{VO_{1.5}}}{X_{VO_{1.5}}} \qquad (42)$$

In this calculation, the mole fraction of vanadium oxide in the slag ($Xvo_{1.5}$) was determined from EDX analysis of the amounts of Ca^{2+}, Al^{3+} and V^{3+} in the slag, by taking species which make up the slag to be CaO, $AlO_{1.5}$ and $VO_{1.5}$.Hence the experimentally determined activity coefficients ($\gamma_{VO_{1.5}}$) also refer to this convention.

Experiment	Temp K	moisture (g/h)	X_{H2O}	P_{H2O} (atm)	K	$a_{VO1.5}$	N $X_{VO1.5}$	95% Confidence limit	$\gamma_{VO1.5}$	Basicity	95% Confidence limit
1	1973	1.70E-02	1.97E-03	1.72E-03	8264.77	0.721	6.24E-02	0.214	11.54	0.90	0.009
2	1973	1.70E-02	1.97E-03	1.73E-03	8264.77	0.724	7.74E-03	0.129	93.52	0.64	0.013
3	1973	1.76E-02	2.04E-03	1.79E-03	8264.77	0.762	5.79E-02	0.208	13.17	1.01	0.014
4	1973	1.72E-02	1.99E-03	1.75E-03	8264.77	0.735	8.69E-02	0.975	8.46	1.70	0.021
5	1973	1.69E-02	1.96E-03	1.71E-03	8264.77	0.715	7.28E-02	0.397	9.82	1.13	0.015
6	1973	1.68E-02	1.95E-03	1.71E-03	8264.77	0.712	6.23E-03	0.067	114.24	0.62	0.004
7	1973	1.68E-02	1.95E-03	1.71E-03	8264.77	0.712	2.21E-02	0.096	32.17	0.63	0.004
8	1973	3.03E-02	3.51E-03	3.08E-03	8264.77	1.717	1.69E-02	0.158	101.83	0.70	0.015
9	1923	0.0156	1.81E-03	1.58E-03	11656.17	0.895	7.42E-02	0.128	12.07	1.00	0.044
10	1923	0.0151	1.75E-03	1.53E-03	11656.17	0.853	9.37E-02	0.699	9.10	1.47	0.009

Table 16: Summary of experiments performed

Before any activity-composition calculations could be performed, the oxidation state of vanadium should first be determined. For a first approximation, the oxidation state of vanadium can be estimated by plotting the oxygen activity as a function of temperature for different vanadium metal and oxide equilibria. (Unit activities of oxide species are assumed). In this case, the equilibrium constant for the different vanadium metal and oxide equilibria was calculated using the correlations of Kubaschewski et al (1992) for the free energy values. At this stage, it should be noted that there appears to be a serious discrepancy between the literature values for the free energies of the vanadium oxide species. For example, the. Kubaschewski et al correlations predict the free energy of solid V_2O_3 to be -1649 244 J/mole, whereas the F.A.C.T. database yields a value of -1673 483 J/mole. This substantial difference - largely due to the difference in the entropy values - changes the equilibrium constant K_2 (see table 17) by a factor 2.1 (being larger if the F.A.C.T. values are used).

$H_2O = H_2 + 0.5O_2$ $K_1 = \frac{p_{H_2}\, p_{O_2}^{0.5}}{p_{H_2O}}$; $\log K_1 = 3.0456 - 13170/T$
$V + 1.5H_2O = VO_{1.5} + 1.5H_2$ $K_2 = \frac{a_{VO_{1.5}}\, p_{H_2}^{1.5}}{a_V\, p_{H_2O}^{1.5}}$; $\log K_2 = -1.8258 + 11331/T$
$2Al + 2VO_{1.5} = Al_2O_3 + 2V$ $K_3 = \frac{a_{Al_2O_3}\, a_V^2}{a_{Al}^2\, a_{VO_{1.5}}^2}$; $\log K_3 = 4.0365 - 25570/T$

Table 17. Equilibrium constants germane to this work
(Correlations fitted for the temperature range 1600°C to 1850°C; temperature in Kelvin for the correlations; reference states are pure solid V, V_2O_3 and Al_2O_3, pure gaseous H_2 and H_2O, and pure liquid Al)

The data point shown in figure 46 indicates the average oxygen activities and the equilibration temperature used to determine the influence of slag composition on the activity coefficient of vanadium oxide. As indicated, the divalent oxidation state of vanadium was expected to be stable for unit activities.

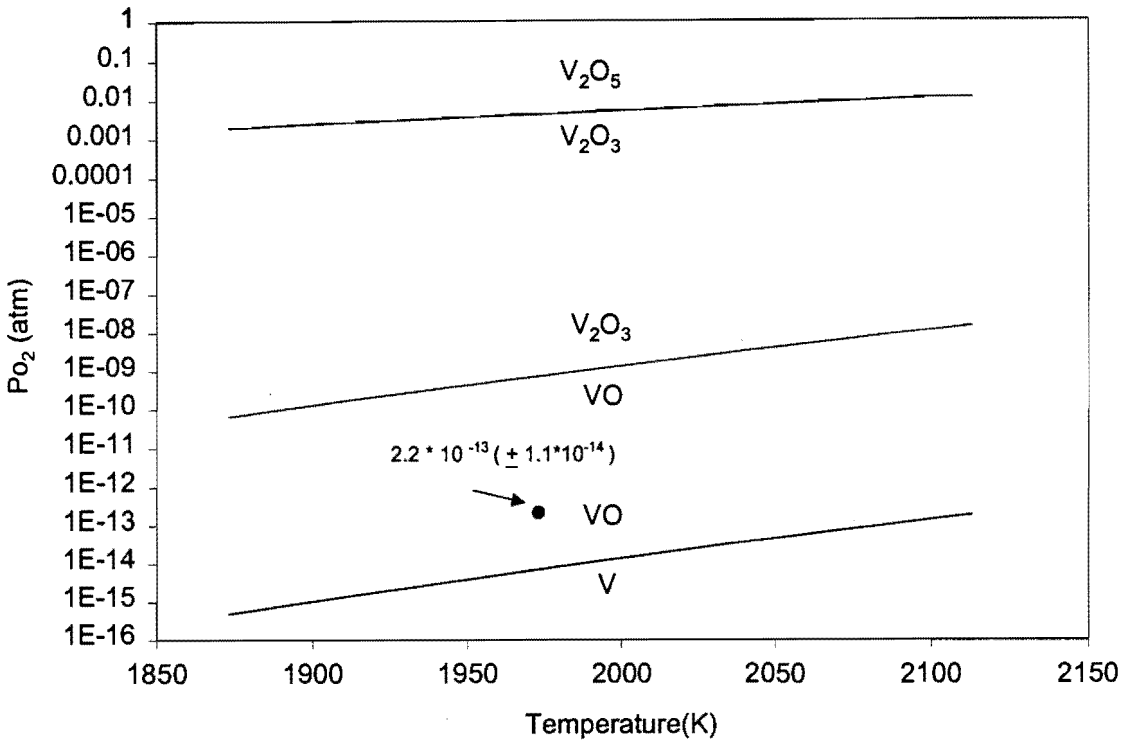

Figure 46: Predicted oxidation state of vanadium. Reference states were pure solid V,VO,V_2O_3 and pure liquid V_2O_5 and the correlations of Kubaschewski et al (1992) were used. Data point indicates experimental conditions.

By conducting an experiment at a higher oxygen activity and at constant basicity and temperature the vanadium oxidation state can be determined more accurately. This was done by changing the water content of the gas mixture to 0.0035 mole fraction water. These results are presented by figure 47, which shows the predicted relative change of the mole fraction of VO_x in the slag as function of the relative change in the oxygen activity for the different equilibria. ($Po_2 = 2.0 \times 10^{-13}$ atm at 1700°C.) The initial water vapour content of 0.0020 yielded an initial mole fraction of VO_x in the slag of 0.0077 (See experiment 2 and 8 in Table 16). The data points on the graph present actual measurements - indicating the best agreement between predicted and measured effects of the change in the oxygen activity to be for the trivalent state.

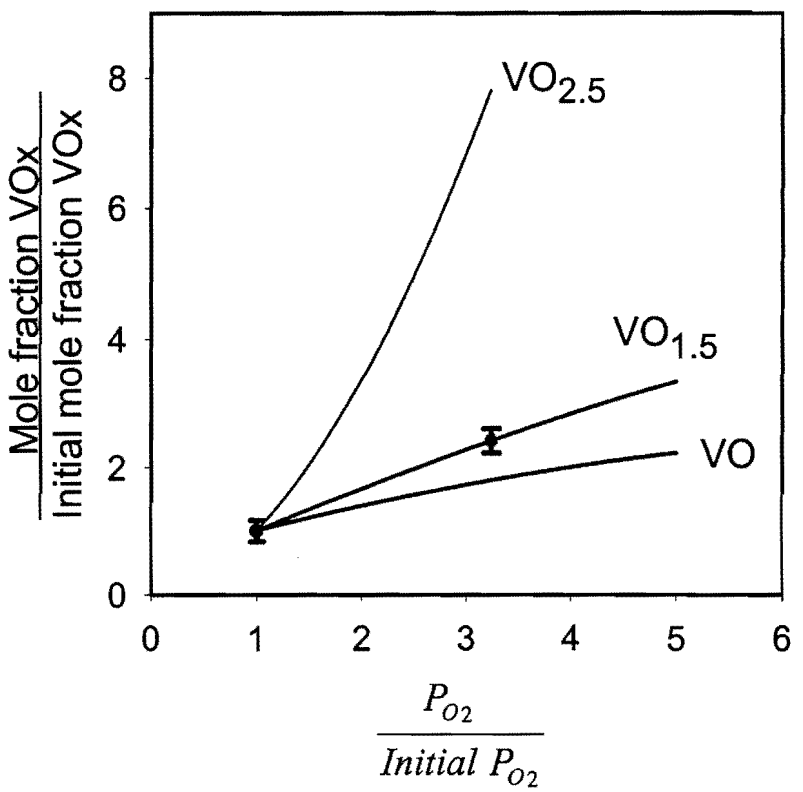

Figure 47: Expected and real vanadium oxide contents of the slag.

The actual mole fraction VO_x as function of the $CaO:Al_2O_3$ ratio is given in figure 48 for experimental conditions as listed in table 16. The effect of the varying of the Po_2 was taken into account during further analysis.

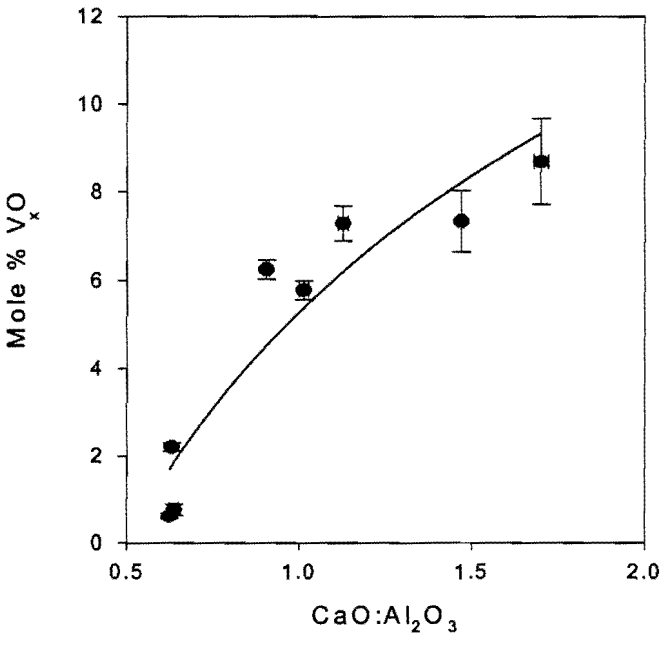

Figure 48: Effect of slag basicity on VO_x content for experimental conditions as listed in Table 16.

Nevertheless, Figure 48 demonstrated the actual amount of soluble vanadium to be strongly dependent on the slag basicity. It is clear, that in order to minimize vanadium loses to the oxide phases the slag basicity should be as low as possible, yielding at best 0.6 mole $\%VO_x$ at a basicity of 0.6 (for the Po_2 values used here).

The determined activity coefficient values of $VO_{1.5}$ are illustrated in figure 49.

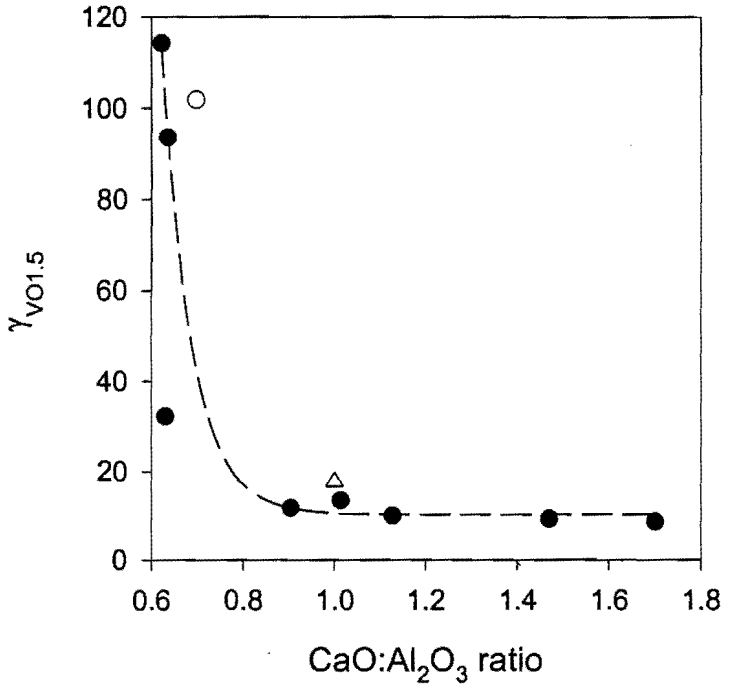

Figure 49. Calculated value of the activity coefficient of $VO_{1.5}$ in CaO-Al_2O_3, based on equilibration runs at 1700°C under a hydrogen-water mixture, with a water mole fraction of 0.002 (filled circles). The open circle (See experiment 8) is for a hydrogen-water mixture (at 1700°C) with a water mole fraction of 0.0035, and the triangle(See experiment 9) for 1650°C.

Figure 49 demonstrates the activity coefficient of $VO_{1.5}$ to be strongly dependent on the slag basicity, with a sharp decrease in the activity coefficient at higher basicities. The measurement of the vanadium oxidation state is indicated by open circle in the figure. Furthermore, the data point shown as a triangle indicates an experiment conducted at 1650°C. As expected, the activity coefficient is not strongly dependent on temperature. This indicates that the laboratory data - conducted at 1700°C - can be used to calculate approximate equilibrium compositions at the furnace tapping temperature of 1840°C.

The reliability of the measured activity coefficients depends on the reliability of the equilibrium constant (which was discussed earlier), and of the gas composition and the chemical analyses. As far as the latter two are concerned, the variation of ±2.5% in the

H_2O content of the gas (as mentioned earlier) yields an uncertainty of ±4% in the activity coefficient (since $a_{VO_{1.5}}$ is proportional to $p_{H_2O}{}^{1.5}$). The largest 95% confidence interval on the vanadium oxide content, expressed relative to the average vanadium oxide content, amounted to 17% for the lower-basicity slags (with the lowest vanadium contents), and 11% for the slags with basicities higher than 0.7. This means that the maximum estimated variability in the activity coefficients (assuming no systematic errors) is ±21% for the lower-basicity slags, and ±15% for the higher-basicity slags. The largest 95% confidence interval on the analysed $CaO:Al_2O_3$ molar ratio was 0.04. See Appendix 2 for the 95 % confidence limits of the experimental results.

From the viewpoint of the ferrovanadium producer, it is clear that efficient recovery of vanadium from the slag is favored by low basicity. This can be achieved by lowering the amount of CaO added to the furnace as burned time.

5. Industrial slag sample investigations

5.1. Introduction

As indicated previously, metal droplet entrainment has been identified as a possible important factor influencing vanadium recovery to the slag. So far, only the effect of slag basicity on the soluble vanadium loss has been discussed. An alteration of the slag composition by adding less CaO will lower the soluble vanadium loss, but inevitably also changing the separation of the solid ferrovanadium phase from the slag phase. One way to assess the effect of slag basicity on metal droplet entrainment is to investigate solidified industrial slag samples.

In addition, the effect of slag basicity on soluble vanadium loss can be compared to the equilibrium results obtained. The purpose of this investigation is, thus, to identify all the phases co-existing in the industrial slag samples as well as to quantify the amounts of vanadium associated with the oxidic and metal phases respectively.

5.2. Oxidic phase analysis

5.2.1. Experimental procedure

5.2.1.1. Sample preparation

A number of factors such as cooling rate, tap temperature and slag volume influence the amount of entrained metal droplets. The amount of entrained droplets is also influenced by the location of the slag samples taken from the bulk slag (i.e. slag closer to the refractory lining solidifies more quickly, resulting in a larger amount of entrained particles). Nevertheless, by taking slag samples at a fixed location within the slag, the effect of slag basicity on droplet entrainment can be assessed semi-quantitatively.

The vertical segregation effect was addressed by investigating the best and worst positions regarding vanadium loss as entrained droplets, by sampling from the top and bottom, at a fixed horizontal position, in the bulk slag sample. See figure 50 below.

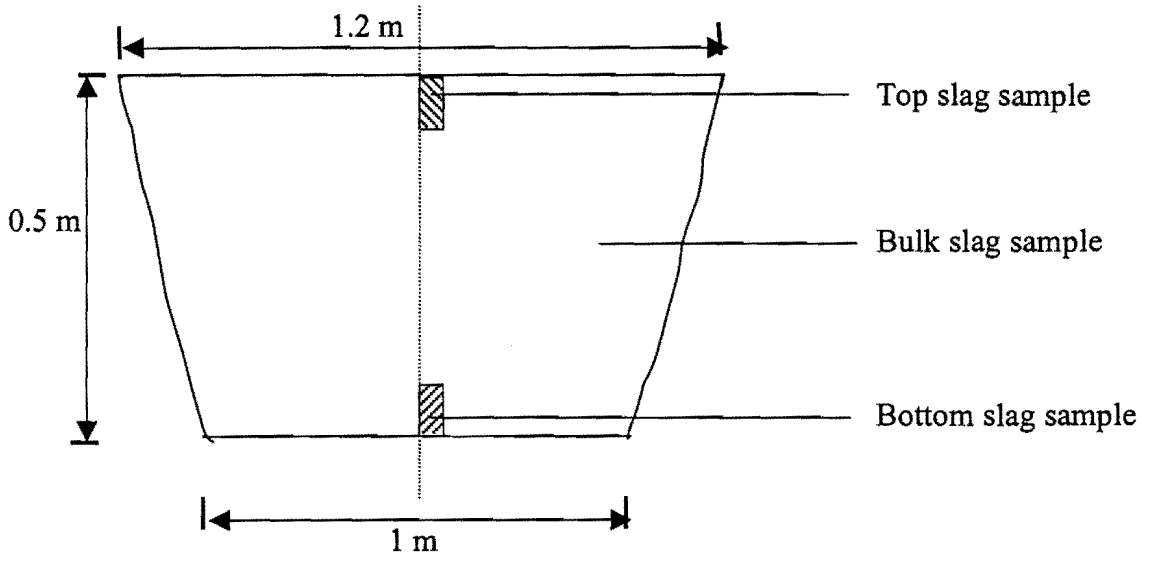

Figure 50: Schematic diagram of a vertical section through the bulk sample showing the location of the samples taken.

To investigate the possible influence of tap temperature on vanadium loss, the slag temperature was also recorded prior to tapping. The temperature readings were taken of the slag pool near the electrodes, through an observation window in the shell, seconds after the arc had been extinquised, using an infra-red pyrometer. Temperature readings of the tap stream could not be obtained due to large dust emissions surrounding the metal tap stream.

The sections were epoxy-impregnated under vacuum, polished, carbon coated and analyzed. Analyses of the oxidic and metal phases were by X-ray diffraction spectroscopy (XRD) and energy dispersive X-ray Spectrometry (EDX). Parts of the samples were milled into powder for XRD analysis. Electron probe microanalyses were done on polished sections using a Jeol 5800 Scanning Electron microscope. Back-scattered electron imaging was first employed to identify all the possible phases, including metal droplets, before quantitative EDX analysis was performed. At first, at least 30 fields were analyzed for a given phase to establish a good mean and small standard deviation. Due to the homogenous nature of the oxidic phases, 10 analyses proved to be sufficient to

establish a good aggregate, and small standard deviation. The following section will focus on investigations performed on the oxidic phase constituent of the slag.

The average chemical composition of the slag samples was determined by performing EDX analysis at the lowest obtainable magnification of 85x. Metal droplets were included in the analysis contributing to higher apparent vanadium levels in the slag. The way in which this was taken into account is discussed later. It was not possible to exclude the metal particles, without raising the magnification and losing the representative nature of the analysis. Around 10 fields were analyzed to establish a good mean and small standard deviation.

5.2.2. Results and discussion

5.2.2.1. Oxidic phase investigations

A back scattered electron image of a slag sample is shown in figure 51:

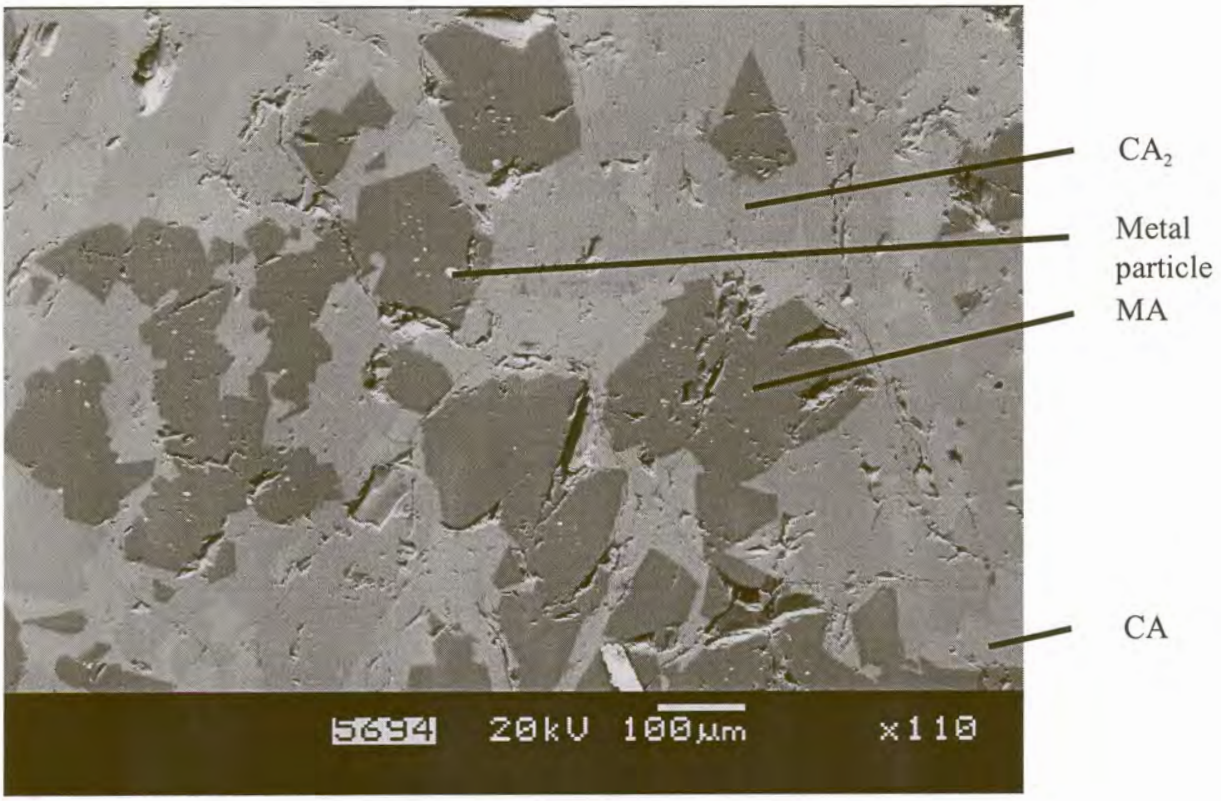

Figure 51: Back-scattered electron image showing the three prominent phases.

The three oxide phases which are visible in figure 51 were identified – based on X-ray diffraction and EDX analysis – as $MgO.Al_2O_3$ (MA), $CaO.Al_2O_3$ (CA), and $CaO.2Al_2O_3$ (CA_2)

All three the phases identified were present in all the slag samples investigated. A fourth phase, shown in figure 52, which is a result of impurities (especially Na) introduced by the vanadium starter material, was also identified in some of the slag samples. Na_2CO_3 or Na_2SO_4 is used as a roasting reagent to react with V_2O_5 in the magnetite ores to form soluble sodium vanadates. Both V_2O_5 and V_2O_3 used as starter vanadium oxide materials in ferrovanadium production are products of the roast / leach process utilized to recover vanadium from ore and vanadium-rich slags. Vanadium pentoxide is mainly exported while V_2O_3 and small quantities of V_2O_5 are used to produce ferrovanadium.

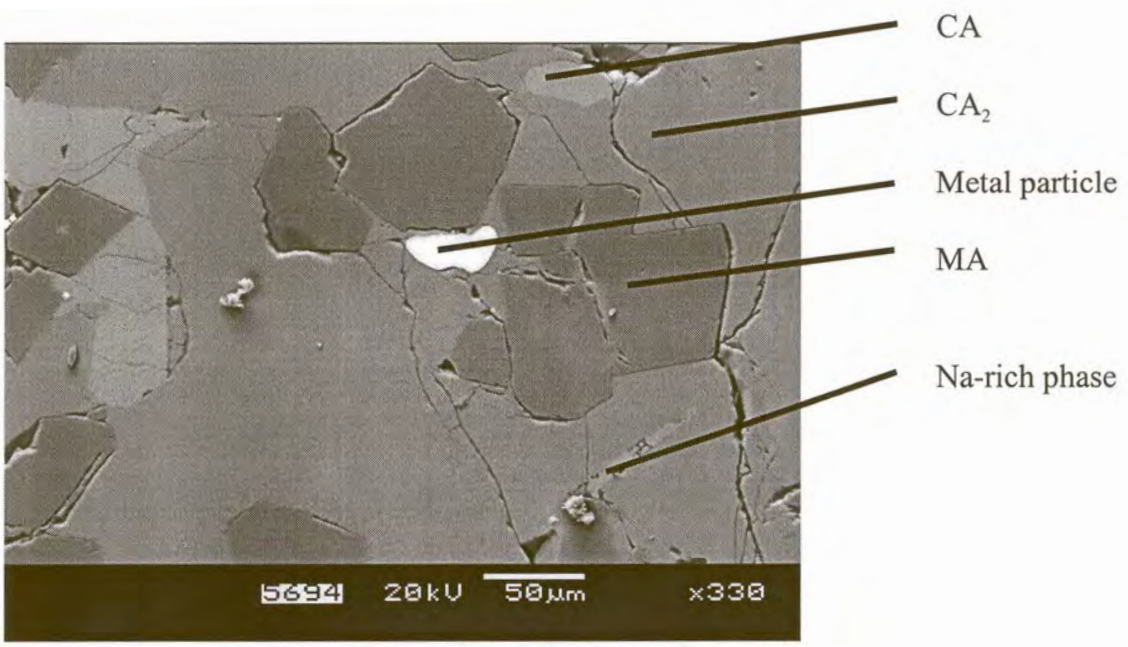

Figure 52: Back-scattered electron image showing the Na – rich phase.

This Na-rich phase usually constituted less than 1 volume % of the slag sample. From time to time vanadium oxide of poor quality was used to produce ferrovanadium, leading to the slag structure shown in figure 53.

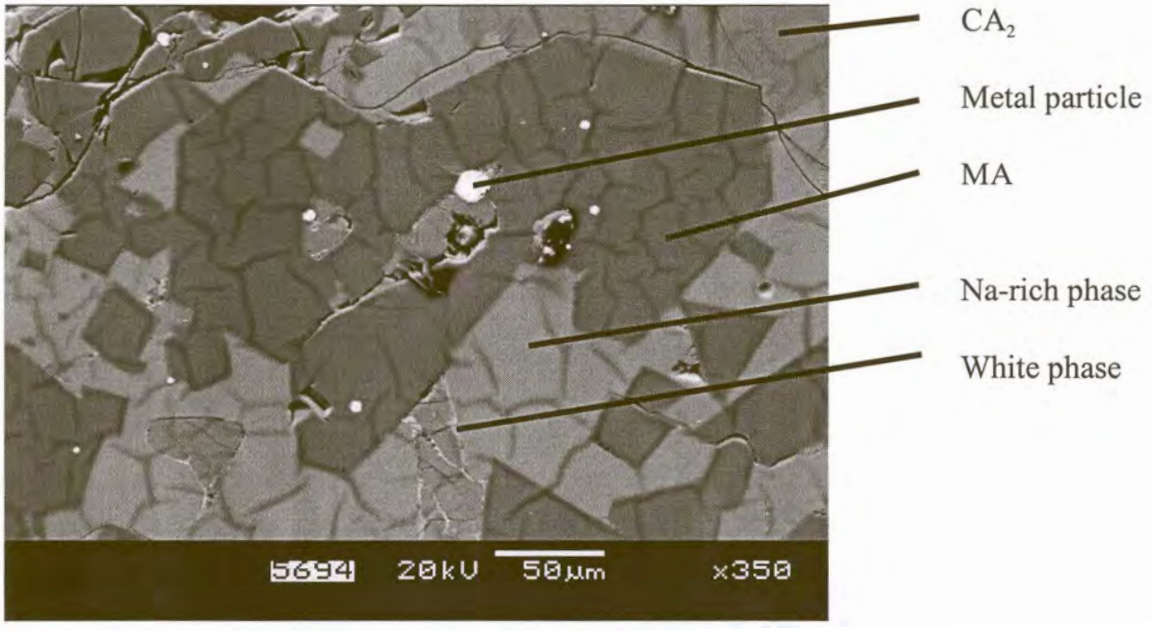

Figure 53: Back – scattered electron image showing a severe case of poor quality vanadium oxide starter material used to produce ferrovanadium.

This figure clearly indicates the Na-rich phase to be present in much larger quantities compared to figure 52. Fortunately, no oxidic vanadium is associated with this phase as indicated by the results shown in Appendix 3 (See slag 7). The detrimental effect of Na in raw material is thus related to higher energy requirements, due to the decrease in exothermicity of the charge, and possibly refractory wear.

For the slags without Na_2O contamination, the locus of the average slag composition lies within the CA-CA_2-MA alkemade triangle, in the primary phase field of MA. During the first stage of crystallization only MA will crystallize from the melt and only solid and liquid will be present, thus enabling crystals of MA to grow. The primary crystals of MA will be large and have an idiomorphic shape since the melt does not hinder their crystallization. The idiomorphic shape of the MA crystals can clearly be seen in figure 51.

It can be concluded that solidification of the ferrovanadium slag follows (to an extent) equilibrium cooling (if the Na-rich phase is neglected, based on the small quantities usually occurring in the slag).

Interestingly, the metal particles occur only on the boundary or within the MA phase as indicated by both figures 51 and 52. The metal droplets (containing mainly V, Fe and Al) have a higher liquidus temperature than the slag (see figure 17), resulting in metal solid formation while the slag is still in the liquid state. On subsequent solidification, the solid metal particles may serve as seed crystals for nucleation of the MA phase, resulting in their occurrence within or on the boundary of the MA phase. It can be concluded that metal droplets occurring in any other phase except the MA phase, are probably the result of entrainment after primary crystallization. This may occur during any slow tapping when molten ferrovanadium is tapped onto semi-solidified slag. The $MgO.Al_2O_3$ (MA) phase was found to be the major repository of oxidic vanadium containing up to 6% V_2O_3 (on a molar basis), compared with less than 0.4% in the CA and CA_2 phases. (See Appendix 3 for chemical analyses)

The calculated chemical composition based on EDX analysis indicates the Al_2O_3-content of the MA phase to vary between 70 and 75%, compared to the (stoichiometric) 72% obtained from the ternary phase diagram. The MgO content of the MA phase never

exceeds 24% (on a mass basis) compared to the 28% given by the phase diagram. The MgO-content of the MA phase is therefore distinctly lower than in the equilibrium MA phase. The MA phase was confirmed, by XRD analysis, to have a spinel-type structure. The general formula of the spinel can be written as $A^{2+}B_2^{3+}O_4$, where A^{2+} can be iron, chromium, magnesium, zinc, vanadium and manganese, and B^{3+} can be aluminium, iron, chromium or vanadium. Vanadium can therefore substitute either magnesium or aluminium in the spinel-type lattice to form a solid solution without altering the lattice spacing of the structure much. The dominant oxidation states of vanadium can be either V^{2+} or V^{3+}.

Such substitution can be clarified by plotting the normalized Mg and V cation fractions of the MA phase - as obtained by EDX analysis- against the Al fraction, as shown in figure 54.

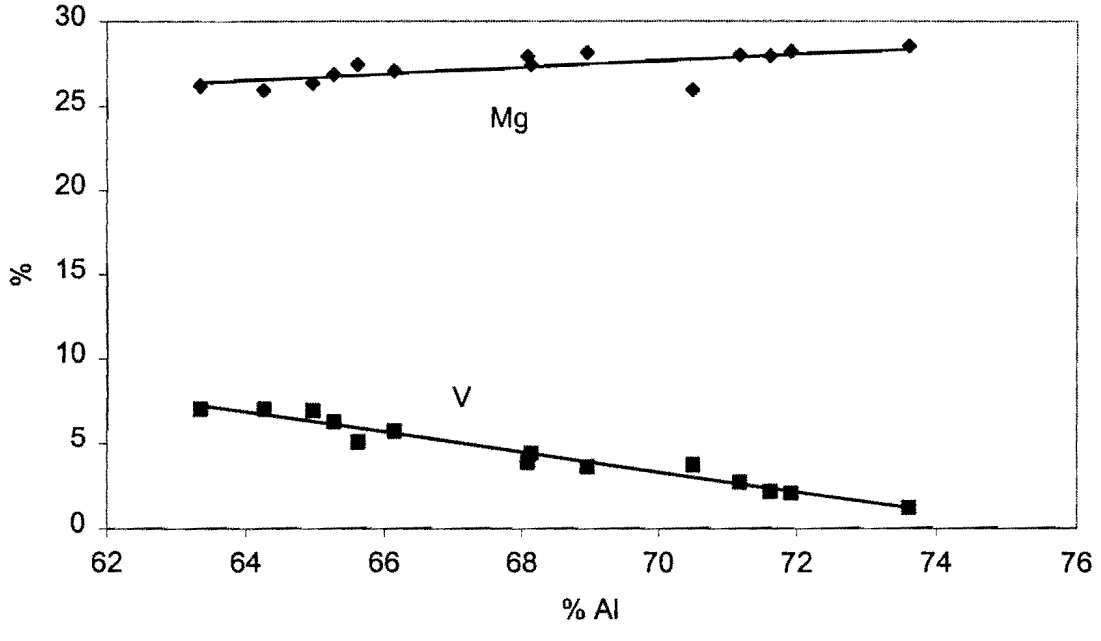

Figure 54: The effect of the Al cation fraction on the fractions of Mg and vanadium in the MA phase as obtained by EDX analysis (mole percentages).

Figure 54 clearly indicates that vanadium substitutes mainly aluminium in the spinel-type structure. The partial substitution vanadium of magnesium is also evident because the actual Mg^{2+} fraction is lower than the expected 31 %. The dominant oxidation state of vanadium in the structure would therefore be V^{3+}. The Al_2O_3 content of the MA phase has

therefore a strong effect on the vanadium content of this phase, as indicated by figure 55 which shows the calculated oxide fractions of the equilibrium MA phase.

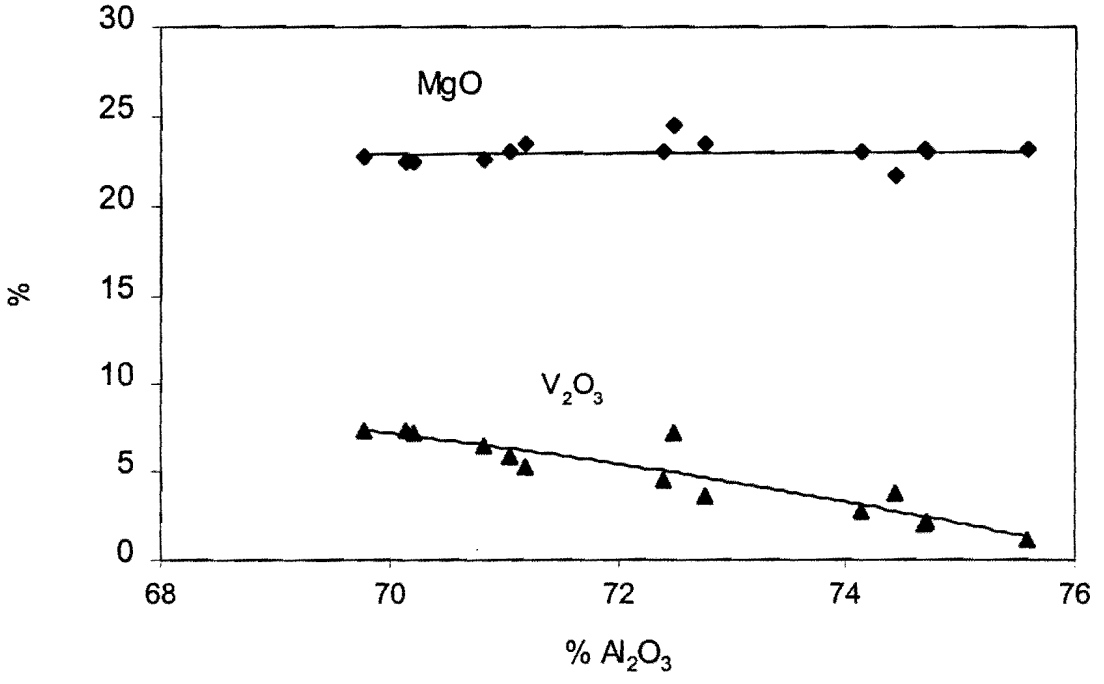

Figure 55: Recalculated chemical compositions of the MA phases showing the effect of alumina on the V_2O_3 content of these phases (mass percentage).

In conclusion, vanadium is associated in the solid state with primarily the MA spinel-type phase where V_2O_3 substitutes Al_2O_3 in this structure to form a solid solution without altering the lattice spacing of the structure much (as deduced from the XRD results). High alumina contents of the ferrovanadium slags are beneficial for the solid state as well as the liquid state interactions between the vanadium and the slags. Furthermore, the MgO content of the slag should be reduced, if possible, to inhibit the formation of the MA phase. However the amount of oxidic vanadium will not necessarily be reduced if the amount of MA phase is reduced because the MA phase can contain up to 6% V_2O_3. In other words, a small amount of MA phase with a high vanadium content can result in a high overall vanadium content in the slag. Nevertheless, vanadium losses are predicted to be much lower for slags with lower CaO and MgO contents due to the similarly strong basic nature of these oxides (as discussed in a previous chapter). Although the effect of the MgO content on the vanadium activity coefficient is not known, the section on equilibrium simulation calculations will incorporate the effect of MgO on the alumina activity which influences the oxidic vanadium content of the slag.

5.2.2.2. Composition relations of the oxidic phase

High temperature equilibrium experiments performed indicate a very strong relationship between the slag composition and the amount of oxidic vanadium in the slag, especially where CaO: $Al_2O_3 < 0.7$ (molar basis). The aim of this section is to determine whether the strong effect of slag basicity on the amount of oxidic vanadium also holds for the industrial slag samples. Because of the higher analyzed vanadium content of the slag sample due droplets included during EDX analysis, the contribution of the metal droplets needed to be quantified. This was done by performing mass balances using the average chemical compositions of each phase, including the droplets, as well as the mean chemical composition of each slag sample. All the vanadium which could not be attributed to the oxidic phases was assigned to the metal droplet phase.

It is worth mentioning at this stage that the analysed vanadium assigned to the metal phase is not the exact amount of vanadium associated with the droplets but just a mere fraction of that amount due to different volumes analyzed by EDX, as shown in figure 56.

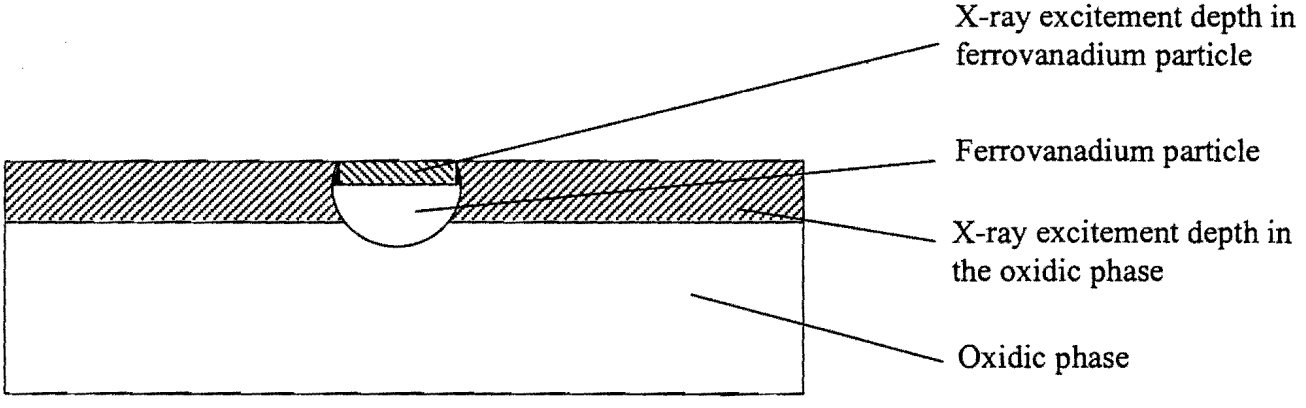

Figure 56: Cross section through a slag sample showing the excitement depth of the oxidic and metal phases in schematic form.

The schematic shows that the excitement depths of metal particles are not as deep compared to oxidic phases An indication of the depth dimension of the interaction volume is given by the following expression (Goldstein et al.,1981)

$$R = 0.0276\ AE_o^{1.67} / Z^{0.889}\rho \quad \mu m \qquad (43)$$

where E_o is given by keV, A in g/mol, ρ in g/cm^3, and Z is the atomic number of the target. Both ρ and Z are higher for metal droplets resulting in a lower depth of excitement, as shown in figure 56. A smaller volume of the metal droplets is exited resulting in lower analysed vanadium levels that would have been obtained if the same depth of excitement had occurred. Thus, only a fraction of the total amount of vanadium present in the metal phase is analysed for if a low magnification EDX analysis is performed. This had no effect on the oxide phase calculations because the Al, Ca and Mg mass balances were performed to estimate the relative amount of each oxide phase and the vanadium balance to determine the amount of vanadium associated with the metallic phase. The results obtained (See Appendices 3 and 4) are summarized in figure 57.

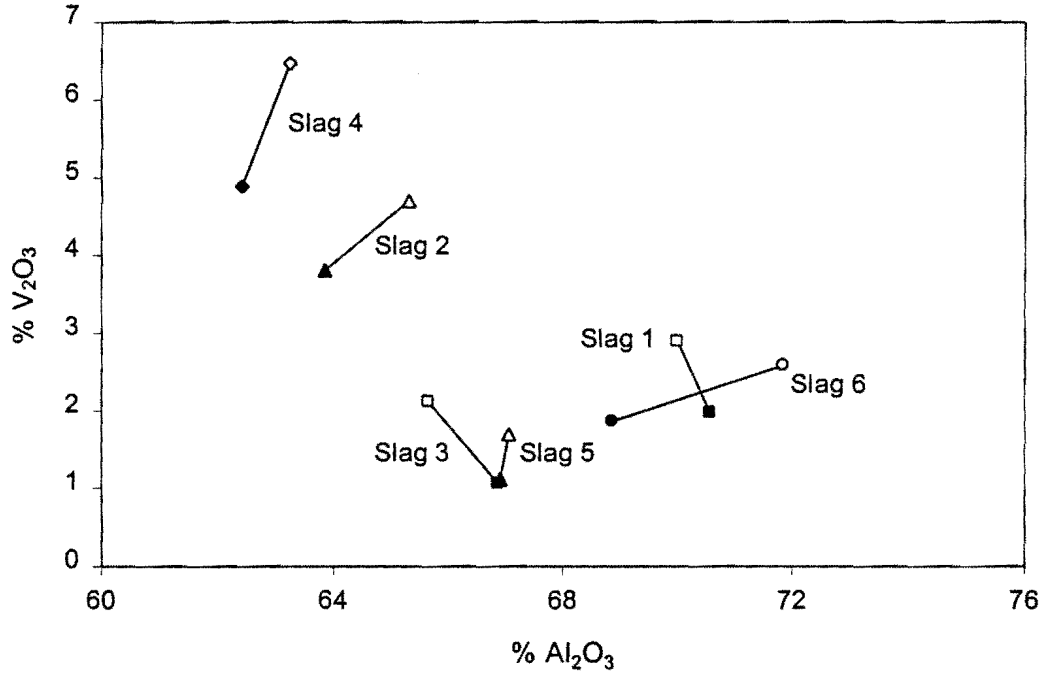

Figure 57: The effect of the alumina content of the industrial slag sample on the oxidic vanadium content. Solid data markers present data of samples taken at the top of the bulk sample and open data markers samples taken from the bottom (mass percentages).

Electric arc smelting processes are known for the poor stirring of the furnace contents resulting in segregation. The segregation of vanadium has an important effect on representative sampling as will be discussed in the next section. The samples taken at the bottom of the bulk slag sample contain up to 1.5% (mass basis) less V_2O_3 compared to the samples taken at the top.

It is not clearly understood whether the segregation indicated by figure 57 is an extension of the segregation in the furnace or a result of the solidification process. Nevertheless, vanadium concentration gradients do occur throughout the bulk slag sample and sampling of the entire bulk sample would be necessary to fully quantify the effect of position on the oxidic vanadium content of the slag. The results obtained in figure 57 (see Appendices 3 and 4) do confirm the laboratory results showing that oxidic vanadium losses are much higher for slags with lower alumina contents. The V_2O_3 content of the slag can be reduced from about 6% to 2% by raising the alumina content from 62% to 67% (mass basis). This confirms the importance of basicity control by control of the CaO additions and MgO refractory wear in such an operation.

5.2.2.3. Industrial slag sampling

The South African ferrovanadium producer under investigation calculates the percentage vanadium recovered per smelt as follows.

$$\% \text{ vanadium recovered} = \frac{\frac{\% V_{FeV}}{100} \times \text{weighed FeV button}}{\frac{\% V_{Hivox}}{100} \times \text{mass of hivox used}} \qquad (44)$$

FeV buttons are the as-cast metal constituent of the electric arc furnace, weighed after shot blasting to remove excess slag (See figure 7). The advantage of this method is that vanadium losses to the slag as oxidic vanadium and entrained droplets are indirectly accounted for by determining the total mass of the button. No time consuming method is necessary to distinguish between the vanadium associated with the slag or entrained metal particles. Thus, this method accounts for all the possible vanadium losses to the slag regardless the type of factor, including reverts (ferrovanadium containing spillages), oxide spillages, metal droplet entrainment or unreduced vanadium oxides, influencing vanadium recovery (See section 2.4.4.). This method is very sensitive regarding the chemical compositions of the hivox and FeV button respectively, and care should be taken that the sampling is representative. Despite the effectiveness of this method, it is absolutely essential for process control purposes that the exact chemical composition of the slag is known. Without the basic knowledge of the chemical compositions of the slag, no process

refinement can be conducted. Strong segregation within the slag sample and the inability of in-line analytical techniques, like the XRF technique, to distinguish between oxidic and metallic vanadium are some of the serious factors hampering the quantitative description of vanadium in the slag.

The ferrovanadium producer under investigation samples the slag prior to tapping by dipping a steel rod into the slag through the observation window in the furnace shell. After dipping, the rod is quickly withdrawn from the slag resulting in the subsequent solidification of the slag onto the rod. Upon cooling the slag is removed from the rod, crushed to a fine powder and sent for X.R.F analysis. Figure 58 shows an electron back-scattered image of such a dipped slag sample.

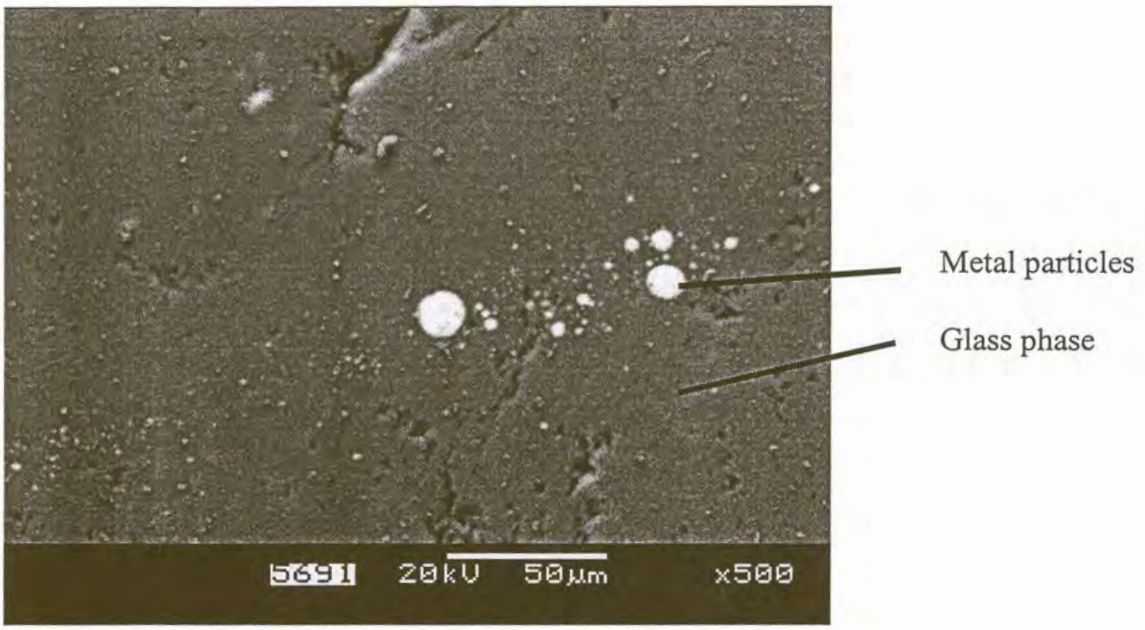

Figure 58: Back-scattered electron image of dipped slag small with metal particles.

This image shows a glass phase formed as a result of very rapid solidification of the thin slag layer on the rod. This image furthermore shows entrained metal particles in the glass phase which must contribute significantly to the average vanadium content of the slag if X.R.F analyses are conducted on the milled dip samples. EDX analysis performed on the entrained metal droplets indicate an average vanadium composition in excess of 93% (See Appendix 5). The absence of Fe in these droplets clearly indicates the poor mixing and

the strong segregation behavior of these slags. This is because initially pure vanadium droplets are formed as a result of the reduction of the vanadium oxide raw materials by aluminium. After agglomeration the pure vanadium droplets form an alloy with the molten scrap iron in the bottom of the furnace. The vanadium detected by X.R.F analysis is therefore likely to be strongly vertical position dependent. The next step is to determine how well the oxidic vanadium content of the dipped sample compares to that of samples taken from the bulk slag sample, at the top and bottom respectively (See slag 6 in Appendices 3 and 4 for chemical analysis), after tapping. A number of pieces of the dipped sample were co-mounted in epoxy resin, polished and analyzed using EDX. Special care had to be taken to ensure that the metal particles were excluded during analysis. At least 40 fields were analyzed to establish a good mean and standard deviation (See Appendix 6 for chemical analysis). The results obtained are summarized in figure 59.

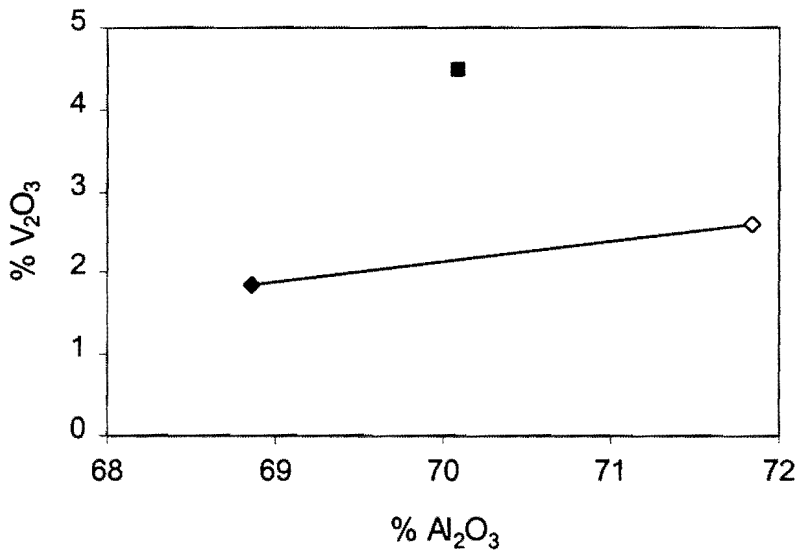

Figure 59: Comparison between vanadium content of dipped sample and samples taken from the bulk solidified sample after tapping. Square data marker represents dipped slag sample and diamond markers samples from the bulk slag sample.

The dipped sample analyzed appreciably higher for V_2O_3 than the two samples taken from the bulk sample. The figure furthermore illustrates that the alumina content of the dipped sample compares well with the average alumina content of the other two samples. The strong segregation behavior of the slag has clear implications for attempts at process refinement because the V_2O_3 content of the slag, determined by X.R.F analysis, may be in

excess of the average vanadium content of the slag. In other words, the in-furnace segregation effect may overshadow any change in vanadium content due to changes made for process improvement. Ways have to be found to address this problem and to ensure that sampling is much more representative of the bulk of the slag. Perhaps one such a way is to sample in the tap stream where the slag is much more subjected to stirring. Further investigations are therefore necessary to address this problem of representative sampling.

5.2.2.4. Industrial X.R.F. relations

Although the vanadium content of the dipped samples is likely to be in excess of the average bulk sample, the industrial X.R.F. analysis may be of some value as long as the sampling procedure is consistent. Historic industrial data, relating to 3 months of production during which in excess of 550 smelts were made, were collected, grouped and are summarized in figures 60-62. The large confidence intervals are a result of extensive scattering of plant data.

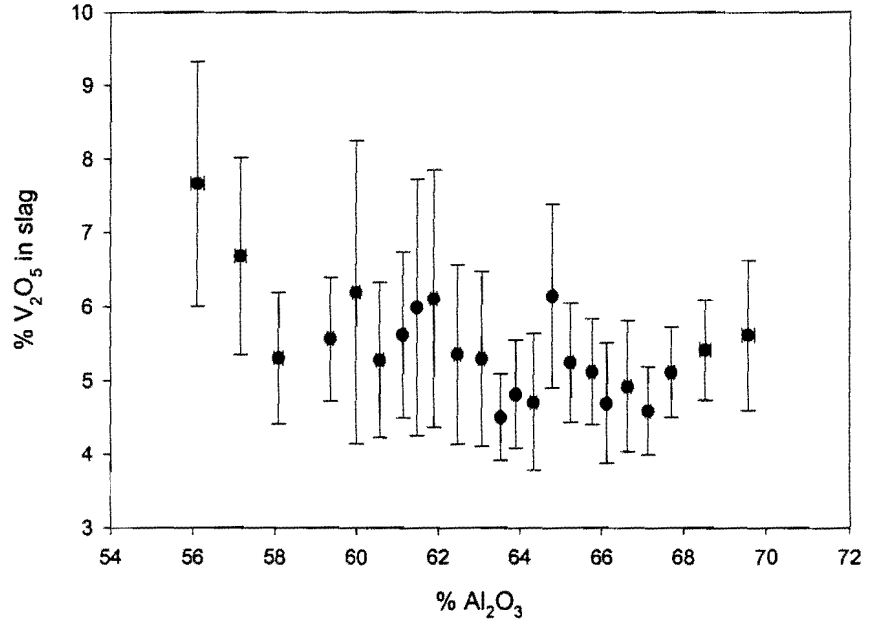

Figure 60 : Total vanadium oxide content as function of the alumina content of the slag based on XRF analyses of dip samples. All the vanadium in slag, including droplets, is reported as V_2O_5.

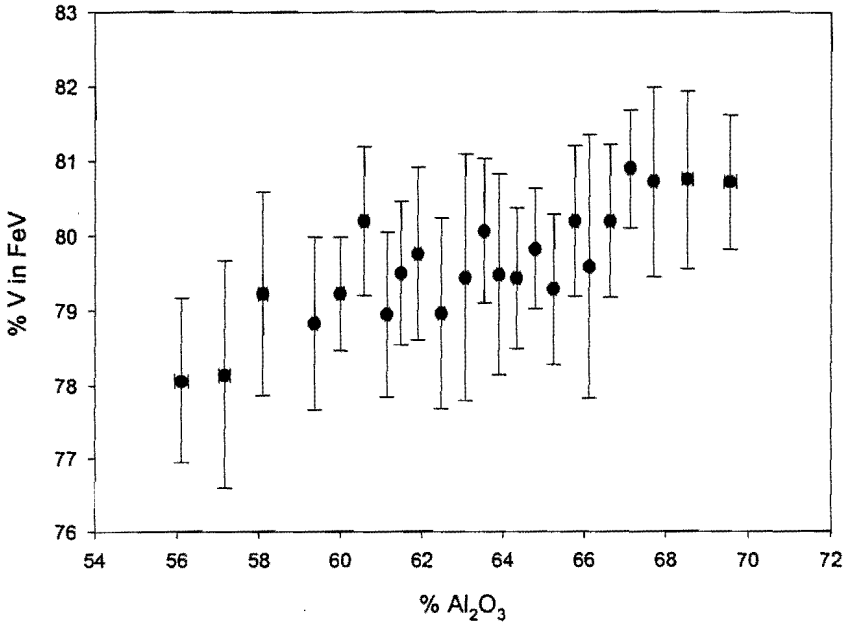

Figure 61: Vanadium content of ferrovanadium as a function of the alumina content of the slag. The XRF analysis technique was used to analise for alumina and vanadium of different dip slag and metal chip samples (taken from the metal buttons), respectively.

Figure 60 shows that high-alumina slags are beneficial for vanadium recovery. The alumina content strongly influences the oxidic amount of vanadium resulting in higher vanadium contents in the metal for increased amounts of alumina in the slag, as depicted by figure 61. In other word high alumina slags result in heavier ferrovanadium buttons with higher vanadium contents. This is in close agreement with the laboratory measurements and EDX results obtained from industrial slag samples.

Because of strict international specifications on the aluminium content of ferrovanadium, some concern may arise on what the effect of higher alumina contents is on the residual aluminium of the ferrovanadium. The effect of higher alumina contents on the vanadium content of the ferrovanadium is shown in figure 62.

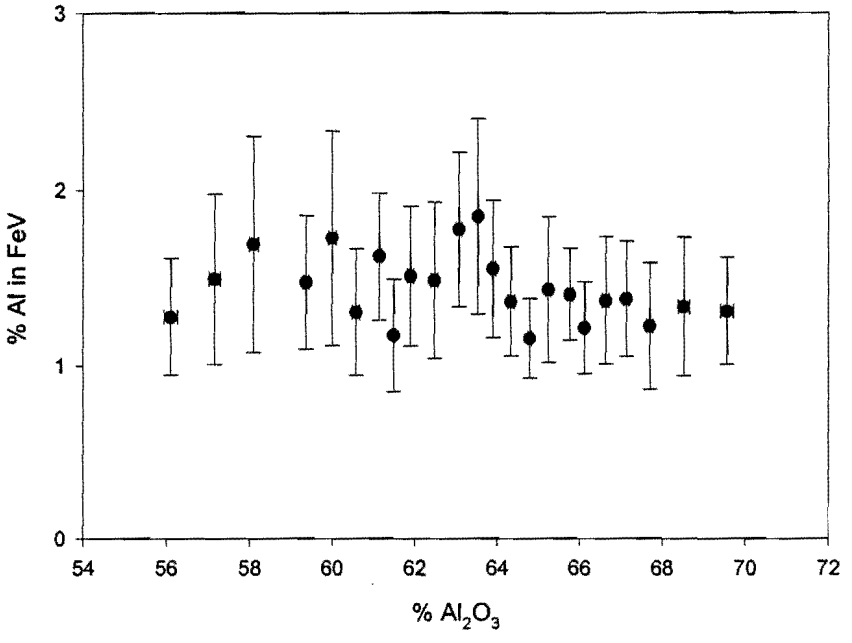

Figure 62: The effect of the slag composition on the aluminium content of the ferrovanadium.

This figure indicates that the aluminium content of the ferrovanadium is expected to remain constant, for slags containing up to 70 % Al_2O_3, if the slag basicity is decreased by lowering the lime additions.

It was previously assumed that MgO (for slags containing from 5 to 15 % of MgO on a mass basis) and CaO are similarly strong basic oxides and would therefore behave similarly in Al_2O_3-rich liquid slags. Because of the scatter in the plant data, no conclusion can be made on this regard. The next section aims to quantify metal droplet entrainment as a possible mechanism of vanadium loss to the slag.

5.3. Metallic phase analysis

5.3.1. Introduction

EDX on industrial slag samples and laboratory results indicate that the Al_2O_3 content of the slag has a strong effect on the soluble vanadium loss to the slag. The decrease of the slag basicity by lowering the lime additions will result in higher liquidus temperatures and hence possibly higher slag viscosities, which may lead to higher metallic losses. It is still uncertain which of the oxidic or metallic loss contributes most strongly to the total vanadium loss in the slag. The aim of this section is to quantify the amount of vanadium typically associated with the metallic phase and to what extent the slag basicity influences metal droplet entrainment.

5.3.2. Experimental procedure

5.3.2.1. Sample preparation

The investigations were carried out on the polished sections (See slags 1-6 in Appendices 3 and 4) previously subjected to oxidic phase analysis, as reported in section 5.2.2.2.

5.3.2.2. Procedure to determine droplet-size distributions and to estimate mass of vanadium associated with the metal particles.

Polished sections were investigated using an optical microscope and photos of the entrained droplets were taken with a digital camera. The y-coordinate of the polished sections (that is vertical in the bulk slag sample) was incrementally increased, while photos were taken randomly along the x-coordinate. Special care was taken to ensure that the photos were representative of the entire sample because of the large difference in the droplet dimensions (0.5 μm - 60 μm apparent diameter). Using the Imagetool software package, the areas of the individual particles as well as the total droplet area expressed as a fraction of the total sample area, were estimated. Subsequently the generated data were used to determine the two-dimensional size distribution of the planar section. Without any additional calculations, the total droplet area fraction can be used to estimate the volume

fraction of metal particles entrained in the slag. The amount of metal droplets in the slag can also be estimated by determining the true spatial size distribution of the droplets entrained in the polished sections. Once the two-dimensional size distribution of the planar section has been determined, equations can be utilized to estimate the spatial size distribution. The true spatial size distribution can be used to determine to what extent each size class interval contributes to the total mass of entrained metal particles. Most of the methods derived to calculate the spatial size distribution make use of the assumption that the particles are spherical. The entrained droplets are almost perfect spheres, as can be seen from the back-scattered images, thus fitting the assumption perfectly. The following correlation was used to calculate the spacial size distribution (Underwood, 1986).

$$N_{v,i} = 1/Di(1.645\ N_{A,i} - 0.4542\ N_{A,i-1} - 0.1173\ N_{A,i-2} - 0.0423\ N_{A,i-3} - 0.01561\ N_{A,i-4} - 0.0083\ N_{A,i-5} - 0.0036\ N_{A,i-6} - 0.0019\ N_{A,i-7} - 0.0009\ N_{A,i-8} - 0.00044\ N_{A,i-9} - 0.00036\ N_{A,i-10} - 0.0001\ N_{A,i-11} - 0.00003\ N_{A,i-12} - 0.00003\ N_{A,i-13} - 0.00001\ N_{A,i-14} \quad (43)$$

$N_{A,i}$ = Planar density of droplets in class interval i (estimated from the planar size distribution) (number/mm^2)

$N_{v,I}$ = Volumetric density of droplets in class interval i (number /mm^3)

Di = maximum droplet diameter in class interval i

Droplet size class intervals were determined by applying the $\sqrt{2}$ - ratio of geometric grouping. This was done by multiplying the pre-determined minimum droplet diameter of the first class interval by $\sqrt{2}$ to establish the upper limit of the size interval. This value was used as the lower limit of the next class interval, for which the upper limit was again calculated by multiplying the lower limit by $\sqrt{2}$. This procedure was repeated until all the droplets could be classed.

The average droplet diameter for each class interval was calculated as the geometric mean of the maximum and minimum diameters of the class interval.

It is further worth mentioning that each class interval should at least contain 7 areas for calculation purposes (Underwood,1986).

5.3.3. Results and discussion

Table 18 gives a summary of the volume % metal particles, droplet composition, droplet and slag densities, mass of vanadium in droplets, percentage oxidic vanadium, mass of V in oxidic phases, total mass of vanadium in slag and the mass percentage V in 1230 kilograms of slag in each slag sample.

Some of the slag samples contained above average-sized entrained metal droplets resulting in the high standard deviations and 95 % confidence limits. Large entrained metal particles hamper representative sample photography because the magnification has to be chosen in such a way that a representative portion of the large particles is included. This causes the small particles not to be optically resolved. This problem was overcome by choosing a magnification which enabled the small particles to be just identified and the number of photographs that was taken, was increased substantially. Nevertheless, some of the large standard deviations could not be substantially reduced.

Slag	Volume % droplets	Standard Deviation	95 % Confidence limits	Droplet composition			Dencities(g/cm^3)		Mass V in droplets (kg)	% V in slag	Mass of oxidic V	Total mass V	% V_T (1230 kg)
				% Al	% V	% Fe	Droplet	Slag					
Slag 1 top	0.10	3.13	1.37	0.1	95	4.90	6.02	3.80	1.80	2.31	28.43	30.23	2.46
Slag 1 bottom	0.87	0.14	0.06	0.2	95	4.80	6.02	3.80	16.02	2.31	28.43	44.44	3.61
Slag 2 top	0.19	0.24	0.11	5.80	83.6	4.40	5.98	3.81	2.99	2.65	32.61	35.60	2.89
Slag 2 bottom	0.22	0.22	0.10	1.12	77.8	16.54	6.42	3.81	3.61	2.38	29.26	32.87	2.67
Slag 3 top	0.15	0.10	0.05	7.34	74.2	8.81	6.14	3.81	2.16	1.56	19.23	21.39	1.74
Slag 3 bottom	1.01	1.33	0.71	2.85	81.5	8.82	6.31	3.79	16.88	0.68	8.36	25.24	2.05
Slag 4 top	0.21	0.18	0.10	0.74	74.1	23.74	6.36	3.71	3.29	3.26	40.13	43.43	3.53
Slag 4 bottom	0.44	0.71	0.36	6.03	82	8.42	5.86	3.81	6.83	3.33	40.97	47.80	3.89
Slag 5 top	0.36	0.36	0.17	1.28	93	0.70	6.19	3.80	6.74	1.16	14.21	20.95	1.70
Slag 5 bottom	2.91	7.24	3.54	11.26	72.3	7.03	5.81	3.80	39.55	1.09	13.38	52.93	4.30

Table 18: Results of metal droplet analysis.

Figure 63 and 64 depict the true spatial size distributions, as calculated using equation 42, for the bottom and top of Slag 1.

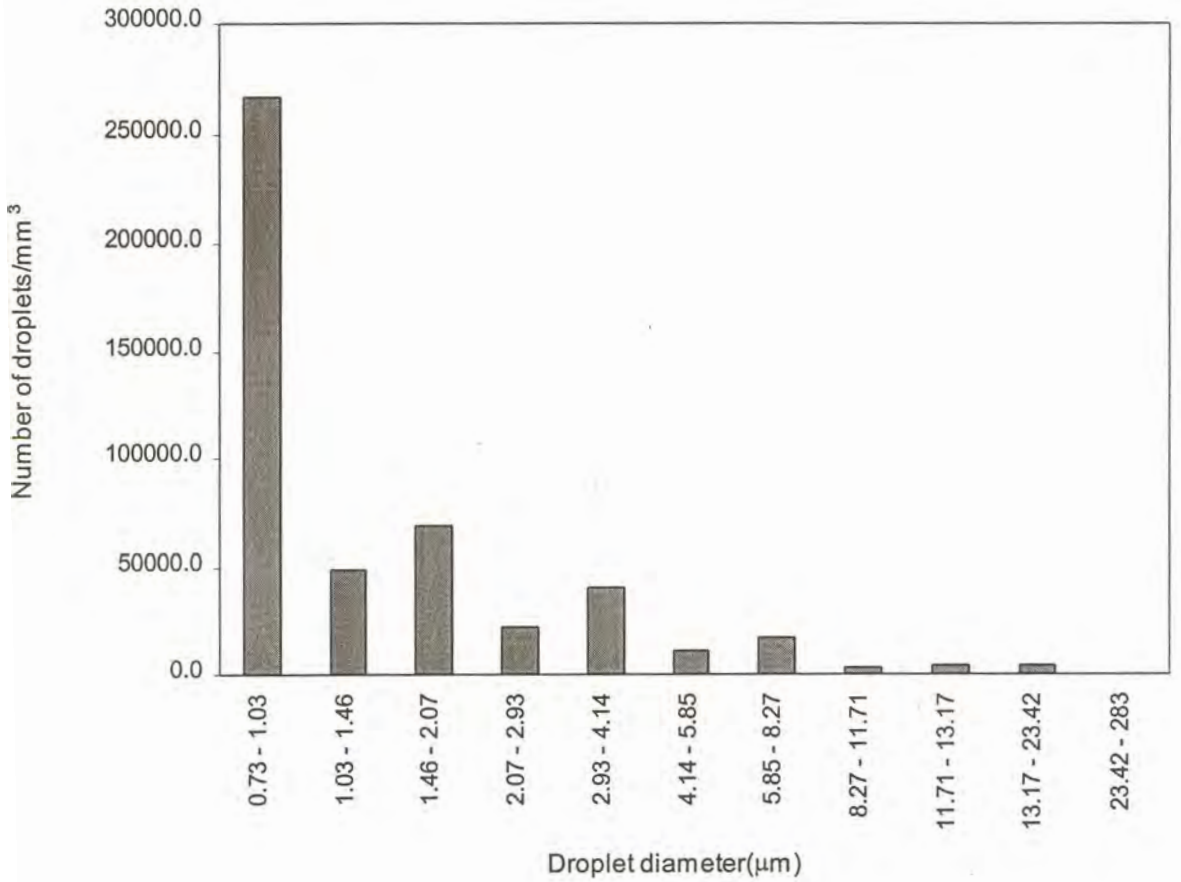

Figure 63: True spatial size distribution of entrained droplets for Slag 1 bottom.

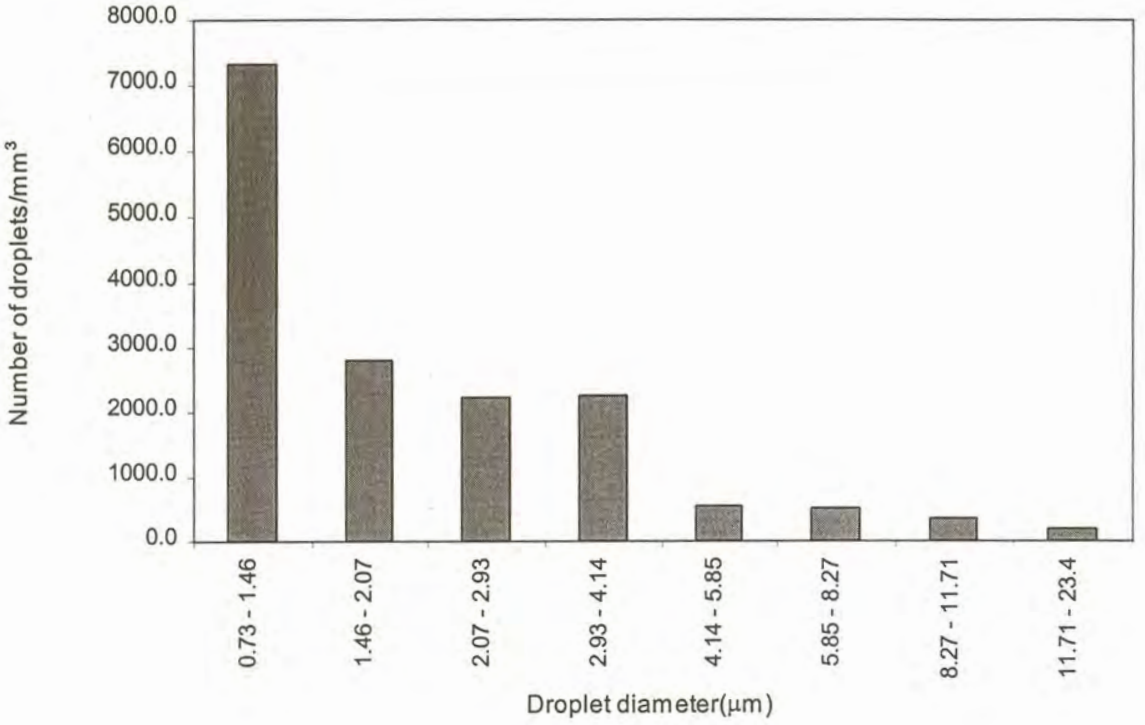

Figure 64: True spatial size distribution of entrained droplets for Slag 1 top.

Figure 65 and 66 depict the volume fraction of particles in each class interval for the bottom and top of slag 1.

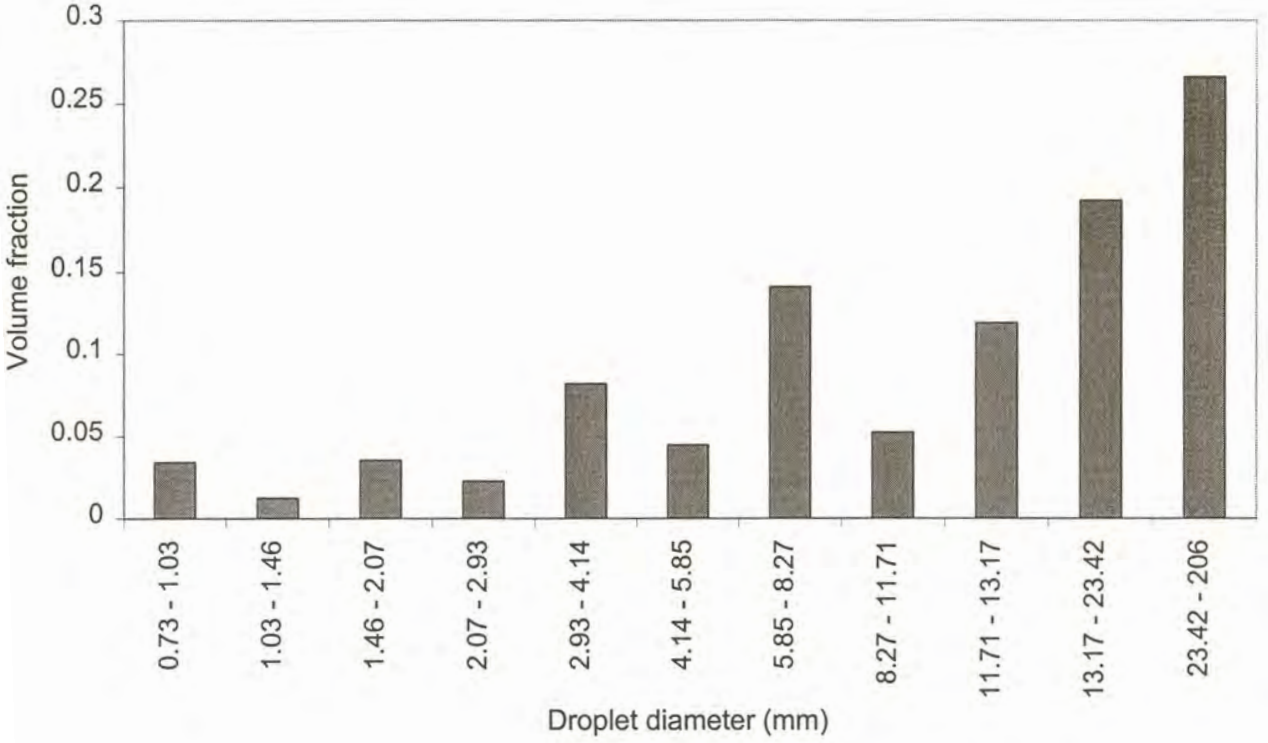

Figure 65: The volume fraction of particles in each class interval for the bottom of Slag 1.

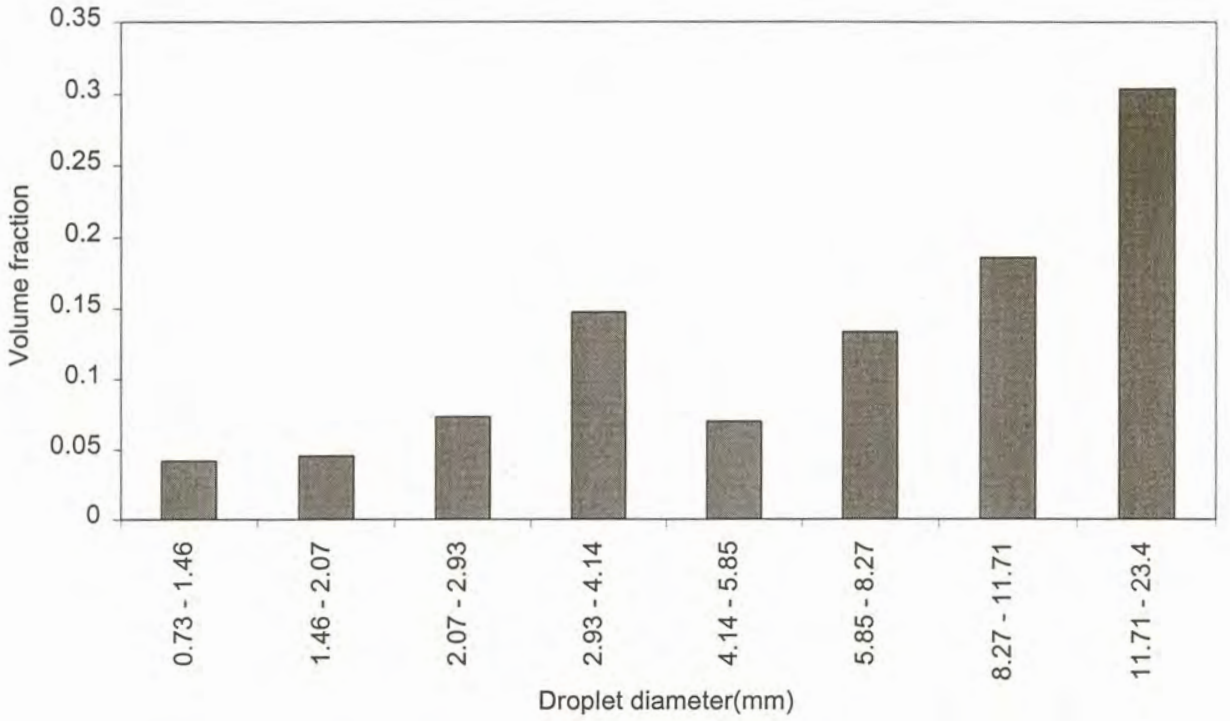

Figure 66: The volume fraction of particles in each class interval for the bottom of Slag 1.

Figures 63 and 64 show that by far the largest number of the metal droplets is smaller than 5 μm and the concentration and size of entrained particles is much larger in case of the bottom slag sample. In contrast to this, figures 65 and 66 show that the largest volume fraction of droplets lies in the class intervals larger than 5 μm. Thus, the mass of entrained metal particles can be estimated by considering only 5 μm particles and larger. Due to the time consuming nature of the droplet size distribution calculations to estimate the volume fraction of the metal particles in the slag, only the area fraction calculations were utilized to estimate the volume fraction of metal particles for the remainder of the slag samples.

The effect of temperature and slag composition on metal droplet entrainment is shown in figure 67.

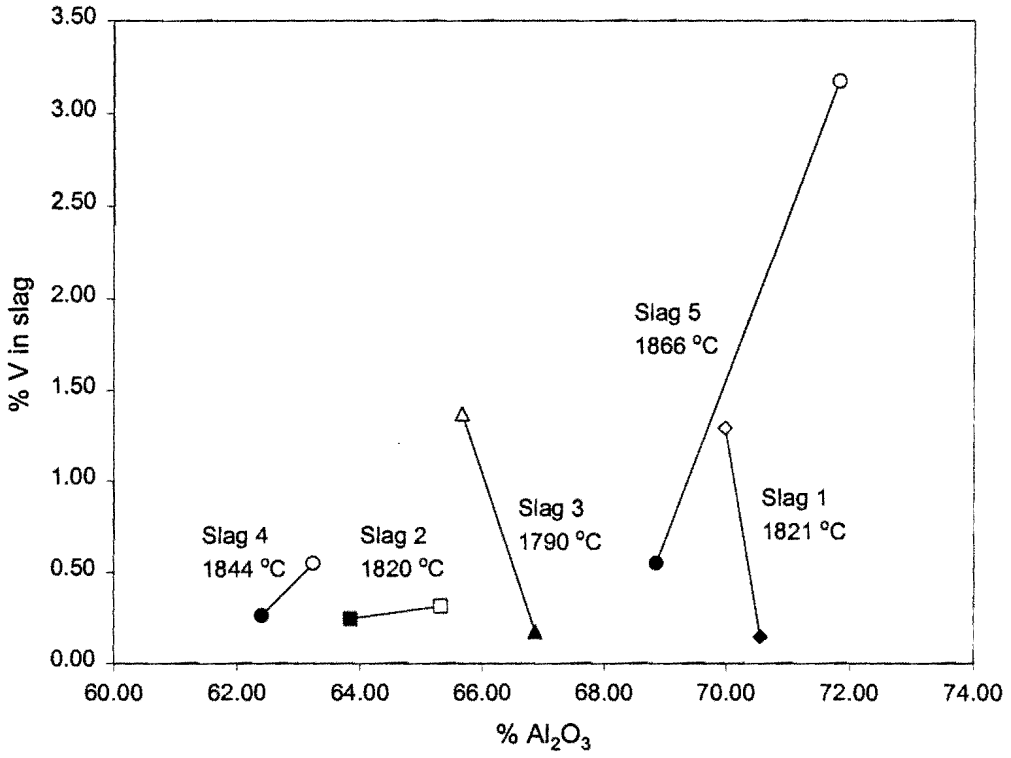

Figure 67: Vanadium losses, with recorded tap temperatures for different slag samples. The % V in the slag is only the vanadium associated with the entrained metal droplets. A slag mass of 1230 kg was assumed. The open data markers and solid data markers present samples taken at the bottom and top of the bulk sample, respectively. The investigations were carried out on the polished sections of which the VO_x content was previously determined. (See section 5.2.2.2)

Before any conclusions relating to the influence of slag composition on droplet entrainment can be drawn, the influence of tap temperature should first be investigated. High tap temperatures will reduce the viscosity and increase the solidification period of the slag, resulting in the reduction of metal droplet entrainment. However, no relation between the amount of droplets entrained and the tap temperature could be observed as

shown in figure 67. The amount of droplets entrained, in this case, is not very sensitive to temperature fluctuations which may be encountered from smelt to smelt (See specially the solid data markers).

Vanadium losses to the slag expressed as % V in metal droplets and total % V in slag (the latter includes oxidic and metallic vanadium) for the top and bottom slag samples, are shown in figure 68 and 69 respectively.

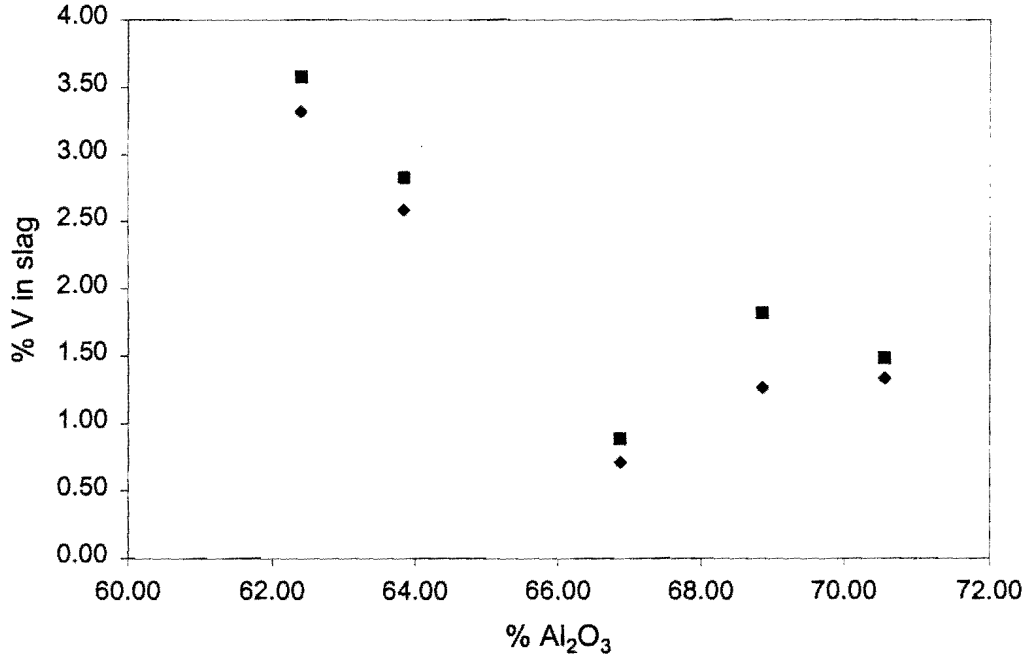

Figure 68: Soluble and total vanadium loss to the slag as function of the slag basicity for the top slag samples. In this figure the squares show the total vanadium composition of the slag (Soluble as well as droplet contributions), and the diamond figures the soluble vanadium content of the slag

Figure 68 indicates that the contribution of the entrained metal particles to the total vanadium loss to the slag is relatively small with the maximum contribution of $\approx$ 0.5 %. This figure depicts, thus, that small adjustments made to the slag basicity by decreasing the fluxing agent additions will increase the metal recoveries. The total vanadium content

of the slag can be reduced from ≈ 3.5 % to ≈ 1.5 % by adjusting the alumina composition from ≈ 60 % to 70 %. Figure 68 appears to have a minimum at around 67 % alumina resulting in a total vanadium loss around 1 %, but this can only confirmed if more analyses on industrial samples are conducted. Nevertheless, higher slag viscosity which is a result of a higher liquidus temperatures appears not to be strongly affecting the entrainment of metal particles for slag samples taken from the top of the industrial bulk slag samples.

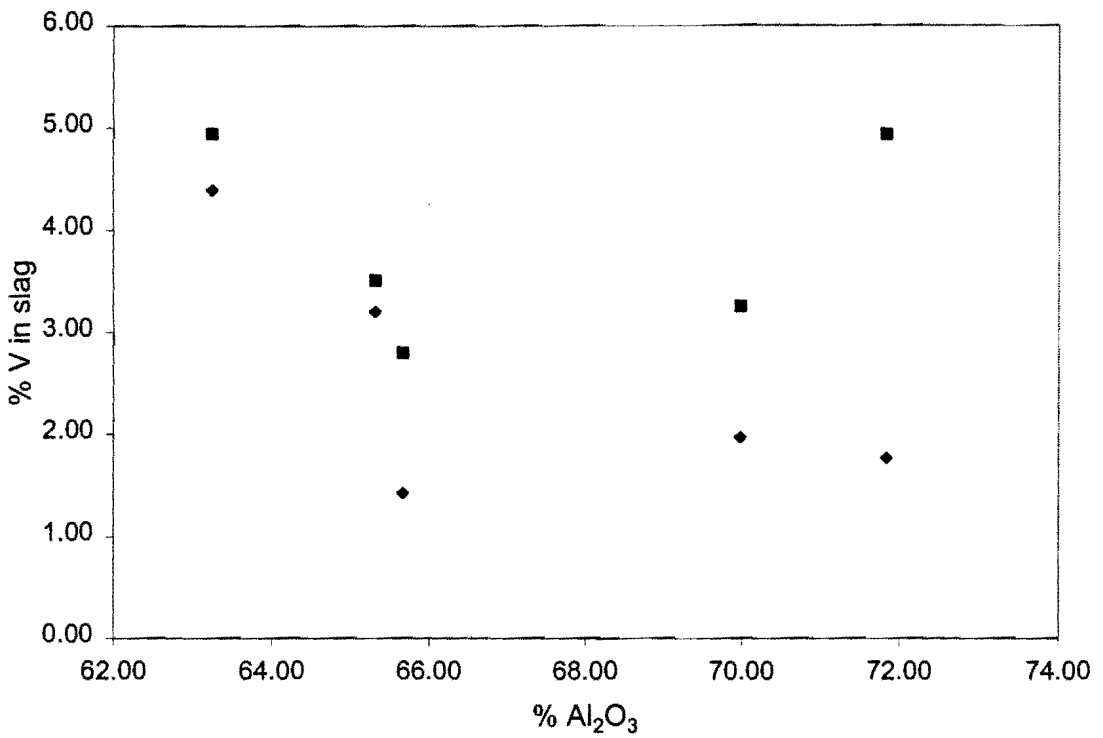

Figure 69: Soluble and total vanadium loss to the slag as function of the slag basicity of the bottom slag samples. In this figure the squares show the total vanadium composition of the slag (Soluble as well as droplet contributions), and the diamond symbols the soluble vanadium content of the slag

Compared to figure 68, figure 69 shows a very strong effect of the slag basicity on the amount of vanadium associated with the entrained metal particles with the maximum around 3.3 %. At this stage, it is worth mentioning that slag samples were taken very

close to the slag-metal interface. The amount of entrained droplets was very dependent on the height within the bulk sample. The first few centimeters along the y-axis of the sample contained most of the entrained droplets, whereafter the concentration strongly declined further along the y-axis. The very high concentration of the droplets close to the interface give rise to unusually high losses of vanadium to the entrained metal particles which are not representative of the entire bulk slag sample. The crowding of the droplets close to the interface should be avoided as far as representative sampling is concerned because this effect is only observed for a very small fraction of the total slag volume.

The influence of slag basicity on metal droplet entrainment is thus better depicted by figure 68 than figure 69. In addition to this, the amount of entrained droplets is also strongly dependent on the horizontal position within the bulk slag sample. Slag closer to the slag pot lining solidifies more rapidly than slag closer to the center, resulting in a higher concentration of metal particles closer to the lining.

It can be concluded from the results that vanadium losses as entrained droplets could not be fully quantified by analyzing samples from the top and bottom of the bulk slag sample. Although the samples taken at the top of the bulk slag sample are expected to be more representative of the entire slag sample, the positional effect on droplet entrainment introduces much uncertainty. In order to fully quantify metal droplet entrainment as a possible cause of vanadium loss to the slag, new sampling methods must be derived. One such way is to sample from both the y and x direction to establish a three-dimensional mapping of the bulk slag sample. Only then will the positional effect on droplet entrainment be fully quantified. A number of slag samples should be subjected to this extended sampling to establish the effect of slag composition on metal droplet entrainment.

6. Equilibrium simulation calculations

6.1. Introduction

Ferrovanadium can be produced from trivalent oxide (V_2O_3) by reduction with aluminium in an electric arc furnace, adding iron in the form of scrap, and lime (CaO) to flux the alumina (Al_2O_3) which is produced by reduction of vanadium oxide. Incompatibility between the refractory and the Al_2O_3-rich slag results in excessive refractory wear. (Industrial slag contains 3-15 % MgO). The effect of MgO on the activity coefficient of $VO_{1.5}$ is not known, but MgO does affect the Al_2O_3 activity. Al_2O_3 is expected to fix the oxygen activity in the slag. Calculations were performed assuming equilibrium to hold between Al_2O_3 and $VO_{1.5}$ in the slag, and Al and V in the metal. The effect of temperature, aluminium activity and MgO content of the slag on oxidic vanadium loss were considered. The activity of Al_2O_3 in CaO-MgO-Al_2O_3 slags and Al activity in Al-Fe-V melts were estimated using a software package of Chemsage (Chemsage,1999).

6.2. Results and discussion

The Chemsage software package was utilized to estimate the activities of species in liquid ferrovanadium and CaO-Al_2O_3-MgO slags. This Solgasmix free energy minimizer uses free energy correlations of all the pure species as well as correlations describing their respective interactions in binary systems. Using these correlations with a mixing model enables the user to estimate activities of species in different melts. The first simulation calculations aimed to compare activities obtained using the software package and experimentally determined activities. The activity of $AlO_{1.5}$ as a function of the mole fraction $AlO_{1.5}$ in $AlO_{1.5}$-CaO slags, published by Rein et al(1965) and the estimated activities using the Chemsage software package are shown in figure 70. Reference states were pure solid V, MgO, CaO and Al_2O_3, pure liquid Al and Fe.

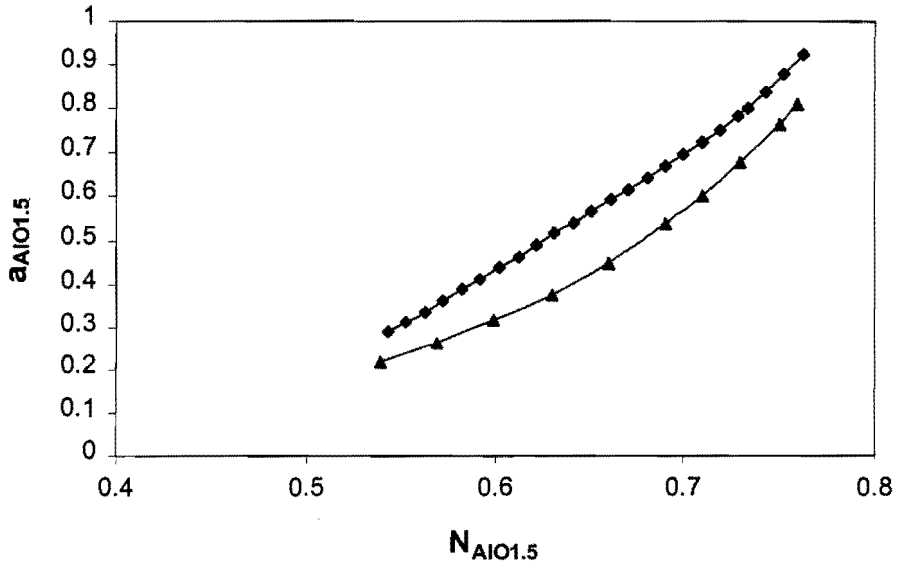

Figure 70: Activity-composition relations of $AlO_{1.5}$ on $AlO_{1.5}$-CaO slags at 1650°C. The triangles show the calculated data points using the Chemsage package and the diamond data markers, the published activities of Rein et al.(1965). Reference states were pure solid CaO and Al_2O_3.

Some error is associated with the published activities of Rein et al since the data were only graphically represented in the published paper. Nevertheless, the graph indicates that the estimated activities for the $AlO_{1.5}$-CaO binary system using the Chemsage software package compares well to the Rein et all published data. Activities in the ternary Al_2O_3-CaO-MgO system were tested against data published in the Slag Atlas(Verein Deutscher Eisenhüttenleute,1995).

Figure 71 shows the activity of MgO in the system Al_2O_3-CaO-MgO at 1687°C.

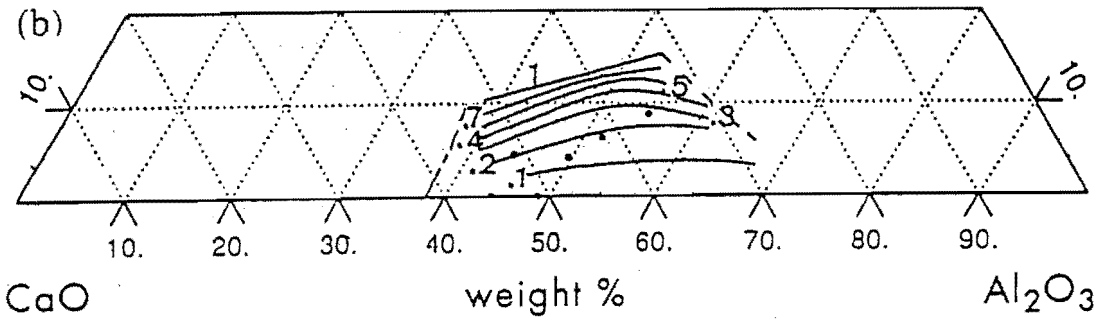

Figure 71: Activity of MgO in the system Al_2O_3-CaO-MgO with the solid lines showing the published activity (Verein Deutscher Eisenhüttenleute,1995) and the data points the estimated activities of 0.2 for different slag compositions utilizing the Chemsage software. Reference states were pure solid MgO, CaO and Al_2O_3.

Figure 71 illustrates that the estimated activities compare remarkably well with the published data. (A large activity coefficient of MgO in MgO-CaO-Al_2O_3 slags is expected because MgO has unit activity at around 12% MgO).

With confidence in the abilities of the Chemsage software to estimate the activities of species in the CaO-MgO-$AlO_{1.5}$ system, the ternary system, illustrated in figure 70, was constructed.

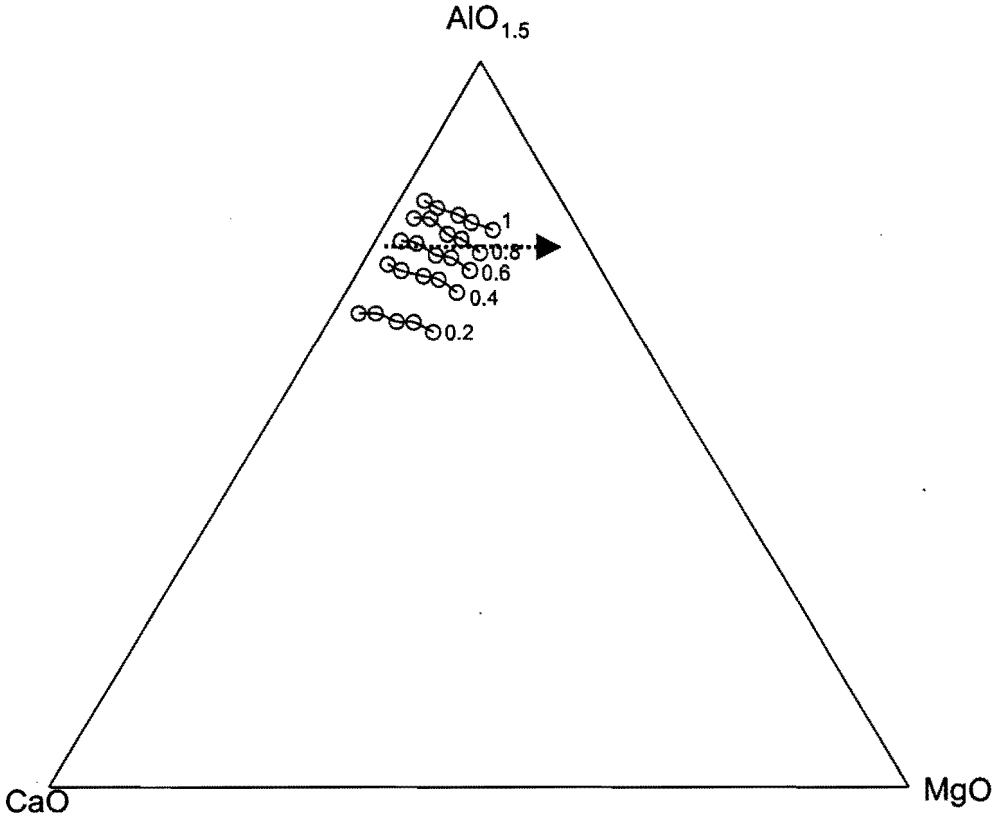

Figure 72: Activity of Al_2O_3 in the system $AlO_{1.5}$-CaO-MgO. Compositions plotted as mole fractions of $AlO_{1.5}$, CaO and MgO. Reference states were pure solid CaO, MgO and Al_2O_3 at 1973 K.

This graph indicates that the activity of $AlO_{1.5}$ is somewhat increased by MgO for a constant $\frac{MgO + CaO}{AlO_{1.5}}$ (mole basis) ratio. Thus, MgO substitutes CaO in the slag resulting in the slag composition changing along the broken line shown in figure 72. The effect on the oxidic vanadium loss of this increasing in the $AlO_{1.5}$ activity by MgO will now be quantified. Calculated vanadium losses to the slag - based on the measured activity coefficients – are presented in figure 73. This figure gives the predicted mass percentage of vanadium oxide in the slag and the total mass of vanadium lost to the slag as oxide, per tonne of ferrovanadium. The calculations were performed by assuming equilibrium to

hold between Al_2O_3 and $VO_{1.5}$ in the slag, and Al and V in the metal. (See third reaction in Table 18.) The Chemsage software was utilized to estimate the activity of aluminum in ferrovanadium. A ferrovanadium composition of 80% V, 1.5% Al and balance Fe, a typical average composition of ferrovanadium produced by the South African producer, was chosen to estimate the aluminum activity. Appendices 10 and 12 contain the calculated activities of Al and Al_2O_3 as a function of ferrovanadium and slag composition. It was further assumed that the aluminum content of the ferrovanadium remains constant, independent of the slag composition. This assumption is supported by industrial data, see figure 62, that the aluminum content of ferrovanadium is not strongly influenced by the slag composition. The other main assumption is a total mass of Al_2O_3 of 800kg per tonne of ferrovanadium. All the calculations were performed at 1973K. The basicity of the slag is expressed as follows:

$$\text{Basicity} = \frac{N_{CaO} + N_{MgO}}{N_{Al_2O_3}} \qquad (45)$$

With N_i = mole fraction of species i in the slag.

It was assumed that the effect of MgO on $\gamma_{VO1.5}$ is similar to that of CaO (on a molar basis).

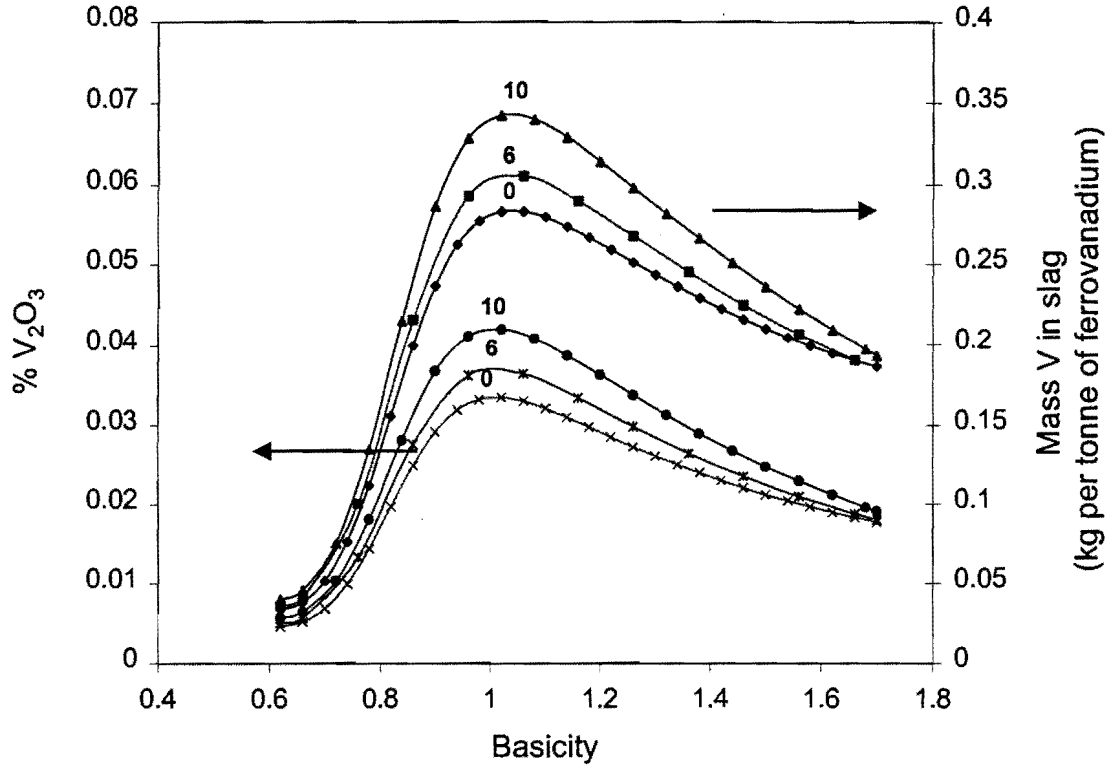

Figure 73: Predicted effect of slag composition on the soluble vanadium loss to the slag, based on activity data given in figure 49 and in Appendices 10 and 12. A constant ferrovanadium composition of 80% V, 1.5% Al and the balance Fe rendering the aluminum and vanadium activities to be 0.00539 and 0.834, respectively. A total mass of Al_2O_3 of 800kg per tonne of ferrovanadium was assumed. The V_2O_3 content of the slag and the total vanadium loss to the slag are shown for different MgO contents at 1973K. The numbers depict the respective mass percentages of MgO in the slag. Reference states were pure solid V, MgO, CaO and Al_2O_3, pure liquid Al and Fe.

The predicted relationships in figure 73 show a strong effect of slag basicity on soluble vanadium losses. At low slag basicities, a small increase in the basicity yields a large increase in vanadium losses, as a result of the sharp decrease in the vanadium oxide activity coefficient.

At higher basicity, the continued decrease in the Al_2O_3 activity (giving a lower oxygen activity at constant aluminum activity) while the $VO_{1.5}$ activity coefficient remains nearly constant, result in somewhat lower predicted vanadium oxide levels in the slag.

Figure 71 further shows MgO retained in the slag to be detrimental to the soluble vanadium loss to the slag. The strong effect of slag basicity on the $VO_{1.5}$ activity coefficient for low basicity slags (Basicity < 0.8) overshadows the small effect of MgO on the activity of Al_2O_3. MgO somewhat increases the activity of Al_2O_3 (at a constant basicity) resulting in lower oxygen activities at a constant aluminum activity. The detrimental effect of the dissolution of the refractory lining and fettling material, and the subsequent uptake of MgO is mainly related to the change of the slag basicity. In addition to the cost associated with the dissolution of the magnesite refractory lining, the uptake of MgO from the lining further increases the soluble vanadium loss to the slag. This confirms that ways have to be found to retard the dissolution of the magnesite refractory lining, which may include fettling with crushed slag or using dolomite instead of lime, rather than with MgO-rich fettling materials.

The typical V_2O_3 content of industrial slag samples (see section 5.2.2.2.) is between 1 and 3% (mass percentage) for high-alumina slags. The calculated vanadium yield (figure 73) is much higher than for the industrial slag samples. The lower oxidic vanadium content predicted is mainly attributed to the aluminum activity estimation, which appears a factor 10 too high. The calculated effect of slag composition on the loss of vanadium oxide assuming activity of aluminium in ferrovanadium chosen to yield vanadium oxide contents of the same order as those measured for industrial slags is shown in figure 74. All the assumptions previously made still hold.

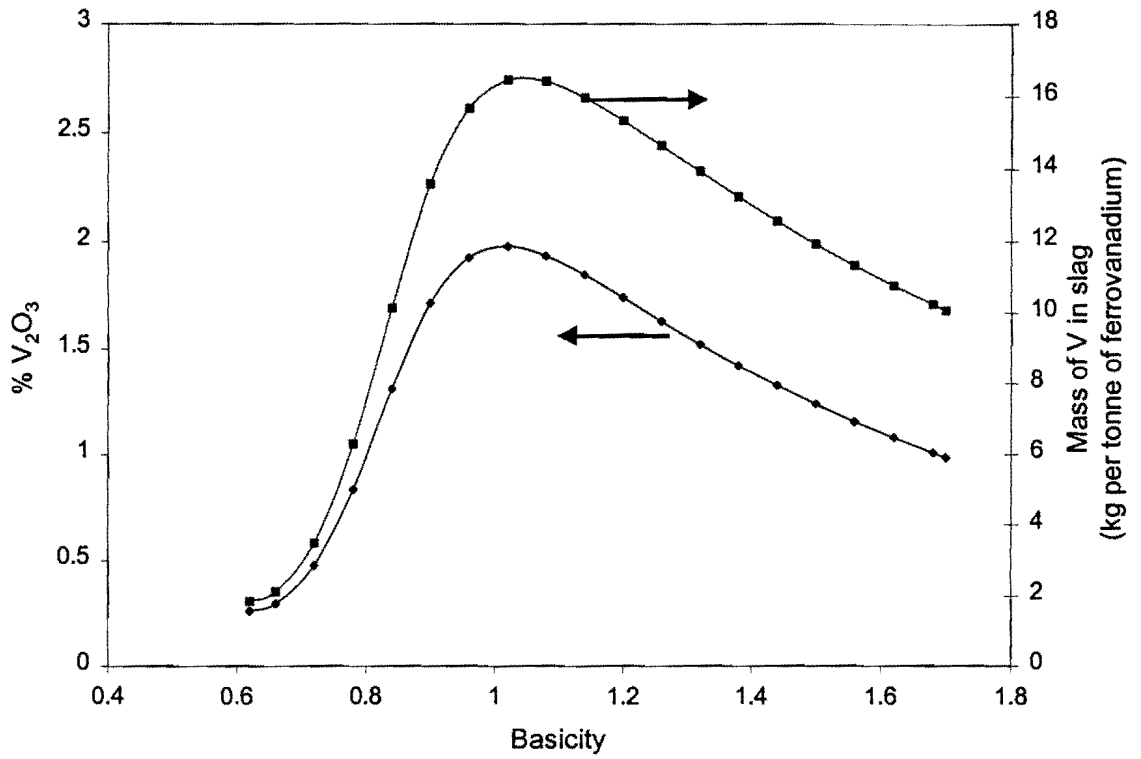

Figure 74: Predicted effect of slag composition on the soluble vanadium loss to the slag, assuming a constant activity of a_{Al}=0.0002 to yield the same vanadium oxide content as previously measured for industrial slag. Activity data given in figure 49 and Appendices 11 and 13 were used to perform the calculations. A total mass of Al_2O_3 of 800kg per tonne was assumed. The V_2O_3 content of the slag containing 10 % MgO and the total vanadium loss to the slag are shown for 2073K.

This figure clearly indicates that a factor 10 change in the aluminum activity will result in a factor 100 change in the mass of vanadium in the slag due to the quadratic dependency on the activity of aluminum in the equilibrium constant (see Table 18). The activity of aluminum in ferrovanadium cannot be fully quantified using the Chemsage software package and uncertainties on the order of the magnitude of the activity coefficient still remain. Experiments should ideally be performed to determine the activity coefficient of aluminum in ferrovanadium. By knowing the activity of aluminum in ferrovanadium the

oxidic vanadium losses to the slag can be fully quantified. Despite the uncertainties of the Chemsage aluminum activity estimates, the values generated using the software package will be used, (due to the lack of better correlations) for the remainder of the simulation calculations to illustrate the effect of temperature and aluminum content of ferrovanadium on the oxidic vanadium loss.

Calculated vanadium losses to the slag, showing the influence of the aluminum content of the ferrovanadium, are presented in Figure 75. This calculation was performed assuming a constant MgO content in the slag of 10%. In addition to this, a ferrovanadium composition with constant vanadium content of 80% V was assumed. All the calculations were performed at 1973K. A constant mass of Al_2O_3 of 800kg was assumed (based on the mass balance shown in Figure 5) which implies that the slag mass increases as the slag basicity is increased. The other main assumption is that the aluminum content of the ferrovanadium remains constant, independent of the slag composition, which is supported by plant data.

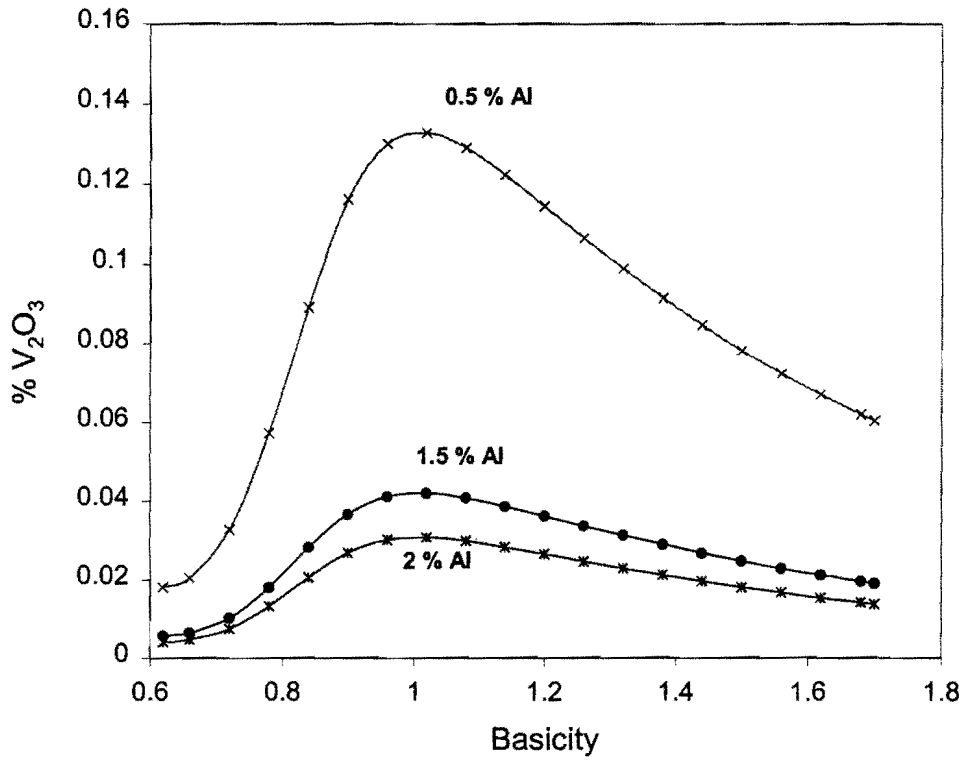

Figure 75: Predicted effect of the aluminum content of the ferrovanadium on the soluble vanadium loss to the slag equilibrated at 1973K. Constant MgO content of the slag and vanadium content of ferrovanadium of 10% and 80%, respectively, and a total mass of Al_2O_3 of 800kg per tonne of ferrovanadium were assumed.

The predicted relationship in figure 75 shows, in addition to the strong effect of slag basicity, also a strong effect of the aluminum content of ferrovanadium on vanadium losses. A 1% decrease, from 1.5% Al – 0.5% Al, in the aluminum levels of the ferrovanadium will increase the mass percentage vanadium in the slag from ≈ 0.04% to ≈ 0.13%. This strong effect is due to the quadratic dependence of a_{V2O3} on a_{Al} in the equilibrium constant expression. This strong effect of aluminum further underlines the necessity to perform equilibrium experiments to fully quantify the aluminium effect on soluble vanadium losses.

The predicted effect of temperature on the soluble vanadium losses to the slag is shown in figure 76. In all the calculations a MgO content of 10% MgO in the slag was assumed. A constant ferrovanadium composition of 80% V, 1.5% Al and the balance Fe was used to estimate the vanadium and aluminum activities utilizing the Chemsage software package. In these calculations, it was assumed that the $VO_{1.5}$ activity coefficients are not strongly dependent on temperature for the entire slag composition range. A constant mass of Al_2O_3 of 800kg was assumed.

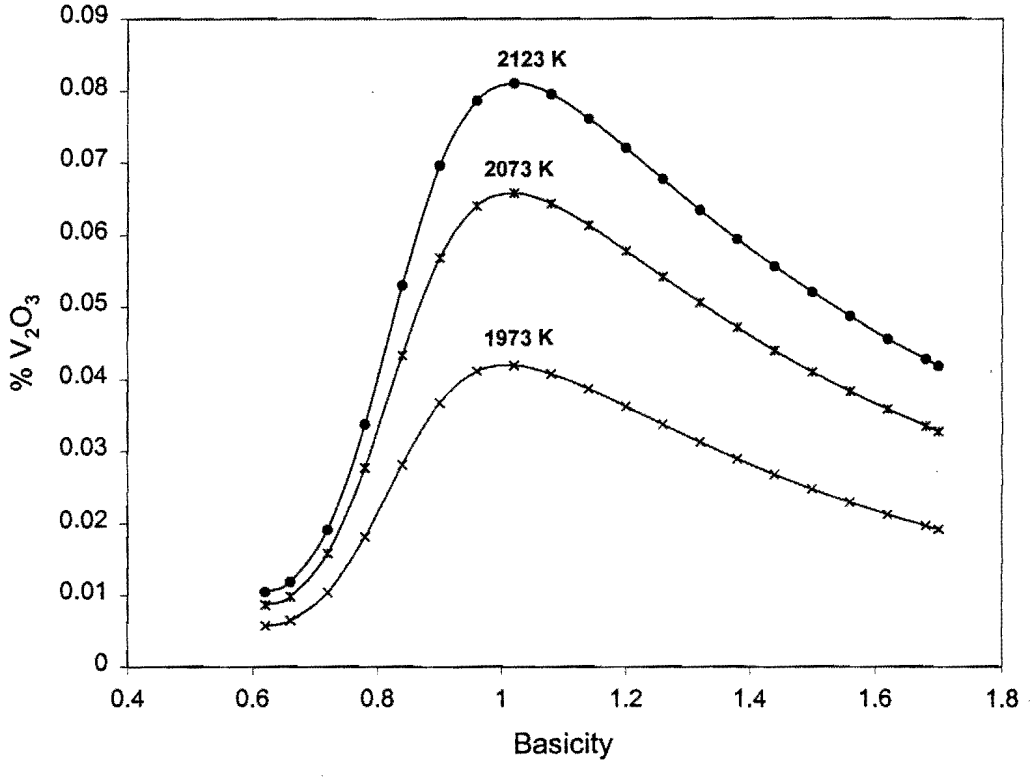

Figure 76: Predicted effect of temperature on oxidic vanadium losses to the slag, assuming a constant ferrovanadium composition of 80% V, 1.5% Al and the balance Fe. See Appendices 11 and 13 for the activities of vanadium and aluminum as a function of temperature utilized to perform the calculations. A total Al_2O_3 mass of 800kg per tonne of ferrovanadium was assumed. Appendix 11 contains the activities of Al_2O_3-CaO-MgO system as a function of temperature.

The predicted relationship of Figure 76 shows the strong effect of temperature on the vanadium losses to the slag. Tapping temperatures of the South African smelter is, as measured by means of an infrared pyrometer, on average around 1820°C.

It is thus expected that a lowering of the tap temperature will increase the vanadium recovery substantially. But from an entrained droplet point of view, lower tap temperatures might be detrimental. At this stage the effect of temperature on droplet entrainment is not fully quantified but the slag samples did not show did not show any strong effect of temperature, this includes temperatures as low as 1740°C, on the amount of droplets entrained. In the meantime it might be worthwhile for the industrial operation to control the tap temperatures around 1750°C and to monitor the effect of temperature on the total vanadium loss over an extended period.

The strong dependence of vanadium losses on the slag composition has clear implications for the operation of the industrial furnace. If it is assumed that the effect of MgO is similar to that of CaO (on a molar basis), the current operation uses the equivalent of a CaO: Al_2O_3 molar ratio of 1.0 (based on the composition shown in Table 3). Figures 73, 75 and 76 indicate that the maximum effects of MgO, Al and temperature, are expected at a CaO: Al_2O_3 molar ratio of 1.0. In addition to the vanadium losses which are expected to be close to the maximum (see figures 73, 75 and 76), the effects of MgO, Al and temperature amplify the maximum vanadium loss at a CaO: Al_2O_3 molar ratio of 1.0 even more. Small decreases in the slag basicity from the current level are expected to cause a large decrease in vanadium oxide loss, as well as to decrease the MgO, Al and temperature effect on soluble vanadium loss. This prediction is supported by analyses of industrial slags (see Figure 57); the slags clearly have lower vanadium oxide contents where the Al_2O_3 contents are higher (lower basicity). In addition to this, lower MgO contents in the slag, higher Al contents in ferrovanadium and lower tap temperature will likely yield lower vanadium oxide losses.

Appendix 1

Comparison between the actual weighed mass of water and the mass of water calculated assuming equilibrium between the water vapour in the gas stream and acid.

Bath temperature (°C)	Measured mass of water (g)	Exposure period (h)	Moisture g/h	Calculated mass of water (g)
42	0.099	5.83	0.0170	0.092
42	0.099	5.75	0.0172	0.091
42	0.095	5.58	0.0170	0.088
42	0.091	5.17	0.0176	0.082
42	0.086	5.00	0.0172	0.079
42	0.086	5.00	0.0172	0.079
42	0.086	5.00	0.0172	0.079
42	0.083	4.92	0.0169	0.078
42	0.092	5.00	0.0184	0.079
42	0.101	6.00	0.0168	0.095
50	0.111	5.00	0.0222	0.131
50	0.114	5.00	0.0228	0.131
55	0.424	14.00	0.0303	0.506
55	0.153	5.00	0.0306	0.181
55	0.158	5.00	0.0316	0.181
55	0.155	5.00	0.0310	0.181
42	0.076	5.00	0.0156	0.079
42	0.078	5.00	0.0156	0.079
42	0.076	5.00	0.0152	0.079
42	0.079	5.20	0.0151	0.082

Appendix 2 : EDX analysis of experimental slags

Experiment 1																									95% Confidence limit
Atom%	1	2	3	4	5	6	7	8	9	10	11	12	13	14	15	16	17	18	19	20	21	22	Ave	Stdev	
Al	63.58	63.57	62.60	63.25	63.60	61.86	62.88	63.12	62.74	63.08	63.40	63.62	63.38	62.04	62.41	61.51	63.00	63.50	63.53	63.53	63.47	63.27	62.99	0.62	0.26
Ca	26.82	26.03	26.10	26.43	25.33	27.28	26.63	27.16	26.40	25.89	26.93	26.41	26.11	26.39	26.52	27.71	26.31	26.79	26.40	26.40	25.24	27.06	26.47	0.60	0.25
Mg	1.73	1.87	2.35	2.21	2.40	1.90	1.73	1.44	2.01	1.79	1.74	2.21	1.99	2.06	1.73	1.94	1.77	2.39	2.15	2.15	2.60	1.45	2.00	0.31	0.13
V	5.50	5.82	6.47	5.89	6.55	6.27	6.13	6.39	6.77	7.05	5.70	5.66	6.41	6.45	6.17	5.18	5.88	5.13	5.88	5.88	6.48	5.59	6.10	0.50	0.21
Sum	97.63	97.29	97.52	97.78	97.88	97.31	97.37	98.11	97.92	97.81	97.77	97.90	97.89	96.94	96.83	96.34	96.96	97.81	97.96	97.96	97.79	97.37	97.56	0.47	0.20
Mole % oxidic component																									
Al_2O_3	50.39	50.38	49.61	50.13	50.40	49.03	49.83	50.02	49.72	49.99	50.25	50.42	50.23	49.17	49.46	48.75	49.93	50.32	50.35	50.35	50.30	50.14	49.92	0.49	0.20
CaO	42.51	41.26	41.37	41.89	40.15	43.24	42.21	43.05	41.84	41.04	42.69	41.86	41.39	41.83	42.04	43.92	41.70	42.46	41.84	41.84	40.01	42.89	41.96	0.95	0.40
MgO	2.74	2.96	3.72	3.50	3.80	3.01	2.74	2.28	3.19	2.84	2.76	3.50	3.15	3.27	2.74	3.07	2.81	3.79	3.41	3.41	4.12	2.30	3.17	0.50	0.21
V_2O_3	4.36	4.61	5.13	4.67	5.19	4.97	4.86	5.06	5.37	5.59	4.52	4.49	5.08	5.11	4.89	4.11	4.66	4.07	4.66	4.66	5.14	4.43	4.83	0.40	0.17
Basicity	0.898	0.878	0.909	0.906	0.872	0.943	0.902	0.906	0.906	0.878	0.904	0.900	0.887	0.917	0.905	0.964	0.891	0.919	0.899	0.899	0.877	0.901	0.904	0.021	0.009

Experiment 2																									95% Confidence limit
Atom%	1	2	3	4	5	6	7	8	9	10	11	12	13	14	15	16	17	18	19				Ave	Stdev	
Al-K	75.29	75.9	77.44	73.96	75.43	75.27	75.19	75.25	75.05	74.7	75.4	75.22	74.29	75.31	76.52	71.97	73.93	74.92	75.09				75.06	1.10	0.49
Ca-K	23.61	23.35	22	24.9	23.5	23.44	24.08	23.61	23.97	24.41	23.41	24.2	24.41	24.08	22.95	25.32	23.74	23.95	23.87				23.83	0.72	0.32
Mg-K	0.02	0	0	0	0	0	0.02	0.01	0	0	0	0.08	0	0.01	0	0	0	0	0				0.01	0.02	0.01
V -K	0.88	0.68	0.51	0.69	0.71	1.01	0.42	0.84	0.66	0.6	0.87	0.49	0.79	0.51	0.41	1.59	0.98	1.12	0.95				0.77	0.29	0.13
Sum	99.8	99.93	99.95	99.55	99.64	99.72	99.71	99.71	99.68	99.71	99.68	99.99	99.49	99.91	99.88	98.88	98.65	99.99	99.91				99.67	0.35	0.16
Mole % oxidic component																									
Al_2O_3	61	61.49	62.74	59.92	61.11	60.98	60.92	60.97	60.8	60.52	61.09	60.94	60.19	61.01	61.99	58.31	59.9	60.7	60.84				60.81	0.89	0.40
CaO	38.26	37.84	35.65	40.35	38.08	37.98	39.02	38.26	38.84	39.55	37.93	39.21	39.55	39.02	37.19	41.03	38.47	38.81	38.68				38.62	1.16	0.52
MgO	0.032	0	0	0	0	0	0.032	0.016	0	0	0	0.13	0	0.016	0	0	0	0	0				0.01	0.03	0.01
V_2O_3	0.713	0.551	0.413	0.559	0.575	0.818	0.34	0.681	0.535	0.486	0.705	0.397	0.64	0.413	0.332	1.288	0.794	0.907	0.77				0.63	0.23	0.10
Basicity	0.628	0.615	0.568	0.673	0.623	0.623	0.641	0.628	0.639	0.654	0.621	0.646	0.657	0.640	0.600	0.704	0.642	0.639	0.636				0.636	0.028	0.013

Experiment3																									95% Confidence limit
Atom%	1	2	3	4	5	6	7	8	9	10	11	12	13	14	15	16	17	18	19	20	21		Ave	Stdev	
Al	61.21	60.71	60.98	59.85	59.88	60.07	61.04	60.88	60.96	60.96	61.82	64.93	60.98	59.68	60.88	61.86	60.63	60.63	59.75	59.9	61.38		60.90	1.12	0.48
Ca	30.89	30.68	30.8	31.48	30.7	31.53	30.7	30.82	31.08	30.96	30.1	29.49	30.55	31.64	30.24	30.39	31.19	30.38	31.3	31.31	30.93		30.82	0.52	0.22
Mg	0	0	0	0	0.02	0	0	0	0	0	0	0	0	0.11	0.08	0.01	0	0.01	0	0	0		0.01	0.03	0.01
V	5.6	5.71	6.18	5.86	5.97	5.97	5.87	5.63	5.39	5.74	5.42	4.16	6.02	6.1	6.25	5.79	5.98	6.17	6.29	6.17	5.22		5.79	0.48	0.20
Sum	97.7	97.1	97.96	97.19	96.57	97.57	97.61	97.33	97.43	97.66	97.34	98.58	97.55	97.53	97.45	98.05	97.8	97.19	97.34	97.38	97.53		97.52	0.40	0.17
Mole % oxidic component																									
Al_2O_3	47.6	47.21	47.42	46.54	46.57	46.71	47.47	47.34	47.41	47.41	48.08	50.49	47.42	46.41	47.34	48.11	47.15	47.15	46.47	46.58	47.73		47.36	0.87	0.37
CaO	48.04	47.72	47.9	48.96	47.75	49.04	47.75	47.94	48.34	48.15	46.82	45.87	47.52	49.21	47.03	47.27	48.51	47.25	48.68	48.7	48.11		47.93	0.81	0.35
MgO	0	0	0	0	0.031	0	0	0	0	0	0	0	0	0.171	0.124	0.016	0	0.016	0	0	0		0.02	0.04	0.02
V_2O_3	4.355	4.44	4.806	4.557	4.643	4.643	4.565	4.378	4.192	4.464	4.215	3.235	4.682	4.744	4.86	4.503	4.65	4.798	4.892	4.798	4.059		4.50	0.37	0.16
Basicity	1.009	1.011	1.01	1.052	1.026	1.05	1.006	1.012	1.02	1.016	0.974	0.908	1.002	1.064	0.996	0.983	1.029	1.002	1.048	1.045	1.008		1.013	0.033	0.014

Experiment4																									95% Confidence limit
Atom%	1	2	3	4	5	6	7	8	9	10	11	12	13	14	15	16	17	18	19	20	21	22	Ave	Stdev	
Al	47.04	47.3	47.85	47.44	47.29	47.04	47.12	47.43	47.6	47.02	47.18	46.63	46.44	48.55	49.42	47.74	48.36	50.34	50.11	47.24	47.83	47.72	47.75	1.01	0.41
Ca	40.89	40.69	40.77	40.51	40.27	40.11	41.27	40.57	40.96	41.08	39.56	40.04	40.84	40.61	40.63	40.81	41.53	39.14	39.17	40.22	41.08	41.41	40.57	0.64	0.26
Mg	0	0	0.05	0.12	0	0	0	0.03	0	0.05	0	0	0.01	0.13	0	0	0	0	0	0	0.01	0	0.02	0.04	0.02
V	9.64	9.64	8.5	8.18	8.52	8.46	9.6	9.58	8.32	8.04	9.3	9.59	8.32	7.18	6.92	8.55	7.39	7.17	6.82	10.06	8.11	8.71	8.48	0.95	0.39
Sum	97.57	97.63	97.17	96.25	96.08	95.61	97.99	97.61	96.88	96.19	96.04	96.26	95.61	96.47	96.97	97.1	97.28	96.65	96.1	97.52	97.03	97.84	96.81	0.71	0.29
Mole % oxidic component																									
Al_2O_3	33.97	34.16	34.56	34.26	34.15	33.97	34.03	34.26	34.38	33.96	34.07	33.68	33.54	35.06	35.69	34.48	34.93	36.36	36.19	34.12	34.54	34.46	34.48	0.73	0.30
CaO	59.06	58.78	58.89	58.52	58.17	57.94	59.61	58.60	59.17	59.34	57.14	57.84	58.99	58.66	58.69	58.95	59.99	56.54	56.58	58.10	59.34	59.82	58.60	0.92	0.38
MgO	0.00	0.00	0.07	0.17	0.00	0.00	0.00	0.04	0.00	0.07	0.00	0.00	0.01	0.19	0.00	0.00	0.00	0.00	0.00	0.00	0.01	0.00	0.03	0.05	0.02
V_2O_3	6.96	6.96	6.14	5.91	6.15	6.11	6.93	6.92	6.01	5.81	6.72	6.93	6.01	5.19	5.00	6.18	5.34	5.18	4.93	7.27	5.86	6.29	6.12	0.69	0.28
Basicity	1.74	1.72	1.71	1.71	1.70	1.71	1.75	1.71	1.72	1.75	1.68	1.72	1.76	1.68	1.64	1.71	1.72	1.56	1.56	1.70	1.72	1.74	1.70	0.05	0.02

Experiment5																								95% Confidence limit
Atom%	1	2	3	4	5	6	7	8	9	10	11	12										Ave	Stdev	
Al	58.09	57.63	57.89	57.83	57.98	58.32	59.84	59.47	58.11	57.75	59.34	58.73										58.42	0.75	0.42
Ca	32.81	33.21	33.24	32.80	33.57	32.93	32.45	32.19	32.60	33.44	32.64	32.67										32.88	0.41	0.23
Mg	0.00	0.10	0.00	0.00	0.00	0.17	0.14	0.00	0.06	0.00	0.01	0.00										0.04	0.06	0.04
V	7.90	7.76	7.42	7.71	7.22	7.35	6.33	6.84	8.01	7.46	6.55	5.74										7.19	0.69	0.39
Sum	98.80	98.70	98.55	98.34	98.77	98.77	98.76	98.50	98.78	98.65	98.54	97.14										98.53	0.46	0.26
Mole % oxidic component																								
Al_2O_3	44.14	43.79	43.99	43.94	44.05	44.31	45.47	45.19	44.15	43.88	45.09	44.62										44.38	0.57	0.32
CaO	49.86	50.47	50.51	49.84	51.01	50.04	49.31	48.92	49.54	50.82	49.60	49.65										49.96	0.63	0.36
MgO	0.00	0.15	0.00	0.00	0.00	0.26	0.21	0.00	0.09	0.00	0.02	0.00										0.06	0.10	0.05
V_2O_3	6.00	5.90	5.64	5.86	5.49	5.58	4.81	5.20	6.09	5.67	4.98	4.36										5.46	0.53	0.30
Basicity	1.13	1.16	1.15	1.13	1.16	1.14	1.09	1.08	1.12	1.16	1.10	1.11										1.127	0.03	0.01

Experiment6																								95% Confidence limit
Atom%	1	2	3	4	5	6	7	8	9	10												Ave	Stdev	
Al	75.65	75.83	75.46	75.96	75.34	75.95	75.81	76.06	75.69	75.81												75.76	0.23	0.14
Ca	23.55	23.56	23.73	23.35	23.87	23.34	23.47	23.47	23.75	23.68												23.58	0.18	0.11
Mg	0.00	0.00	0.00	0.00	0.00	0.00	0.00	0.00	0.00	0.05												0.01	0.02	0.01
V	0.64	0.60	0.61	0.67	0.79	0.71	0.72	0.47	0.55	0.46												0.62	0.11	0.07
Sum	99.84	99.99	99.80	99.98	100.0	100.0	100.0	100.0	100.0	100.0												99.96	0.07	0.05
Mole % oxidic component																								
Al_2O_3	61.31	61.46	61.16	61.56	61.06	61.55	61.44	61.64	61.34	61.44												61.40	0.18	0.11
CaO	38.17	38.19	38.46	37.85	38.69	37.83	38.04	38.04	38.50	38.38												38.22	0.29	0.18
MgO	0.00	0.00	0.00	0.00	0.00	0.00	0.00	0.00	0.00	0.08												0.01	0.03	0.02
V_2O_3	0.52	0.49	0.49	0.54	0.64	0.58	0.58	0.38	0.45	0.37												0.50	0.09	0.05
Basicity	0.62	0.62	0.63	0.61	0.63	0.61	0.62	0.62	0.63	0.63												0.62	0.01	0.00

Experiment7																													95% Confidence limit
Atom%	1	2	3	4	5	6	7	8	9	10	11	12	13	14	15	16	17	18	19	20	21	22	23	24	25	26	27	Ave	Stdev	
Al	73.8	73.8	74.4	74.3	74.6	74.3	74.4	74.3	73.9	74.1	73.8	74.1																74.2	0.3	0.2
Ca	23.9	23.7	23.4	23.4	23.4	23.4	23.3	23.5	23.7	23.1	23.4	23.1																23.4	0.3	0.1
Mg	0.0	0.0	0.0	0.0	0.0	0.1	0.0	0.0	0.0	0.0	0.0	0.0																0.0	0.0	0.0
V	2.1	2.3	2.1	2.1	2.0	2.0	2.2	2.1	2.4	2.5	2.3	2.5																2.2	0.2	0.1
Sum	99.8	99.8	99.9	99.8	100	99.9	99.9	99.9	100	99.6	99.6	99.6																99.8	0.1	0.1
Mole % oxidic component																														
Al_2O_3	59.6	59.7	60.1	60.1	60.3	60.0	60.1	60.0	59.8	59.9	59.7	59.9																60.0	0.2	0.1
CaO	38.6	38.3	37.8	37.9	37.8	37.9	37.6	38.1	38.2	37.3	37.9	37.3																37.8	0.4	0.2
MgO	0.0	0.0	0.0	0.0	0.0	0.2	0.0	0.0	0.0	0.0	0.0	0.0																0.0	0.1	0.0
V_2O_3	1.7	1.8	1.7	1.7	1.6	1.6	1.8	1.7	1.9	2.0	1.9	2.0																1.8	0.1	0.1
Basicity	0.6	0.6	0.6	0.6	0.6	0.6	0.6	0.6	0.6	0.6	0.6	0.6																0.6	0.0	0.0

Experiment8																													95% Confidence limit
Atom%	1	2	3	4	5	6	7	8	9	10	11	12	13	14	15	16	17	18	19	20	21	22	23	24	25	26	27	Ave	Stdev	
Al	72.6	71.5	74.7	74.6	73.2	72.1	74.4	74.8	73.2	75.3	72.9	70.3	72.8	72.3	72.3	75.0	69.6	70.2	72.4	70.7	70.3	72.6	72.6	70.4	70.9	70.6	73.4	72.30	1.6	0.55
Ca	25.0	25.2	23.7	24.2	23.7	24.3	24.1	23.9	24.3	23.6	25.0	26.6	25.0	25.3	25.0	23.7	26.5	26.4	25.0	26.4	26.6	25.1	25.0	26.3	26.3	26.8	25.1	25.20	1.0	0.35
Mg	0.0	0.0	0.0	0.0	0.0	0.0	0.0	0.0	0.0	0.0	0.0	0.0	0.0	0.0	0.0	0.0	0.0	0.0	0.0	0.0	0.0	0.0	0.0	0.0	0.0	0.0	0.0	0.00	0.0	0.00
V	1.9	2.1	1.2	1.0	2.4	2.7	1.1	1.2	1.9	1.0	1.2	2.0	1.5	1.7	1.5	1.1	2.3	2.2	1.2	2.0	2.1	1.5	1.6	2.1	1.9	1.7	1.0	1.68	0.5	0.16
Sum	99.4	98.8	99.7	99.7	99.3	99.1	99.5	99.9	99.4	99.9	99.1	98.9	99.3	99.3	98.9	99.8	98.4	98.8	98.5	99.1	98.9	99.2	99.1	98.8	99.1	99.1	99.5	99.18	0.4	0.13
Mole % oxidic component																														
Al_2O_3	58.3	57.5	60.1	60.0	58.9	57.9	59.8	60.1	58.9	60.6	58.6	56.5	58.5	58.2	58.1	60.3	56.0	56.4	58.2	56.9	56.5	58.4	58.4	56.6	57.0	56.8	59.0	58.14	1.3	0.45
CaO	40.1	40.5	38.2	38.8	38.1	39.1	38.7	38.5	39.1	37.9	40.2	42.8	40.3	40.7	40.2	38.1	42.6	42.5	40.1	42.4	42.7	40.4	40.2	42.3	42.2	43.1	40.4	40.53	1.6	0.56
MgO	0.0	0.0	0.0	0.0	0.0	0.0	0.0	0.0	0.0	0.0	0.0	0.0	0.0	0.0	0.0	0.0	0.0	0.0	0.0	0.0	0.0	0.0	0.0	0.0	0.0	0.0	0.0	0.00	0.0	0.00
V_2O_3	1.5	1.7	1.0	0.8	1.9	2.1	0.9	1.0	1.5	0.8	0.9	1.6	1.2	1.3	1.2	0.9	1.8	1.8	0.9	1.6	1.7	1.2	1.2	1.7	1.6	1.4	0.8	1.35	0.4	0.13
Basicity	0.7	0.7	0.6	0.6	0.6	0.7	0.6	0.6	0.7	0.6	0.7	0.8	0.7	0.7	0.7	0.6	0.8	0.8	0.7	0.7	0.8	0.7	0.7	0.7	0.7	0.8	0.7	0.70	0.0	0.01

Experiment9 phase 1																											95% Confidence limit
Atom%	1	2	3	4	5	6	7	8	9	10	11	12	13	14											Ave	Stdev	
Al	61.9	60.6	60.5	59.6	58.5	58.5	60.7	59.5	60.9	60.8	60.5	61.9	58.2	57.7											59.94	1.32	0.69
Ca	32.3	33.2	33.4	33.5	34	34.5	32.3	33.5	32.5	32.8	33.6	32.1	35.0	35.1											33.40	0.98	0.51
Mg	0	0	0	0	0	0	0	0	0	0	0	0	0	0											0	0	0
V	5.17	5.21	6.37	6.4	6.5	6.0	6.0	6.0	5.7	5.4	5.2	5.3	5.9	6.1											5.77	0.45	0.24
Sum	99.0	98.9	99.4	99.4	98.9	98.9	99.1	99.0	99.2	98.9	99.3	99.3	99.1	98.9											99.06	0.18	0.09
Mole % oxidic component																											
Al_2O_3	46.9	46.1	46.1	45.4	44.5	44.5	46.2	45.4	46.4	46.3	46.1	47.2	44.3	43.9											45.66	1.01	0.53
CaO	49.1	50.5	50.9	51.0	51.8	52.5	49.3	51.0	49.5	49.9	51.2	48.9	53.3	53.5											50.89	1.49	0.78
MgO	0	0	0	0.0	0.0	0	0	0	0	0	0	0	0	0											0	0	0
V_2O_3	3.9	4.0	4.3	4.9	4.9	4.6	4.6	4.6	4.4	4.1	4.0	4.1	4.5	4.7											4.39	0.34	0.18
Basicity	1.0	1.1	1.1	1.1	1.2	1.2	1.1	1.1	1.1	1.1	1.1	1.0	1.2	1.2											1.12	0.06	0.03

Experiment9 phase 2																											95% Confidence limit
Atom%	1	2	3	4	5	6	7	8	9	10	11	12	13	14	15	16	17								Ave	Stdev	
Al	74.8	74.8	74.5	75.3	75.1	74.8	75.2	74.7	75.1	74.4	75.1	74.4	75.1	75.2	74.8	75.2	74.4								74.85	0.32	0.15
Ca	22.5	22.7	22.9	22.6	22.8	22.9	22.9	23.1	22.6	23.4	22.8	22.9	22.7	22.3	22.9	22.5	22.9								22.78	0.25	0.12
Mg	0	0	0	0	0	0	0	0	0	0	0	0	0	0	0	0	0								0	0	0
V	2.3	2.1	1.41	1.9	1.7	2.04	1.9	1.9	2.14	1.87	1.57	2.23	1.94	2.46	2.17	2.14	2.23								2.00	0.27	0.13
Sum	99.6	99.6	98.7	99.7	99.7	99.7	99.9	99.6	99.8	99.6	99.5	99.5	99.7	99.9	99.8	99.8	99.4								99.63	0.27	0.13
Mole % oxidic component																											
Al_2O_3	61.3	61.3	61.0	61.6	61.5	61.3	61.6	61.2	61.5	60.9	61.5	61.5	61.5	61.6	61.2	61.6	60.9								61.31	0.26	0.12
CaO	36.9	37.2	37.5	37.0	37.3	37.5	37.4	37.8	37.0	38.3	37.4	37.2	37.2	36.5	37.5	36.8	37.4								37.31	0.41	0.20
MgO	0	0	0	0	0	0	0	0	0	0	0	0	0	0	0	0	0								0	0	0
V_2O_3	1.9	1.7	1.2	1.52	1.42	1.67	1.57	1.54	1.75	1.53	1.29	1.59	1.59	2.0	1.78	1.75	1.83								1.64	0.22	0.10
Basicity	0.6	0.61	0.61	0.6	0.61	0.61	0.61	0.62	0.60	0.63	0.61	0.60	0.60	0.59	0.61	0.60	0.61								0.61	0.01	0.00

Experiment10																										95% Confidence limit
Atom%	1	2	3	4	5	6	7	8	9	10	11	12	13	14	15	16	17	18	19	20	21	22	23	Ave	Stdev	
Al	51.2	51.4	50.7	52.7	53.0	50.8	51.3	51.3	51.0	54.6	55.0	50.9	51.0	51.1	51.2	51.6	51.5	51.4	51.4	51.0	51.4	51.7	52.1	51.95	1.41	0.51
Ca	37.4	38.0	37.8	38.4	37.7	37.1	37.6	37.4	37.4	39.3	39.4	38.3	38.0	37.8	37.8	37.8	37.9	38.3	38.4	37.9	37.6	38.3	37.8	38.10	0.63	0.23
Mg	0.0	0.0	0.0	0.1	0.0	0.1	0.1	0.0	0.1	0.0	0.0	0.1	0.1	0.1	0.1	0.1	0.0	0.0	0.1	0.1	0.1	0.1	0.0	0.05	0.05	0.02
V	10.9	10.0	10.8	8.4	8.5	11.5	10.6	10.5	10.9	5.9	5.2	10.1	10.5	10.7	10.3	10.2	10.0	9.9	9.3	10.8	10.5	9.7	9.7	9.37	1.92	0.70
Sum	99.5	99.5	99.3	99.6	99.2	99.4	99.4	99.3	99.4	99.8	99.6	99.3	99.5	99.7	99.4	99.6	99.4	99.5	99.2	99.7	99.5	99.7	99.7	99.48	0.16	0.06
Mole % oxidic component																										
Al_2O_3	37.4	37.6	37.0	38.5	38.7	37.1	37.4	37.5	37.3	39.9	40.2	37.2	37.2	37.3	37.4	37.7	37.6	37.5	37.5	37.2	37.6	37.7	38.1	37.95	1.03	0.37
CaO	54.6	55.6	55.3	56.1	55.1	54.2	54.9	54.7	54.6	57.4	57.5	55.9	55.5	55.2	55.2	55.2	55.4	55.9	56.1	55.4	54.9	55.9	55.3	55.65	0.92	0.33
MgO	0.0	0.0	0.0	0.1	0.0	0.1	0.1	0.0	0.1	0.0	0.0	0.2	0.1	0.1	0.2	0.2	0.0	0.0	0.2	0.1	0.1	0.1	0.0	0.08	0.08	0.03
V_2O_3	8.0	7.3	7.9	6.2	6.2	8.4	7.7	7.7	8.0	4.3	3.8	7.3	7.7	7.8	7.5	7.4	7.3	7.2	6.8	7.9	7.6	7.1	7.1	6.85	1.40	0.51
Basicity	1.5	1.5	1.5	1.5	1.4	1.5	1.5	1.5	1.5	1.4	1.4	1.5	1.5	1.5	1.5	1.5	1.5	1.5	1.5	1.5	1.5	1.5	1.5	1.47	0.02	0.01

Appendix 3 : Industrial slag analysis

Slag 1 bottom

MA phase							Ave	Stdev	95 % Confidence limit
Na	0.02	0.05	0.08	0	0.18	0.08	0.07	0.06	0.05
Mg	24.27	24.35	24.2	24.2	23.83	24.05	24.15	0.19	0.15
Al	66.87	66.62	66.88	67.21	65.2	66.78	66.59	0.71	0.57
Si	0	0	0.16	0	0.05	0	0.04	0.06	0.05
P	0	0	0.08	0	0	0	0.01	0.03	0.03
S	0.03	0	0.1	0.01	0	0.06	0.03	0.04	0.03
Ca	0.4	0.56	0.45	0.21	0.3	0.35	0.38	0.12	0.10
V	8.09	8.07	7.47	7.79	9.55	8.08	8.18	0.72	0.57
Fe	0.13	0	0	0.09	0.11	0.17	0.08	0.07	0.06

CA phase							Ave	Stdev	95 % Confidence limit
Na	1.2	0.33	0.37	0.29	0.49	0.54	0.54	0.34	0.27
Mg	0	0	0	0	0	0.02	0.00	0.01	0.01
Al	52.95	53.78	53.81	54.3	53.6	54.07	53.75	0.46	0.37
Si	0.03	0.03	0.11	0	0	0.16	0.06	0.07	0.05
P	0.03	0.17	0	0.06	0.08	0.13	0.08	0.06	0.05
S	0.14	0	0	0.08	0	0	0.04	0.06	0.05
Ca	44.8	45.06	45.28	44.99	44.98	44.05	44.86	0.43	0.34
V	0.19	0.14	0.3	0.04	0.37	0.64	0.28	0.21	0.17
Fe	0.24	0	0	0	0.27	0	0.09	0.13	0.11

A_2 phase						Ave	Stdev	95 % Confidence limit
Na	0.54	0.21	0.17	0.12	0.19	0.25	0.17	0.15
Mg	0	0	0	0	0	0.00	0.00	0.00
Al	68	68.37	68.38	68.58	68.11	68.29	0.23	0.20
Si	0	0	0	0	0	0.00	0.00	0.00
P	0.04	0.04	0.15	0	0	0.05	0.06	0.05
S	0.13	0.09	0	0.04	0	0.05	0.06	0.05
Ca	30.39	30.81	30.78	30.37	30.82	30.63	0.23	0.20
V	0.27	0.18	0.15	0.47	0.44	0.30	0.15	0.13
Fe	0.1	0.06	0	0	0.22	0.08	0.09	0.08

Average slag analysis								Ave	Stdev	95 % Confidence limit
Na	1.72	0.86	0.99	0.46	0.44	0.82	1.81	1.01	0.55	0.34
Mg	9.52	7.57	8.47	10.01	8.31	10.25	12.5	9.52	1.63	1.01
Al	62.64	62.98	63.04	61.35	64.11	61.69	62.34	62.59	0.92	0.57
Si	0.13	0	0.11	0.18	0.2	0.22	0	0.12	0.09	0.06
P	0	0.01	0	0.17	0.04	0.05	0.08	0.05	0.06	0.04
S	0.04	0	0.12	0.06	0.13	0.17	0.2	0.10	0.07	0.04
K	0.75	0.14	0.5	0.17	0.26	0.33	1.21	0.48	0.38	0.24
Ca	20.77	24.16	22.63	22.28	21.84	21.29	16.57	21.36	2.37	1.47
V	4.14	4.03	4	5.19	4.51	4.84	5.19	4.56	0.52	0.32
Fe	0	0.14	0	0	0.15	0.04	0.04	0.05	0.07	0.04

Slag 1 top

MA phase											Ave	Stdev	95 % Confidence limit
Na	0	0	0.11	0	0.02	0	0	0	0	0	0.01	0.03	0.00
Mg	23.13	22.46	23.54	22.82	24.27	23.61	24.09	24.25	24.04	24.27	23.65	0.66	0.41
Al	60.43	64.56	63.57	61.28	65.3	63.56	64.99	65.23	65.21	63.62	63.78	1.70	1.06
Si	0.13	0.07	0	0	0	0.1	0	0	0.04	0	0.03	0.05	0.03
Ca	0.62	0.87	0.44	0.72	0.19	0.46	0.38	0.3	0.47	0.45	0.49	0.20	0.12
V	15.36	11.84	11.32	14.62	9.89	11.76	10.06	9.91	9.91	10.81	11.55	1.97	1.22
Fe	0	0.09	0.11	0	0	0	0.1	0	0.03	0.23	0.06	0.08	0.00

CA phase						Ave	Stdev	95 % Confidence limit
Na	0.14	0	0	0.03	0.02	0.04	0.06	0.00
Mg	0	0	0.06	0	0	0.01	0.03	0.02
Al	54.1	53.92	54.35	54.45	53.76	54.12	0.29	0.19
Si	0	0	0	0	0	0.00	0.00	0.00
Ca	44.71	45.1	44.99	45.03	45.71	45.11	0.37	0.24
V	0.22	0.45	0	0.24	0.09	0.20	0.17	0.11
Fe	0.37	0	0	0.13	0	0.10	0.16	0.00

CA_2 phase						Ave	Stdev	95 % Confidence limit
Na	0.05	0	0.05	0.13	0	0.05	0.05	0.00
Mg	0	0.03	0	0.14	0	0.03	0.06	0.04
Al	68.58	69.26	69.2	68.34	68.15	68.71	0.50	0.35
Si	0	0	0	0	0	0.00	0.00	0.00
Ca	30.45	30.1	30.23	30.59	31.04	30.48	0.37	0.25
V	0.57	0.47	0.26	0.43	0.42	0.43	0.11	0.08
Fe	0.28	0	0.06	0.07	0.27	0.14	0.13	0.00

Average slag analysis								Ave	Stdev	95 % Confidence limit
Na	0.13	0.36	0.16	0.73	0.45	0.03	0.92	0.40	0.33	0.20
Mg	4.45	3.47	5	4.16	3.83	3.68	4.04	4.09	0.51	0.32
Al	64.83	62.41	64.91	62.77	63.79	64.41	62.87	63.71	1.04	0.64
Si	0	0	0	0	0	0	0	0.00	0.00	0.00
P	0.04	0	0	0	0	0.01	0	0.01	0.01	0.01
S	0.04	0.16	0.05	0.04	0.12	0	0.17	0.08	0.07	0.04
Cl	0	0	0.07	0	0.1	0	0	0.02	0.04	0.03
K	0.15	0.12	0.23	0.14	0	0.02	0.43	0.16	0.14	0.09
Ca	27.47	30.65	26.68	29.43	28.9	28.47	28.52	28.59	1.29	0.80
V	2.81	2.75	2.52	2.61	2.63	3.35	2.67	2.76	0.28	0.17
Fe	0	0	0.1	0	0	0.02	0	0.02	0.04	0.02

Slag 2 bottom

MA phase									Ave	Stdev	95 % Confidence limit
Na	0.03	0	0	0	0	0.1	0	0.01	0.02	0.03	0.02
Mg	24.28	23.89	23.77	24.19	24.31	24.72	24.26	23.79	24.15	0.32	0.22
Al	66.79	65.37	64.7	54.34	66.71	66.45	66.66	61.99	64.13	4.27	2.96
Si	0.08	0	0.11	0	0	0	0.18	0	0.05	0.07	0.05
P	0	0	0.13	0	0.02	0	0.03	0	0.02	0.04	0.03
S	0	0	0.1	0.09	0	0.12	0.01	0	0.04	0.05	0.04
Cl	0	0.27	0	0.03	0.07	0.09	0	0.11	0.07	0.09	0.06
K	0.2	0	0.14	0	0.03	0.02	0.11	0.01	0.06	0.08	0.05
Ca	0.21	0.56	0.44	0.51	0.25	0.4	0.25	0.33	0.37	0.13	0.09
V	8.34	9.73	10.17	9.37	8.39	7.8	8.3	12.9	9.38	1.64	1.14
Fe	0	0.11	0.02	0.25	0	0	0.01	0.19	0.07	0.10	0.07

CA phase									Ave	Stdev	95 % Confidence limit
Na	0.05	0.08	0.24	0	0.23	0	0	0.19	0.10	0.11	0.07
Mg	0	0.08	0.03	0	0	0.03	0.01	0.21	0.05	0.07	0.05
Al	54.36	54.75	53.78	53.09	53.93	54.24	54.28	54.46	54.11	0.51	0.35
Si	0.03	0.15	0.08	0.17	0.05	0.05	0.06	0	0.07	0.06	0.04
P	0	0.19	0.13	0	0.09	0	0.09	0	0.06	0.07	0.05
S	0	0.04	0	0	0	0	0.07	0	0.01	0.03	0.02
Cl	0.12	0	0.06	0	0	0.04	0.13	0	0.04	0.06	0.04
K	0	0	0	0	0.05	0	0	0	0.01	0.02	0.01
Ca	44.87	44.65	45.46	46.71	45.05	45.39	44.66	44.99	45.22	0.67	0.46
V	0	0	0.02	0.03	0.15	0.17	0.21	0.08	0.08	0.08	0.06
Fe	0.25	0	0.07	0	0.28	0.07	0.21	0.02	0.11	0.12	0.08

CA_2 phase									Ave	Stdev	95 % Confidence limit
Na	0	0	0	0	0	0	0.02	0.08	0.01	0.03	0.02
Mg	0.04	0	0	0	0.05	0	0	0	0.01	0.02	0.01
Al	68.77	68.66	68.43	68.49	68.82	68	69.47	68.46	68.64	0.42	0.29
Si	0.01	0	0	0	0.03	0.19	0	0	0.03	0.07	0.05
P	0.11	0.16	0	0	0.03	0.15	0	0	0.06	0.07	0.05
S	0.16	0.08	0.13	0	0.08	0.03	0	0	0.06	0.06	0.04
Cl	0	0	0	0.15	0.04	0	0	0.04	0.03	0.05	0.04
K	0.1	0	0.06	0	0.1	0	0.02	0.01	0.04	0.04	0.03
Ca	30.31	30.68	31.14	30.66	30.35	31.05	30.11	30.81	30.64	0.36	0.25
V	0.45	0.39	0.24	0.62	0.1	0.56	0.33	0.53	0.40	0.17	0.12
Fe	0	0.03	0	0	0.03	0	0	0.06	0.02	0.02	0.02

Na-rich phase									Ave	Stdev	95 % Confidence limit
Na	0.64	0.44	0.62	0.41	0.77	0.65	0.47	0.5	0.56	0.13	0.09
Mg	0.02	0.19	0.15	0	0.09	0.19	0	0.06	0.09	0.08	0.06
Al	41.56	41.79	41.16	40.53	39.43	40.72	41.69	40.84	40.97	0.78	0.54
Si	0.86	0.72	0.71	1.03	3.73	0.8	0.82	0.98	1.21	1.03	0.71
P	0.14	0.21	0.1	0.11	0.08	0	0.16	0.13	0.12	0.06	0.04
S	0.08	0.08	0	0.07	0.01	0.07	0.12	0	0.05	0.04	0.03
Cl	0	0.16	0.01	0	0	0.09	0.02	0.01	0.04	0.06	0.04
K	0.09	0.05	0.01	0.11	0.02	0.02	0	0.12	0.05	0.05	0.03
Ca	56.25	55.83	57.04	57.19	55.44	57.13	56.71	56.87	56.56	0.65	0.45
V	0.15	0.33	0.13	0.46	0.22	0.24	0	0.16	0.21	0.14	0.10
Fe	0.21	0.16	0.07	0	0.05	0	0.01	0.12	0.08	0.08	0.05

Average slag analysis											Ave	Stdev	95 % Confidence limit
Na	0.4	0.49	0.47	0.39	0.51	0.1	0.38	0.37	0.75	0.52	0.44	0.16	0.10
Mg	13.39	12.59	13.16	11	11.94	24.72	14.1	12.69	13.04	12.39	13.90	3.89	2.41
Al	57.84	57.9	58.26	60.67	57.62	66.45	59.54	58.31	58.62	54.64	58.99	3.04	1.88
Si	0.42	0.1	0.2	0.23	0.13	0	0.24	0.18	0.08	0.22	0.18	0.11	0.07
P	0.15	0.11	0.01	0.09	0	0	0.17	0.06	0.03	0.16	0.08	0.07	0.04
S	0.08	0	0.02	0	0	0.12	0	0.15	0.13	0.01	0.05	0.06	0.04
Cl	0	0.08	0.12	0	0	0.09	0	0.02	0.02	0	0.03	0.05	0.03
K	0.13	0	0.11	0.06	0.1	0.02	0	0.04	0.02	0.01	0.05	0.05	0.03
Ca	21.53	22.71	21.3	23.11	24.39	0.4	19.67	22.8	21.68	22.84	20.04	7.02	4.35
V	5.62	5.42	5.7	4.26	4.94	7.8	5.87	5.15	5.42	6.37	5.66	0.94	0.58
Fe	0.2	0	0.29	0.03	0.13	0	0	0.02	0.17	0.25	0.11	0.11	0.07

Slag 2 top

MA phase									Ave	Stdev	95 % Confidence limit
Na	0.03	0	0.01	0.09	0	0.04	0.01	0.05	0.03	0.03	0.02
Mg	24.05	23.79	24.05	23.91	22.9	24.09	24.28	23.67	23.84	0.42	0.29
Al	63.94	66.49	66.33	65	57.56	65.96	65.59	66.26	64.64	2.98	2.07
Si	0.19	0	0	0.03	0.04	0.02	0	0.07	0.04	0.06	0.04
P	0	0	0.01	0.1	0	0	0	0.09	0.03	0.04	0.03
S	0	0	0	0	0.01	0	0	0	0.00	0.00	0.00
Cl	0	0	0	0	0.07	0	0	0.03	0.01	0.03	0.02
K	0	0.03	0	0.15	0.04	0	0	0	0.03	0.05	0.04
Ca	0.51	0.31	0.42	0.31	0.41	0.48	0.54	0.33	0.41	0.09	0.06
V	10.9	9.25	8.62	10.08	18.21	8.95	9.33	9.08	10.55	3.18	2.20
Fe	0.02	0	0.02	0	0.06	0	0	0	0.01	0.02	0.01

CA phase									Ave	Stdev	95 % Confidence limit
Na	0.04	0.14	0.19	0.16	0.02	0.23	0.07	0.18	0.13	0.08	0.05
Mg	0.05	0	0	0.06	0.04	0.14	0	0	0.04	0.05	0.03
Al	54.82	54.7	54.36	54.31	54.37	54.71	55.16	54.18	54.58	0.33	0.23
Si	0.04	0	0.14	0.06	0	0.06	0.02	0	0.04	0.05	0.03
P	0	0.03	0	0.09	0	0.17	0.05	0.07	0.05	0.06	0.04
S	0	0	0.01	0.01	0.03	0.1	0	0.05	0.03	0.04	0.02
Cl	0.01	0.01	0.06	0.04	0.03	0	0.07	0	0.03	0.03	0.02
K	0	0.05	0.07	0.01	0	0	0	0	0.02	0.03	0.02
Ca	44.78	44.91	44.53	44.69	45.24	44.19	44.22	45.16	44.72	0.39	0.27
V	0.19	0.09	0.38	0.15	0.27	0.14	0.12	0.16	0.19	0.09	0.07
Fe	0	0.09	0.23	0.13	0	0.07	0.23	0.2	0.12	0.09	0.07

CA_2 phase									Ave	Stdev	95 % Confidence limit
Na	0	0	0.06	0.13	0.1	0.12	0	0.01	0.05	0.06	0.04
Mg	0.05	0	0.11	0	0.02	0.06	0	0	0.03	0.04	0.03
Al	69.36	68.77	68.49	69.14	68.75	69.38	69.79	68.92	69.08	0.42	0.29
Si	0	0	0	0	0	0	0.05	0	0.01	0.02	0.01
P	0	0.05	0	0.01	0.07	0	0.01	0.07	0.03	0.03	0.02
S	0.02	0.13	0.09	0	0	0	0	0.04	0.04	0.05	0.03
Cl	0	0.1	0.08	0	0.04	0	0	0.04	0.03	0.04	0.03
K	0	0.02	0	0	0.04	0	0	0.04	0.01	0.02	0.01
Ca	29.98	30.3	30.87	30.32	30.47	29.81	29.56	30.35	30.21	0.41	0.28
V	0.48	0.39	0.25	0.38	0.48	0.58	0.45	0.41	0.43	0.10	0.07
Fe	0	0.08	0	0	0	0.04	0	0	0.02	0.03	0.02

Na-rich phase									Ave	Stdev	95 % Confidence limit
Na	0.74	1.12	0.45	0.95	0.61	0.7	0.59	1.11	0.78	0.25	0.17
Mg	0.06	0.18	0	0	0.2	0.1	0.03	0.12	0.09	0.08	0.05
Al	42.47	39.83	41.4	39.86	41.52	41.5	40.7	38.58	40.73	1.25	0.86
Si	0.46	2.24	0.76	2.22	0.54	1.65	1.9	3.74	1.69	1.10	0.77
P	0.09	0.16	0.12	0.04	0.16	0.17	0.01	0.11	0.11	0.06	0.04
S	0.14	0.23	0.13	0.03	0.11	0.11	0.05	0.35	0.14	0.10	0.07
Cl	0.04	0.15	0.09	0.03	0	0.17	0.08	0.09	0.08	0.06	0.04
K	0.03	0.1	0.02	0.09	0	0.18	0.11	0.1	0.08	0.06	0.04
Ca	55.7	55.84	56.71	56.14	56.21	55.17	56.06	55.63	55.93	0.46	0.32
V	0.07	0.05	0.08	0.34	0.19	0.09	0.25	0	0.13	0.12	0.08
Fe	0.06	0.11	0.11	0	0.16	0.02	0	0	0.06	0.06	0.04

Average slag analysis											Ave	Stdev	95 % Confidence limit
Na	0.64	0.29	0.62	0.55	0.88	0.66	0.4	0.91	0.87	0.44	0.63	0.21	0.13
Mg	6.12	11.43	12.5	9.14	4.13	11.04	10.54	8.37	11.05	11.64	9.60	2.68	1.66
Al	55.86	57.79	58.4	57.37	54	57.81	56.92	57.22	55.89	57.49	56.88	1.29	0.80
Si	0.18	0.29	0.22	0.34	0.24	0.09	0.14	0.25	0.73	0.13	0.26	0.18	0.11
P	0.12	0.24	0.09	0	0.02	0	0.17	0.13	0.14	0	0.09	0.08	0.05
S	0.12	0.17	0.04	0.05	0.15	0.09	0.15	0.08	0.42	0.1	0.14	0.11	0.07
Cl	0.09	0.09	0	0.1	0	0	0.05	0	0.22	0.06	0.06	0.07	0.04
K	0	0.02	0.09	0.08	0.17	0.01	0.08	0.02	0.2	0.18	0.09	0.08	0.05
Ca	33.68	25.04	21.86	27.98	37.04	25.15	26.85	28.91	23.76	24.56	27.48	4.69	2.91
V	3.04	4.36	5.81	4	2.88	5.16	4.53	3.85	5.46	5.09	4.42	0.99	0.61
Fe	0.13	0.13	0.1	0.02	0.07	0	0.13	0	0.84	0.07	0.15	0.25	0.15

Slag 3 bottom

MA phase									Ave	Stdev	95 % Confidence limit
Na	0	0	0	0.06	0	0.03	0.02	0.05	0.02	0.02	0.02
Mg	24.91	25.15	24.89	25.01	25.34	25.08	25.43	25.14	25.12	0.19	0.13
Al	71.01	70.75	71.67	71.88	72.49	73	72.72	71.99	71.94	0.79	0.55
Si	0	0.21	0.1	0	0	0.09	0.06	0	0.06	0.07	0.05
P	0.05	0.04	0	0.24	0.04	0	0	0	0.05	0.08	0.06
S	0.02	0	0.06	0	0	0	0	0.11	0.02	0.04	0.03
Cl	0	0	0	0	0.03	0	0.08	0.17	0.04	0.06	0.04
K	0	0.03	0.03	0	0	0.06	0.12	0.04	0.04	0.04	0.03
Ca	0.22	0.34	0.34	0.35	0.4	0.31	0.31	0.37	0.33	0.05	0.04
V	3.79	3.35	2.69	2.22	1.7	1.37	1.25	2.01	2.30	0.92	0.64
Fe	0	0.14	0.21	0.24	0	0.06	0	0.13	0.10	0.10	0.07

CA phase										Ave	Stdev	95 % Confidence limit
Na	0.09	0	0.08	0.29	0	0.01	0	0	0.1	0.06	0.10	0.06
Mg	0.07	0	0	0	0	0	0	0.01	0.1	0.02	0.04	0.02
Al	54.35	54.53	54.17	54.88	54.36	54.64	53.86	53.49	54.56	54.32	0.42	0.28
Si	0	0.05	0	0.12	0.05	0.09	0	0	0.05	0.04	0.04	0.03
P	0	0	0	0	0	0	0.01	0	0	0.00	0.00	0.00
S	0	0.01	0.09	0	0.08	0	0	0	0.02	0.02	0.04	0.02
Cl	0.02	0.01	0.1	0	0	0.07	0.04	0.05	0.13	0.05	0.05	0.03
K	0	0	0	0.04	0.14	0.07	0.11	0.03	0.16	0.06	0.06	0.04
Ca	45.09	45.21	45.39	44.67	45.37	45.12	45.7	46.37	44.89	45.31	0.50	0.32
V	0.03	0.05	0	0	0	0	0.14	0.05	0	0.03	0.05	0.03
Fe	0.35	0.14	0.18	0	0	0.01	0.15	0	0	0.09	0.12	0.08

CA_2 phase									Ave	Stdev	95 % Confidence limit
Na	0.07	0.18	0.02	0.01	0	0.08	0	0.12	0.06	0.07	0.05
Mg	0	0	0	0	0.03	0	0.14	0.08	0.03	0.05	0.04
Al	68.52	69.18	68.06	69.02	68.9	68.43	68.35	68.52	68.62	0.38	0.26
Si	0	0	0	0	0	0	0	0	0.00	0.00	0.00
P	0	0	0.03	0.03	0.11	0.03	0	0.03	0.03	0.04	0.02
S	0	0	0	0.18	0	0.07	0.03	0.12	0.05	0.07	0.05
Cl	0.02	0	0	0	0	0.03	0.05	0	0.01	0.02	0.01
K	0.01	0	0.08	0	0	0.08	0.03	0.13	0.04	0.05	0.03
Ca	31.22	30.64	31.69	30.61	30.75	30.93	31.18	30.6	30.95	0.39	0.27
V	0.06	0	0	0	0.08	0.18	0	0.31	0.08	0.11	0.08
Fe	0.1	0	0.11	0.15	0.13	0.18	0.23	0.08	0.12	0.07	0.05

Na-rich phase									Ave	Stdev	95 % Confidence limit
Na	1.19	0.65	0.55	0.94	0.69	1.26	0.2	1.26	0.84	0.38	0.27
Mg	0.05	1.01	0.24	0.2	0.05	0.03	0.05	0.33	0.25	0.33	0.23
Al	42.12	41.61	42.18	47.74	43.93	36.17	46.07	41.37	42.65	3.47	2.41
Si	0.94	1.16	1	1.26	2.78	1.98	1.36	0.92	1.43	0.65	0.45
P	0.03	0.09	0.03	0.07	0.26	0.07	0.05	0.04	0.08	0.08	0.05
S	0.06	0	0.05	0.11	0.15	2.94	0.53	0.21	0.51	1.00	0.69
Cl	0.01	0	0.05	0	0	0	0	0.02	0.01	0.02	0.01
K	0.36	0.39	0.06	0.37	0.19	0.24	0.04	0.22	0.23	0.14	0.09
Ca	55.11	54.9	55.59	49.11	51.96	57.16	51.35	55.44	53.83	2.71	1.88
V	0.15	0.16	0.03	0.2	0.01	0.05	0.13	0.18	0.11	0.07	0.05
Fe	0	0.03	0.22	0	0	0.09	0.22	0	0.07	0.10	0.07

Average slag analysis												Ave	Stdev	95 % Confidence limit
Na	0.54	0.51	0.85	0.62	86	0.69	1.07	0.92	0.94	1	0.51	8.51	25.70	15.93
Mg	12.82	13.87	12.95	12.26	7.8	13.08	13.69	13.72	13.99	12.96	12.97	12.74	1.72	1.07
Al	59.4	59.68	61.75	60.26	58.61	60.27	60.17	59.88	58.59	58.98	59	59.69	0.93	0.58
Si	0.33	0	0.09	0.22	0.37	0.28	0.2	0.1	0.15	0.18	0.24	0.20	0.11	0.07
P	0	0.14	0	0	0.2	0.15	0.1	0.01	0	0.05	0	0.06	0.08	0.05
S	0.04	0.23	0.09	0	0.07	0.1	0.24	0.09	0.08	0.17	0.08	0.11	0.07	0.05
Cl	0	0.03	0	0	0	0.1	0	0.11	0.03	0.11	0.16	0.05	0.06	0.04
K	0.18	0.14	0.16	0.08	0	0.09	0.26	0	0.07	0	0.09	0.10	0.08	0.05
Ca	24.16	21.93	21.82	23.93	31.11	22.42	21.05	21.52	22.78	23.62	23.54	23.44	2.75	1.70
V	2.3	3.48	2.04	2.46	0.98	2.69	3.17	3.39	2.67	2.88	3.3	2.67	0.73	0.45
Fe	0.22	0	0.24	0.16	0	0.12	0.06	0.26	0.7	0.06	0.11	0.18	0.20	0.12

Slag 3 top

MA phase								Ave	Stdev	95 % Confidence limit
Na	0	0.01	0.01	0	0	0	0.12	0.02	0.04	0.03
Mg	24.88	24.5	24.85	24.44	24.76	24.46	24.66	24.65	0.19	0.14
Al	70.33	70.82	69.92	70.39	69.22	66.43	69.82	69.56	1.47	1.09
Si	0.18	0.05	0.06	0.21	0	0.19	0	0.10	0.09	0.07
P	0.14	0	0.01	0	0	0.05	0.01	0.03	0.05	0.04
S	0.1	0	0	0.12	0.03	0	0.07	0.05	0.05	0.04
Cl	0.22	0.07	0.04	0.12	0.1	0	0.11	0.09	0.07	0.05
K	0	0.04	0	0	0	0	0	0.01	0.02	0.01
Ca	0.24	0.26	0.38	0.24	0.56	0.41	0.45	0.36	0.12	0.09
V	3.91	4.26	4.73	4.47	5.31	8.27	4.61	5.08	1.47	1.09
Fe	0	0	0	0	0.02	0.19	0.14	0.05	0.08	0.06

CA phase								Ave	Stdev	95 % Confidence limit
Na	0.25	0.34	0.12	0	0.1	0	0.25	0.15	0.13	0.10
Mg	0	0	0	0	0	0.12	0	0.02	0.05	0.03
Al	55.24	53.5	54.67	54.53	54.17	54.48	54.15	54.39	0.54	0.40
Si	0.18	0.77	0	0.14	0.44	0.24	0.23	0.29	0.25	0.19
P	0	0	0.12	0.07	0	0.01	0.06	0.04	0.05	0.03
S	0.06	0.05	0.05	0.15	0	0.05	0	0.05	0.05	0.04
Cl	0.07	0	0.07	0.01	0.1	0.02	0	0.04	0.04	0.03
K	0.02	0.01	0.08	0.04	0	0.05	0	0.03	0.03	0.02
Ca	44.1	45.32	44.83	44.95	45.19	45.03	45.28	44.96	0.42	0.31
V	0	0.01	0.02	0	0	0.01	0.03	0.01	0.01	0.01
Fe	0.07	0	0.04	0.11	0	0	0	0.03	0.04	0.03

CA_2 phase								Ave	Stdev	95 % Confidence limit
Na	0	0.03	0	0.05	0.15	0.12	1.28	0.23	0.47	0.34
Mg	0.01	0	0.01	0	0.09	0	0.23	0.05	0.09	0.06
Al	69.56	69.82	69.31	69.18	66.37	69.48	68.03	68.82	1.22	0.91
Si	0.16	0.07	0	0	0.79	0.05	0.04	0.16	0.28	0.21
P	0.01	0.17	0	0.04	0.04	0	0.07	0.05	0.06	0.04
S	0.07	0.06	0	0.04	0.25	0.07	0.13	0.09	0.08	0.06
Cl	0.03	0.11	0	0.07	0.38	0.03	0.09	0.10	0.13	0.10
K	0	0	0.01	0.09	0.69	0	0.13	0.13	0.25	0.19
Ca	29.77	29.49	30.45	30.1	30.73	30.18	29.7	30.06	0.44	0.33
V	0.3	0.25	0.2	0.43	0.43	0.05	0.22	0.27	0.13	0.10
Fe	0.09	0	0.02	0	0.08	0	0.09	0.04	0.04	0.03

Na-rich phase								Ave	Stdev	95 % Confidence limit
Na	1.11	0.68	0.95	1.06	1.32	1.2	0.92	1.03	0.21	0.15
Mg	0	0.03	0.05	0.11	0.06	0.36	0.26	0.12	0.13	0.10
Al	40.76	42.69	39.21	38.75	38.08	40.55	39.57	39.94	1.54	1.14
Si	5.04	3.34	4.84	4.11	4.57	1.92	3.26	3.87	1.10	0.82
P	0.08	0.08	0.08	0.07	0.14	0	0.04	0.07	0.04	0.03
S	0.07	0.07	0.08	0.14	0.08	0.19	0.26	0.13	0.07	0.05
Cl	0.04	0.02	0	0.08	0.09	0.08	0.11	0.06	0.04	0.03
K	0.18	0.06	0.19	0.33	0.16	0.14	0.08	0.16	0.09	0.07
Ca	52.49	52.96	54.26	55.16	55.21	55.4	55.27	54.39	1.21	0.89
V	0.21	0.08	0.14	0.17	0.29	0.17	0	0.15	0.09	0.07
Fe	0.03	0	0.21	0.03	0	0	0.24	0.07	0.11	0.08

Average slag analysis										Ave	Stdev	95 % Confidence limit
Na	0.88	0.59	0.85	0.61	0.64	0.81	0.55	0.7	0.76	0.71	0.12	0.08
Mg	13.51	10.95	10.86	10.49	12.25	12.81	12.22	11.43	9.4	11.55	1.27	0.83
Al	59.56	58.83	58.44	58.68	59.61	59.18	58.95	58.93	58.07	58.92	0.50	0.32
Si	0.38	0.43	0.45	0.69	0.25	0.28	0.66	0.53	0.36	0.45	0.15	0.10
P	0	0.04	0.04	0	0	0.03	0.13	0.09	0.01	0.04	0.05	0.03
S	0	0.03	0.01	0.09	0.24	0	0	0	0.16	0.06	0.09	0.06
Cl	0	0	0	0.17	0.11	0	0	0.09	0	0.04	0.07	0.04
K	0.18	0.09	0.07	0.03	0.19	0	0.17	0.04	0.1	0.10	0.07	0.05
Ca	22.28	26.56	25.73	26.6	23.91	23.89	24.12	25.55	28.99	25.29	1.99	1.30
V	2.92	2.46	3.35	2.58	2.49	2.72	2.9	2.64	2.15	2.69	0.34	0.22
Fe	0.29	0.03	0.19	0.05	0.31	0.28	0.29	0	0	0.16	0.14	0.09

Slag 4 bottom

MA phase											Ave	Stdev	95 % Confidence limit
Na	0	0	0	0	0	0	0	0	0	0	0.00	0.00	0.00
Mg	23.23	22.92	23.18	23.01	23.34	23.26	23.25	23.22	23.65	22.97	23.20	0.21	0.13
Al	64.13	64.34	64.36	63.73	64.05	64	64.45	63.74	61.6	60.38	63.48	1.36	0.85
Si	0.02	0.06	0.12	0.02	0.13	0.01	0.07	0	0.01	0.16	0.06	0.06	0.04
P	0	0	0	0	0	0	0	0	0	0	0.00	0.00	0.00
S	0	0	0	0	0	0	0	0	0	0	0.00	0.00	0.00
Cl	0	0	0	0	0	0	0	0	0	0	0.00	0.00	0.00
K	0	0	0	0	0	0	0	0	0	0	0.00	0.00	0.00
Ca	0.46	0.42	0.29	0.54	0.46	0.42	0.33	0.46	0.77	0.39	0.45	0.13	0.08
V	12.06	12.18	12.04	12.71	12.01	12.31	11.9	12.58	13.98	15.92	12.77	1.26	0.78
Fe	0	0	0	0	0	0	0	0	0	0	0.00	0.00	0.00

CA phase										Ave	Stdev	95 % Confidence limit
Na	0	0	0	0	0	0	0	0	0	0.00	0.00	0.00
Mg	0	0.13	0.02	0.07	0	0	0	0	0	0.02	0.05	0.03
Al	53.47	53.59	53.59	53.62	54.22	53.8	54.21	54.41	53.65	53.84	0.35	0.23
Si	0.01	0	0	0	0.07	0.05	0.03	0.2	0.11	0.05	0.07	0.04
P	0	0	0	0	0	0	0	0		0.00	0.00	0.00
S	0	0	0	0	0	0	0	0		0.00	0.00	0.00
Cl	0	0	0	0	0	0	0	0		0.00	0.00	0.00
K	0	0	0	0	0	0	0	0		0.00	0.00	0.00
Ca	46.42	45.99	46.02	46.03	45.47	45.69	45.48	44.97	45.8	45.76	0.42	0.28
V	0.1	0.29	0.36	0.28	0.24	0.32	0.22	0.3	0.09	0.24	0.09	0.06
Fe	0	0	0	0	0	0	0	0	0	0.00	0.00	0.00

CA_2 phase										Ave	Stdev	95 % Confidence limit
Na	0	0	0	0	0	0	0	0		0.00	0.00	0.00
Mg	0.1	0.06	0	0.13	0	0	0	0.04		0.04	0.05	0.04
Al	67.87	67.39	67.73	67.7	68.05	68.16	69.17	68.29		68.05	0.54	0.37
Si	0	0	0.04	0.01	0	0	0	0.07		0.02	0.03	0.02
P	0	0	0	0	0	0	0	0		0.00	0.00	0.00
S	0	0	0	0	0	0	0	0		0.00	0.00	0.00
Cl	0	0	0	0	0	0	0	0		0.00	0.00	0.00
K	0	0	0	0	0	0	0	0		0.00	0.00	0.00
Ca	31.42	31.61	31.78	31.53	31.07	31.02	30.52	30.83		31.22	0.43	0.30
V	0.61	0.94	0.46	0.63	0.8	0.75	0.31	0.61		0.64	0.20	0.14
Fe	0	0	0	0	0	0	0	0		0.00	0.00	0.00

Na-rich phase										Ave	Stdev	95 % Confidence limit
Na	1	0.83	1.12	1.12	1.03	2.83	0.85	1.2	0.9	1.21	0.62	0.41
Mg	0.2	0.25	0.21	0.21	0.38	0.13	0.23	0.56	0.17	0.26	0.13	0.09
Al	41.47	41.26	42.41	41.41	42.23	45.53	43.59	42.25	46.5	42.96	1.88	1.23
Si	0.37	0.4	0.45	0.45	0.33	1.25	0.48	0.37	1.08	0.58	0.34	0.22
P	0	0	0	0	0	0	0	0	0	0.00	0.00	0.00
S	0	0	0	0	0	0	0	0	0	0.00	0.00	0.00
Cl	0	0	0	0	0	0	0	0	0	0.00	0.00	0.00
K	0	0	0	0	0	0.62	0.16	0.06	0	0.09	0.20	0.13
Ca	57.64	56.95	55.54	55.54	55.69	51.47	54.59	54.82	50.77	54.78	2.29	1.50
V	0.32	0.3	0.24	0.24	0.26	0.16	0.1	0.3	0.35	0.25	0.08	0.05
Fe	0	0	0	0	0	0	0	0	0	0.00	0.00	0.00

Average slag analysis											Ave	Stdev	95 % Confidence limit
Na	0.12	0.17	0.27	0.16	0.22	0.27	0.3	0.3	0.24	0.41	0.25	0.08	0.05
Mg	13.78	13.07	14.02	13.19	12.65	12.75	13.16	13.39	14.53	13.86	13.44	0.60	0.37
Al	57.24	56.52	57.66	56.36	57.56	55.72	56.72	58.22	57.53	56.46	57.00	0.76	0.47
Si	0.4	0.78	0.07	0.23	33	0.32	0.09	0.4	0.22	0.2	3.57	10.34	6.41
P	0.12	0	0	0	0	0.2	0	0.1	0.08	0.05	0.06	0.07	0.04
S	0.03	0.15	0	0.13	0	0.12	0	0.08	0.15	0	0.07	0.07	0.04
Cl	0.02	0.08	0	0	0.09	0.06	0	0.09	0.02	0	0.04	0.04	0.02
K	0.05	0	0.17	0.16	0.13	0.19	0	0	0.06	0.05	0.08	0.07	0.05
Ca	20.42	20.84	19.7	21.63	21.42	22.3	21.98	19.89	18.82	21.43	20.84	1.12	0.69
V	7.83	7.44	7.95	8.03	7.36	7.54	7.69	7.24	8.27	7.11	7.65	0.37	0.23
Fe	0	0.96	0.17	0.11	0.23	0.54	0.06	0.29	0.09	0.44	0.29	0.29	0.18

Slag 4 top

MA phase									Ave	Stdev	95 % Confidence limit
Mg	23.04	22.62	23.56	23.37	23.51	23.29	23.25	21.89	23.07	0.56	0.39
Al	62	61.54	64	62.5	62.35	63.23	63.76	55.82	61.90	2.60	1.80
Si	0	0.08	0.11	0.26	0.25	0.37	0.32	0.24	0.20	0.13	0.09
P	0	0	0	0	0	0.08	0.08	0	0.02	0.04	0.03
S	0	0	0.03	0	0	0.07	0.16	0.14	0.05	0.07	0.05
Cl	0	0.05	0	0.02	0.03	0.07	0	0.04	0.03	0.03	0.02
K	0	0.11	0	0	0	0.08	0	0	0.02	0.04	0.03
Ca	0.35	0.23	0.4	0.47	0.53	0.38	0.49	0.57	0.43	0.11	0.08
V	11.06	12.24	10.87	13.37	12.88	10.37	11.92	21.01	12.97	3.41	2.36
Fe	0	0.02	0.16	0	0.29	0	0.01	0.3	0.10	0.13	0.09

CA phase								Ave	Stdev	95 % Confidence limit
Mg	0	0	0	0.04	0	0	0.09	0.02	0.03	0.03
Al	55.07	54.77	55.59	54.71	55.01	54.68	54.95	54.97	0.31	0.23
Si	0.29	0.34	0.24	0.35	0.24	0.22	0.25	0.28	0.05	0.04
P	0.05	0	0	0.09	0	0	0	0.02	0.04	0.03
S	0.02	0	0.01	0.08	0	0.03	0.03	0.02	0.03	0.02
Cl	0.19	0.11	0	0.04	0	0.4	0	0.11	0.15	0.11
K	0.11	0	0	0.03	0	0.11	0.03	0.04	0.05	0.04
Ca	43.91	44.24	43.6	44.35	44.7	44.64	44.43	44.27	0.39	0.29
V	0.2	0.25	0.23	0.22	0.01	0.17	0.15	0.18	0.08	0.06
Fe	0	0.21	0.33	0.01	0	0	0	0.08	0.14	0.10

CA_2 phase								Ave	Stdev	95 % Confidence limit
Mg	0.1	0.05		0.07	1.22	0	0.04	0.25	0.48	0.38
Al	69.63	68.76		65.09	68.42	68.88	69.36	68.36	1.66	1.33
Si	0	0.22		0.01	0.13	0	0.21	0.10	0.11	0.08
P	0	0		0.08	0	0	0	0.01	0.03	0.03
S	0	0		0.02	0.05	0.15	0	0.04	0.06	0.05
Cl	0.13	0.04		0.01	0	0.03	0.07	0.05	0.05	0.04
K	0.04	0		0	0.01	0.09	0	0.02	0.04	0.03
Ca	29.34	29.84		28.39	28.96	30.15	29.35	29.34	0.62	0.50
V	0.76	0.87		0.59	1.16	0.66	0.89	0.82	0.20	0.16
Fe	0	0.03		0.05	0.05	0	0	0.02	0.02	0.02

Na-rich phase								Ave	Stdev	95 % Confidence limit
Mg	0.07	0	0.18	0.03	0	0.18	0.21	0.10	0.09	0.07
Al	40.82	38.92	39.26	40.28	39.15	42.93	42.51	40.55	1.63	1.21
Si	2.39	4.15	4.89	1.56	1.688	3.1	0.63	2.63	1.51	1.12
P	0.04	0	0	0	0.04	0.03	0	0.02	0.02	0.01
S	0.07	0.06	0.15	0	0.01	0.04	0	0.05	0.05	0.04
Cl	0	0.08	0.08	0.04	0.05	0.01	0	0.04	0.03	0.03
K	0.05	0.21	0.11	0.01	0.13	0.3	0.14	0.14	0.10	0.07
Ca	55.88	55.52	53.96	53.61	53.17	30.9	55.6	51.23	9.03	6.69
V	0.02	0.26	0.1	0.03	0.01	0.6	0.25	0.18	0.21	0.16
Fe	0.01	0	0.12	0.01	0.2	0	0.23	0.08	0.10	0.07

Average slag analysis										Ave	Stdev	95 % Confidence limit
Mg	7.41	10.48	10.14	8.3	9.85	9.09	10.44	10.22	11.75	9.74	1.29	0.85
Al	54.35	56.32	55.73	55.38	53.53	55.2	55.36	55.39	56.64	55.32	0.94	0.61
Si	0.25	0.36	0.3	0.29	0.45	0.5	0.86	0.74	0.19	0.44	0.23	0.15
P	0	0	0	0	0	0	0	0.01	0.09	0.01	0.03	0.02
S	0.25	0.02	0.09	0.08	0.02	0.05	0	0	0	0.06	0.08	0.05
Cl	0.1	0.15	0.1	0	0.15	0.04	0	0	0	0.06	0.07	0.04
K	0.06	0.02	0.13	0.01	0.08	0.01	0.03	0.22	0	0.06	0.07	0.05
Ca	31.72	25.53	27.26	29.74	26.62	29.49	27.26	26.15	23.99	27.53	2.39	1.56
V	5.2	6.69	6.11	5.04	6.27	5.45	5.78	6.68	7.05	6.03	0.71	0.46
Fe	0.47	0.17	0	0.08	0	0.06	0	0.14	0.06	0.11	0.15	0.10

Slag 5 bottom

MA phase									Ave	Stdev	95 % Confidence limit
Na	0	0	0	0	0.11	0.09	0	0.08	0.04	0.05	0.03
Mg	25.02	25	24.55	25.08	24.67	24.74	24.82	24.85	24.84	0.18	0.13
Al	70.88	69.95	70.08	70.6	70.01	70.17	70.58	69.97	70.28	0.36	0.25
Si	0.02	0	0.01	0	0	0.16	0.04	0.17	0.05	0.07	0.05
P	0	0	0.07	0.13	0.15	0.06	0	0.13	0.07	0.06	0.04
S	0.06	0	0.02	0.06	0.03	0.03	0	0.1	0.04	0.03	0.02
Cl	0.07	0	0.01	0	0	0	0.19	0.04	0.04	0.07	0.05
K	0.06	0.1	0	0.17	0.11	0	0	0.01	0.06	0.06	0.04
Ca	0.28	0.4	0.4	0.28	0.48	0.57	0.49	0.29	0.40	0.11	0.08
V	3.37	3.71	4.38	3.64	4.31	3.99	3.89	3.96	3.91	0.34	0.23
Fe	0.02	0.31	0	0.03	0	0.08	0	0.01	0.06	0.11	0.07

CA phase									Ave	Stdev	95 % Confidence limit
Na	0.17	0.16	0.08	0	0.13	0.14	0	0.07	0.09	0.07	0.05
Mg	0	0.15	0.09	0.06	0	0.01	0	0	0.04	0.06	0.04
Al	53.45	53.63	54	53.79	53.08	53.56	53.62	53.17	53.54	0.30	0.21
Si	0.08	0.05	0.04	0	0.1	0.03	0.11	0.1	0.06	0.04	0.03
P	0.09	0.02	0.12	0.08	0.11	0.06	0	0	0.06	0.05	0.03
S	0.04	0.11	0.23	0.06	0.14	0.06	0.2	0	0.11	0.08	0.06
Cl	0	0.13	0	0	0	0	0	0	0.02	0.05	0.03
K	0	0.27	0.07	0.11	0.01	0.05	0.2	0.34	0.13	0.13	0.09
Ca	46.11	45.16	45.01	45.63	45.85	45.99	45.75	45.9	45.68	0.39	0.27
V	0.05	0.2	0.19	0	0.16	0	0.1	0	0.09	0.09	0.06
Fe	0	0	0.07	0.09	0.37	0.1	0	0	0.08	0.13	0.09

CA_2 phase									Ave	Stdev	95 % Confidence limit
Na	0	0	0.16	0.08	0.09	0	0.11	0.09	0.07	0.06	0.04
Mg	0	0.07	0.05	0	0	0	0	0	0.02	0.03	0.02
Al	68.6	68.46	68	67.82	67.83	68.16	68.17	67.34	68.05	0.40	0.28
Si	0	0.02	0.04	0.03	0	0	0	0	0.01	0.02	0.01
P	0	0.14	0.09	0.13	0	0.14	0	0.22	0.09	0.08	0.06
S	0	0	0.02	0	0.17	0.02	0	0.03	0.03	0.06	0.04
Cl	0.13	0.15	0	0	0.15	0	0.05	0.1	0.07	0.07	0.05
K	0	0	0.1	0.08	0.2	0	0.19	0.21	0.10	0.09	0.06
Ca	31.24	30.85	31.11	31.02	30.9	31.46	30.82	31.55	31.12	0.28	0.19
V	0	0.01	0	0.1	0.06	0.11	0.16	0.09	0.07	0.06	0.04
Fe	0.03	0.25	0.06	0.31	0.2	0	0.31	0.08	0.16	0.13	0.09

Na-rich phase						Ave	Stdev	95 % Confidence limit
Na	3.91	2.41	2.24	4.26	6.85	3.93	1.86	1.63
Mg	0.59	1.19	0.25	0.42	1.13	0.72	0.42	0.37
Al	28.83	24.89	33.4	29.82	30.51	29.49	3.08	2.70
Si	3.83	2.58	3.42	3.46	2.67	3.19	0.54	0.48
P	0.07	0.28	0	0.09	0.12	0.11	0.10	0.09
S	0.09	0.22	0	0	0.04	0.07	0.09	0.08
Cl	0.13	0	0	0.12	0	0.05	0.07	0.06
K	2.64	1.56	1.7	2.86	2.7	2.29	0.61	0.54
Ca	57.41	45.01	58.36	56.32	45.32	52.48	6.72	5.89
V	2.49	5.06	0.01	0.61	1.48	1.93	1.98	1.74
Fe	0.01	0.04	0.15	0	0.05	0.05	0.06	0.05

Average slag analysis									Ave	Stdev	95 % Confidence limit
Na	1.57	0.74	1.32	0.6	1.89	2.02	1.44	1.04	1.33	0.51	0.35
Mg	10.56	10.1	10.88	10.13	10.73	11.8	11.82	11.46	10.94	0.69	0.48
Al	60.72	58.95	59.65	59.89	55.08	59.25	58.6	59.1	58.91	1.68	1.16
Si	0.1	0.02	0.07	0.23	0.56	0.02	0.2	0.11	0.16	0.18	0.12
P	0.04	0.13	0.11	0	0.31	0.2	0.07	0.11	0.12	0.10	0.07
S	0.07	0.17	0	0.12	0	0	0.08	0.14	0.07	0.07	0.05
Cl	0.07	0	0	0.08	0	0.12	0.09	0.01	0.05	0.05	0.03
K	1.08	0.5	0.91	0.62	4.94	2.27	2.28	1.46	1.76	1.45	1.01
Ca	23.73	27.28	24.63	26.24	21.4	22.09	22.81	24.19	24.05	2.00	1.39
V	2.05	1.93	2.4	2	4.42	2.22	2.53	2.22	2.47	0.81	0.56
Fe	0	0	0.02	0.04	0.43	0	0.07	0.04	0.08	0.15	0.10

Slag 5 top

MA phase											Ave	Stdev	95 % Confidence limit
Na	0.02	0	0	0.04	0	0.1	0.03	0	0.02	0	0.02	0.03	0.02
Mg	24.8	24.76	24.68	23.91	24.53	24.06	25.28	24.75	24.43	24.79	24.60	0.39	0.24
Al	70.71	70.96	70.44	66.61	70.44	68.34	70.84	71.52	70.31	69.74	69.99	1.46	0.91
Si	0.05	0	0	0	0	0.13	0	0.03	0.39	0.04	0.06	0.12	0.08
P	0	0.15	0.04	0	0.29	0.16	0	0.07	0.15	0	0.09	0.10	0.06
S	0	0.1	0	0.11	0.02	0.16	0.03	0	0.08	0	0.05	0.06	0.04
Cl	0	0	0	0.15	0.08	0	0	0.15	0	0	0.04	0.06	0.04
K	0.04	0	0.04	0	0	0.13	0.05	0.04	0.45	0.22	0.10	0.14	0.09
Ca	0.35	0.39	0.32	1.82	0.43	1.46	0.41	0.44	0.36	0.38	0.64	0.54	0.33
V	3.77	3.57	3.68	6.82	4.16	4.79	3.23	2.42	3.83	4.55	4.08	1.17	0.72
Fe	0.21	0	0	0	0	0	0	0.26	0	0	0.05	0.10	0.06

CA phase											Ave	Stdev	95 % Confidence limit
Na	0.09	0.13	0.21	0.08	0	1.64	0.06	0.17	0.13	0.07	0.26	0.49	0.30
Mg	0	0.09	0.12	0.01	0.11	0.1	0.01	0.08	0.09	0.14	0.08	0.05	0.03
Al	53.41	54.01	53.9	54.25	53.39	53.46	54.58	54.36	54.87	53.6	53.98	0.52	0.32
Si	0	0	0	0	0.06	0.11	0.22	0.01	0.18	0.01	0.06	0.08	0.05
P	0	0	0.02	0	0	0	0.13	0.05	0.01	0.06	0.03	0.04	0.03
S	0.04	0.05	0	0.08	0	0.08	0	0.11	0	0	0.04	0.04	0.03
Cl	0.07	0	0.07	0.01	0.04	0	0	0	0	0.01	0.02	0.03	0.02
K	0.01	0.22	0	0.07	0	0.64	0	0.03	0.07	0.37	0.14	0.21	0.13
Ca	46.03	45.18	45.36	45.3	46.11	43.54	44.88	44.84	44.41	45.32	45.10	0.75	0.47
V	0	0	0.03	0.15	0.08	0.17	0	0	0.05	0.14	0.06	0.07	0.04
Fe	0.11	0	0	0.05	0	0	0.07	0	0	0.28	0.05	0.09	0.06

CA_2 phase											Ave	Stdev	95 % Confidence limit
Na	0	0.12	0	0	0.08	0.15	0	0.11	0.06	0	0.05	0.06	0.04
Mg	0	0.05	0	0	0	0.05	0	0	0.62	0	0.07	0.19	0.12
Al	68.77	68.72	68.74	68.3	67.63	68.4	68.81	68.92	66.94	68.05	68.33	0.63	0.39
Si	0	0	0	0.03	0	0	0	0	0	0	0.00	0.01	0.01
P	0	0	0.06	0.06	0	0.01	0.06	0	0	0.14	0.03	0.05	0.03
S	0.03	0	0	0.2	0.18	0.05	0.32	0	0.2	0.05	0.10	0.11	0.07
Cl	0	0	0	0.08	0	0	0.08	0.03	0.2	0.02	0.04	0.06	0.04
K	0.02	0.1	0.02	0.05	0.03	0.02	0.09	0	1.48	0.17	0.20	0.45	0.28
Ca	30.77	30.46	30.67	30.95	31.28	30.87	30.08	30.48	29.96	30.81	30.63	0.40	0.25
V	0.4	0.28	0.36	0.23	0.31	0.18	0.37	0.01	0.06	0.44	0.26	0.14	0.09
Fe	0	0.15	0	0	0.29	0.02	0.04	0.15	0.22	0.33	0.12	0.13	0.08

Na-rich phase											Ave	Stdev	95 % Confidence limit
Na	0.32	2.29	4.73	3.95	1.14						2.49	1.85	1.28
Mg	0.83	0.42	0.32	1.44	0.32						0.67	0.48	0.33
Al	23.33	28.57	36.5	25.34	43.2						31.39	8.29	5.75
Si	1.59	2.14	2.52	1.11	1.94						1.86	0.54	0.37
P	0.15	0.13	0.05	0.02	0.2						0.11	0.07	0.05
S	0	4.24	0.05	0.03	0.27						0.92	1.86	1.29
Cl	0.03	0	0	0.01	0.01						0.01	0.01	0.01
K	0.14	1.78	4.85	2.52	0.69						2.00	1.85	1.28
Ca	49.14	58.36	50.21	47.4	50.87						51.20	4.21	2.92
V	6.49	0.03	0.07	7.67	0.66						2.98	3.77	2.61
Fe	0.08	0	0.12	0.33	0.09						0.12	0.12	0.09

Average slag analysis											Ave	Stdev	95 % Confidence limit
Na	0.24	0.34	0.26	0.32	0.78	0.35	0.44	0.23			0.37	0.18	0.12
Mg	7.48	6.91	5.94	8.11	6.7	3.9	9.86	6.66			6.95	1.71	1.19
Al	61.84	60.19	59.55	60.92	60.18	56.36	60.87	58.87			59.85	1.67	1.16
Si	0	0	0.14	0.12	0	0.08	0.09	0.09			0.07	0.06	0.04
P	0	0.09	0	0.09	0.12	0.1	0.15	0.14			0.09	0.06	0.04
S	0.13	0	0.05	0.01	0.13	0.13	0	0.25			0.09	0.09	0.06
Cl	0.13	0.02	0.03	0	0	0.17	0	0.14			0.06	0.07	0.05
K	0.2	0.19	0.21	0.19	0.24	0.28	0.28	0.13			0.22	0.05	0.03
Ca	27.35	30.31	32.2	27.78	30.16	37.41	25.42	31.39			30.25	3.67	2.54
V	2.42	1.89	1.44	2.44	1.69	1.23	2.32	1.83			1.91	0.45	0.32
Fe	0	0	0.18	0.02	0	0	0.09	0.15			0.06	0.07	0.05

Slag 6 bottom

MA phase									Ave	Stdev	95 % Confidence limit
Na	0	0	0	0.16	0.1	0	0	0	0.03	0.06	0.04
Mg	22.38	23.13	22.49	23.74	22.64	22.77	23.09	22.77	22.88	0.44	0.30
Al	69.52	69.14	69.45	68.03	69.09	68.88	68.36	68.7	68.90	0.52	0.36
Si	0.53	0.36	0.37	0.48	0.62	0.61	0.4	0.57	0.49	0.11	0.07
P	0	0.04	0	0.07	0.08	0.02	0.03	0	0.03	0.03	0.02
S	0.15	0.23	0	0.08	0.04	0	0.04	0	0.07	0.08	0.06
	0	0	0.04	0	0.03	0.04	0.04	0.14	0.04	0.05	0.03
K	0.06	0.01	0.13	0	0	0.16	0.14	0	0.06	0.07	0.05
	0.3	0.36	0.27	0.41	0.07	0.3	0.17	0.42	0.29	0.12	0.08
V	6.87	6.57	7.05	6.64	7.33	6.94	7.64	6.73	6.97	0.36	0.25
Fe	0	0	0	0.17	0.01	0	0	0.32	0.06	0.12	0.08

CA phase								Ave	Stdev	95 % Confidence limit
Na	1.4	0.1	0.07	0	0.17	0	0.05	0.26	0.51	0.38
Mg	0.11	0	0	0.02	0.01	0.05	0	0.03	0.04	0.03
Al	48.74	51.95	53.64	52.75	57.38	52.39	52.63	52.78	2.55	1.89
Si	0.48	0.24	0.62	0.37	0.6	0.34	0.46	0.44	0.14	0.10
P	0.05	0	0.09	0.26	0.1	0.13	0.11	0.11	0.08	0.06
S	0.16	0.05	0.16	0.03	0.13	0.12	0.02	0.10	0.06	0.05
Cl	0.03	0.05	0.08	0	0.07	0.05	0.1	0.05	0.03	0.02
K	1.83	0.16	0.16	0.25	0.19	0.15	0	0.39	0.64	0.47
Ca	46.73	46.95	44.47	46	40.91	46.49	46.49	45.43	2.16	1.60
V	0.12	0.41	0.39	0.14	0.42	0.14	0.11	0.25	0.15	0.11
Fe	0	0	0	0.16	0	0	0	0.02	0.06	0.04

CA_2 phase									Ave	Stdev	95 % Confidence limit
Na	0	0.04	0.22	0	0	0	0	0	0.03	0.08	0.05
Mg	0	0.1	0.19	0	0	0.07	0	0	0.05	0.07	0.05
Al	67.91	66.93	66.82	67.23	67.1	66.91	67.36	66.57	67.10	0.41	0.28
Si	0.27	0.27	0.53	0.33	0.45	0.39	0.07	0.13	0.31	0.15	0.11
P	0.07	0.21	0.07	0	0.03	0	0.11	0.08	0.07	0.07	0.05
S	0	0.12	0.22	0.01	0.02	0.2	0.1	0.29	0.12	0.11	0.08
Cl	0	0.07	0.13	0.02	0.19	0.13	0.1	0.04	0.09	0.06	0.04
K	0	0.13	0.41	0.04	0	0.1	0	0.01	0.09	0.14	0.10
Ca	31.44	31.4	31.07	32.12	31.44	31.92	31.84	32.27	31.69	0.41	0.29
V	0.31	0.39	0.35	0.21	0.36	0.16	0.13	0.28	0.27	0.10	0.07
Fe	0	0.04	0	0	0.29	0	0.13	0.13	0.07	0.10	0.07

Na-rich phase									Ave	Stdev	95 % Confidence limit
Na	7.82	11.8	7.79	11.8	7.79	15.87	14.59	12.13	11.20	3.15	2.18
Mg	0.13	0	0	0	0	0.05	0.02	0.16	0.05	0.06	0.04
Al	51.32	53.58	53.25	53.58	53.25	54.31	52.85	52.37	53.06	0.90	0.63
Si	2.79	1.18	1.48	1.18	1.48	1.62	2.63	0.59	1.62	0.74	0.52
P	0.08	0.09	0	0.09	0	0.12	0.11	0.21	0.09	0.07	0.05
S	0.13	0.1	0.01	0.1	0.01	0.02	0	0.29	0.08	0.10	0.07
Cl	0.2	0.07	0	0.07	0	0	0.07	0.19	0.08	0.08	0.06
K	2.68	2.5	2.28	2.5	2.28	2.62	5.65	4.37	3.11	1.23	0.85
Ca	34.34	30.5	35.16	30.5	35.16	25.1	23.87	29.18	30.48	4.36	3.02
V	0.47	0.03	0.01	0.03	0.01	0.02	0.2	0.32	0.14	0.18	0.12
Fe	0.04	0	0	0	0	0	0	0.04	0.01	0.02	0.01

Average slag analysis											Ave	Stdev	95 % Confidence limit
Na	0.34	0.13	0.39	0.15	0.19	0.13	0.24	0.07	0.22	0.17	0.20	0.10	0.06
Mg	7.17	11.2	8.24	7.56	10.38	11.91	9.68	12.66	8.92	7.8	9.55	1.93	1.20
Al	65.14	66.51	64.55	64.57	65.47	65.23	64.27	64.59	65.4	64.53	65.03	0.67	0.42
Si	1.18	0.96	0.83	0.84	0.59	0.84	0.86	1.05	0.79	0.55	0.85	0.19	0.12
P	0.26	0	0.07	0.12	0.03	0.28	0.24	0.25	0.03	0.08	0.14	0.11	0.07
S	0.21	0.23	0.11	0.07	0	0.16	0.06	0.18	0.08	0	0.11	0.08	0.05
Cl	0.05	0	0.04	0.2	0.16	0.04	0.13	0	0.23	0.22	0.11	0.09	0.06
K	0.41	0.1	0.3	0.2	0.17	0.36	0.13	0.28	0.1	0.25	0.23	0.11	0.07
Ca	22.34	16.73	21.99	23.66	18.19	16.61	19.79	15.69	20.55	23.18	19.87	2.93	1.81
V	2.39	3.74	3.31	2.56	4.08	4	4.01	4.74	3.32	3.15	3.53	0.73	0.45
Fe	0.36	0.29	0.02	0	0.24	0.27	0.11	0.21	0.13	0	0.16	0.13	0.08

Slag 6 top

MA phase									Ave	Stdev	95 % Confidence limit
Na	0	0	0.01	0.04	0	0.22	0	0	0.03	0.08	0.05
Mg	22.71	22.38	23.27	22.72	23.21	22.37	23.53	22.65	22.86	0.43	0.30
Al	60.63	59.64	65.28	61.16	65.59	61.08	65.88	63.15	62.80	2.50	1.74
Si	0	0.01	0.29	0.42	0.28	0.45	0.39	0.3	0.27	0.17	0.12
P	0.05	0.03	0	0.22	0.04	0.18	0.06	0.09	0.08	0.08	0.05
S	0.06	0	0.05	0.06	0.05	0.04	0.01	0.01	0.04	0.02	0.02
Cl	0	0	0	0.01	0.19	0.05	0.03	0	0.04	0.07	0.05
K	0.02	0	0.05	0.03	0	0.05	0.02	0	0.02	0.02	0.01
Ca	0.52	0.57	0.33	0.21	0.11	1.64	0.12	0.62	0.52	0.50	0.34
V	15.75	16.9	9.77	14.5	9.86	14.53	9.78	12.59	12.96	2.88	2.00
Fe	0	0.01	0.4	0.21	0.28	0	0	0	0.11	0.16	0.11

CA phase											Ave	Stdev	95 % Confidence limit
Na	0.09	0.38	0.09	0	0.05	0.02	0.013	0.12	0.08	0.23	0.11	0.12	0.07
Mg	0	0.13	0	0	0	0.06	0.01	0.05	0	0	0.03	0.04	0.03
Al	51.24	51.35	51.89	53.33	52.94	55.33	53.09	53.49	50.52	53.61	52.68	1.43	0.88
Si	0.16	0.34	0.45	0.1	0.22	0.11	0.03	0.17	0.26	0.89	0.27	0.25	0.15
P	0.14	0.55	0.1	0.11	0.01	0.09	0.2	0.17	0.09	0.11	0.16	0.15	0.09
S	0.08	0.36	0.09	0	0.02	0.07	0.05	0.09	0.25	0.08	0.11	0.11	0.07
Cl	0.12	0.18	0.18	0.03	0.07	0	0.13	0.06	0	0.14	0.09	0.07	0.04
K	0.09	0.28	0.14	0.02	0.05	0.2	0.08	0.01	0.2	0.26	0.13	0.10	0.06
Ca	47.52	46.28	46.02	46.14	46.26	43.76	45.48	45.44	48.07	44.23	45.92	1.31	0.81
V	0.06	0.05	0.35	0.09	0.11	0.27	0.17	0.1	0.1	0.31	0.16	0.11	0.07
Fe	0.2	0	0.41	0.17	0.12	0.05	0.22	0	0.24	0.04	0.15	0.13	0.08

CA_2 phase										Ave	Stdev	95 % Confidence limit
Na	0	0	0	0	0.02	0.08	0	0	0	0.01	0.03	0.02
Mg	0	0.07	0.04	0	0.02	0.03	0.19	0.07	0	0.05	0.06	0.04
Al	68.07	68	67.39	67.72	67.71	67.11	67.93	67.75	68.45	67.79	0.39	0.25
Si	0.01	0	0	0	0	0.09	0.07	0	0	0.02	0.04	0.02
P	0	0	0.11	0.13	0.14	0.11	0.02	0	0.08	0.07	0.06	0.04
S	0	0.12	0.15	0.14	0.16	0	0	0	0.02	0.07	0.07	0.05
Cl	0.04	0.04	0	0.02	0.02	0	0	0	0	0.01	0.02	0.01
K	0.03	0	0.06	0	0.01	0	0.07	0.35	0.05	0.06	0.11	0.07
Ca	31.53	31.45	31.86	31.56	31.18	31.84	30.85	31.49	30.59	31.37	0.43	0.28
V	0.22	0.32	0.39	0.42	0.3	0.46	0.4	0.35	0.34	0.36	0.07	0.05
Fe	0	0	0	0.01	0.12	0.13	0.02	0.1	0	0.04	0.06	0.04

Average slag analysis									Ave	Stdev	95 % Confidence limit
Na	0.11	0.15	0.36	0.22	0.31	0.24	0.16	0.09	0.21	0.10	0.07
Mg	2.5	4	3.67	2.68	3.81	3.43	3.17	3.81	3.38	0.55	0.38
Al	48.89	62.56	61.17	62.41	63.36	63.13	63.88	65.13	61.32	5.15	3.57
Si	1.08	0.59	1	0.19	0.18	0.41	0.21	0.15	0.48	0.38	0.26
P	0.3	0.11	0.05	0.05	0	0.12	0.2	0.17	0.13	0.10	0.07
S	0.51	0.09	0.19	0	0.27	0.21	0.18	0	0.18	0.17	0.11
Cl	0	0.05	0.29	0.05	0	0	0	0	0.05	0.10	0.07
K	0.22	0.23	0.28	0.17	0.25	0.2	0.07	0.11	0.19	0.07	0.05
Ca	42.65	29.3	30.08	31.61	28.93	29.68	28.84	27.72	31.10	4.80	3.33
V	2.49	2.67	2.18	2.05	2.9	2.25	2.65	2.59	2.47	0.29	0.20
Fe	0.34	0	0.3	0.11	0	0	0.06	0.2	0.13	0.14	0.10

Slag 7 bottom

MA phase										Ave	Stdev	95 % Confidence limit
Na	0	0.04	0	0	0	0	0	0	0.03	0.01	0.02	0.01
Mg	24.84	24.47	24.92	24.87	25.06	24.72	24.56	24.74	24.86	24.78	0.18	0.12
Al	68.14	67.6	67.04	67.07	67.4	67.06	67.5	67.52	67.17	67.39	0.36	0.23
Si	0.28	0.03	0.1	0.17	0	0.32	0.16	0	0	0.12	0.12	0.08
P	0.03	0.02	0	0.14	0	0.03	0.04	0	0.12	0.04	0.05	0.03
S	0	0.09	0.09	0	0.03	0.04	0.08	0.07	0.04	0.05	0.04	0.02
Cl	0	0.1	0	0	0.01	0	0	0.04	0	0.02	0.03	0.02
K	0	0	0	0	0	0	0	0.01	0.01	0.00	0.00	0.00
Ca	0.33	0.31	0.38	0.43	0.48	0.37	0.52	0.46	0.44	0.41	0.07	0.05
V	5.64	6.85	7	7.04	6.88	6.91	6.46	7.02	6.86	6.74	0.45	0.29
Fe	0.38	0.01	0.18	0.24	0.15	0.1	0	0	0.04	0.12	0.13	0.08

Na-rich phase									Ave	Stdev	95 % Confidence limit
Na	1.95	1.83	2.62	2.05	2.28	2.08	2.46	2	2.16	0.27	0.18
Mg	0.58	0.67	0.33	0.72	0.6	0.41	0.59	0.72	0.58	0.14	0.09
Al	41.67	41.72	41.93	42.32	41.73	41.8	41.9	42.35	41.93	0.27	0.17
Si	0.01	0.2	0.03	0	0.16	0	0.08	0.11	0.07	0.08	0.05
P	0.17	0.19	0.1	0	0.12	0	0	0.05	0.08	0.08	0.05
S	0.29	0.33	0.49	0.43	0.33	0.46	0.38	0.17	0.36	0.10	0.07
Cl	0.07	0.09	0	0	0	0.16	0	0	0.04	0.06	0.04
K	0.55	0.43	0.63	0.54	0.77	0.61	0.55	0.58	0.58	0.10	0.06
Ca	54.33	54.15	53.56	53.53	53.57	53.89	53.93	53.72	53.84	0.29	0.19
V	0.15	0.1	0.29	0.22	0.18	0.25	0.09	0	0.16	0.10	0.06
Fe	0.04	0.28	0	0	0	0.24	0	0	0.07	0.12	0.08

CA_2 phase									Ave	Stdev	95 % Confidence limit
Na	0.04	0.11	0.02	0.01	0	0.04	0	0.07	0.04	0.04	0.02
Mg	0.03	0	0	0.04	0.05	0.12	0.14	0	0.05	0.05	0.04
Al	53.49	53.19	53.18	54.33	54.44	54.14	53.84	54.22	53.85	0.51	0.33
Si	0	0.08	0.18	0.08	0.06	0	0.09	0.02	0.06	0.06	0.04
P	0.2	0.15	0.11	0	0.05	0.01	0	0	0.07	0.08	0.05
S	0.11	0.02	0	0.02	0	0.07	0.04	0.03	0.04	0.04	0.02
Cl	0.06	0.07	0	0	0	0	0	0	0.02	0.03	0.02
K	0.04	0	0.09	0	0.01	0	0.11	0.11	0.05	0.05	0.03
Ca	45.5	45.89	46.09	45.13	45.23	45.48	45.23	45.33	45.49	0.34	0.22
V	0.27	0.2	0.14	0.25	0.16	0.14	0.1	0	0.16	0.09	0.06
Fe	0	0	0	0.12	0	0	0.04	0	0.02	0.04	0.03

White phase									Ave	Stdev	95 % Confidence limit
Na	0.88	0.34	0.17	0.14	0.03	0.55	0.47	0	0.32	0.30	0.20
Mg	1.88	6.89	5.27	3.96	5.9	8.3	6.32	1.11	4.95	2.48	1.62
Al	27.1	32.86	32.54	34.83	31.07	30.86	29.36	32.97	31.45	2.41	1.58
Si	11.47	7.47	8.17	6.84	8.3	6.41	8.73	9.58	8.37	1.61	1.05
P	0.29	0.16	0.12	0.16	0.16	0.09	0.33	0.48	0.22	0.13	0.09
S	0.27	0.08	0.09	0.01	0	0.1	0.03	0.14	0.09	0.09	0.06
Cl	0.03	0	0	0.04	0	0.11	0	0.17	0.04	0.06	0.04
K	0.29	0.15	0.19	0.2	0.08	0.29	0.35	0.05	0.20	0.11	0.07
Ca	56.81	49.73	50.64	51.94	50.67	50.79	52.22	54.59	52.17	2.39	1.56
V	0.96	2.31	2.36	1.67	2.75	1.77	1.69	0.9	1.80	0.66	0.43
Fe	0	0	0.03	0	0.36	0.22	0	0	0.08	0.14	0.09

Average slag analysis										Ave	Stdev	95 % Confidence limit
Na	0.34	0.41	0.67	0.83	0.65	0.5	0.36	0.51	0.33	0.51	0.17	0.11
Mg	13.36	13.07	10.42	9.28	9.23	10.49	13.15	13.2	14.15	11.82	1.93	1.26
Al	53.76	54.2	51.19	50.46	50.13	52.54	53.52	52.8	54.78	52.60	1.67	1.09
Si	0.34	0.27	0.15	0.44	0.51	0.3	0.31	0.13	0.22	0.30	0.12	0.08
P	0.09	0	0.03	0.2	0.26	0.12	0.03	0.01	0.01	0.08	0.09	0.06
S	0.19	0.11	0.18	0.19	0.18	0.17	0.05	0.13	0.05	0.14	0.06	0.04
Cl	0.06	0.07	0	0.05	0	0.09	0.01	0.19	0	0.05	0.06	0.04
K	0.19	0.17	0.29	0.24	0.19	0.09	0.06	0.24	0.09	0.17	0.08	0.05
Ca	27.4	27.7	33.83	35.64	35.95	31.83	28.92	28.77	25.6	30.63	3.80	2.49
V	4.02	3.8	2.99	2.64	2.67	3.18	3.29	3.85	4.54	3.44	0.65	0.42
Fe	0.09	0.18	0	0	0.03	0.48	0	0.17	0	0.11	0.16	0.10

Slag 7 top

MA phase										Ave	Stdev	95 % Confidence limit
Na	0	0	0	0	0	0	0	0	0	0.00	0.00	0.00
Mg	23.21	24.61	25.01	24.67	24.65	24.67	24.78	24.47	25.06	24.57	0.54	0.44
Al	62.03	67.69	66.84	66.11	67	67.67	66.64	67.43	67.43	66.54	1.77	1.23
Si	0.23	0.23	0	0	0.02	0	0	0.17	0.35	0.11	0.14	0.09
P	0.24	0	0	0	0.06	0	0	0	0	0.03	0.08	0.06
S	0.55	0	0.05	0.06	0.11	0.05	0	0.05	0.15	0.11	0.17	0.12
Cl	0	0.09	0.1	0.12	0	0	0.14	0.09	0	0.06	0.06	0.04
K	0.12	0	0	0.09	0	0	0	0.07	0	0.03	0.05	0.03
Ca	0.92	0.33	0.35	0.69	0.29	0.31	0.56	0.43	0.27	0.46	0.22	0.15
V	7	6.99	7.25	7.89	7.59	7.11	7.84	6.66	6.6	7.21	0.47	0.33
Fe	0.08	0	0	0	0	0	0.04	0.29	0.09	0.06	0.10	0.07

Na-rich phase									Ave	Stdev	95 % Confidence limit
Na	2.55	2.54	2.33	2.6	2.25	2.45	2.16	2.09	2.37	0.19	0.17
Mg	0.61	0.56	0.53	0.79	0.63	0.42	0.51	0.51	0.57	0.11	0.10
Al	42.74	42.45	42.27	42.55	42.02	41.88	41.96	41.61	42.19	0.38	0.33
Si	0.01	0	0.06	0.17	0.09	0.02	0.26	0	0.08	0.09	0.08
P	0.03	0	0	0.09	0	0.14	0.25	0	0.06	0.09	0.08
S	0.44	0.21	0.37	0.52	0.11	0.36	0.29	0.53	0.35	0.15	0.13
Cl	0.13	0.12	0.09	0	0	0.12	0.05	0.11	0.08	0.05	0.05
K	0.6	0.69	0.85	0.64	1	0.66	0.68	0.54	0.71	0.15	0.13
Ca	52.58	52.86	53.08	52.19	53.65	53.28	53.33	54.1	53.13	0.60	0.53
V	0.12	0.01	0.04	0.22	0	0.04	0.29	0	0.09	0.11	0.10
Fe	0.06	0.37	0	0.23	0	0.26	0	0.25	0.15	0.15	0.13

CA_2 phase									Ave	Stdev	95 % Confidence limit
Na	0.1	0	0.03	0	0.04	0	0	0.01	0.02	0.03	0.03
Mg	0.06	0	0.04	0.23	0.74	0	0	0	0.13	0.26	0.23
Al	54.16	54.19	53.94	53.96	51.63	53.54	53.16	54.11	53.59	0.87	0.76
Si	0.07	0.01	0.01	0.24	0.78	0.19	0.13	0.01	0.18	0.26	0.23
P	0	0	0.05	0.07	0.04	0.04	0.03	0.03	0.03	0.02	0.02
S	0.18	0.03	0	0.05	0.04	0.21	0.12	0	0.08	0.08	0.07
Cl	0.05	0	0.1	0.06	0	0.14	0	0	0.04	0.05	0.05
K	0	0.1	0	0.07	0.06	0.01	0	0	0.03	0.04	0.04
Ca	45.03	45.33	45.59	45.02	46.26	45.62	46.28	45.69	45.60	0.48	0.42
V	0.05	0.13	0.14	0.05	0.23	0	0.06	0	0.08	0.08	0.07
Fe	0.13	0.1	0.07	0.09	0	0	0	0.02	0.05	0.05	0.05

White phase									Ave	Stdev	95 % Confidence limit
Na	0.5	0.54	0.21	0.02	1.69	1.07	0.32	0.14	0.56	0.56	0.49
Mg	6.99	1.41	4.84	0.26	2.75	1.26	5.26	0.93	2.96	2.44	2.14
Al	31.48	31.83	33.26	33.59	36.69	29.54	34.21	23.38	31.75	3.98	3.49
Si	7.59	7.5	6.95	9.49	3.33	6.91	6.07	12.83	7.58	2.74	2.40
P	0.15	0.2	0.11	0.05	0.23	0.15	0.03	0.19	0.14	0.07	0.06
S	0.07	0	0.04	0.24	0.1	0.12	0.11	0	0.09	0.08	0.07
Cl	0.05	0.06	0.05	0.1	0.05	0	0.05	0.06	0.05	0.03	0.02
K	0.14	0.22	0.33	0.02	0.84	0.48	0.27	0.06	0.30	0.27	0.23
Ca	50.52	56.13	51.71	53.95	52.61	57.76	51.74	60.64	54.38	3.50	3.07
V	1.92	1.69	1.72	2.09	0.87	2.4	1.65	1.39	1.72	0.46	0.40
Fe	0	0.23	0.15	0.11	0	0	0	0.39	0.11	0.14	0.13

Avera	slag analysis								Ave	Stdev	95 % Confidence limit
Na	0.5	0.46	0.31	0.45	0.71	0.34	0.41	0.29	0.43	0.13	0.09
Mg	12.32	13.59	13.85	11.95	12.99	14.7	12.83	13.83	13.26	0.90	0.63
Al	52.24	53.62	53.72	52.57	52.5	54.24	52.69	53.85	53.18	0.76	0.52
Si	0.51	0.34	0.15	0.2	0.26	0.15	0.35	0.33	0.29	0.12	0.08
P	0.16	0.03	0.11	0.05	0.13	0	0.04	0.11	0.08	0.06	0.04
S	0.2	0	0.19	0.16	0.16	0.03	0.14	0.25	0.14	0.09	0.06
Cl	0	0.02	0.01	0	0	0.18	0.09	0	0.04	0.07	0.05
K	0.15	0.27	0.2	0.13	0.22	0.17	0.21	0.12	0.18	0.05	0.04
Ca	30.06	27.17	26.74	30.88	28.68	25.33	29.46	27	28.17	1.90	1.32
V	3.64	4.08	4.39	3.42	3.67	4.62	3.66	3.86	3.92	0.41	0.29
Fe	0	0.29	0.03	0.04	0.21	0.05	0	0	0.08	0.11	0.08

Appendix 4: Summary of slag analysis

	$\%Al_2O_3$	$\%V_2O_3$	% CaO	% MgO
Slag 1 top	70.56	1.97	23.48	4.00
Slag 1 bottom	69.98	2.89	17.70	9.43
Slag 2 top	63.84	3.80	22.86	9.49
Slag 2 bottom	65.32	4.70	23.09	13.53
Slag 3 top	66.87	1.05	19.48	12.61
Slag 3 bottom	65.67	2.10	20.90	11.34
Slag 4 top	62.40	4.88	23.03	9.69
Slag 4 bottom	63.25	6.46	17.14	13.15
Slag 5 top	66.90	1.10	25.06	6.94
Slag 5 bottom	67.06	1.70	18.17	10.95
Slag 6 top	68.86	1.86	25.89	3.38
Slag 6 bottom	71.83	2.59	16.28	9.30

Appendix 5: Metal droplet analysis of dipped sample (mass basis)

					Average	Stdev	95 % Confidence limit
Na	0	0	0	0	0.00	0.00	0.00
Mg	0.03	0	0.02	0	0.01	0.02	0.01
Al	6.22	5.31	6.35	5.61	5.87	0.49	0.48
Si	0.17	0.21	0.25	0.48	0.28	0.14	0.14
P	0.17	0.16	0	0.17	0.13	0.08	0.08
S	0.02	0.08	0.03	0.02	0.04	0.03	0.03
Cl	0	0.03	0	0.02	0.01	0.02	0.01
K	0	0	0	0	0.00	0.00	0.00
Ca	0.09	0.4	0.5	0.02	0.25	0.23	0.23
V	93.5	94	93.1	94.15	93.69	0.48	0.47
Fe	0.02	0.1	0.05	0.03	0.05	0.04	0.03

Appendix 6: Chemical composition of dipped sample

	1	2	3	4	5	6	7	8	9	10	11	12	13	14	15	16	17	18	19	20	21	22	23	24	25	26	27	28	29	30	31	32	33	34	35	36	37	Ave	Sdev	95 % Confidence limit
Na	0.2	0.0	0.0	0.1	0.3	0.1	0.4	0.3	0.0	0.1	0.4	0.2	0.1	0.2	0.4	0.2	0.0	0.1	0.0	0.2	0.2	0.0	0.3	0.0	0.4	0.2	0.2	0.1	0.6	0.3	0.2	0.2	0.2	0.0	0.1	0.3	0.3	0.18	0.14	0.04
Mg	2.9	2.8	3.4	4.3	1.4	3.3	2.9	3.7	4.2	3.0	2.8	2.8	2.7	3.6	5.1	3.0	2.6	2.7	0.6	3.6	3.3	3.9	4.7	3.5	4.0	1.1	2.3	2.9	3.6	6.6	0.9	4.3	3.1	4.0	4.3	4.3	2.3	3.26	1.16	0.36
Al	61.7	64.7	65.3	60.8	63.5	63.5	60.9	59.6	62.7	62.2	62.5	62.7	62.5	62.0	62.0	64.5	64.4	63.0	62.7	62.2	63.4	63.5	60.8	65.0	59.3	60.0	62.6	65.2	59.8	62.9	66.4	62.3	62.6	63.8	64.2	61.3	62.7	62.68	1.67	0.52
Si	1.1	0.8	1.1	1.2	0.8	1.0	1.2	3.0	0.7	0.9	0.9	0.9	0.7	0.6	0.8	1.0	1.0	1.2	1.0	0.9	1.0	0.8	1.0	0.9	1.1	0.9	0.9	0.8	1.2	1.0	0.7	0.9	0.8	0.9	0.8	1.0	1.2	0.99	0.37	0.11
P	0.1	0.0	0.0	0.1	0.0	0.2	0.1	0.0	0.0	0.0	0.1	0.1	0.0	0.0	0.0	0.0	0.0	0.1	0.0	0.2	0.3	0.1	0.0	0.1	0.0	0.1	0.0	0.2	0.0	0.0	0.1	0.0	0.0	0.0	0.1	0.0	0.0	0.06	0.07	0.02
Si	0.0	0.3	0.2	0.1	0.1	0.1	0.1	0.1	0.1	0.0	0.1	0.3	0.2	0.1	0.2	0.1	0.1	0.2	0.0	0.1	0.0	0.1	0.1	0.0	0.1	0.1	0.1	0.0	0.2	0.3	0.1	0.1	0.0	0.1	0.1	0.0	0.1	0.10	0.08	0.03
Cl	0.1	0.0	0.1	0.0	0.0	0.1	0.0	0.2	0.0	0.0	0.1	0.1	0.0	0.1	0.2	0.0	0.1	0.1	0.2	0.2	0.0	0.0	0.1	0.0	0.0	0.1	0.2	0.0	0.2	0.0	0.2	0.2	0.2	0.0	0.1	0.1	0.1	0.08	0.08	0.02
K	0.2	0.1	0.2	0.3	0.2	0.2	0.3	0.3	0.2	0.3	0.3	0.2	0.3	0.2	0.2	0.0	0.0	0.1	0.1	0.4	0.1	0.1	0.2	0.1	0.3	0.4	0.4	0.0	0.8	0.4	0.1	0.2	0.5	0.2	0.2	0.1	0.1	0.22	0.15	0.05
Ca	28.7	26.5	26.8	26.1	29.8	25.5	27.6	26.0	25.2	27.8	27.7	27.5	28.0	26.7	22.8	26.2	27.5	26.1	31.6	26.0	25.9	24.6	24.8	25.3	27.8	33.0	29.6	27.5	29.9	23.8	29.4	25.4	27.3	24.9	23.7	25.7	28.4	26.94	2.15	0.67
V	4.5	4.6	2.2	7.0	3.8	5.6	6.4	6.4	6.6	5.4	4.8	5.0	5.2	5.9	8.0	4.9	4.0	5.9	3.3	6.0	5.8	6.5	7.2	4.6	6.5	3.4	3.5	3.0	3.3	4.5	1.6	6.4	5.0	5.7	6.3	7.0	4.3	5.13	1.47	0.45
Fe	0.2	0.0	0.2	0.0	0.0	0.4	0.0	0.3	0.1	0.0	0.2	0.0	0.2	0.4	0.2	0.2	0.0	0.2	0.2	0.1	0.1	0.1	0.3	0.3	0.2	0.3	0.1	0.3	0.0	0.0	0.0	0.1	0.1	0.0	0.2	0.1	0.0	0.13	0.12	0.04
Mn	0.2	0.0	0.5	0.0	0.0	0.0	0.1	0.2	0.2	0.4	0.2	0.0	0.0	0.0	0.0	0.0	0.0	0.4	0.1	0.3	0.0	0.3	0.2	0.0	0.2	0.3	0.1	0.0	0.5	0.1	0.0	0.1	0.4	0.1	0.1	0.2	0.5	0.15	0.16	0.05
Cr	0.0	0.0	0.0	0.0	0.1	0.0	0.0	0.0	0.0	0.0	0.0	0.2	0.1	0.1	0.0	0.0	0.2	0.0	0.2	0.1	0.0	0.0	0.2	0.2	0.2	0.0	0.0	0.1	0.1	0.2	0.2	0.0	0.0	0.4	0.0	0.0	0.0	0.07	0.10	0.03

Appendix 7: Metal droplet analysis (mass basis)

Slag 1 bottom				Average	Stdev	95 % Confidence limit
Na	0.03	0.05	0.07	0.05	0.02	0.01
Mg	0.03	0	0	0.01	0.02	0.01
Al	0.2	0.2	0.2	0.20	0.00	0.00
Si	0	0	0	0.00	0.00	0.00
P	0.08	0.01	0	0.03	0.04	0.03
S	0.05	0.03	0.04	0.04	0.01	0.01
Cl	0	0	0.03	0.01	0.02	0.01
K	0	0	0	0.00	0.00	0.00
Ca	0	0	0	0.00	0.00	0.00
V	95	95	95	95.00	0.00	0.00
Fe	4.61	4.71	4.66	4.66	0.05	0.03
Mn	0	0	0	0.00	0.00	0 0 0
Cr	0	0	0	0.00	0.00	0.00

Slag 1 top				Average	Stdev	95 % Confidence limit
Na	0.13	0	0	0.04	0.08	0.08
Mg	0.13	0.1	0	0.08	0.07	0.08
Al	0.1	0.1	0.2	0.13	0.06	0.07
Si	0	0	0	0.00	0.00	0.00
P	0	0	0	0.00	0.00	0.00
S	0	0	0	0.00	0.00	0.00
Cl	0	0	0	0.00	0.00	0.00
K	0	0	0	0.00	0.00	0.00
Ca	0	0.01	0	0.00	0.01	0.01
V	95	95	95	95.00	0.00	0.00
Fe	4.64	4.79	4.8	4.74	0.09	0.10
Mn	0	0	0	0.00	0.00	0.00
Cr	0	0	0	0.00	0.00	0.00

Slag 2 top											Average	Stdev	95 % Confidence limit
Na	0.78	0.08	0.14	0.22	0.15	0	0.05	0.42	0.27	0.48	0.26	0.24	0.15
Mg	4.88	0.13	2.1	1.27	2.86	0.2	0.27	0.1	10.5	6.07	2.83	3.40	2.11
Al	9.51	0.19	4.45	2.05	6.06	0.28	0.82	0.23	21.7	12.7	5.80	7.05	4.37
Si	0.63	0.51	0.83	0.96	0.97	0.74	0.93	0.43	0.59	0.76	0.74	0.19	0.12
P	0	0.04	0	0	0.05	0	0	0.07	0	0	0.02	0.03	0.02
S	0.02	0.01	0.08	0.05	0	0	0.01	0	0.04	0.05	0.03	0.03	0.02
Cl	0.02	0	0.05	0	0	0	0	0	0.01	0.01	0.01	0.02	0.01
K	0	0	0	0	0	0	0	0	0	0	0.00	0.00	0.00
Ca	0.36	0.97	0.17	0.17	0.21	0.06	0.14	0.32	0.31	0.14	0.29	0.26	0.16
V	76.9	92	86.3	90.2	84.2	92.5	90.6	89.6	59.9	73.8	83.59	10.48	6.49
Fe	4.8	3.09	3.76	2.91	3.65	4.54	5.31	6.67	4.91	4.35	4.40	1.12	0.70
Mn	0.35	0.37	0.36	0.55	0.51	0.27	0.17	0.41	0.43	0.34	0.38	0.11	0.07
Cr	1.72	2.63	1.81	1.62	1.34	1.43	1.72	1.73	1.43	1.29	1.67	0.38	0.24

Slag 2 bottom											Average	Stdev	95 % Confidence limit
Na	0.04	0.12	0	0	0.21	0	0.16	0.05	0.09	0.18	0.09	0.08	0.05
Mg	0.08	0	0.07	0.16	0.07	2.47	0.07	0.12	3.18	0.13	0.64	1.17	0.72
Al	0.11	0.21	0.2	0.3	0.09	4.43	0.1	0.15	5.43	0.13	1.12	2.03	1.26
Si	0.39	0.4	0.72	0.36	0.64	0.6	0.47	0.63	0.41	0.84	0.55	0.16	0.10
P	0.1	0.02	0.07	0.11	0.07	0.04	0.07	0.01	0.18	0.01	0.07	0.05	0.03
S	0.05	0.03	0	0	0.03	0	0.01	0	0.03	0.14	0.03	0.04	0.03
Cl	0	0	0.02	0	0	0	0.02	0.02	0.06	0	0.01	0.02	0.01
K	0	0	0	0	0	0	0	0	0	0	0.00	0.00	0.00
Ca	0.1	0.53	0.3	0.99	0.4	0.31	0.3	0.27	0.17	0.25	0.36	0.25	0.15
V	74.9	79.8	75.6	80.5	81.6	73.9	80.6	81.2	69.2	80.5	77.78	4.16	2.58
Fe	21.9	16.1	21.3	15.5	13.2	15.5	15.5	13.7	19	13.8	16.54	3.13	1.94
Mn	0.72	1.02	0.54	0.47	1.08	0.61	0.63	0.8	0.83	0.8	0.75	0.20	0.12
Cr	1.93	1.74	1.2	1.65	2.62	2.12	2.07	3.08	1.47	3.2	2.11	0.67	0.41

Slag 3 top											Average	Stdev	95 % Confidence limit
Na	0	0	0.05	0	0.08	0.01	0.71	0.07	0.05	0	0.09	0.21	0.12
Mg	0.83	0.02	0.24	1.46	0.03	0	2.9	1.17	0.83	21.7	2.96	6.32	3.74
Al	1.26	0.23	2.27	2.73	0.04	0.08	6.07	4.73	1.23	55.2	7.34	16.06	9.49
Si	0.27	0.62	0.58	0.48	0.42	0.77	0.71	0.87	2.26	0.3	0.74	0.55	0.32
P	0.06	0.06	0.09	0	0	0.05	0.11	0.01	0.12	0	0.05	0.04	0.03
S	0.11	0.05	0.06	0	0	0	0.05	0.07	0.01	0	0.03	0.04	0.02
Cl	0.03	0	0	0	0.03	0.02	0.04	0	0.09	0.03	0.03	0.03	0.02
K	0	0	0	0	0	0	0	0	0	0.03	0.00	0.01	0.01
Ca	0.48	0.61	1.94	0.53	0.4	0.15	0.77	2.21	0.14	0.33	0.88	0.80	0.47
V	82.4	83.7	80.5	82.5	80.5	80.3	71.1	81.6	74.6	19.5	74.18	18.52	10.94
Fe	8.2	8.05	8.29	6.37	12.9	14.2	13.9	3.14	18.5	2.32	8.82	5.51	3.26
Mn	0.77	0.73	0.37	0.84	0.8	0.58	0.6	0.18	0.18	0	0.53	0.29	0.17
Cr	5.57	5.96	5.63	5.11	4.81	3.83	3.03	5.91	1.96	0.6	4.34	1.78	1.05

Slag 3 bottom											Average	Stdev	95 % Confidence limit
Na	0.1	0.1	0.63	0.09	0.24	0	0.21	0.09	0.03	0.23	0.17	0.18	0.11
Mg	0.19	0.04	0.22	0.04	10.7	1.07	0	0.14	0.01	0.18	1.26	3.34	2.07
Al	0.17	0.11	2.21	0.14	23.2	1.64	0.21	0.28	0.22	0.24	2.85	7.20	4.46
Si	0.47	0.54	0.5	1.43	0.47	0.68	0.74	1.41	1.62	2.62	1.05	0.71	0.44
P	0.08	0.12	0.09	0.12	0.04	0.02	0.06	0.17	0	0.05	0.08	0.05	0.03
S	0	0	0.11	0.08	0.12	0.01	0.01	0.01	0.03	0	0.04	0.05	0.03
Cl	0.03	0.03	0.01	0.01	0	0.04	0.03	0.01	0	0.02	0.02	0.01	0.01
K	0	0	0	0	0	0	0	0	0	0	0.00	0.00	0.00
Ca	0.56	0.73	1.31	0.12	2.92	0.11	0.2	0.79	0.38	0.24	0.74	0.85	0.53
V	85.3	83.9	79.8	83	54.6	83.6	86.1	79.7	89.1	90.1	81.51	10.04	6.22
Fe	9.44	10.7	10.7	11.9	5.54	9.31	8.73	13.5	4.77	3.64	8.82	3.22	2.00
Mn	3.13	3.03	3.46	2.76	1.79	2.74	2.85	3.47	3.21	2.23	2.87	0.53	0.33
Cr	0.56	0.77	1	0.26	0.28	0.82	0.82	0.39	0.6	0.49	0.60	0.25	0.15

Slag 4 top											Average	Stdev	95 % Confidence limit
Na	0	0	0.16	0	0.1	0.26	0	0.12	0	0.05	0.06	0.09	0.05
Mg	0.05	0.92	2.37	0.6	3.48	4.67	3.89	0.04	0.03	0.02	1.88	1.96	1.16
Al	3.26	1.65	4.03	1.29	6.95	9.7	9.83	2.59	14.7	2.24	6.03	4.47	2.64
Si	0.35	1.04	0.83	0.52	0.37	0.4	0.31	0.4	0.22	0.3	0.46	0.25	0.15
P	0.12	0.13	0.01	0.04	0	0.08	0	0.01	0.05	0.06	0.05	0.05	0.03
S	0.01	0.03	0.04	0.03	0.05	0.05	0	0.11	0	0.02	0.03	0.03	0.02
Cl	0.06	0.08	0	0.11	0	0.1	0.09	0.04	0.06	0.02	0.05	0.04	0.02
K	0	0	0	0	0	0	0	0	0	0	0.00	0.00	0.00
Ca	1.18	0.15	0.13	0.45	0.17	0.2	0.53	1.49	4.53	1.3	0.97	1.28	0.76
V	88.7	81.8	72.1	90.8	80.1	76.8	77.4	90	78	88.5	82.04	6.39	3.78
Fe	6.3	14.2	20.4	6.21	8.8	7.74	7.93	5.16	2.46	7.46	8.42	4.89	2.89

Slag 4 bottom					Average	Stdev	95 % Confidence limit
Na	0.45	0.36	0.05	0.15	0.25	0.18	0.18
Mg	0.03	0	0.02	1.12	0.29	0.55	0.54
Al	0.1	0.23	0.16	2.45	0.74	1.14	1.12
Si	0.17	0.21	0.25	0.48	0.28	0.14	0.14
P	0.17	0.16	0	0.17	0.13	0.08	0.08
S	0.02	0.08	0.17	0.11	0.10	0.06	0.06
Cl	0	0.03	0	0.02	0.01	0.02	0.01
K	0	0	0	0	0.00	0.00	0.00
Ca	0.09	0.4	0.42	0.23	0.29	0.16	0.15
V	77.6	75.2	74.2	69.4	74.10	3.47	3.40
Fe	21.3	23.3	24.8	25.6	23.74	1.85	1.82

Slag 5 top							Average	Stdev	95 % Confidence limit
Na	0	0.14	0.01	0.17	0	0	0.05	0.08	0.06
Mg	0.27	0	0.15	0.07	0.14	0	0.11	0.10	0.08
Al	0.56	0.1	0.48	0.84	1.26	4.45	1.28	1.60	1.28
Si	1.7	0.31	1.63	1.26	0.5	1.34	1.12	0.58	0.47
P	0.03	0.02	0.06	0.11	0	0	0.04	0.04	0.03
S	0	0.07	0.02	0	0.03	0	0.02	0.03	0.02
Cl	0.02	0	0	0	0	0	0.00	0.01	0.01
K	0	0	0	0	0	0	0.00	0.00	0.00
Ca	0.67	0.9	0.44	0.71	0.8	2.45	1.00	0.73	0.58
V	93.7	93.1	94.6	93.5	93.8	89.1	92.96	1.95	1.56
Fe	0.76	0.9	0.48	0.91	0.77	0.24	0.68	0.26	0.21
Mn	0.15	0	0.49	0.5	0.82	0.88	0.47	0.35	0.28
Cr	2.19	2.8	1.64	1.93	1.89	1.52	2.00	0.46	0.37

Slag 5 bottom											Average	Stdev	95 % Confidence limit
Na	0.05	0.01	0.06	0.3	0.03	6.76	0.15	0.25	0.01	0.13	0.71	2.01	1.19
Mg	0.15	0.03	0.06	11.4	23.3	0	0.12	0.6	0	0	3.25	7.46	4.41
Al	0.23	0.24	0.79	57.5	63.2	0.24	0.14	1.13	0.16	0.17	11.26	24.30	14.36
Si	0.76	0.73	0.81	0.05	0.4	0.69	1.49	0.75	1.13	1.31	0.83	0.40	0.24
P	0.13	0.15	0.12	0.01	0	0.02	0.02	0.12	0.02	0.19	0.07	0.07	0.04
S	0.06	0	0	0.09	0.17	0.03	0.03	0.01	0.07	0.01	0.04	0.05	0.03
Cl	0	0	0	0	0	0	0.03	0.02	0	0.01	0.01	0.02	0.01
K	0	0	0	0.37	0.03	0.07	0	0	0.72	0	0.11	0.23	0.14
Ca	0.69	0.68	0.66	25.8	0.38	0.27	0.03	0.47	0	0.12	2.66	7.69	4.55
V	89.7	88.6	88.2	3.52	12.1	83.7	84	91.2	84.6	83.6	72.30	32.05	18.94
Fe	5.48	6.72	6.7	0.31	0.13	5.76	13.2	3.26	11.9	13	7.03	4.73	2.79
Mn	0.5	0.53	0.56	0.35	0	0.41	0.3	0.61	0.36	0.37	0.44	0.21	0.13
Cr	2.25	2.36	2.04	0	0	2.04	0.5	1.58	0.99	1.09	1.23	0.88	0.52

Slag 6 bottom									Average	Stdev	95 % Confidence limit
Na	0.09	2.34	0.08	0	0	0.01	0	0.06	0.32	0.82	0.57
Mg	0.08	0.58	0	0.03	0.1	0	1.86	0	0.33	0.65	0.45
Al	0.09	14.5	0.14	0.22	0.11	0.18	4.47	0.11	2.48	5.10	3.53
Si	1.17	1.46	0.46	0.31	0.49	0.85	2.02	0.36	0.89	0.61	0.43
P	0.02	0.25	0.01	0	0.01	0.1	0.06	0.01	0.06	0.08	0.06
S	0	0.48	0.02	0	0.08	0	0.11	0.02	0.09	0.16	0.11
Cl	0	0.26	0.06	0.06	0.02	0.02	0.01	0.03	0.06	0.08	0.06
K	0	2.61	0	0	0	0	0	0	0.33	0.92	0.64
Ca	0.15	5.03	0.56	0.25	0.5	0.44	0.88	0.4	1.03	1.63	1.13
V	92.6	65.3	93	93.3	90.3	91.2	81.1	93.6	87.55	9.87	6.84
Fe	2.68	0.78	1.07	1.79	1.86	3.45	6.76	1.07	2.43	1.96	1.36
Mn	0.24	1.38	0.66	0.51	1.06	0.61	0.29	0.29	0.63	0.40	0.28
Cr	2.86	4.99	3.93	3.57	5.43	3.16	2.46	4.01	3.80	1.02	0.71

Slag 6 top										Average	Stdev	95 % Confidence limit
Na	0.13	0.05	0.07	0	0	0.09	0.04	0	0.02	0.04	0.05	0.03
Mg	0.13	0	0.12	0.02	0.07	0	0	0.1	0	0.05	0.06	0.04
Al	1.35	0.78	2.07	0.36	0.63	0.47	0.58	0.59	0.58	0.82	0.55	0.36
Si	1.42	1.87	5.07	1.92	1.16	1.35	1.23	0.98	1.3	1.81	1.26	0.82
P	0.08	0.01	0	0	0	0.01	0.08	0.07	0.05	0.03	0.04	0.02
S	0.05	0.03	0.04	0	0	0.04	0.03	0.02	0.06	0.03	0.02	0.01
Cl	0	0	0.03	0.02	0.02	0	0	0	0.01	0.01	0.01	0.01
K	0	0	0	0	0	0	0	0	0	0.00	0.00	0.00
Ca	1.32	1.19	1.33	0.95	1.03	0.83	1.06	0.93	1.12	1.08	0.17	0.11
V	88.1	87.6	86.1	91.9	91.5	89	89.5	91.2	91.2	89.58	2.04	1.33
Fe	5.23	5.87	1.36	0.62	2.22	5.65	4.88	3.01	3.5	3.59	1.93	1.26
Mn	0.63	0.38	0.36	0.68	0.39	0.5	0.62	0.49	0.23	0.48	0.15	0.10
Cr	1.53	2.18	3.5	3.5	2.95	2.07	1.98	2.59	1.97	2.47	0.71	0.46

Appendix 8

Estimated activity data of species in the $CaO-Al_2O_3$ system according to the Chemsage software package. Temperature :1973 K.

N_{CaO}	$N_{AlO1.5}$	a_{CaO}	$a_{AlO1.5}$	a_{Al2O3}	Basicity
0.46	0.54	0.445	0.2178	0.05	0.85
0.43	0.57	0.3516	0.263	0.07	0.75
0.4	0.6	0.2725	0.3153	0.10	0.67
0.37	0.63	0.205	0.377	0.14	0.59
0.34	0.66	0.1486	0.4496	0.20	0.52
0.31	0.69	0.1028	0.5369	0.29	0.45
0.29	0.71	0.078	0.604	0.36	0.41
0.27	0.73	0.0577	0.6794	0.46	0.37
0.25	0.75	0.0414	0.7631	0.58	0.33
0.24	0.76	0.0347	0.8082	0.65	0.32

Activity data of species in the $CaO-Al_2O_3$ system according Chipman et al . Temperature :1973 K

(%CaO)	$N_{AlO1.5}$	N_{Al2O3}	a_{Al2O3}	a_{CaO}	$a_{AlO1.5}$	Basicity
48	0.54374	0.373	0.0831	0.28	0.29	1.68
47	0.55367	0.3824	0.0975	0.25	0.31	1.62
46	0.56358	0.3919	0.1134	0.23	0.34	1.55
45	0.57347	0.4016	0.1308	0.21	0.36	1.49
44	0.58334	0.4113	0.1497	0.19	0.39	1.43
43	0.5932	0.4212	0.1701	0.18	0.41	1.37
42	0.60303	0.4312	0.1919	0.16	0.44	1.32
41	0.61285	0.4414	0.215	0.15	0.46	1.27
40	0.62265	0.4516	0.2395	0.14	0.49	1.21
39	0.63243	0.462	0.2651	0.12	0.51	1.16
38	0.64219	0.4725	0.292	0.11	0.54	1.12
37	0.65194	0.4832	0.32	0.11	0.57	1.07
36	0.66166	0.4939	0.3494	0.10	0.59	1.02
35	0.67137	0.5049	0.3801	0.09	0.62	0.98
34	0.68106	0.5159	0.4125	0.08	0.64	0.94
33	0.69073	0.5271	0.4469	0.08	0.67	0.90
32	0.70038	0.5385	0.4836	0.07	0.70	0.86
31	0.71002	0.55	0.5233	0.07	0.72	0.82
30	0.71963	0.5616	0.567	0.06	0.75	0.78
29	0.72923	0.5734	0.6155	0.06	0.78	0.74
28.5	0.73402	0.5794	0.6421	0.06	0.80	0.73
27.5	0.7436	0.5914	0.701	0.05	0.84	0.69
26.5	0.75315	0.6036	0.7694	0.05	0.88	0.66
25.5	0.76269	0.616	0.8501	0.05	0.92	0.62

With N_i = mole fraction of specie i in the slag
a_i = Raoultion activity of specie i.

Appendix 9

Estimated activity data of MgO in the $CaO-Al_2O_3-MgO$ system according to the Chemsage software package.

N_{MgO}	$N_{AlO1.5}$	N_{CaO}	a_{MgO}
0.01	0.47	0.52	0.02
0.03	0.47	0.51	0.07
0.05	0.47	0.48	0.16
0.08	0.47	0.45	0.31
0.11	0.47	0.43	0.45
0.13	0.47	0.40	0.54

N_{MgO}	$N_{AlO1.5}$	N_{CaO}	a_{MgO}
0.03	0.52	0.45	0.05
0.05	0.52	0.43	0.11
0.08	0.52	0.40	0.22
0.11	0.52	0.37	0.33
0.13	0.52	0.35	0.40

N_{MgO}	$N_{AlO1.5}$	N_{CaO}	a_{MgO}
0.03	0.54	0.43	0.05
0.05	0.54	0.41	0.10
0.08	0.54	0.38	0.20
0.11	0.54	0.35	0.30
0.13	0.54	0.33	0.37

N_{MgO}	$N_{AlO1.5}$	N_{CaO}	a_{MgO}
0.03	0.57	0.40	0.04
0.05	0.57	0.38	0.09
0.08	0.57	0.35	0.17
0.11	0.57	0.32	0.27
0.13	0.57	0.30	0.33

With N_i = mole fraction of specie i in the slag
a_i = Raoultion activity of specie i.

Appendix 10

Estimated activity data of Al_2O_3 in the CaO-Al_2O_3-MgO system according to the Chemsage software package. Temperature :1973 K

N_{MgO}	N_{CaO}	$N_{AlO1.5}$	$a_{AlO1.5}$	a_{Al2O3}	Basicity
0	0.56	0.44	0.088	0.008	1.273
0	0.54	0.46	0.125	0.016	1.174
0	0.52	0.48	0.137	0.019	1.083
0	0.5	0.5	0.162	0.026	1.000
0	0.48	0.52	0.187	0.035	0.923
0	0.46	0.54	0.218	0.047	0.852
0	0.43	0.57	0.263	0.069	0.754
0	0.4	0.6	0.315	0.099	0.667
0	0.37	0.63	0.377	0.142	0.587
0	0.34	0.66	0.450	0.202	0.515
0	0.31	0.69	0.537	0.288	0.449
0	0.29	0.71	0.604	0.365	0.408
0	0.27	0.73	0.679	0.462	0.370
0	0.25	0.75	0.763	0.582	0.333
0	0.24	0.76	0.808	0.653	0.316

Estimated activity data of Al_2O_3 in the CaO-Al_2O_3-MgO system according to the Chemsage software package. Temperature :1973 K

N_{MgO}	$N_{AlO1.5}$	N_{CaO}	a_{MgO}	a_{CaO}	$a_{AlO1.5}$	a_{Al2O3}	Basicity
0.08	0.43	0.49	0.43	0.95	0.069	0.005	1.306
0.08	0.45	0.47	0.36	0.76	0.092	0.008	1.206
0.08	0.47	0.45	0.3	0.62	0.116	0.013	1.114
0.08	0.49	0.43	0.26	0.51	0.141	0.020	1.029
0.08	0.51	0.41	0.23	0.43	0.163	0.027	0.952
0.08	0.53	0.39	0.21	0.35	0.197	0.039	0.880
0.08	0.55	0.37	0.19	0.29	0.229	0.052	0.814
0.08	0.57	0.35	0.17	0.24	0.264	0.070	0.752
0.08	0.59	0.33	0.16	0.19	0.303	0.092	0.695
0.08	0.61	0.31	0.15	0.15	0.347	0.120	0.642
0.08	0.63	0.29	0.14	0.12	0.395	0.156	0.592
0.08	0.65	0.27	0.13	0.09	0.450	0.202	0.545
0.08	0.67	0.25	0.12	0.07	0.511	0.261	0.501
0.08	0.69	0.23	0.11	0.05	0.578	0.334	0.459
0.08	0.70	0.22	0.11	0.04	0.615	0.378	0.420
0.08	0.71	0.21	0.11	0.03	0.652	0.426	0.401
0.08	0.72	0.20	0.1	0.03	0.692	0.479	0.392
0.08	0.74	0.18	0.1	0.02	0.776	0.602	0.357
0.08	0.76	0.16	0.09	0.01	0.866	0.749	0.323
0.08	0.77	0.15	0.09	0.01	0.912	0.832	0.299
0.08	0.79	0.13	0.09	0.01	1.000	1.000	0.266

Estimated activity data of Al_2O_3 in the CaO-Al_2O_3-MgO system according to the Chemsage software package. Temperature :1973 K

N_{MgO}	$N_{AlO1.5}$	N_{CaO}	a_{MgO}	a_{CaO}	$a_{AlO1.5}$	a_{Al2O3}	Basicity
0.13	0.41	0.46	0.84	1	0.005	2.632E-05	1.453
0.13	0.43	0.44	0.709	0.847	0.007	4.900E-05	1.340
0.13	0.45	0.42	0.603	0.671	0.009	8.464E-05	1.238
0.13	0.47	0.40	0.524	0.538	0.117	0.014	1.145
0.13	0.49	0.38	0.463	0.434	0.144	0.021	1.059
0.13	0.50	0.37	0.438	0.391	0.158	0.025	0.980
0.13	0.52	0.35	0.395	0.315	0.189	0.036	0.908
0.13	0.54	0.33	0.361	0.252	0.223	0.050	0.840
0.13	0.56	0.31	0.333	0.198	0.261	0.068	0.778
0.13	0.58	0.29	0.309	0.154	0.304	0.092	0.720
0.13	0.60	0.27	0.289	0.116	0.352	0.124	0.665
0.13	0.62	0.25	0.271	0.086	0.406	0.165	0.615
0.13	0.64	0.23	0.256	0.061	0.467	0.218	0.567
0.13	0.66	0.21	0.242	0.042	0.535	0.286	0.522
0.13	0.68	0.19	0.23	0.028	0.610	0.372	0.480
0.13	0.69	0.18	0.224	0.023	0.650	0.422	0.440
0.13	0.70	0.17	0.219	0.018	0.691	0.478	0.421
0.13	0.71	0.16	0.214	0.014	0.734	0.539	0.412
0.13	0.73	0.14	0.204	0.009	0.824	0.680	0.376
0.13	0.75	0.12	0.195	0.005	0.918	0.843	0.342
0.13	0.77	0.1	0.187	0.003	1.014	1.000	0.299

Appendix 11

Estimated activity data of Al_2O_3 in the CaO-Al_2O_3-MgO system according to the Chemsage software package. Temperature : 2073 K

N_{MgO}	$N_{AlO1.5}$	N_{CaO}	$a_{AlO1.5}$	a_{Al2O3}	Basicity
0.13	0.41	0.46	0.059	0.003	1.45
0.13	0.43	0.44	0.076	0.006	1.34
0.13	0.45	0.42	0.096	0.009	1.24
0.13	0.47	0.40	0.119	0.014	1.14
0.13	0.49	0.38	0.144	0.021	1.06
0.13	0.50	0.37	0.157	0.025	0.98
0.13	0.52	0.35	0.185	0.034	0.91
0.13	0.54	0.33	0.217	0.047	0.84
0.13	0.56	0.31	0.251	0.063	0.78
0.13	0.58	0.29	0.289	0.084	0.72
0.13	0.60	0.27	0.332	0.110	0.67
0.13	0.62	0.25	0.379	0.143	0.61
0.13	0.64	0.23	0.431	0.186	0.57
0.13	0.66	0.21	0.488	0.238	0.52
0.13	0.68	0.19	0.550	0.303	0.48
0.13	0.69	0.18	0.583	0.340	0.44
0.13	0.70	0.17	0.617	0.381	0.42
0.13	0.71	0.16	0.652	0.425	0.41
0.13	0.73	0.14	0.725	0.526	0.38
0.13	0.75	0.12	0.800	0.640	0.34
0.13	0.77	0.10	0.876	0.767	0.30

Estimated activity data of Al_2O_3 in the CaO-Al_2O_3-MgO system according to the Chemsage software package. Temperature :2123 K

N_{MgO}	$N_{AlO1.5}$	N_{CaO}	$a_{AlO1.5}$	a_{Al2O3}	Basicity
0.13	0.41	0.46	0.062	3.87E-03	1.45
0.13	0.43	0.44	0.079	6.19E-03	1.34
0.13	0.45	0.42	0.098	9.62E-03	1.24
0.13	0.47	0.40	0.120	0.014	1.14
0.13	0.49	0.38	0.144	0.021	1.06
0.13	0.50	0.37	0.157	0.025	0.98
0.13	0.52	0.35	0.184	0.034	0.91
0.13	0.54	0.33	0.214	0.046	0.84
0.13	0.56	0.31	0.247	0.061	0.78
0.13	0.58	0.29	0.283	0.080	0.72
0.13	0.60	0.27	0.322	0.104	0.67
0.13	0.62	0.25	0.366	0.134	0.61
0.13	0.64	0.23	0.415	0.172	0.57
0.13	0.66	0.21	0.467	0.218	0.52
0.13	0.68	0.19	0.524	0.275	0.48
0.13	0.69	0.18	0.554	0.307	0.44
0.13	0.70	0.17	0.585	0.342	0.42
0.13	0.71	0.16	0.617	0.381	0.41
0.13	0.73	0.14	0.682	0.465	0.38
0.13	0.75	0.12	0.750	0.563	0.34
0.13	0.77	0.10	0.818	0.669	0.30

Appendix 12

Estimated activity data of V and Al in the FeV system according to the Chemsage software package. Temperature : 1973 K.

N_{Al}	N_V	N_{Fe}	a_{Al}	a_V
0.01	0.76	0.23	1.69E-03	0.73
0.01	0.77	0.22	1.69E-03	0.75
0.01	0.78	0.21	1.69E-03	0.77
0.01	0.79	0.20	1.69E-03	0.78
0.01	0.80	0.19	1.69E-03	0.80
0.01	0.81	0.18	1.68E-03	0.82
0.01	0.82	0.17	1.67E-03	0.84
0.01	0.83	0.16	1.66E-03	0.86
0.01	0.84	0.15	1.65E-03	0.88
0.01	0.85	0.14	1.64E-03	0.90
0.02	0.76	0.22	3.52E-03	0.73
0.02	0.77	0.21	3.51E-03	0.75
0.02	0.78	0.20	3.51E-03	0.77
0.02	0.79	0.19	3.50E-03	0.79
0.02	0.80	0.18	3.49E-03	0.81
0.02	0.81	0.17	3.47E-03	0.83
0.02	0.82	0.16	3.46E-03	0.85
0.02	0.83	0.15	3.44E-03	0.87
0.02	0.84	0.14	3.41E-03	0.89
0.02	0.85	0.13	3.39E-03	0.90
0.03	0.76	0.21	5.47E-03	0.74
0.03	0.77	0.20	5.46E-03	0.76
0.03	0.78	0.19	5.45E-03	0.78
0.03	0.79	0.18	5.43E-03	0.80
0.03	0.80	0.17	5.41E-03	0.82
0.03	0.81	0.16	5.39E-03	0.83
0.03	0.82	0.15	5.35E-03	0.85
0.03	0.83	0.14	5.32E-03	0.87
0.03	0.84	0.13	5.28E-03	0.89
0.03	0.85	0.12	5.23E-03	0.91

0.04	0.76	0.20	7.55E-03	0.75
0.04	0.77	0.19	7.54E-03	0.76
0.04	0.78	0.18	7.52E-03	0.78
0.04	0.79	0.17	7.49E-03	0.80
0.04	0.80	0.16	7.45E-03	0.82
0.04	0.81	0.15	7.41E-03	0.84
0.04	0.82	0.14	7.36E-03	0.86
0.04	0.83	0.13	7.31E-03	0.88
0.04	0.84	0.12	7.25E-03	0.90
0.04	0.85	0.11	7.18E-03	0.91

0.06	0.76	0.18	1.21E-02	0.76
0.06	0.77	0.17	1.21E-02	0.77
0.06	0.78	0.16	1.20E-02	0.79
0.06	0.79	0.15	1.20E-02	0.81
0.06	0.80	0.14	1.19E-02	0.83
0.06	0.81	0.13	1.18E-02	0.85
0.06	0.82	0.12	1.17E-02	0.87
0.06	0.83	0.11	1.16E-02	0.88
0.06	0.84	0.10	1.15E-02	0.90
0.06	0.85	0.09	1.14E-02	0.92

0.08	0.76	0.16	1.72E-02	0.76
0.08	0.77	0.15	1.71E-02	0.78
0.08	0.78	0.14	1.70E-02	0.80
0.08	0.79	0.13	1.69E-02	0.82
0.08	0.80	0.12	1.68E-02	0.84
0.08	0.81	0.11	1.67E-02	0.85
0.08	0.82	0.10	1.65E-02	0.87
0.08	0.83	0.09	1.63E-02	0.89
0.08	0.84	0.08	1.61E-02	0.91
0.08	0.85	0.07	1.59E-02	0.92

Appendix 13

Estimated activity data of V and Al in the FeV system according to the Chemsage software package. Temperature : 2073 K

N_{Al}	N_V	N_{Fe}	a_{Al}	a_V
0.03	0.76	0.21	6.17E-03	0.70
0.03	0.77	0.20	6.16E-03	0.72
0.03	0.78	0.19	6.14E-03	0.73
0.03	0.79	0.18	6.11E-03	0.75
0.03	0.80	0.17	6.08E-03	0.77
0.03	0.81	0.16	6.04E-03	0.79
0.03	0.82	0.15	6.00E-03	0.80
0.03	0.83	0.14	5.96E-03	0.82
0.03	0.84	0.13	5.91E-03	0.84
0.03	0.85	0.12	5.85E-03	0.86

Estimated activity data of V and Al in the FeV system according to the Chemsage software package. Temperature 2173 K

N_{Al}	N_V	N_{Fe}	a_{Al}	a_V
0.03	0.76	0.21	6.53E-03	0.68
0.03	0.77	0.20	6.51E-03	0.70
0.03	0.78	0.19	6.48E-03	0.72
0.03	0.79	0.18	6.45E-03	0.73
0.03	0.80	0.17	6.42E-03	0.75
0.03	0.81	0.16	6.37E-03	0.77
0.03	0.82	0.15	6.33E-03	0.78
0.03	0.83	0.14	6.28E-03	0.80
0.03	0.84	0.13	6.22E-03	0.82
0.03	0.85	0.12	6.16E-03	0.83

7. Conclusions

The following can be concluded:

- Measured activity coefficients of vanadium oxide in $CaO\text{-}Al_2O_3$ slags confirm that vanadium is present as V^{3+} under conditions present in industrial operations.

- The Al_2O_3 content of the slag has a strong effect on the vanadium activity coefficient.

- Industrial slag samples indicate that the $MgO\text{-}Al_2O_3$ phase is the major repository of oxidic vanadium in solidified slag.

- The strong dependence of the vanadium oxide content of the solidified slag sample on the Al_2O_3 content is associated with V_2O_3 substituting Al_2O_3 in the $MgO\text{-}Al_2O_3$ spinel-type phase.

- Analyses of industrial slags indicate that slags with higher Al_2O_3 contents clearly have lower vanadium oxide contents.

- Slag samples taken for industrial X.R.F. analyses contain metal droplets and the oxidic constituent is not representative of the average bulk composition.

- Industrial X.R.F. analyses taken over 3 months show that high-alumina slags are beneficial for vanadium recovery. Furthermore, the aluminium content of the ferrovanadium is not strongly dependent on the alumina content of the slag.

- The amount of droplets entrained for the slag samples analysed is not strongly dependent on the tap temperature.

- Vanadium losses as entrained metal droplets could not be fully quantified due to the strong segregation behaviour and crowding close to the slag metal interface. The positional effect of droplet entrainmnet introduces too much uncertainty. A 3-D mapping of the slag sample must be established in order to fully quantify the positional effect on droplet entrainment.

- The predicted relationships show a strong effect of slag basicity on the soluable vanadium loss.

- Although the effect of retained MgO on the vanadium activity coefficient is not known, MgO is detrimental to the soluble vanadium loss due to the lowering of the alumina activity.

- The lower predicted vanadium content compared to industrial slag samples is a result of the aluminium activity in ferrovanadium which could not be fully quantified.

- Lower MgO contents, higher aluminium contents in ferrovanadium and lower tap temperatures will yield lower vanadium oxide losses.

8. Recommendations for future work

- New sampling methods must be derived to quantify the amount of droplets entrained in the slag to quantify the effect of slag basicity on metal droplet entrainment. Special care has to be taken to ensure that the determined amount of entrained droplets is representative of the bulk slag sample. One such way is to sample from both the y and x direction to establish a three-dimensional mapping of the bulk slag sample. Only then will the positional effect on droplet entrainment be fully quantified. A number of slag samples should be subjected to this new form of sampling to establish the effect of slag composition on metal droplet entrainment.

- Because of the many uncertainties regarding the aluminium activity in liquid ferrovanadium, experiments should be performed for oxygen activities in the same order as previously used in experiments.

9. References

Arkhipov, O.A., Berezin, N.M. and Shtengel'meier, S.V., *Influence of the physicochemical properties of the slag on the separation of liquid phases in the production of high-percentage ferrovanadium by the aluminothermic method*, Paper from phenomena in metallurgical processes consultants Bureau of Enteprises (Inc), New York, 1965. pp224-226.

Baker (ed), H., *ASM Handbook, volume 3: Alloy phase diagrams.*, ASM International, Metals Park, Ohio,1992.

Bedford, R.E., *Reference tables for Platinum-40 % Rodium/ Platinum-20 % Rodium thermocouples*, The Review of the scientific instruments, vol 36,1965, pp 1571-1580.

Belton, G.R., *Personal communication*, Marks Point, New South Wales, 1998.

Belton, G. R. and Belton. R.A., *On the rate of desulfurization of liquid iron by hydrogen*, Transaction of ISIJ, 1980, vol 20, pp. 87-91.

Chipman. J. and Gokcen, N.A., *Aluminum-oxygen equilibrium in liquid iron*, Journal of metals, 1953, pp. 173-178.

Chemsage technical thermochemistry, Chemsage Standard and extended versions 4.15, GTT-Technologies, Kaiserstrasse 100, 52134 Herzogenrath, Germany.

Darken, L.S. and Gurry R.W., *The system iron iron-oxygen. Equilibrium and the thermodynamics of liquid oxide and other phases.*, Journal of American Chemical Society, vol 68,1945, pp 1398-1412.

FACT thermochemical database. http:/www.crct.polymtl.ca/fact/fact.htm.

Fruehan,R.J., *The making, shaping and treating of steel., Steelmaking and refining volume*, 11th edition, Pittsburgh,U.S.A.,1998,p. 56.

Goldstein, J.I., Newbury, D.E., Echlin, P., Joy, D.C., Fiori, C. and Lifshin,E., *Scanning Electron Microscopy and X-ray* Microanalysis., Plenum Press, New York,1981, pp.63-111.

Gupta,C.K. and Krishnamurthy,N., *Extractive metallurgy of vanadium*, Process Metallurgy 8, Amsterdam, Netherlands, 1992.

Hayward,C.R., *An outline of metallurgical practice*, 3rd edition, Van Nonstrand, New York, 1952.

Janaf Table, *Temperature - oxygen fugacity tables for selected gas mixtures in the system C-H-O at one atmosphere total pressure*, Joint Army, Airforce Thermochemical Tables edited by D.R. Stull et al with subsequent supplements, Dow Chemical Co., Midland, Michigan, 1965, pp.11-15.

Khodorovsky, Y. and Dunn.H.E., *Production of ferroalloys*, MIR Publishers, Moscow,1967.

Kubaschewski, O., Alcock, C.B. and Spencer, P.J., *Materials Thermochemistry*, 6th edition, Pergamon, Oxford, 1993, pp.258-338.

MacRae, D.R, Gold, R.G., Thomson, C.D. and Sandall,W.R., *Ferrovanadium production by plasma carbothermic reduction of vanadium oxide*, Proceedings of the ISS/AIME 34th Electric Furnace Converence,1976,pp. 96-100.

Mannion, F.J., Fruehan, R.J., Belton, G.R. and Sasaki, Y., *Rate of decarburization of Fe-C_{sat} melts by H_2O at 1523 and 1873 K*, Metallurgical Transactions B, vol. 23B, 1992, pp. 45-51.

Minu, N., Dastur and Chipman, J., *Elimination of the thermal-diffusion error in studies of gas-metal equilibrium,* Journal of American Chemical Society , 1948, pp. 100-108.

Nagasaka,T. and Fruehan, R.J., *Kinetics of the reaction of H2O gas with liquid iron,* Metallurgical Transactions B, vol. 25B, 1994, pp. 245-253.

Nelson, G.O., *Gas mixtures: preparation and control,* Lewis Publishers, Chelsea, 1992, pp 159-223

Nyirfa, J., *Industrial experience in the aluminothermic manufacture of ferrovanadium (Translation : Mintek-TR-1260),* Koshazat, vol. 118, no. 9., 1985, pp. 382-388.

Perry, F.H. and Green. D., *Perry's Chemical Engineers' handbook,* sixth edition, McGraw-Hill,1984.

Pretorius, E.B., *Activity-composition relations of chromium oxide in silicate melts,* PhD Thesis, University of Pennsylvania, 1989, pp. 19.

Reddy, R.G. and Yen, J.G., *Effect of solid particles on the viscosity of slags, The Paul E. Queneau International Symposium : Extractive metallurgy of copper, nickel and cobalt,* vol. 1 : Fundamental aspects, The Minerals, Metals and Materials Society, 1993, pp. 309-323.

Rein, R.H. and Chipman, J., *Activities in the liquid solution SiO_2-CaO-MgO-Al_2O_3,*Transactions of the Metallurgical Society of AIME, 1965, vol. 223, pp. 415-425.

Sieveking, H.A., *Some electrical supply aspects of ferro-alloy manufacture,* Journal of Institute of Electrical Engineering, vol XC,1945.

Sigworth, G.K. and Elliott, J.F., *The thermodynamics of liquid dilute iron alloys*, Metal Science, vol. 8, 1974, pp. 298-309.

Szekely,J. and Themelis,N.J., *Rate phenomena in process metallurgy.*, Canada, Wiley-Interscience, 1971, pp. 368-369

Verein Deutscher Eisenhüttenleute (ed.): Slag atlas, 2nd edition, Verlag Stahleisen, Düsseldorf, 1995, pp. 104, 226 & 550.

Weast, R.C., *Handbook of chemistry and Physics*, 62nd eddition, 1982, pp. F-175.

Wills, B.A., *Mineral processing technology*, New York, Pergamon Press, 3rd edition,1985, pp 260-301.

Yücel. O., Cinar, F., Addemir, O. and Tekin, O., *The preparation of ferroboron and ferrovanadium by aluminothermic reduction, High temperature materials and processes*, Vol. 15, 1996, pp. 103-109.